Role of JmjC Histone Demethylases in Hypoxia Induced NF-κB Response

Thesis submitted in accordance with the requirements of the University of Liverpool for the degree of Doctor in Philosophy

Dilem Shakir

December 2022

Acknowledgement

First of all, I would like to express my greatest appreciation to my supervisor, Prof Sonia Rocha, for giving me every opportunity to improve my scientific skills, and for encouraging me to work on a research project that I am interested in. Her curiosity and enthusiasm for science has been very inspirational. Her continuous guidance and motivation provided me a very supportive and enjoyable PhD experience. Beyond all, I am very thankful for her support during covid phase; finding a family, away from mine gave me the strength and joy to live through the unpredictable times.

Secondly, I would like to express my gratitude to Michael Batie, who patiently taught me everything I needed in the lab, always encouraged me to learn new techniques, and tirelessly supported me to improve my scientific thinking and understanding skills. Having a skilful postdoc like him in the group made this project and my PhD journey a much easier and enjoyable experience.

I have been extremely lucky to do this project in a very supportive and friendly group. For that, I would like to thank to past and present SR lab members. In particular, thanks to James, Julianty and Mark for welcoming me to the group and supporting me in the lab. Thanks to Laura for being a very helpful resource of information and motivating and helping me to adapt to the PhD. Also, thanks to Fraser, Jimena, Temi, Harry, Adam, Chun, Jiahua and Hao.

Last but not least, I would like to thank to my secondary supervisor Dr Niall Kenneth, for his valuable comments in the lab meetings, which directed me to think about different aspects of the project. Also, thanks to my independent progress assessment panel members, Prof Patrick Eyers and Dr Jill Madine for their support throughout these years.

Abstract

Reduced oxygen availability or increased demand for oxygen create an imbalance called hypoxia, which is an essential condition for regulating many physiological processes such as development, and also pathological conditions such as cancer and ischaemic diseases. Molecular responses to hypoxia involve alterations in gene expression levels, including changes in gene transcription, to maintain homeostasis in cells. This transcriptional response is coordinated at the chromatin level by multiple mechanisms that also involve Jumonji-C domain containing histone lysine demethylases (KDMs) that depend on oxygen for activity. Responses to hypoxia involve many transcription factors, including NF-κB, which is a main regulator of critical biological functions, such as immune and inflammatory responses. Previous work has shown hypoxia induces changes in histone methylation, linked to altered activities of KDMs. In addition, hypoxia induced histone methylation highlights an NF-κB target gene signature. However, the mechanism regulating the hypoxia-induced NF-κB transcriptional response at the chromatin level is unknown. This project finds that hypoxia-induced NF-κB target genes have increased histone-3 lysine-4 trimethylation (H3K4me3), and this response could be mimicked by KDM5A depletion. In addition, enzymatic activity of KDM4A and KDM4B is suggested as a potential regulator of the H3K36me3 levels at NF-κB target genes in response to hypoxia. Previous work has identified methylated lysine sites on NF-κB RelA protein, which are important for RelA activity and are demethylated by KDM2A. This project demonstrates that these lysine residues are conserved across different NF-κB subunits and provides analysis of their importance to NF-κB activity and provides preliminary evidence for an additional layer of crosstalk between KDMs, hypoxia and NF-κB. Lastly, this project reports hypoxia-inducible NF-κB target gene signatures in different cell lines by analysing publicly available hypoxia transcriptomics data, integrated with known NF-κB target genes. The cell type-specific and the core hypoxia-inducible NF-κB target genes signature is a significant resource for future work uncovering the mechanisms involved in hypoxia stimulated NF-κB transcriptional response.

List of Contents

List of Figures

List of Tables

List of Abbreviations

2-OG - 2-Oxoglutarate

A20/ TNFAIP3 - Tumour Necrosis Factor Alpha-Induced Protein 3

AP-1 - Activator Protein-1

ARID - AT-Rich Interaction Domain

ATAC-seq - Assay for Transposase-Accessible Chromatin using sequencing

ATP - Adenosine Triphosphate

BAFF - B-cell Activation Factor

Bcl-3 - B-cell lymphoma 3-encoded protein

bHLH-PAS - basic Helix-Loop-Helix-containing Per/ARNT/Sima

BHLHE40 - Basic Helix-Loop-Helix Family Member E40

BMP2 - Bone Morphogenetic Protein 2

BNIP3 - BCL2 Interacting Protein 3

CA9 - Carbonic Anhydrase 9

CaMK2 - Calcium/ Calmodulin-dependent Kinase 2

CBP - CREB Binding Protein

CDK - Cyclin-Dependent Kinase

CDYL1 - Chromodomain Y-Like

CH_3 - Methyl

CHD - Chromodomain Helicase DNA-binding

ChIP - Chromatin Immunoprecipitation

ChIP-seq - Chromatin Immunoprecipitation-sequencing

CK2 - Casein Kinase-II

CRISPR - Clustered Regularly Interspaced Short Palindromic Repeats

CSB - DNA excision repair protein ERCC-6

CTAD - C-Terminal Transactivation Domain

CXCL2 - C-X-C Motif Chemokine Ligand 2

DEG - Differentially Expressed Genes

DFX - Desferrioxamine

DM - Double Mutant

DNA - Deoxyribonucleic Acid

DUSP1 - Dual Specificity Phosphatase 1

EDN1 - Endothelin 1

EV - Empty Vector

EZH1-2 - Enhancer of Zeste 1 Polycomb Repressive Complex 1-2

FDR - False Discovery Rate

FIH - Factor Inhibiting

FTH1 - Ferritin Heavy Chain 1

G9A/ EHMT2 - Euchromatic Histone Lysine Methyltransferase 2

GEO - Gene Expression Omnibus

GLP/ EHMT1 - Euchromatic Histone Lysine Methyltransferase 1

GO - Gene Ontology

GSEA - Gene Set Enrichment Analysis

HER2 - Human Epidermal Growth Factor Receptor 2

HIF - Hypoxia Inducible Factor

HIV-1 LTR - Human Immunodeficiency Virus-1 Long Terminal Repeat

HMT - Histone Methyltransferase

HRE - Hypoxia Response Element

HUVEC - Human Umbilical Vein Endothelial Cells

IAP - Inhibitor of Apoptosis

IgG - Immunoglobulin G

IGV - Integrative Genomics Viewer

IKK - Inhibition of *κ*B Kinase

IL - Interleukin

IL-1R - Interleukin-1 Receptor

INO80 - INO80 Complex ATPase Subunit

IP - Immunoprecipitation

ISWI - Imitation Switch

I*κ*B - Inhibitor of *κ*B

I*κ*BNS - Nuclear I*κ*Bs

JmjC - Jumonji-C

JUN - Jun Proto-Oncogene, AP-1 Transcription Factor Subunit

KAT5 - Histone Acetyl Transferase 5

KDM - Jumonji-C domain-containing Lysine Demethylase

KMT - Histone Lysine Methyltransferase

LMP1 - Latent Membrane Protein-1

LPS - Lipopolysaccharide

LRR - Leucin-Rich Repeat

LSD1 - Lysine Demethylase

LTbR - Lymphotoxin-b Receptors

MAFF - MAF BZIP Transcription Factor F

MARCKS - Myristoylated Alanine-Rich C-Kinase Substrate

MEF - Mouse Embryonic Fibroblast cells

MLL1-4 - Mixed Lineage Leukemia protein1-4

MMP2 - Matrix Metallopeptidase 2

MSigDB - Molecular Signature Database

MTorck1 - Mammalian Target of rapamycin complex 1

MYC - MYC Proto-Oncogene, BHLH Transcription Factor

NCBI - National Center for Biotechnology Information

NES - Normalised Enrichment Score

NF-κB - Nuclear Factor kappa-light-chain-enhancer of activated B cells

NIK - NF-κB Inducing Kinase

NSD1-3 - Nuclear receptor-binding SET Domain-containing protein 1-3

NTAD - N-terminal Transactivation Domain

O_2 - Oxygen

ODD - Oxygen Dependent Domain

PHD - Prolyl Hydroxylase Domain

PHD* - Plant Homeobox Domain

PHF20 - Plant Homeodomain Finger protein 20

PP2A - Protein Phosphatase 2

PRC2 - Polycomb Repressive Complex 2

PRDM9 - PR/ SET Domain zinc finger protein 9

PTM - Post Translational Modification

PTPN13 - Protein Tyrosine Phosphatase Non-Receptor Type 13

RANKL - Receptor Activator of NF-κB Ligand

RHD - Rel Homology Domain

RNA - Ribonucleic Acid

RNApolII - RNA polymerase II

RPL30 - Ribosomal Protein L30

SAM - S-Adenosyl Methionine

SET - Su(var)3-9 Enhancer of Zeste Trithorax

SETD1A/ B - SET Domain Containing 1A/ B

SETD2 - SET Domain Containing 2

SETD7/ 9 - SET Domain Containing 7/ 9

SETDB1 - SET Domain Bifurcated Histone Lysine Methyltransferase 1

SGK1 - Serum/Glucocorticoid Regulated Kinase 1

SIN3A - SIN3 Transcription Regulator Family Member A

SM - Single Mutant

SOCS1 - Suppressor of Cytokine Signalling 1

SRA - Sequencing Read Archive

STAT - Signal Transducer and Activator of Transcription

SWI/SNF - SWItch/Sucrose Non-Fermentable

TAD - Transactivation Domain

TAK1 - Transforming growth factor-beta-Activated Kinase 1

TES - Transcription End Site

TET - Ten Eleven Translocation

TGF - Tumour Growth Factor

TLR - Toll-Like Receptors

TNF-α - Tumour Necrosis Factor-alpha

TNFR - Tumour Necrosis Factor Receptor

TSC22D1 - Transforming Growth Factor Beta-1-Induced Transcript 4 Protein

TSS - Transcription Start Site

Ubc13 - Ubiquitin-conjugating enzyme 13

UV - Ultraviolet

VHL - Von Hippel-Lindau

WebGestalt - WEB-based Gene Set Analysis Toolkit

WIZ - G9A/GLP-associating zinc finger

WT - Wild Type

XIAP - X-linked Inhibitor of Apoptosis Protein

Chapter 1 - Introduction

1.1. Gene Transcription

Gene transcription is a fundamental biological process that enables the cell and ultimately the whole organism to respond to a variety of intra- and extra-cellular signals. This process aims to define the cell's physiology during development and maintain its homeostasis throughout its lifespan by coordinating different cellular activities. Essentially, transcription is processed by the interaction of cis- and trans-regulatory factors within the cell nucleus that regulate the expression of targeted genes. The cis- regulatory elements are the non-coding DNA regions, such as promoters and enhancers, which regulate the transcription of nearby genes, and trans-regulatory factors include sequence-specific transcription factors (e.g., HIF and NF-κB), chromatin modifying complexes (e.g., histone methyltransferases), and general transcription factors (GTFs), including RNA polymerase II (RNApolII) (1). RNA polymerase is an enzyme that transcribes DNA into RNA. In eukaryotes, there are 3 classes of RNA polymerases, with RNApolII responsible for transcribing the majority of genes, including protein coding genes.

The pre-initiation step of gene transcription starts when RNApolII binds to the template DNA strand of the target gene at its promoter region through AT-rich DNA sequence (the TATA box) that is around 30 base pair (bp) upstream (5' end) of the transcription start site (TSS) (2-4). Following assembly of the pre-initiation complex (PIC), which includes RNApolII and the GTFs TFIIA-H, transcription initiation, elongation and termination can proceed (2). Transition from transcription initiation to elongation is promoted by phosphorylation of the C-terminal domain (CTD) of RNApolII, which predominantly occur at Serine 2 and Serine 5 sites (2, 4). Several kinases can phosphorylate Serine 5, including Cyclin-dependent kinase 7 (CDK7) of TFIIH, which facilitates the promoter escape and abortive transcription (4). Subsequent to the Serine 5 phosphorylation at the promoter region, Serine 2 phosphorylation of the RNApolII, increases downstream of the TSS by CDK9 or CDK12 and initiates the productive elongation phase of transcription. As RNApolII moves from 5' to 3' end of the DNA, phosphorylation of serine residues at its CTD coordinate the recruitment of factors necessary for elongation process and transcript formation (reviewed in

(5)). Following the elongation step, transcription termination involves dissociation of RNApolII transcription complex from the transcript, which is proposed to occur in two ways (reviewed in (2, 4)).

1.2. Chromatin

Eukaryotic genomes are packaged in the nucleus in a complex three-dimensional structure, termed chromatin (6). Organisation and regulation of chromatin controls all stages of the transcription and consequently, gene expression.

1.2.1. Chromatin structure

Chromatin is a dynamic structure composed of nucleosomes, which includes 147 bp DNA wrapped 1.65 times around an octamer of histones (7) (**Figure 1.1**). The histone octamer contains two copies of each of the core histones H2A, H2B, H3 and H4 and the linker histone, H1, which connects and stabilises the nucleosomes (7). Each core histone protein shares a common structural domain that contains three α-helices separated by 2 loops, called the histone fold, which enables H2A-H2B and H3-H4 heterodimerisations (8). These links between histone proteins are the fundamental structural units of the chromatin that are essential for the interaction of nucleosome with DNA (8). Apart from the core histones, there are other histone variants, such as H2A.X and H3.3, which are majorly expressed throughout the cell cycle and support the structure of the nucleosome (reviewed in (9)).

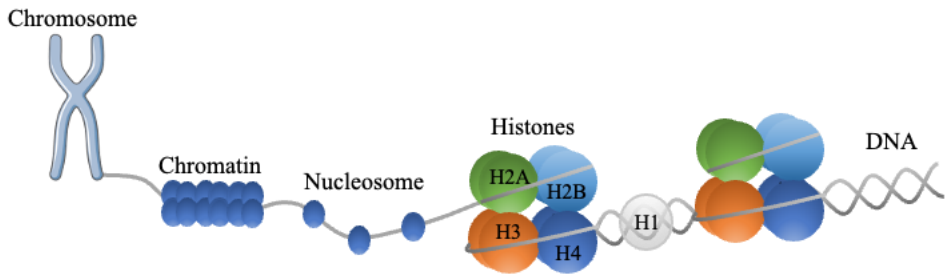

Figure 1.1. Schematic diagram of simplified chromatin structure. The structure contains nucleosomes that is composed of double-stranded DNA wrapped around core histone octamers, H2A, H2B, H3 and H4, and a linker histone, H1. Chromosome icon was obtained from <https://bioicons.com>.

Nucleosomes are the repeating units of chromatin, which are connected to each other by 10-70 bp of linker DNA. These nucleosomal arrays form short-range interactions with adjacent nucleosomes to form chromatin fibres. The fibre-fibre interactions contribute to the high degree of compaction establishing the condensed form of the chromosome (10). The beads-on-a-string organisation of individual nucleosomes are known as the primary structure of the chromatin, which then defines the secondary and the tertiary higher-order chromatin structures (8, 11). The high affinity of histone octamers for DNA keeps the nucleosome tightly assembled together through electrostatic interactions, hydrogen bonds and salt bridges, which forms a barrier for proteins requiring DNA access (8, 12). These structural organisations can vary based on the DNA sequence that is being organised, and also based on the amino acid sequence and combinations of post-translational modifications (PTMs) of the histones (11). In addition to the components of the nucleosomes, there are more elements that contribute to the organisation of the chromatin structure, including architectural chromatin proteins and nucleosome binding proteins, histone chaperons and ATP-dependent chromatin remodellers including SWI/SNF, INO80, ISWI, and CHD (reviewed in (13, 14)). Functional interactions between chromatin remodelling enzymes and histone modifications create a network of mechanisms that control chromatin dynamics. Slight changes by these elements can significantly affect the nucleosome structure and stability and essentially its accessibility to numerous proteins that regulate the gene expressions.

Two major states of chromatin are defined according to its compaction: heterochromatin and euchromatin (15). The compact heterochromatin (i.e., silent) is inaccessible and transcriptionally inactive, and an open (i.e., active) form, euchromatin is accessible to DNA binding proteins such as transcription factors (7). However, imaging approaches have identified additional variations in chromatin compaction levels (16). Importantly, the three-dimensional chromatin organisation also includes topologically associating chromatin domains and loops, linking proximal and distal regulatory elements (6). These three-dimensional chromatin interactions play a key role in modulating gene transcription.

When considering chromatin structure, post translational modifications (PTMs) on histones are one of the many elements that alter the dynamical structural states of nucleosomes, and they function as recruitment sites for chromatin binding proteins, and regulation of gene expression. Histones contain many amino acid residues that can be modified, such as acetylation, phosphorylation, ubiquitylation, sumoylation and methylation. In this study, there is a focus on histone methylation.

1.2.2. Histone lysine methylation and KMTs

Histone methylation is catalysed by histone methyltransferases (HMTs), also referred as "writers" that transfer methyl groups (CH_3) from S-adenosyl-L-methionine (SAM) to either arginine (R) or lysine (K) residues mainly on N-terminal histone tails (17). In the human proteome, there are two domains with lysine methyltransferase (KMT) activity; the SET (Su(var)3-9, Enhancer of Zeste, Trithorax) domain and the seven-beta-strand (7βS) domain, which includes the hDOT1L (18) (**Figure 1.2**, **B**). Lysine residues can be mono (me1)-, di (me2)-, or tri (me3)-methylated, and depending on the site and degree of methylation, this modification can be associated with transcriptional activation or repression (**Figure 1.2**, **A**). In humans, the best understood lysine methylation sites are histone 3 lysine 4 (H3K4), H3K9, H3K27, H3K36, and H3K79, and H4K20. Different histone modification patterns are associated with distinctive parts of the genome, discovered by chromatin immunoprecipitation (ChIP) experiments using antibodies specific to targeted histone modifications (19). As such, methylation of H3K4, H3K36 and H3K79 has been associated with active genes, whereas methylation of H3K27, H3K9 and H4K20 has been associated with inactive genes (20). Overall, H3K9 and H4K20 methylation marks are identified to have a homogenous distribution on the repressed genes. On the other hand, H3K27me3 is found, but not restricted to, the promoter regions of the repressed genes. On the actively transcribed genes, H3K4me3 methylation mark is found at the promoter area or around the TSS, whereas H3K36me3 methylation mark is identified downstream of the TSS in gene bodies.

A.

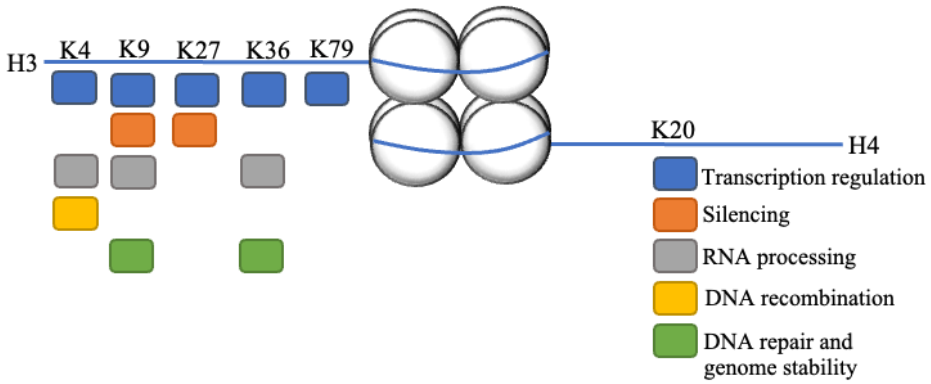

B.

Methylation targets	H3K4	H3K9	H3K27	H3K36	H3K79	H4K20
KMTs	SETD1A */ **/ ***	Suv39H1-2 **/ ***	EZH1-2 **/ ***	SETD2 ***	hDOT1L */ **/ ***	SET8 *
	SETD1B */ **/ ***	SETDB1 */ **		NSD1-3 */ **		Suv420H1-2 **/ ***
	MLL1-2 */ **/ ***	G9A/ EHMT2 */ **		ASH1L **		
	MLL3-4 */ **	GLP/ EHMT1 */ **				
	SETD7 *					
	PRDM9 */ **/ ***					

Figure 1.2. Histone lysine methylation sites, their functions and associated KMT enzymes. A. Main lysine (K) methylation sites and chromatin functions. **B.** Histone lysine methyltransferases (KMTs) targeting the corresponding histone lysine residues. Methylation state specificities determined as follows: * me1, ** me2, *** me3 (Adapted from (21, 22)).

Histone KMTs are selective enzymes, for instance, dimethylation of the H3K36 (H3K36me2) can be generated by NSD1, NSD2, NSD3 and ASH1L, whereas SETD2 is the only identified methyltransferase that synthesises trimethylation of H3K36 (H3K36me3) (23, 24). Furthermore, methylation of H3K79 is only identified to be generated by hDOT1L (18). SET8 only mono-methylates the H3K20, with the H3K20 di- or trimethylations being generated by the KMTs, SUV420-H1 and -H2 (25). MLL1 and MLL2 can catalyse H3K4 mono-, di- and tri-methylation, whereas MLL3 and MLL4 are restricted to H3K4-me1 and -me2 (26). SETD7 (also known as SET7/9) is an H3K4 mono-methyltransferase (27), whereas SETD1A, SETD1B and PRDM9 can also catalyse H3K4-me2 and -me3 (28-30). In addition,

there are less well characterised lysine methylation sites on the histones such as H3K23, H3K63, H4K12 that are also found to be methylated by various KMTs (reviewed in (21)).

Furthermore, to their histone methylation role, KMTs are also identified to modify non-histone proteins (reviewed in (31-33)). For instance, SETD7, G9A, GLP and SETD8 can methylate p53 protein and other non-histone substrates (31). In addition, SETD7 can methylate DNA methyltransferase 1 (DNMT1), oestrogen receptor α (ERα), and the transcription factor NF-κB RelA (reviewed in (34)). Also, NSD1 is shown to methylate NF-κB RelA protein (35). Overall, these modifications regulate the protein-protein interactions and stability, their localisation, and activities that are necessary in diverse cellular processes.

1.2.3. Histone lysine demethylation and KDMs

Methylation on lysine residues is reversible and can be removed by lysine demethylase enzymes, also referred as "erasers". The first histone demethylase that was identified is the lysine-specific demethylase 1 (LSD1) (36). Since then, an additional class of lysine demethylases was discovered. This family of enzymes contain a JmjC domain in their structure, which catalyses demethylation through the oxidation of methyl groups (**Figure 1.3**). Jumonji C (JmjC) lysine demethylase enzymes (KDMs) depend on α-ketoglutarate, molecular oxygen, and iron (Fe^{2+}) as cofactors for their function (37). In humans, 32 JmjC family members have been discovered with 23 of them having histone demethylase activity in cells (reviewed in (38, 39)).

All KDM family members share a JmjC domain and depending on the degree of homology and structural similarities with other domains, they are further classified into subfamilies that usually share substrate specificity (39) (**Figure 1.3**). In some of the enzymes JmjN domain is observed with the JmjC domain, which both are essential for their enzymatic activity (40). Each KDM has various DNA binding domains, including plant homeobox domain (PHD*), AT-rich interaction domain (ARID), or Zinc finger domains including C5HC2-ZF and CXXC-ZF (41). In addition, KDM2 family contains F-box and leucin-rich repeat (LRR) domains in their structure. F-Box binds a protein called S-phase kinase-

associated protein 1 (SKP1) that is part of a ubiquitin ligase complex, thus it has been suggested that KDM2 proteins might identify target proteins for their ubiquitylation (42). KDM4A, KDM4B and KDM4C contains an additional domain in their C-terminal region, called the Tudor domain, which is identified to be critical in regulating chromatin localisation and their enzymatic function by binding to methylated histone proteins (43, 44).

While KDMs are known primarily for demethylating histones, non-histone substrates for KDMs are emerging. For instance, KDM2A is shown to demethylate the NF-κB RelA protein (35). KDM4 isoforms, -A, -B and -C are identified to demethylate chromatin repressor proteins, WIZ, CDYL1, CSB and G9A (45). Furthermore, KDMs are also known to have demethylation independent functions (42, 46-48). This includes interaction of KDM2B with the ATPase subunit of SWI/SNF chromatin remodelling complexes and directly recruiting RNApolII to the interleukin 6 (IL6) promoter, which then initiates the inflammatory immune responses (47). Also, KDM2 proteins shape RNApolII occupancy on the CpG islands that are associated with the gene promoter regions and recruiting chromatin modifying enzymes (42). Thus, KDMs can be described as multifunctional proteins. However, JmjC containing KDMs' need for molecular oxygen, makes them attractive and potential oxygen sensors in the cell.

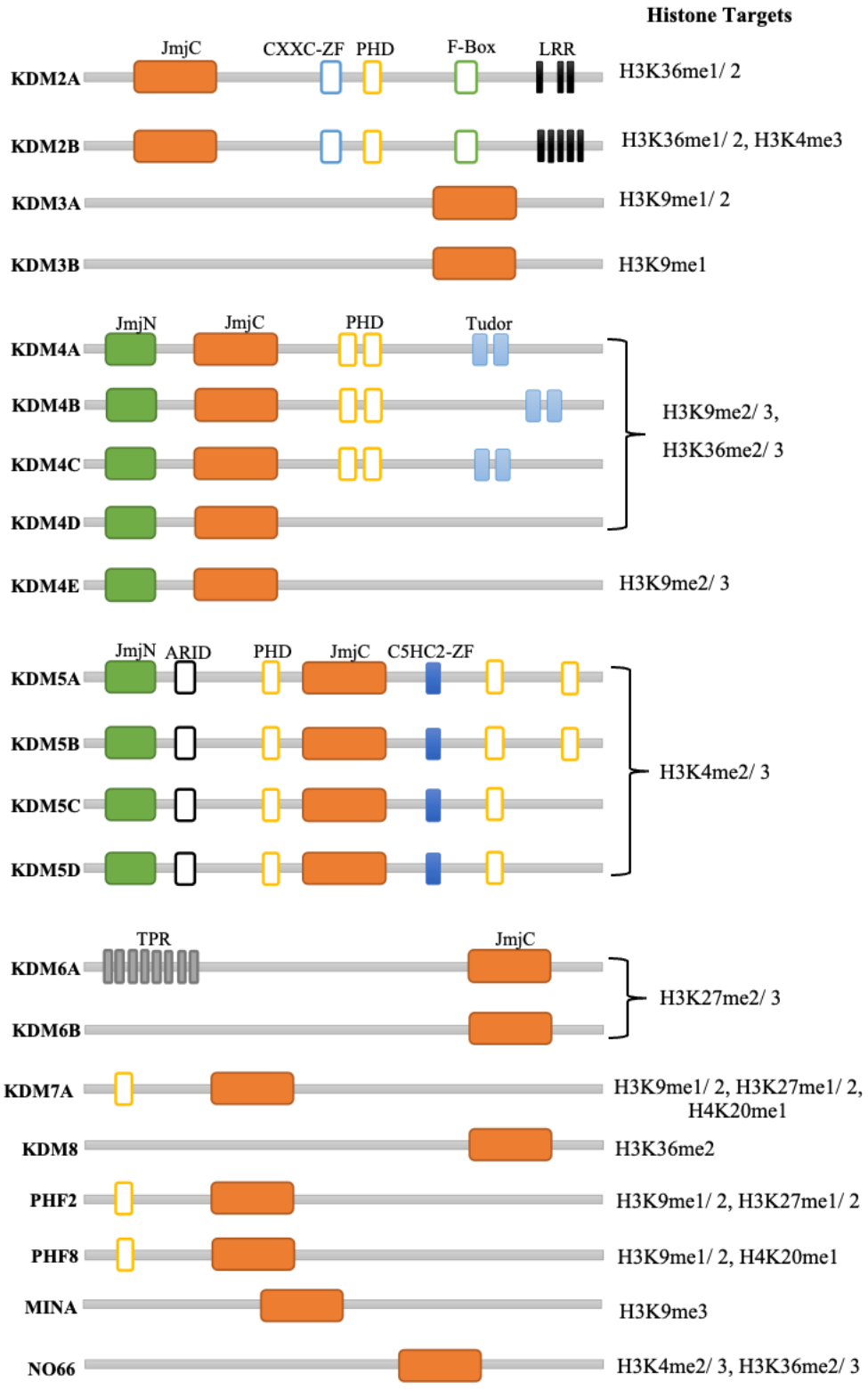

Figure 1.3. Schematic diagram of KDM subunits and their histone targets. ARID, AT-rich interactive domain; C5HC2-ZF, zinc finger domain; CXXC-ZF, zinc finger domain; F-Box, F-box domain; JmjC, Jumonji-C domain; JmjN, Jumonji-N domain; LRR, leucine-rich repeat domain (F-box associated domain); TPR, tetratricopeptide domain; Tudor, Tudor domain. (Adapted from (39))

1.3. Hypoxia

Molecular oxygen utilisation is an essential feature for the majority of living organisms. Eukaryotes have evolved sophisticated and co-ordinated mechanisms for sensing and responding to changes in oxygen availability (49). Hypoxia can be defined as the deficiency of molecular oxygen levels in the tissue, which is part of both physiological and pathological conditions (50-52). In human tissues, oxygen concentration can range from 1% and 14%, depending on the tissue type, which is termed as physiological hypoxia, since the values are below 21% that is considered as the normal atmospheric oxygen level (53). Physiological hypoxia impact variety of biological processes, including embryonic development (54), angiogenesis (55), energy metabolism (56), wound healing (57) and adaptation to high altitudes (58). Also, hypoxia is associated with wide range of diseases, including different cancer types and ischemia (59-61).

In response to hypoxia, cells undergo specific alterations in gene expression patterns to promote cell survival and maintain homeostasis in the cells and ultimately the whole organism (50). This cellular response to hypoxia is predominantly coordinated by the transcription factor family, hypoxia-inducible factor (HIF).

1.3.1. HIF subunits and structures

HIF subunits are members of the basic helix-loop-helix (bHLH)-containing Per/ARNT/SIM (PAS) domains family of transcription factors (**Figure 1.4**) (62, 63), which these domains mediate heterodimerisation and DNA binding of HIF subunits (64). In the mammalian genome there are three oxygen-sensitive alpha subunits, namely HIF-1α, HIF-2α, and HIF-3α, and a continuously expressed beta subunit, HIF-1β (known as aryl hydrocarbon receptor nuclear translocator, ARNT) (65). Overall, HIF-1α and HIF-2α subunits have been extensively studied, however HIF-3α remains poorly understood. HIF-1α and HIF-2α have similar sequence identity and protein domains, including the oxygen-dependent domain (ODD), and the C-terminal transactivation domain (CTAD), in contrast, HIF-3α does not contain CTAD, representing a distinct functional role in hypoxia-induced regulatory system

(50). The CTAD has been shown to be necessary for binding with the co-activators CBP/ p300 (66). The N-terminal transactivation domain (NTAD) is thought to contribute to the target gene specificity in different HIF isoforms (67). Importantly, all HIF-α subunits contain an ODD with hydroxylation sites that are important for determining the protein stability of the subunits in response to oxygen. On the other hand, HIF-1β does not contain the ODD and thus is not sensitive to changes in oxygen levels (68).

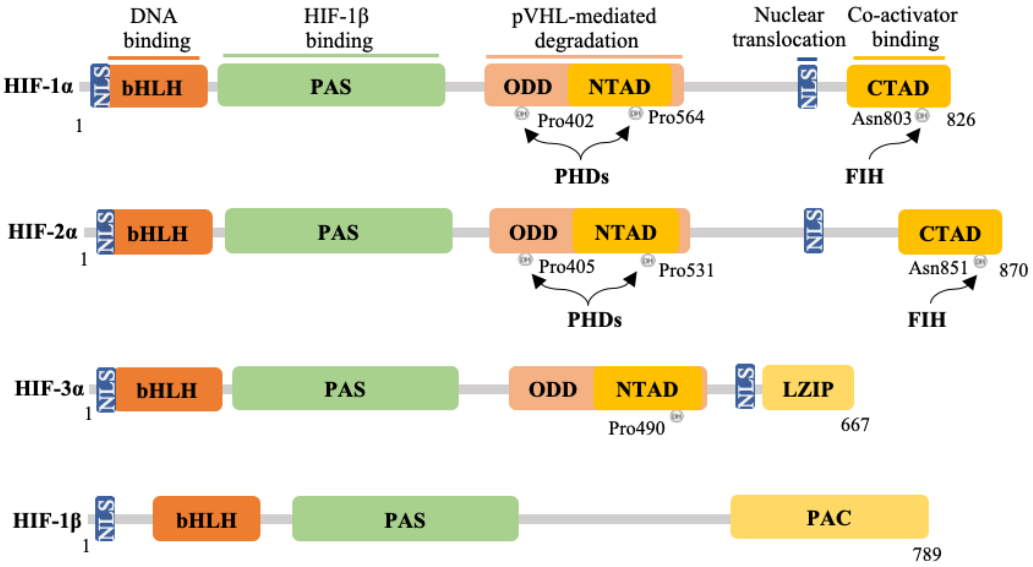

Figure 1.4. Schematic diagram of HIF subunits. Coloured bars represent different structural domains. bHLH, basic Helix Loop Helix; CTAD, C-terminal Transactivation Domain; LZIP, Leucine Zipper Domain; NLS, Nuclear Localization Signal; NTAD, N-terminal Transactivation Domain; ODD, Oxygen-Dependent Domain; PAS, Per/ARNT/Sim domain; PAC, PAS-Associated C-terminal domain. Domains with particular interaction regions are shown. Residues hydroxylated by PHDs and FIH enzymes are indicated. Pro, Proline; Asn, Asparagine; OH, hydroxylation.

1.3.2. HIF regulation in hypoxia

Under sufficient oxygen concentrations, HIF-α subunits are hydroxylated by Prolyl hydroxylase domain-containing proteins (PHDs), which are members of the iron- and 2-oxoglutarate (2-OG)-dependent dioxygenase family that require molecular oxygen for their hydroxylation function (69, 70) (**Figure 1.5**). Due to their dependence on oxygen, and their reduced hydroxylation activity over reduced physiological oxygen concentrations, these enzymes are referred to as oxygen sensors. Hydroxylation by PHDs targets HIF-α for

ubiquitin-mediated degradation by the von Hippel-Lindau tumour suppressor (VHL), which is part of an E3 ubiquitin ligase complex (71). Four PHD isoforms are identified, from which only PHD1, PHD2, and PHD3 have been shown to hydroxylate HIF (70). PHD2 was shown to have higher affinity for HIF-1α while PHD1 and PHD3 have higher affinity for HIF-2α (72).

In addition to PHD enzymes, HIF-α can also be regulated by another 2-OG-dependent dioxygenase family, known as Factor inhibiting HIF (FIH) (73). The C-terminal transactivation domain of HIF-α undergoes oxygen-dependent hydroxylation at asparagine residues by FIH, this prevents the recruitment of the key transcriptional co-activators CREB-binding protein (CBP)/ p300, which is necessary for at least 40% of all HIF-dependent target gene expressions (66, 73). PHD and FIH enzymes have different affinity for oxygen; FIH remains active at lower oxygen concentrations compared to PHDs and hence blocks HIF-α proteins that escaped the destructive mechanism in moderate hypoxia from full transcriptional activity (74). In hypoxic conditions, PHD and FIH enzymes are not active, this stabilises the HIF-α proteins, HIF-α translocate into the nucleus, where it binds to HIF-1β protein and their co-regulators. Consequently, the HIF complex binds to the hypoxia response elements (HRE) on its target genes, inducing transcription of genes necessary for the adaptive response to hypoxia.

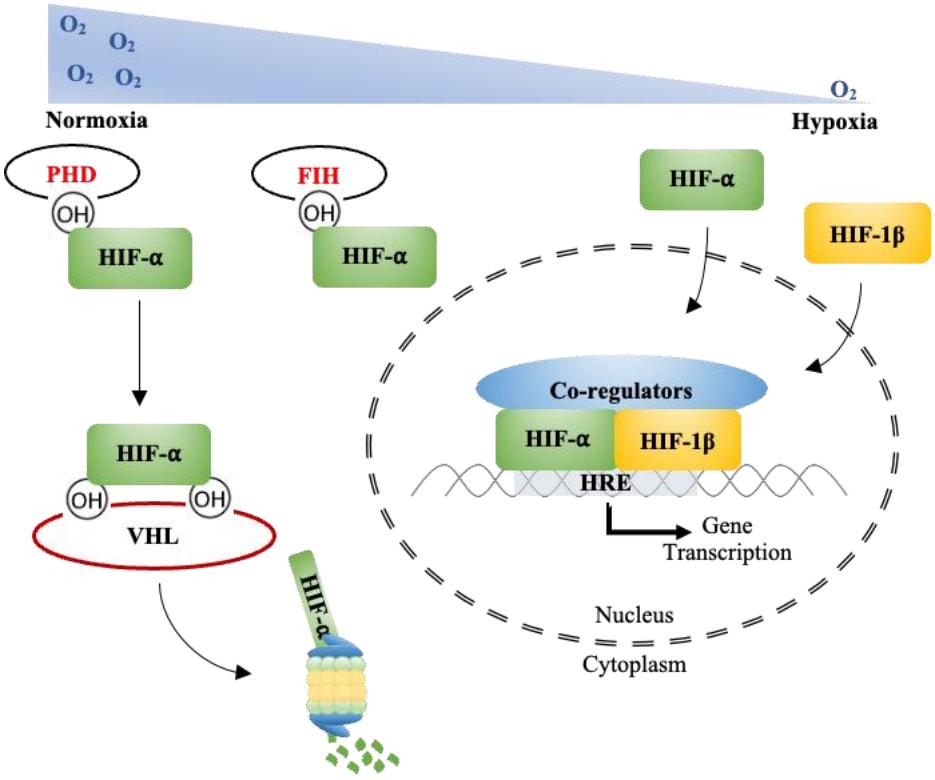

Figure 1.5. Schematic diagram of the HIF pathway. In normoxia, HIF-α protein is subject to oxygen-dependent prolyl hydroxylation (OH) that is mediated by PHDs or asparaginyl hydroxylation by FIH. Prolyl hydroxylation sites are recognised by VHL protein of the E3 ubiquitin ligase complex and HIF-α is targeted for proteasomal degradation, whereas asparaginyl hydroxylation by FIH prevents the recruitment of HIF co-regulators, CBP/p300. In hypoxic conditions, FIH and PHDs are inhibited due to decreased oxygen availability. This stabilises HIF-α and leads its translocation into the nucleus where HIF-α binds with its dimerization partner, HIF-1β and transactivates HIF target genes containing hypoxia response elements (HREs) in their enhancer/ promoter regions.

1.3.3. HIF target genes

The majority of hypoxia-induced genes are HIF dependent, consisting of HIF direct and indirect target genes (reviewed in (75, 76)). HIFs typically function as a HIF-α-HIF-1β heterodimer, binding to the DNA sites containing consensus nucleotide sequence 5'RCGTG-3' (R; A or G) within the HRE of the HIF target genes (77), and transactivating genes via release of paused RNApolII (78-80). Although the HRE consensus sequence is highly abundant in the genome, genome-wide analysis of HIF chromatin occupancy identified that HIF dimers occupy only less than 1% of these potential transcription sites (81-83). This suggests that apart from the consensus sequence, there are other factors contributing to the HIF-DNA binding, which includes epigenetic modifications affecting the chromatin accessibility. In addition, although HRE sites are mainly located at the proximal promoter

regions of target genes, they could also regulate the targeted genes from long distances, which might challenge the detection of direct HIF target genes (84). Furthermore, HIFs are thought to predominantly bind HRE regions that have DNAse I hypersensitivity, RNApolII enrichment, histone modifications, and higher levels of basal gene expression patterns prior to hypoxia induction (79, 82, 83), all these conditions likely contribute to cell type-specific responses to hypoxia. Additionally, there are a number of identified HIF co-regulators which likely play a role in HIF target gene selection and are required for transcriptional responses to hypoxia. These include the cyclin dependent kinase 8 (CDK8) mediator complex (79), histone acetyl transferase KAT5 (85), SET1B (86) and CBP/ p300 (66).

More than 100 validated direct HIF target genes have been identified, which are involved in numerous biological processes (87, 88) (**Figure 1.6**). Interestingly, although HIF-1α and HIF-2α bind the same HRE consensus sequence, they have overlapping but also separate target genes (89, 90). In addition to target gene selectivity by different HIF-α subunits, cell-type specific response to hypoxia have also been identified. For instance, a recently performed meta-analysis study based on 33 different cell types discovered that endothelial cells are deficient in the induction of a large set of genes in response to hypoxia, including many enzymes involved in glucose metabolism (91). Another study comparing HIF transcriptional response in various cell types found that epithelial cells induce higher amount of HIF target genes compared to mesenchymal cells (92). Apart from the cell types, duration, and concentration of hypoxia, the presence of functional destructive HIF mechanisms, such as VHL, and PHDs in different cell lines, as well as cooperation with other transcription factors that occupy the HRE regions can also influence the transcriptional output (reviewed in (93)). In addition, chromatin regulation is an important part of controlling transcriptional responses following hypoxia stimulation, which is detailed further in the following sections.

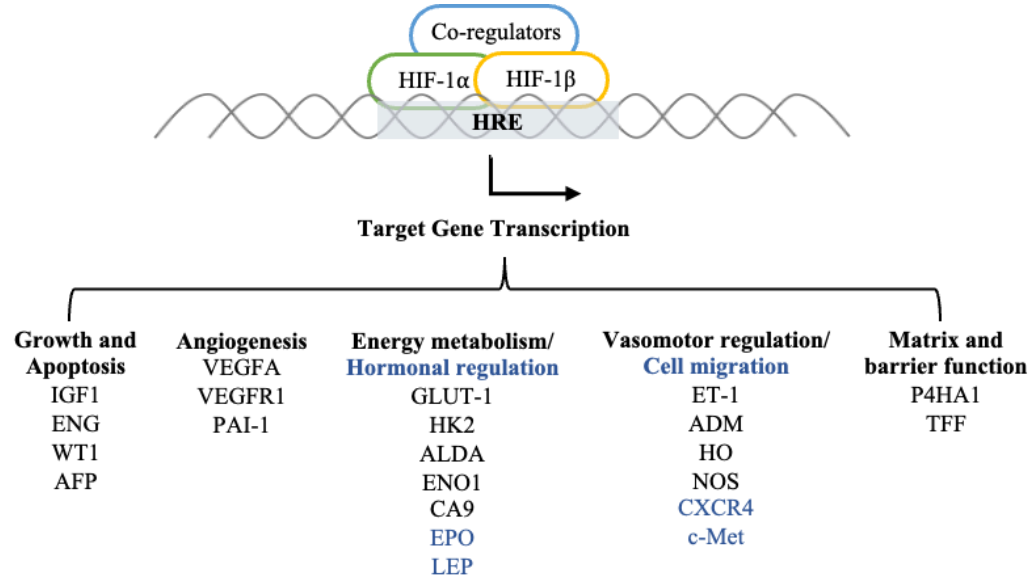

Figure 1.6. HIF target genes. Examples of direct transcriptional targets of HIF, grouped according to their functions. IGF1; insulin-like growth factor binding protein 1, ENG; endoglin, WT1; wilm's tumour suppressor, AFP; Alpha fetoprotein, VEGFA; vascular endothelial growth factor A, VEGFR1; vascular endothelial growth factor receptor 1, PAI-1; plasminogen activator inhibitor 1, GLUT-1; glucose transporter 1, HK2; hexokinase 2, ALDA; Aldolase A, ENO1; enolase 1, CA9; carbonic anhydrase 9, EPO; erythropoietin, LEP; leptin, ET-1; endothelin 1, ADM; adrenomedullin, HO; haem oxygenase, NOS; nitric-oxide synthase, CXCR4; chemokine receptor, c-Met; tyrosine-protein kinase, P4HA1; procollagen prolyl hydroxylase alpha 1, TFF; trefoil factor (adapted from (94)).

1.3.4. Hypoxia and Chromatin

While transcriptional responses to hypoxia have been extensively characterised (75, 91, 95), less is known regarding the chromatin response to hypoxia. ATAC-sequencing studies mapping genome wide chromatin accessibility have shown that hypoxia induces dynamic changes in chromatin accessibility in cell culture models, with changes in local chromatin accessibility enriched at hypoxia responsive genes (96-98).

Hypoxia stimulation can alter chromatin post-translational modifications either by directly inhibiting oxygen dependent enzymes, or via recruitment or increased expression of chromatin modifying enzymes (reviewed in (39, 93, 99-101)). Several chromatin remodellers are known to regulate HIF-mediated transcriptional response, including chromatin remodelling complexes, SWI/ SNF and ISWI (102, 103), and nucleosome remodelling deacetylase complex, metastasis-associated 1 (MTA1) (104). Furthermore, apart from the HIF hydroxylases, PHDs and FIH, there are many other 2-OG dependent dioxygenases in humans,

some of which have been identified as oxygen sensors (reviewed in (105, 106)). This includes certain KDMs and ten eleven translocation (TET) DNA demethylases, which are involved in histone methylation and DNA methylation changes in response to hypoxia respectively (reviewed in (105, 106)).

1.3.5. Histone lysine methylation in hypoxia, a focus on KDMs

Hypoxia-induced histone lysine methylation and gene expression can be regulated through several ways. This includes HIF mediated upregulation and/ or recruitment of KMTs and KDMs; oxygen-dependent hydroxylation of KMTs by proline and asparagine hydroxylases, PHDs and FIH; and oxygen sensing by KDMs (reviewed in (107)).

KDMs, similar to HIF hydroxylases, PHDs and FIH, require molecular oxygen for their enzymatic activity. So far, the oxygen affinity (K_m value) of only few of the KDMs has been measured and compared to HIF hydroxylases, these KDMs were found to have similar K_m value as PHD enzymes (108, 109), suggesting that KDMs can sense oxygen while regulating their enzymatic activity. Many studies have reported that hypoxia increases variety of histone methylation marks in different cell types (100, 110-115). Batie *et al.* and Chakraborty *et al.* have shown that upon hypoxia stimulation, chromatin can sense the change in oxygen levels via the inhibition of KDMs, which increases the histone methylation marks and alter transcriptional responses, independently of HIF activity (100, 110, 116). Hypoxia upregulation of H3K4me3 at a subset of hypoxia upregulated genes has been associated with reduced KDM5A activity in hypoxia (117). More recently it has been shown that PHD1 hydroxylates H3 proline 16 (H3P16oh), which recruits KDM5A to chromatin, and in hypoxia, loss of this modification, due to reduced PHD1 activity, leads to release of KDM5A from chromatin, and correlates with an increase in H3K4me3 and gene expression at a group of hypoxia responsive genes (118, 119). Thus, there may be multiple oxygen sensing mechanisms that involves KDM5A and H3K4me3. Hypoxia-induced changes in H3K4me3 have also been shown to be dependent on the recently identified HIF co-activator, SET1B (86) adding further complexity to H3K4me3 responses to hypoxia. In addition to KDM inactivation in hypoxia,

many KDMs are induced by hypoxia and some of them are recognised as HIF target genes (39, 107). For instance, both KDM2 and KDM5 family members are shown to be regulated by HIF-1 in response to hypoxia (111, 120). Also, some KDMs retain their activity in hypoxia and function as HIF co-regulators. KDM4C is shown to decrease the H3K9me3 and increase the HIF-1α binding to HREs on HIF target genes (121). Also, following hypoxia stimulation, HIF-1α induced KDM3A is shown to reduce H3K9 methylation on HIF target gene promoters, leading to their transcriptional activation (122).

1.3.6. Other transcription factors involved in hypoxia induced transcriptional changes

In response to decreased oxygen levels, apart from HIF, there are many other transcription factors involved in regulating the transcriptional response. Some of these are STATs, MYC, p53 and AP-1 (reviewed in (50, 123)). Importantly, hypoxia stimulation can also induce the major immune and inflammatory response transcription factor family, NF-κB, which is further detailed in the next section.

1.4. NF-κB

The transcription factor NF-κB was discovered in 1986 as a nuclear factor that binds to the enhancer element of the immunoglobulin kappa light-chain of activated B cells (NF-κB) (124). Since its discovery, NF-κB has been involved in a vast number of studies and recognised as a critical transcription factor for extensive range of biological functions, including immune and inflammatory responses (125), cell survival (126, 127), cell maturation (128, 129), and DNA damage responses (130, 131). NF-κB is tightly associated with many pathological conditions such as chronic inflammation, cancer, and autoimmune diseases (132), therefore understanding the regulatory mechanisms and function of the NF-κB signalling pathway is important not only for revealing the fundamental principles of cellular biology, but also critical to understand different human diseases and study on the possible treatment options.

1.4.1. NF-κB subunits and structures

NF-κB transcription factor family is composed of seven distinct proteins that are encoded by five different genes, namely RelA (p65), RelB, cRel, NF-κB1 (p105/p50), and NF-κB2 (p100/p52) (**Figure 1.7**) (133). All of the NF-κB subunits possess about 300 amino acid N-terminal domain, called the Rel homology domain (RHD), which contains residues required for DNA binding, dimerization, nuclear localisation and NF-κB inhibitor, IκB binding (133). In contrast to the other NF-κB family members, NF-κB1 and NF-κB2 are synthesised as pro-forms, p105 and p100, which are proteolytically processed to their active form, p50 and p52, respectively (134). All NF-κB protein members contain a transactivation domain (TAD), except NF-κB1 and NF-κB2. The TAD is essential for the regulation of NF-κB target genes, and it is important for interacting with different transcriptional regulatory proteins (135, 136), and chromatin remodelling complexes (137).

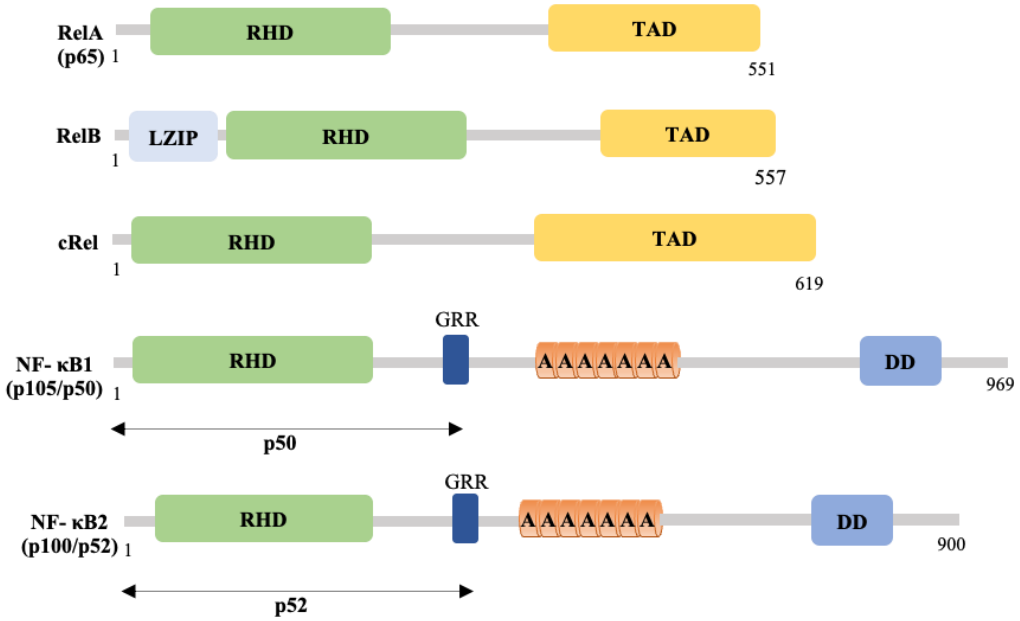

Figure 1.7. Schematic diagram of NF-κB subunits. Coloured bars represent different structural domains. The highly conserved amino-terminal Rel homology domain (RHD) is responsible for NF-κB subunits' dimerization, nuclear translocation, DNA binding and interaction with the inhibitory IκB proteins. RelA, RelB and cRel contain a carboxyl-terminal transactivation domain (TAD) that initiates transcription at the NF-κB binding sites of NF-κB target genes. Precursor proteins, p105 and p100, contain ankyrin repeats (A) that is an IκB-like C-terminal domain and proteolytically processed to p50 and p52, respectively. DD, Death Domain; LZIP, leucine zipper domain; GRR, glycine reach region.

All active members of the NF-κB protein family form homo- or hetero-dimers, except RelB, which only forms heterodimers (133). The most common NF-κB heterodimer is composed of p50 and RelA and is involved in most biological activities associated with NF-κB (138). In the quiescent state of the pathway, NF-κB dimers are bound to inhibitory molecules of NF-κB, namely the IκB family of proteins (133). These inhibitors contain ankyrin repeats, which associate with the NF-κB subunits by binding to their DNA-binding domains thereby making them transcriptionally inactive. The precursors of p50 and p52, p105 and p100, also contain ankyrin repeats within their structure that acts as their own internal inhibitors and need to be cleaved for their activation (139). Also, as p50 and p52 dimers do not contain TAD in their structure, they inherent transcriptional regulation of selected target genes through their association with nuclear IκB proteins such as Bcl-3 and IκBNS (140). Overall, whether an NF-κB dimers leads to transcriptional activation or repression depends on the DNA regions they bind to and their interaction with other transcription regulators (140). The arrangement of NF-κB dimerization can vary depending on the cell type, stimulus, or the duration of the exposure to the stimulus (138, 141, 142). Furthermore, NF-κB subunits contain numerous sites of post-translational modifications (PTMs), which are crucial for their activation and crosstalk with other signalling pathways (143).

1.4.2. NF-κB pathways

The activation of the NF-κB dimers can occur through the stimulation of distinct pathways, namely canonical (classical), non-canonical (alternative) and atypical (mostly IKK independent) pathways, which all are induced through various stimuli (**Figure 1.8**). The canonical activation pathway is stimulated through Toll-like receptors (TLRs), Interleukin-1 receptor (IL-1R), tumour necrosis factor receptor (TNFR) and antigen receptors. The typical receptor stimulating signalling molecules include the pro-inflammatory cytokines, tumour necrosis factor α (TNF-α), and interleukin-1 (IL-1), and bacterial products such as lipopolysaccharides (LPS). Stimulation through the canonical pathway receptors leads to

activation of IκB kinase (IKK) complex. The IKK complex is composed of a regulatory subunit, IKKγ (Nemo), and two catalytic kinases, IKKα, and IKKβ. Activated IKK complex mediates the phosphorylation of IκBα, which normally holds the NF-κB dimers inactive in the cytoplasm (133). Phosphorylation of IκBα leads to lysine-48-linked polyubiquitylation and proteasomal degradation. This process, releases NF-κB dimers from the cytoplasm which then are able to translocate into the nucleus.

The non-canonical pathway, also known as alternative pathway of NF-κB activation is initiated through the stimulation of the CD40, lymphotoxin-β receptors (LTβR), B-cell activation factor (BAFF), LPS and latent membrane protein-1 (LMP1) of Epstein Barr virus (144). Here, activation of IKKα by the NF-κB inducing kinase (NIK) results in the formation of p52 by ubiquitylation and partial degradation of p100, leading to the release of the RelB-p52 dimer (145). On the other hand, the atypical NF-κB pathway activation is an IKK-independent process that involves different mechanisms (146). For instance, treatment with ultraviolet (UV) light, or expression of the HER2 oncogene in breast cancer cells, can phosphorylate IκBα by casein kinase-II (CK2) (147). Also, IκBα phosphorylation occurs upon hypoxia or hydrogen peroxide stimulation, and treatment with nerve growth factor (NGF) (133).

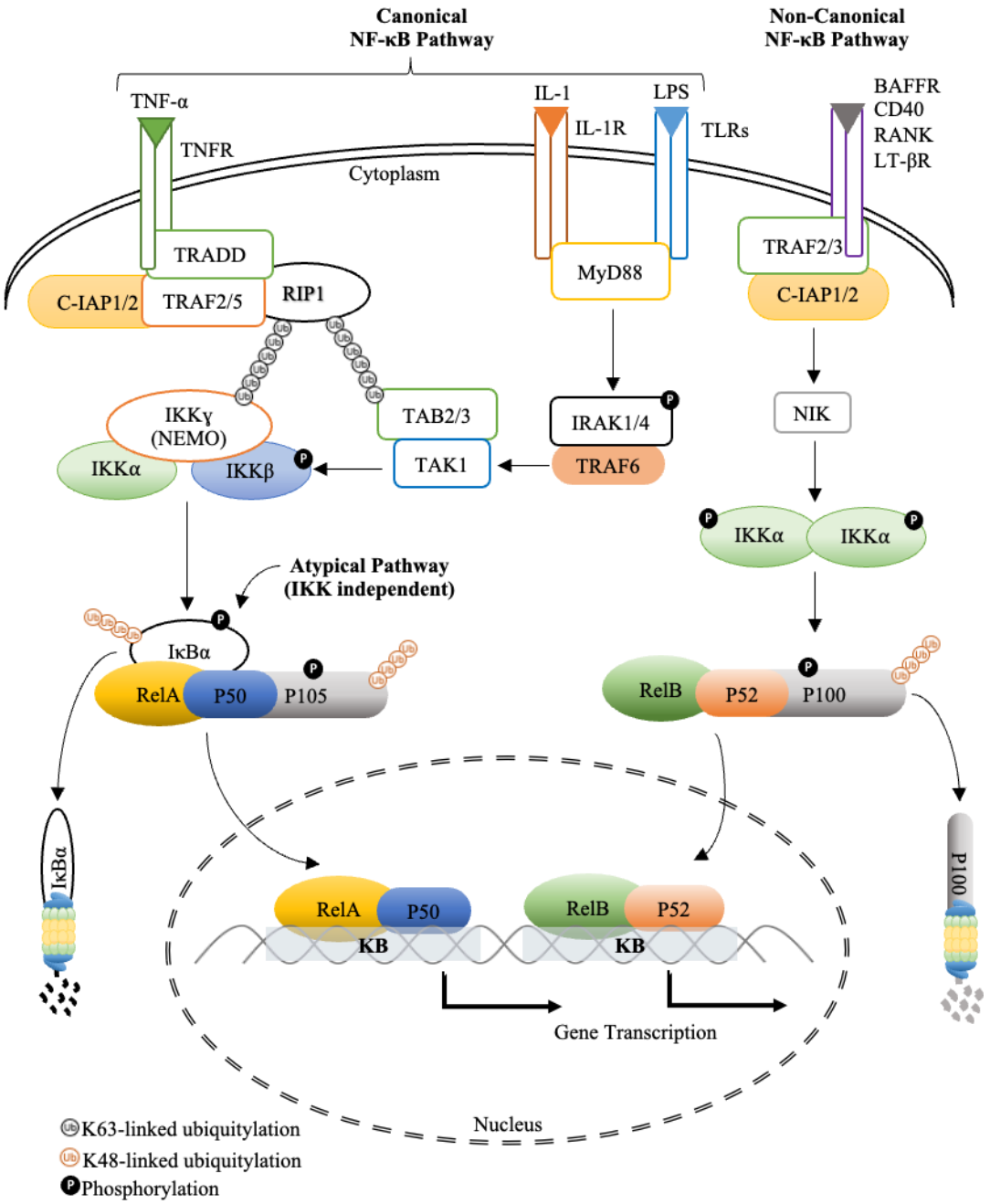

Figure 1.8. Schematic diagram of simplified NF-κB pathways. In the canonical pathway, stimulation of TNFR leads into the activation of TAK1 and IKK complex, mediating the phosphorylation and proteasomal degradation of IκB. Subsequently, NF-κB dimer is released and translocated into the nucleus. Alternatively, the TAK and IKK complex can be activated by another group of ligands binding to the TLR or IL-1R. This triggers the recruitment of the adaptor protein Myd88, and the subsequent activation of TAK and IKK complex through TRAF6. In the atypical pathway, NF-κB is activated in ligand independent manner, resulting in the NF-κB release. In the non-canonical pathway, another group of ligands triggers the activation of NIK, and then IKK-α. Activation of IKK-α phosphorylates p100, leading to its processing into p52. The RelB and p52 dimer translocate into nucleus and leads into transcriptional activation.

1.4.3. Hypoxia induction of NF-κB

Besides inflammatory cytokines and pathogen associated molecular stimuli, hypoxia stimulation also activates the NF-κB pathway, by mechanisms that have been described in numerous studies (148-152). It has been discovered in the Rocha laboratory that NF-κB response to hypoxia is a rapid process, which happens in a time frame varying from 5 to 30 minutes. This stimulation leads to IKK-mediated phosphorylation of IκBα at Serine 32/ 36 sites, and DNA binding of NF-κB (148). More specifically, upon hypoxia treatment, IKK activity is induced through calcium/ calmodulin-dependent kinase 2 (CaMK2)-dependent pathway leading to activation of Transforming growth factor-β (TGF-β)-activated kinase 1 (TAK1) and an E2 ubiquitin conjugating enzyme, Ubc13, and potentially, the E3 ubiquitin ligase, XIAP (148, 149, 153). It was also shown that in contrast to canonical NF-κB inducers, hypoxia stimulation does not result in IκBα degradation, instead ubiquitylation is inhibited and replaced with SUMOylation (148).

HIF subunits are shown to have a role in regulating the NF-κB transcriptional response. As such, HIF-1α is able to prevent full NF-κB transcriptional activation in mammalian cells and *Drosophila melanogaster* (154). In contrast, HIF-1β is shown to be required for NF-κB activation (155). Both HIF and NF-κB transcription factors are shown to regulate many common target genes, such as VEGF, IL-8, BNIP3 (156). However, it is still not clear if these genes are targeted by both HIF and NF-κB together, or independently, or if they are co-regulated following shared stimuli.

Besides HIF, other oxygen sensing molecules such as PHDs and FIH are also suggested to regulate NF-κB activity (reviewed in (106)). In addition, another group of 2-OG-dependent dioxygenases, JmjC proteins are also known to have a role on NF-κB pathway activation, which is described more in detail in **section 1.4.5**.

1.4.4. NF-κB target genes

Once NF-κB dimers accumulate in the nucleus, they bind to consensus κB sites with the DNA sequence 5'-GGGRN (A/T) YYCC-3' (R; purine, Y; pyrimidine, N; any nucleotide) in promoters and enhancers of target genes to induce or repress their transcription (157). There is a vast amount of consensus κB sites in the human genome and affinity and specificity of NF-κB DNA binding to these sites can be affected by many additional mechanisms. This includes ability of individual subunits to form homo- or hetero-dimers in different cellular contexts and stimulus, post-translational modifications targeting NF-κB subunits, as well as chromatin accessibility, recruitment of co-regulators and interactions with other transcription factors (157, 158). The DNA binding of NF-κB regulates the expression of about 500 genes, which are listed in https://www.bu.edu/nf-kb/gene-resources/target-genes/. The listed genes include many different types of molecular regulators, such as cytokines and chemokines, immunoreceptors, stress response genes, apoptosis regulators, growth factor and their modulators (**Figure 1.9**).

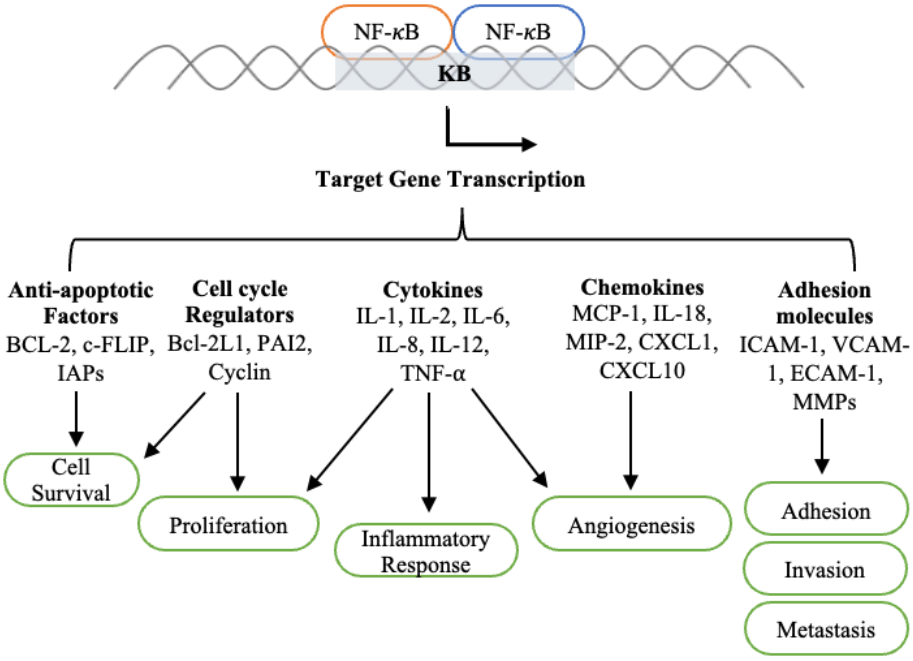

Figure 1.9. NF-κB target genes. Examples for direct NF-κB transcriptional targets genes, grouped according to their biological functions. BCL-2; B-cell lymphoma 2, IAP; inhibitor of apoptosis, PAI2; plasminogen activator inhibitor, IL; interleukin, TNF-α; tumour necrosis factor alpha, MCP-1; monocyte chemoattractant protein, MIP-2; macrophage inflammatory protein, CXCL; chemokine ligand, I/V/ECAM-1; Intracellular/ vascular/ epithelial cell adhesion molecule, MMP; matrix metallopeptidase (adapted from (159)).

1.4.5. Chromatin and NF-κB

The kinetics of NF-κB recruitment to target genes is highly variable as some genes are expressed shortly after stimulating the NF-κB pathway, while others are expressed following minutes to hours later (160). Although it is shown that NF-κB subunits enter the nucleus rapidly following stimulation, they only bind to a subset of them initially, suggesting that change in chromatin structure/ accessibility contributes to selectivity of the NF-κB response. NF-κB activating stimuli leads to alterations in chromatin accessibility, which are mediated through multiple mechanisms including post-translational modifications of histones and energy-dependent chromatin remodelling complexes (reviewed in (161, 162)).

1.4.6. Histone lysine methylation and NF-κB

NF-κB activating stimuli lead to changes in a large set of activating and repressive histone marks. These modifications were shown to occur in different time points. While H3K9/ K14 acetylation accumulates at the early phases of the LPS stimulation regardless of the timing of transcriptional gene induction, H3K4me3 appears at a later phase and associates with transcriptional activation (163). Several other studies have implicated H3K4 methylation and its associated methyltransferases as essential for the transactivation of NF-κB target genes. For instance, SET7/9 knockdown reduced the H3K4 methylation, and TNF-α-induced recruitment of NF-κB RelA to inflammatory gene promoters and thus decreasing the target gene expression (164). SETD1B was shown to promote RelA recruitment to the promoter regions of its target genes, IL-1β, IL-6, and MMP2, through H3K4 trimethylation of the gene promoters (29), suggesting that histone modifications are necessary for NF-κB RelA recruitment and thus regulating its target gene expressions. In contrast, NF-κB-dependent histone modifications has also been described. For instance, following TNF-α stimulation, translocation of methyltransferase MLL1 onto the promoters of NF-κB target genes was dependent on NF-κB RelA (165). In addition, another methyltransferase, SETD6-mediated methylation of RelA protein at lysine (K)310 site was recognised by G9A-like protein (GLP), which under basal conditions, promoted repressed chromatin state at RelA target genes

through GLP-mediated H3K9 dimethylation (166). In response to TNF-α and LPS, RelA was phosphorylated by the atypical protein kinase C, PKCζ at serine 311, which blocked the interaction between GLP and methylated RelA, resulting in transcription activation (166). This study showed a link between NF-κB protein post-translational modifications (PTMs) and NF-κB transcriptional response, which is detailed further in **section 1.4.7**.

JmjC containing proteins are also involved in NF-κB transactivation response via reversing repressive histone modifications. For instance, KDM6A was reported to promote transcription of IL-6 by demethylating H3K27me3 (167). KDM4A and KDM4D were shown to be required for activating genes that are involved in innate immune response by reversing H3K9me2 and H3K9me3 marks (168, 169).

1.4.7. Lysine methylation of NF-κB proteins

NF-κB is controlled by multiple post-translational modifications, namely ubiquitylation, phosphorylation, acetylation, sumoylation, nitrosylation and methylation (35, 147, 166, 170-174). To date, methylation of NF-κB has been mainly studied on the RelA subunit, occurring on both lysine and arginine residues (35, 174). A total of six lysine (K) methylation sites has been identified on RelA, namely K37, K218, K221, K310, K314, and K315, which are modified by various methylation associated enzymes (35, 166, 172, 173, 175). K37, K218 and K221 are located on the Rel homology domain (RHD) of the RelA protein, which is functionally important for protein dimerization, inhibition of NF-κB-IκB interaction, and also nuclear localisation and DNA binding (176) whereas, K310, K314, and K315 sites are found at the linker region between RHD and TAD (**Figure 1.10**). It has been shown in various studies that under different experimental conditions, RelA lysine methylation can regulate NF-κB nuclear translocation, transcriptional activity and NF-κB target gene expression.

Importantly, it has been discovered that following the methylation of RelA on K218/ K221 sites by the lysine methylase, the nuclear receptor-binding SET domain-containing protein 1 (NSD1), RelA can be demethylated by the lysine demethylase, KDM2A (35, 170).

While methylation of RelA at these sites was shown to increase the NF-κB transcriptional activity, their demethylation downregulated NF-κB activity. Particularly, Lu and colleagues discovered that about 80% of the RelA induced genes are downregulated by either K218/ K221 sites' alteration or KDM2A overexpression in mouse embryonic fibroblast cells (MEFs) (35). These findings indicated that RelA methylation is reversible and has an important role in regulating NF-κB transcriptional response. Also, Zhang and colleagues have shown that following TNF-α stimulation, RelA methylation at the K218/ K221 sites is necessary for the interaction of plant homeodomain finger protein 20 (PHF20) with RelA, which is shown to promote NF-κB transcriptional activity (177). In this study, methylation-dependent interaction of PHF20 with RelA interrupted the recruitment of protein phosphatase 2 (PP2A) to RelA, and thus maintained a persistent phosphorylation of RelA protein.

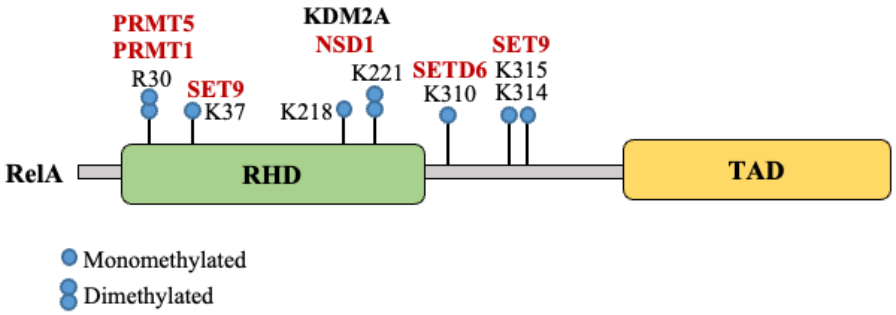

Figure 1.10. A schematic diagram of RelA and its methylation sites. Figure shows the location of the methylation sites on NF-κB RelA structure, and the methylation associated enzymes for each site. Rel homology domain (RHD, amino acids 19-301), the linker region (amino acids 302-427) and the transactivation domain (TAD, amino acids 428-551). Blue circles represent the methylation modifications on either Lysine (K) or Arginine (R) residues of NF-κB RelA. R30 and K221 are dimethylated, rest of the sites are monomethylated. Methyltransferases PRMT1 and PRMT5 methylate the R30 site; SET9 methylates K37, K314 and K315 sites; SETD6 methylates K310 site; and NSD1 methylates K218 and K221 sites, which both can be demethylated by KDM2A. (Adapted from (175))

Furthermore, the RelA protein was shown to be mono-methylated by Set-domain containing protein 9 (SET9) at K37 in response to IL-1β and TNF-α stimulations (172). SET9 mediated methylation of RelA increases its DNA binding ability and is necessary for NF-κB target genes expression (172). On the other hand, Yang and colleagues identified that SET9-mediated mono-methylation of RelA at K314 and K315 sites inhibits NF-κB by promoting

proteasomal degradation of RelA (173). Overall, these studies suggest that the methylated lysine sites can function as positive or negative regulators, depending on the modified lysine residues.

1.5. Aims and objectives

It has been described that hypoxia induces changes to histone methylation and controls chromatin through the deregulation of oxygen-sensitive histone lysine demethylases. Also, it is known that hypoxia promotes NF-κB-mediated transcriptional response. However, the link between the role of hypoxia-induced histone methylation and the NF-κB transcriptional response has not been established. This project aimed to determine the effect of hypoxia on NF-κB transcriptional response at the chromatin level by investigating the active histone marks, H3K4me3 and H3K36me3, as well as their associated demethylases, KDM5A and KDM4A/ B/ C and KDM2A, respectively.

Although multiple lysine methylation sites were identified on RelA protein, so far, no information has been reported about other NF-κB subunits. Also, only two of the RelA methylation sites were linked with demethylation function via a KDM. This project aimed to investigate the functional significance of specific lysine residues in other NF-κB subunits. In addition, it was hypothesised that methylated NF-κB lysine sites could potentially be demethylated by KDMs. Thus, association of KDMs with NF-κB proteins was aimed to be determined.

Hypoxia stimulates both cell type-specific genes, as well as a group of genes that are common to most cell types. However, if this is also true for the hypoxia inducible NF-κB target gene signature in different cell types is unknown. Therefore, this project aimed to elucidate if hypoxia induced NF-κB targets are shared or cell specific, using a bioinformatic approach.

Chapter 2 - Materials and Methods

2.1. Cell Culture

2.1.1. Cell lines and Growth Conditions

Human cervical carcinoma HeLa, human lung carcinoma A549, human osteosarcoma U2OS, and human embryonic kidney HEK293 cells were obtained from the American Type Culture Collection (ATCC). All cells were maintained at 5% CO_2 and 37ºC in Dulbecco's modified Eagle's medium (DMEM, Lonza) supplemented with 10% v/v foetal bovine serum (FBS, Invitrogen), 1% penicillin-streptomycin (Lonza), and 1% L-glutamine (Lonza). Cells were cultured not more than 30 passages. All cell lines were routinely tested for mycoplasma contamination using MycoAlert kit (Lonza).

Hypoxia response element (HRE) luciferase stable cell lines were previously created in the lab via co-transfection of an HRE-luciferase reporter vector (gift from Prof. G. Melillo, National Institute of Health, USA) with a puromycin resistance construct (103). HeLa-κB luciferase cells, containing an integrated copy of the κB ConA luciferase reporter plasmid, and are described in (178), were kindly gifted by Prof. Ron Hay (School of Life Sciences, University of Dundee, UK). U2OS-κB and A549-κB luciferase cells were previously generated in the lab, by transfecting with NF-κB-reporter construct gGL4.32[luc2P/NF-κB-RE/Hygro], selecting the individual clones based on their response to TNF-α. Selected cells were then maintained with 150 μg/ml Hygromycin B (Roche) (179).

2.2. Cell Transfection

2.2.1. siRNA Transfection

Small interfering RNA oligonucleotides were purchased from Eurofins Genomics and used in a final concentration of 27 nM. siRNA transfections in all cell lines were performed using interferin (polyplus) according to manufacturer's instructions. For experiments performed using 35 mm plates, cells were seeded at a density of 1.5×10^5 in a 2 ml media, 24 hours prior to media change and transfection. Cells were then incubated and harvested 48 hours post-transfection. Oligonucleotide sequences used for siRNA knockdown are shown in **Table 2.1**.

Table 2.1. List of oligonucleotide sequences used for siRNA-mediated knockdown

siRNA	Sequence 5' → 3'
Control	CAGUCGCGUUUGCGACUGGTT
KDM2A	GUGCAGAAGUACUGUCUAA
KDM4A_1	GAGUUAUCAACUCAAGAUATT
KDM4A_2	UUGAAGAGCUCGAGCGGAA
KDM4B_1	CGGCCACAUUACCCUCCAATT
KDM4B_2	GACCUGUACAGCAUCAACUTT
KDM4C	GGCGCCAAGUGAUGAAGAATT
KDM5A_1	GAAGAAUUCUAGCCAUACATT
KDM5A_2	GGAAAUACCCAGAGAAUGATT
RelA/p65_1	GCCCUAUCCCUUUACGUCA
RelA/p65_2	GCUGAUGUGCACCGACAAG
IKK-a	GCAGGCUCUUUCAGGGACATT
Nemo	ACAGGAGGUGAUCGAUAAG

2.2.2. DNA Transfection

DNA plasmid overexpression in HEK293 cells were performed using the calcium phosphate transfection method. 24 hours prior to the transfection, cells were seeded at a density of 1.5×10^5 into 35 mm plates containing 2 ml media. Transfection complex was prepared by adding 1 μg DNA into 194.4 μL 2 M $CaCl_2$, that was prepared using distilled sterile water. Also, 200 μL 2X HBS (0.137 M NaCl, 0.75 M Na_2HPO_4, 20 mM HEPES pH 7.0) was added to the mixture before evenly pipetting onto the cells. Cells were kept in an incubator and their media was changed after 24 hours. Then cells were harvested 48 hours post-transfection.

DNA plasmid overexpression in rest of the cell lines was performed using Turbofect (ThermoFisher Scientific) according to manufacturer's instructions. 35 mm plates were seeded with 1.5×10^5 cells in a 2 ml media, 24 hours prior to DNA transfection. Cell media was changed after 24 hours, and cells were harvested 48 hours post-transfection. Plasmids used in this study are listed in **Table 2.2**.

Table 2.2. List of plasmids used in this project

Name	Plasmid vector/ tag	Source (catalogue #)
Control	pcDNA3.1/ HA-Flag	Addgene (52535)
Control	pEBB/ HA	a kind gift from Dr Niall Kenneth, University of Liverpool, UK
cRel	pEBB/ HA-cRel	
RelB	pEBB/ HA-RelB	
RelA	pcDNA3.1/cFlag-RelA	Addgene (20012)
KDM5A	pcDNA3.1/ HA-FLAG-RBP2	Addgene (14800)
KDM4A	pCMV/ HA-JMJD2A	Addgene (24180)
KDM4B	pCMV/ HA-JMJD2B	Addgene (24181)

2.3. Mutagenesis

The rel homology domain mutants of the NF-κB subunits were generated by site directed mutagenesis using KOD hot start DNA polymerase kit (Millipore) on an Agilent SureCycler 8800 thermocycler polymerase chain reaction (PCR) machine. Each reaction tube contained 50 µl total reaction volume (100 ng template DNA, 5 µl 10x KOD buffer, 2 µl $MgSO_4$, 5 µl dNTPs mix, 2 µl DMSO, 33 µl ddH_2O, 2 µl primer mix including 10 µM forward and 10 µM reverse primers, and 1 µl KOD polymerase). Primers used in each reaction is summarised in **Table 2.3**. PCR cycling conditions used for all reactions are as follow; step 1, 95°C for 2 minutes, step 2, 95°C for 30 seconds, step 3, 50,52 and 55°C for 30 seconds, step 4, 70°C for 6 minutes (steps 2-4 were repeated 20 cycles), and step 5, 70°C for 10 minutes. Following the PCR reactions, 2 µl of DpnI (New England Biolabs) was added to each PCR reaction tube and samples were incubated at 37°C for 2 hours on a heating block. 2 µl of 6x DNA loading dye (New England Biolabs) was added to 10 µl of each PCR sample and ran on a 1% agarose TAE (40 mM Tris, 20 mM acetic acid and 1 mM EDTA) gel containing 1:2000 diluted SYBR safe (ThermoFisher Scientific) at 110 v for 1 hour. The DNA band was then purified using DNA gel extraction kit (Qiagen, QIAquick Gel Extraction Kit #28704) following manufacturer's instructions with DNA eluted in a final volume of 20 µL. Alternatively, bacterial transformation and DNA extraction protocol was followed as

described in the next section (see section **2.4.)**. Plasmids were sequenced using Eurofins TubeSeq service to confirm mutations.

Table 2.3. Rel homology domain loss of function mutant primers of NF-κB subunits

Primer Name	Mutation Point	Sequence 5' → 3' (Forward)	Sequence 3' → 5' (Reverse)
RelA	K218A	AGATCTTCCTACTGTGTGAC**GC** **G**GTGCAGAAAGAGGACATTG	CAATGTCCTCTTTCTGCACCGC GTCACACAGTAGGAAGATCT
	K221A	TACTGTGTGACAAGGTGCAG**G** **CA**GAGGACATTGAGGTGTATT	AATACACCTCAATGTCCTCTGC CTGCACCTTGTCACACAGTA
	Double	TACTGTGTGAC**GCG**GTGCAG**G** **CA**GAGGACATTGAGGTGTATTT	AAATACACCTCAATGTCCTCTG CCTGCACCGCGTCACACAGTA
c-Rel	K210-A	ATGAAATATTTCTACTTTGTGA C**GCA**GTTCAGAAAGATGACA	TGTCATCTTTCTGAACTGCGTC ACAAAGTAGAAATATTTCAT
	K213A	TACTTTGTGACAAAGTTCAG**GC** **A**GATGACATAGAAGTTCGTT	AACGAACTTCTATGTCATCTGC CTGAACTTTGTCACAAAGTA
	Double	TACTTTGTGAC**GCA**GTTCAG**GC** **A**GATGACATAGAAGTTCGTTT	AAACGAACTTCTATGTCATCTG CCTGAACTGCGTCACAAAGTA
RelB	K327A	AGCTCTACTTGCTCTGCGAC**GC** **G**GTGCAGAAAGAGGACATAT	ATATGTCCTCTTTCTGCACCGC GTCGCAGAGCAAGTAGAGCT
	K330A	TGCTCTGCGACAAGGTGCAG**G** **CA**GAGGACATATCAGTGGTGT	ACACCACTGATATGTCCTCTGC CTGCACCTTGTCGCAGAGCA
	Double	TGCTCTGCGAC**GCG**GTGCAG**G** **CA**GAGGACATATCAGTGGTGTT	AACACCACTGATATGTCCTCTG CCTGCACCGCGTCGCAGAGCA

2.4. Competent Cell Preparation and Plasmid Transformation

Escherichia coli strain DH5α was used as the chemically competent bacterial cells to transform and grow the plasmid constructs. DH5α cells were propagated using a protocol adapted from (180). Cells were streaked onto an LB agar (Formedium) plate and incubated overnight on a shaking incubator at 37ºC and 240 rpm. The next day, a colony was picked and inoculated 25 mL LB broth (Formedium) in a 250 mL flask. Bacteria was grown until it was reached to OD0.6, which was measured using a spectrophotometer. After bacterial culture was reached to the desired OD level, flask was incubated at 4ºC for 2 hours. Culture was then transferred to a 50 mL tube and centrifuged at 5000 rpm at 4ºC for 10 minutes. Pellet was resuspended using 10 mL ice-cold RF1 buffer (100 mM RbCl, 30 mM Potassium acetate, 10 mM $CaCl_2.2H_2O$, 50 mM $MnCl_2.4H_2O$, 15% v/v Glycerol, solution was adjusted to pH 5.8) and incubated on ice for 5 minutes. Cells were then centrifuged at 5000 rpm at 4ºC for 10 minutes. Pellet was resuspended using 1 mL ice-cold RF2 buffer (10 mM MOPS, 75 mM

$CaCl_2.2H_2O$, 10 mM RbCl 15% v/v Glycerol, solution was adjusted to pH 6.8) and incubated on ice for 15 minutes before aliquoting to store at a -80ºC freezer.

For each transformation, 10-50 ng of purified plasmid DNA was added to 25 µL of the competent cells and incubated on ice for 30 minutes, followed by heat shock at 42°C on a heating block for 90 seconds and incubation on ice for 90 seconds. Then, 200 µL LB broth (Formedium) was added and cells were incubated for 1 hour at 37°C in a shaking incubator. Cells were then plated on LB agar (Formedium) plate containing appropriate antibiotics and incubated at 37°C overnight to allow bacterial colony formation.

2.5. Plasmid DNA Isolation

For isolating plasmid DNA up to 20 µg, a single colony was inoculated in 5 mL of LB broth containing the appropriate selection antibiotic and incubated overnight at 37°C in a shaking incubator. The DNA was isolated using Qiagen miniprep kit (Qiagen, QIAprep Spin Miniprep Kit #27104) following manufacturer's instructions. For isolating plasmid DNA up to 1 mg, a single bacterial colony was inoculated into a 5 mL of LB broth containing the appropriate selection antibiotic. The culture was grown for 8 to 10 hours at 37°C in a shaking incubator before getting transferred to 250 mL of TB broth (Formedium) containing the required selection antibiotic in a 2 L conical flask. The culture was incubated overnight at 37°C in a shaking incubator. Plasmid DNA was then extracted from the bacterial culture with a maxiprep kit (ThermoFisher Scientific, PureLink HQ Mini Plasmid DNA Purification Kit #K210001) following manufacturer's instructions.

2.6. Cell Treatments

For stimulating the inflammatory response, human recombinant TNF-α (Peprotech) was dissolved in sterile PBS and added to the cells at a final concentration of 10 ng/mL. Hypoxia treatments were performed in an InVivo300 hypoxia workstation (Ruskin, UK) at 1% O_2, 5% CO_2 and 37ºC. For hypoxia mimetic conditions, cells were treated with desferroxamine mesylate (DFX, Sigma) at the final concentration of 200 µM.

2.7. Luciferase assay

Cell lines stably transfected with a luciferase reporter gene (κB or HRE luciferase reporter) were seeded in 35 mm plates at a density of $2x10^5$ cells in a 2 ml media and transfected with appropriate siRNA or DNA plasmid, according to procedures previously described in the previous section (see section **2.2.**). Then, cells were stimulated with TNF-α, or hypoxia as described in the previous section (see section **2.5.**). Cells were then harvested with 400 μL of Passive Lysis Buffer (Promega) and kept in -20°C freezer until frozen. After the freeze-thaw cycle, luciferase activity was measured according to the manufacturer's instructions, and normalised to protein concentration determined by Bradford assay (Bio-Rad).

2.8. RNA extraction and Real Time quantitative PCR analysis

Total RNA from cells was extracted using peqGOLD total RNA kit (VWR Life Sciences) according to manufacturer's instructions. RNA was converted to cDNA using iscript reverse transcription kit (Bio-Rad). iQ sybr green supermix (Bio-Rad) or power-track sybr green master mix (Applied Biosystems) was used to analyse cDNA samples on the Mx3005P qPCR platform with MX3005P 96-well plates (Stratagene/Agilent). Actin or 18S was used as a normalising gene. RT-qPCR results were analysed by the ΔΔCt method. Primers used for the gene expression analysis are listed in **Table 2.4**.

Table 2.4. List of primers used for RT-qPCR

Gene	Sequence 5' → 3' (Forward)	Sequence 3' → 5' (Reverse)
Actin	CTGGGAGTGGGTGGAGGC	TCAACTGGTCTCAAGTCAGTG
18S	AAACGGCTACCACATCCAAG	CGCTCCCAAGATCCAACTAC
RelA	CTGCCGGGATGGCTTCTAT	CCGCTTCTTCACACACTGGAT
BHLHE40	GGGAAGTCACGAAGGATTG	CAGCTGATGTGTATCGAAGG
FTH1	AGTGCCGTTGTTCAGTTC	AGACAGCCACACCTTAGT
DUSP1	GCTCCTTGAGAGGAGAAATG	GACGCTAAGTCATCACCATAA
MARCKS	CTTCCTCTGCCTTGTTTCTC	CCCACCCATCTCCTTCATA
EDN1	GACTGGGAGTGGGTTTCTCC	TCTCTGCTGTTTGTGGCTTG
KDM6B	TTCGAGAGTCCTACCTTTCC	AGATAGATGCTGGGTGTAGG
JUN	AAGAACTCGGACCTCCTC	CGTTGCTGGACTGGATTAT
MAFF	GAGGTGACACGGCTCAA	GCTCCGACTTCTGCTTCT
IKK-a	GCAGAAGTCATATTTAGGATGTG	GCAGAGAGGAGGACCTGTTG
Nemo	CTGGCTTGGAAATGCAGAAG	CTGCCTGGAGGAGAATCAAG
Ca9	CTTTGCCAGAGTTGACGAGG	CAGCAACTGCTCATAGGCAC
KDM5A/ JARID1A	GAGCTGTGTTCCTCTTCCTAAA	CCTTCGAGACCGCATACAAA
KDM4A/ JMJD2A	TGTGCTGTGCTCCTGTAG	GTCTCCTTCCTCTCCATCC
KDM4B/ JMJD2B	GGGGAGGAAGATGTGAGTGA	GACGGCTTTTGGAGGGTAAT
KDM4C/ JMJD2A	CGAGGTGGAAAGTCCTCTGAA	GGGCTCCTTTAGACTCCATGTAT
KDM2A/ JHDM1A	CAGGAGGCCGGGCTCTCAGT	CGGGTCTGGGACTCCTGGGG

2.9. Protein Lysis

Before collecting cell lysates, cell media was removed, cells were washed with PBS (Life Technologies) and then cells in 35 mm plates were harvested using 100 µL RIPA lysis buffer (50 mM Tris-HCl pH 8.0, 150 mM NaCl, 1% v/v NP-40, 0.25% w/v Sodium deoxycholate, 0.1% w/v SDS, 10 mM NaF, 2 mM Na_3VO_4, and 1 Pierce protease inhibitor tablet (ThermoFisher Scientific) per 10 mL of lysis buffer). Cells containing the lysis buffer scraped into 1.5 mL Eppendorf tubes and incubated on ice for 10 minutes to complete the lysis process before spinning them down in a centrifuge for 15 minutes at 13,000 rpm at 4°C. The supernatant was collected and stored at -80°C. Cells treated with hypoxia were harvested in the hypoxia chamber to prevent reoxygenation. Protein concentration of cell lysates were determined using Bradford assay (BioRad).

2.10. Western Blotting

Unless stated, 20 µg of protein was prepared in 2x SDS loading buffer (100 mM Tris-HCl pH 6.8, 20% v/v glycerol, 4% w/v SDS, 200 mM DTT and Bromophenol Blue), and incubated for 5 minutes at 95ºC before loading into previously prepared SDS-page gel (Tris-HCL poly-acrylamide gel). The gel was run at 80-120 volts in running buffer (25 mM Tris, 0.195 M glycine and 0.1% w/v SDS) for 2 hours and then transferred with a semi-dry transfer (BioRad) on a PVDF membrane (Millipore) for 2 hours at 15 volts/ 0.8 mA in transfer buffer (50 mM Tris, 40 mM glycine, 0.001% SDS and 10% methanol). The membrane was then blocked with 10% milk in TBS-tween buffer (20 mM Tris pH 7.6, 150 mM sodium chloride and 0.1% v/v Tween) for 10 minutes, followed by three 5 minutes washes with TBS-tween buffer. Membranes were incubated with primary antibodies diluted in an antibody dilution buffer (2% w/v BSA and 0.5% w/v sodium azide in TBS-tween buffer) for between 30 minutes to 1 hour at room temperature or overnight at 4ºC. After three 5 minutes washes with TBS-tween buffer the membranes were incubated with the appropriate secondary HRP antibody diluted with 5% w/v milk in TBS-tween buffer for 30 minutes to 2 hours. After three 5 minutes washes with TBS-tween buffer the membranes were developed using ECL solution (Pierce). Primary and secondary antibodies used in this study are shown in **Table 2.5** and **Table 2.6**, respectively.

Table 2.5. Primary antibodies used for Western Blots and relative information

Antibody	Manufacturer (catalogue #)	Species	Dilution
β-Actin	Proteintech (66009-1-lg)	Mouse	1:10000
RelA	Santa Cruz (sc-372)	Rabbit	1:2000
RelA	Santa Cruz (sc-8008)	Mouse	1:2000
cRel	Cell Signalling (4727)	Rabbit	1:1000
RelB	Cell Signalling (10544)	Rabbit	1:1000
p52/p100	Millipore (05-361)	Mouse	1:4000
c-IAP1	Cell Signalling (7065)	Rabbit	1:1000
BHLHE40	Proteintech (17895-1-AP)	Rabbit	1:1000
Claspin	Cell Signalling (2800)	Rabbit	1:1000
Cyclin D1	Cell Signalling (2978)	Rabbit	1:1000
KDM5A/ JARID1A	Cell Signalling (3876)	Rabbit	1:1000
KDM4A/ JMJD2A	Cell Signalling (5328S)	Rabbit	1:1000
KDM4B/ JMJD2B	Cell Signalling (8639S)	Rabbit	1:1000
KDM4C/ JMJD2C	Thermo Fisher (703380)	Rabbit	1:1000
KDM2A/ JHDM1A	Bethyl (A301-475A)	Rabbit	1:1000
CA9	Cell Signalling (5649)	Rabbit	1:1000
Mono-methyl Lysine	Cell Signalling (14679)	Rabbit	1:1000
Di-methyl Lysine	Cell Signalling (14117)	Rabbit	1:1000
Tri-methyl Lysine	Cell Signalling (14680)	Rabbit	1:1000

Table 2.6. List of secondary HRP antibodies and relative information

Antibody	Manufacturer (catalogue #)	Dilution
Anti-mouse IgG, HRP-linked	Cell Signalling (7076)	1:2000
Anti-rabbit IgG, HRP-linked	Cell Signalling (7074)	1:2000

2.11. Immunoprecipitation

Unless stated, 500 μg of protein from RIPA cell lysates were diluted with the same amount of Buffer D (20 mM Hepes pH 7.9, 1 mM DTT, 0.1% v/v NP-40, 20% v/v glycerol, 1 mM PMSF, 5 mM NaF, 500 μM Na_3VO_4, and 1 Pierce Protease Inhibitor Mini Tablet (ThermoFisher Scientific) per 10 mL of buffer). Samples were then incubated overnight on a rotating wheel at 4°C with the addition of IP or IgG antibodies with dilutions shown in **Table 2.7**. Immune complexes were captured by incubating the samples on a rotating wheel at 4°C for 2 hours with 20 μL Protein G-Sepharose beads (Generon). Precipitates were washed once with PBS containing 0.05% Tween and twice with PBS only. 20 μL 2X loading buffer was

added to the beads and the spared 10% input sample, which were then heated for 5 minutes at 95°C heat block and analysed by Western Blotting (see **section 2.9.**).

Table 2.7. List of primary IP antibodies and relative information

Antibody	Manufacturer (catalogue #)	Species	Amount
NF-κB p50	Millipore (06-886-I)	Rabbit	2 µg
RelA	Santa cruz (sc-372)	Rabbit	2 µg
Anti-rabbit IgG	Sigma (I5006)	Rabbit	2 µg

2.12. Immunofluorescence

Cells were seeded at a density of 1.5×10^5 onto 19 mm sterilised glass coverslips (VWR) placed into 35 mm plates. After 24 hours, cells were transfected as explained in the previous section (see section **2.2.**). Cell media was removed, and cells were washed with PBS (Life Technologies). Cells were then fixed onto coverslips and cell membrane was permeabilized by incubating them with 100% ice cold methanol at -20°C for 5 minutes. Cells were washed with PBS for 5 minutes then placed inside a humidified chamber and blocked with 120 µL blocking agent (1% v/v donkey serum (Sigma-Aldrich) diluted with PBS containing 0.05% v/v Tween (Sigma-Aldrich)) for 30 minutes at room temperature. Cells were washed with PBS for 5 minutes then placed inside a humidified chamber and incubated overnight at 4°C with the primary antibody diluted with 120 µL blocking agent. Cells were washed once with PBS containing 0.05% v/v Tween for 5 minutes then washed three times with PBS for 5 minutes. Cells were then placed inside a humidified chamber and incubated for 2 hours at room temperature with the secondary antibody diluted with 120 µL blocking agent. Afterwards, washing steps were repeated, cells were placed inside a humidified chamber and incubated for 2 minutes with Hoescht nuclear stain (invitrogen) diluted to 1:15,000 in 120 µL of distilled water. Cells were washed with water and coverslips were mounted on microscope slides (VWR) using Vectashield mounting medium (Vector Laboratories) and sealed with nail varnish. Images were acquired using an Epifluorescence microscope (Zeiss Axio Observer Z.1). Quantification of the antibody signal per cell and

representative image production was performed using OMERO open microscopy environment (181). Antibodies used in this study are listed in **Table 2.8**.

Table 2.8. List of IF antibodies and relative information

Antibody	Manufacturer (catalogue #)	Species	Dilution
H3K36me3	Abcam (9050)	Rabbit	1:250
Anti-rabbit Alexa flour 488	Cell Signalling (4412)	Rabbit	1:500

2.13. Chromatin Immunoprecipitation for qPCR

Chromatin Immunoprecipitation (ChIP) was performed based on the protocol adapted from (182). HeLa cells were seeded on 150 mm plates at a density of about 2.5×10^6 in a final volume of 16 mL media and grown to 80-90% confluency. After hypoxia stimulation or siRNA transfection as described in previous sections (see sections **2.2.** and **2.5.**), proteins were crosslinked to chromatin by adding 1% v/v formaldehyde for 10 minutes inside the incubator or hypoxia chamber. To quench the cross-linking, glycine was added at a final concentration of 0.125 M for 5 minutes. Cells were then washed two times with cold PBS, harvested with 450 µL ChIP lysis buffer (1% w/v SDS, 10 mM EDTA, 50 mM Tris-HCl pH 8.1, 1 protease inhibitor tablet) and incubated on ice for 10 minutes to complete the lysis process. Samples were then sonicated at 4ºC, twenty times for 15 seconds with 30 seconds gap between each sonication cycle at 50% amplitude using Sonics Vibra Cell #VCX130 sonicator. Samples were centrifuged at 12,000 rpm for 10 minutes at 4ºC and supernatant containing the sheared chromatin was transferred into a new tube to be used for rest of the experiment. 10 µL of each sample was reserved as the input and stored at -20ºC until they were processed later steps. Samples were split into 100 µL aliquots, one for each IP that is intended to run, and diluted 10-fold with dilution buffer (1% v/v Triton X-100, 2 mM EDTA, 150 mM NaCl, 20 mM Tris-HCl pH 8.1). Diluted samples were pre-cleared using 2 µg sheared salmon sperm DNA and 20 µL protein G-Sepharose slurry (Generon) on a rotating wheel at 4ºC for 2 hours. After the pre-clearing, samples were centrifuged at 1000 rpm for 1 minute and supernatants were transferred into new Eppendorf tubes. Immunoprecipitation was performed by incubating the

samples overnight on a rotating wheel at 4°C with 0.1% v/v Brij-35 (ThermoFisher Scientific) and antibodies with manufacturer's recommended concentrations (see **Table 2.9**). Immune complexes were captured by incubating the samples with 2 µg sheared salmon sperm DNA and 30 µL protein G-Sepharose slurry on a rotating wheel at 4°C for 1 hour. Captured complexes were washed on a rotating wheel at 4°C for 5 minutes once with each of the following solutions; wash buffer 1 (0.1% w/v SDS, 1% v/v Triton X-100, 2 mM EDTA, 20 mM Tri-HCl pH 8.1, 150 mM NaCl), wash buffer 2 (0.1% w/v SDS, 1% v/v Triton X-100, 2 mM EDTA, 20 mM Tris-HCl pH 8.1, 500 mM NaCl), wash buffer 3 (0.25 M LiCl, 1% v/v NP-40, 1% w/v sodium deoxycholate, 1 mM EDTA, 10 mM Tris-HCl pH 8.1) and twice with TE buffer (10 mM Tris-HCl pH 8.1, 1 mM EDTA). After every wash step, samples were centrifuged at 1000 rpm and supernatant was discarded using an aspirator. The complex was eluted by incubating the beads for 1 hour on a rocker at room temperature with 100 µL elution buffer (1% w/v SDS, 0.1 M $NaHCO_3$). Elutes were centrifuged at 1000 rpm at room temperature and transferred into new Eppendorf tubes. All samples, including the input were reverse crosslinked by incubating them with 0.2 M NaCl overnight on a thermomixer at 65°C and 500 rpm. Proteins were digested by incubating the samples with 20 µg proteinase K, 40 mM Tris-HCl pH 6.5, 10 mM EDTA pH 8 for 1 hour on a thermomixer at 45°C and 500 rpm. DNA was purified using QIAquick PCR purification kit (Qiagen) following manufacturer's instructions, eluting the samples in 40 µL volume. 3 µL DNA was used for qRT-PCR analysis with primers specifically designed on promoter regions of interest (see **Table 2.10**). Data obtained was normalised to the input sample.

Table 2.9. List of ChIP antibodies and relative information

Antibody	Manufacturer (catalogue #)	Species	Amount per 1 mL ChIP (∝g)
H3K36me3	Active motif (61101)	Rabbit	10
H3K36me3	Cell Signalling (4909)	Rabbit	3.06
H3K4me3	Active motif (39915)	Rabbit	3
H3K4me3	Cell Signalling (9751)	Rabbit	2.73
Anti-rabbit IgG	Sigma (I5006)	Rabbit	Same amount as the corresponding ChIP antibody

Table 2.10. List of primers used for RT-qPCR on ChIP samples

Gene	Enriched methylation site	Sequence 5' → 3' (For)	Sequence 3' → 5' (Rev)
MARCKS	H3K36me3	CAGAAGCACATGAAGTTTGC	TATCACAGCTTGGTTGAGTTTA
BHLHE40		CCTGATTGCTGATCGTGTTT	GCTTTACAAATAAAGGCAACGA
FTH1		CTCTCACACACACACACAA	CCTTTCACAAACACTTGACTAC
DUSP1		GGGACATCGAATCAAATTCATATT	ACTAAGCCCAACCTCTGT
EDN1	H3K4me3	GGAAGTGTGGACACACAAA	GTGAGGGATTGGCAAGAAA
KDM6B		CCTCATCCCTAGTCCTTCTC	CTACTTTCACGGTCACATCC
JUN		GGACTCCGACGACTTGT	ACCGGTTGTTGAACTTGG
DUSP1		AGTTATTGCATTTCTCCTCTCA	CCATTACGACCTCTCCCA
MARCKS		ATGTATTTAGGGCGAAAGAGG	AACGCCCTTTGGAAGAAG

2.14. CUT&RUN

To perform the CUT&RUN experiments, cells were seeded to 35 mm plates at a density of $1.5x10^5$ cells in 2 mL media and after 24 hours they were stimulated with TNF-α, or hypoxia as described in the previous section (see section **2.5.**). The CUT&RUN assay was performed according to manufacturer's instructions (CUT&RUN Assay Kit, Cell Signalling #86652). To ensure each reaction tube contains 100,000 cells in 100 µL cell solution, cells were counted using a haemocytometer (Hawksley) and harvested with appropriate amount of 1X wash buffer (kit provided). Hypoxia treated cells were crosslinked for 2 minutes using 0.1% formaldehyde and crosslinking reaction was stopped by incubating the cells for 5 minutes with 0.125 M glycine. After the wash steps described in the kit protocol, cells were harvested with appropriate amount of 1X wash buffer. Formaldehyde fixed cells and the input

sample were sonicated to fragment the chromatin at 4°C using the same sonicator set-up described in the previous section (see section **2.12.**). DNA was purified from input and enriched chromatin samples using the QIAquick PCR purification kit (Qiagen) following manufacturer's instructions, eluting the samples in 40 µL volume. 3 µL DNA was used for the qPCR analysis with RPL30 positive control primers provided by the kit or negative control primers and primers specifically designed on promoter regions of interest (**Table 2.12**). Data obtained was normalised to the input sample. Antibodies used in this study are listed in **Table 2.11**.

Table 2.11. List of CUT&RUN antibodies and relative information

Antibody	Manufacturer (catalogue #)	Species	Dilution
H3K4me3	Cell Signalling (9751)	Rabbit	0.546 µg in 100 µL CUT&RUN
NF-κB p65	Active motif (39369)	Rabbit	1 µg in 100 µL CUT&RUN
NF-κB p65	Cell Signalling (8242)	Rabbit	1 µg in 100 µL CUT&RUN
Anti-rabbit IgG	Cell Signalling (66362)	Rabbit	Same amount as the corresponding CUT&RUN IP antibody

Table 2.12. List of CUT&RUN primers and relative information

Gene	Sequence 5' → 3' (Forward)	Sequence 3' → 5' (Reverse)
IL8 κB	AAGAAAACTTTCGTCATACTCCG	TGGCTTTTTATATCATCACCCTAC
IL8-κB Negative Control	ATCATGGGTCCTCAGAGGTCAGAC	GGTGGGAGGTGTTATG
RPL30	Kit provided	Kit provided
Gene Desert	GGCTAATCCTCTATGGGAGTCTGTC	CCAGGTGCTCAAGGTCAACATC

2.15. ChIP-sequencing data analysis

HeLa ChIP-sequencing datasets for control (21% Oxygen) and 1 hour hypoxia (1% Oxygen) H3K4me3 and H3K36me3 were obtained from Michael Batie (100) (GSE120339). HeLa ChIP-sequencing control and 6 hours hypoxia datasets (86) (GSE159128) were downloaded from NCBI Gene Expression Omnibus (183) and processed by Michael Batie. Coverage tracks displaying H3K4me3 and H3K36me3 bindings were produced using Integrative Genomics Viewer, IGV (184). Hallmark gene set association analysis was performed using WEB-based Gene SeT AnaLysis Toolkit (WebGestalt) (185) in over-

representation analysis mode with the Molecular Signatures Database (MSigDB) hallmark gene sets (186, 187). NF-κB target genes were downloaded from the Gilmore lab website (https://www.bu.edu/nf-kb/gene-resources/target-genes/) and hallmark NF-κB target genes were downloaded from MSigDB. HeLa 24-hours hypoxia upregulated genes determined by RNA-sequencing were downloaded from (98). Overlapping of gene lists and production of gene overlap Venn diagrams were done using InteractiVenn (188). Gene ontology association analysis was performed using WebGestalt in over-representation analysis mode with FDR ≤ 0.05 (185, 189). The topmost significant terms in the molecular process ontology were selected to show the functional characteristics of the given set of genes.

2.16. RNA-sequencing data analysis

RNA-sequencing reads were downloaded from NCBI Sequence Read Archive (SRA) using the SRA toolkit (https://hpc.nih.gov/apps/sratoolkit.html). Sequencing reads were aligned to the human genome assembly version GRCh38 provided by Ensembl using the STAR sequence aligner (190) to generate coordinate-sorted binary alignment map (bam) files. Read counts for each gene from Ensembl GRCh38 gene annotations were calculated using the featureCounts function of Subread (191). Differential expression analysis was performed using R Bioconductor package DESeq2 (192) with filtering for effect size (> 0.58 log2 fold change) and statistical significance (FDR <0.05) to identify significantly differentially expressed genes (DEGs). Sample to sample distance comparison heatmaps using rlog transformed read count data were generated using R Bioconductor packages DESeq2 and pheatmap. Volcano plots for display of differential expression analysis were generated using R Bioconductor package EnhancedVolcano. NF-κB target genes were downloaded from the Gilmore laboratory website (https://www.bu.edu/nf-kb/gene-resources/target-genes/) and converted to Ensembl gene annotation format using R Bioconductor package biomaRt (193). Core hypoxia upregulated genes were downloaded from hypoxia transcriptomics meta-analysis (91) and converted to Ensembl gene annotation format using R Bioconductor package biomaRt. Geneset enrichment analysis (GSEA) (186) was performed using WebGestalt (185).

Statistical significance of gene list overlaps between hypoxia upregulated genes and NF-κB target genes were calculated using the Fisher's exact test from the newGeneOverlap function of R Bioconductor package GeneOverlap.

2.17. Statistical analysis

Statistical significance for qPCR, ChIP-qPCR, luciferase assay and immunofluorescence microscopy analysis were determined via Student's t-test using Microsoft Excel, comparing two different conditions. Statistical significance of gene overlaps in Venn diagrams were determined via hypergeometric test using an online tool (https://flaski.app/venndiagram/). For all other statistical analysis, default settings of the particular analysis tool were used. In all statistical analysis p-values * = $p<0.050$; ** = $p<0.010$ and *** = $p<0.001$.

Chapter 3 - NF-κB target genes are enriched in H3K4me3 sites following hypoxia in HeLa cells

3.1. Introduction

Histone methylation, which usually occurs at the lysine (K) residues of N-terminal histone H3 and H4 tails by adding methyl (CH_3) groups, is one of the most important post-translational modifications (PTMs) (194). The lysine residues of the histones can be mono-, di-, and tri-methylated (me1, me2, and me3, respectively), which leads into activation or repression of gene expressions. Beyond regulating transcriptional responses, histone methylation also involves in other functions, such as DNA replication (195) and DNA repair (196).

Depending on the degree of methylation and the location of the methylated amino acid residue, different molecular functions can be regulated. In general, H3K4 is considered as an activating methylation mark as it occupies the actively transcribed gene regions in chromatin. These methylation marks are highly enriched at enhancer and promoter regions, as well as transcription start sites (TSS). Specifically, H3K4me3 has been associated with active transcription or with genes that are poised for activation (197, 198).

Histone methylation can be reversed by a group of enzymes called histone demethylases (HDMs). Among two different classes of HDMs, Jumonji C (JmjC) domain containing lysine demethylases (KDMs), like the key regulators of the hypoxia response, prolyl hydroxylase domain (PHD) and factor inhibiting hypoxia inducible factor (FIH), are known to be 2-oxoglutarate dependent dioxygenases that require oxygen for their enzymatic activity (39, 99). Changes in histone methylation have been described in hypoxia in different cellular systems (39, 199). Also, recently it has been shown in multiple studies that chromatin can sense oxygen changes and regulate gene expression through the inactivation of KDMs in hypoxia, independent of the main hypoxia stimulated transcription factor family, hypoxia inducible factor (HIF) (110, 117). Specifically, KDM5A that is known to control demethylation of H3K4me3 was found to contribute to hypoxia induced gene regulations (117).

Activation of the NF-κB (Nuclear factor kappa-light-chain-enhancer of activated B cells) is a critical component in the transcriptional response to hypoxia. It has been shown

previously that hypoxia stimulation can modulate NF-κB dependent gene expressions (148). In addition, the same study discovered a link between the role of hypoxia induced H3 modulation, acetylation and the NF-κB transcriptional response. Independent to hypoxia stimulation, H3K4me3 histone methylation (200, 201) and histone demethylase KDM5A have been associated with NF-κB by regulating immune and inflammatory responses (202, 203). However, further research is needed to elucidate the link between hypoxia and NF-κB transcriptional response in the context of histone methylation.

In this chapter, the H3K4me3 levels in response to hypoxia were investigated for their association with the NF-κB transcriptional response. Using Chromatin immunoprecipitation-sequencing (ChIP-seq) datasets, hallmark pathway enrichment analysis was performed focusing on NF-κB transcriptional signature. Identified potential NF-κB target genes were validated for hypoxia stimulation and H3K4me3 methylation. Also, the role of KDM5A in modulating NF-κB activity was determined. This work demonstrates that both hypoxia stimulation and KDM5A depletion regulates the NF-κB target gene signature by coordinating H3K4me3 levels.

3.2. Identification and validation of potential NF-κB target genes enriched with H3K4me3 with hypoxia stimulation

Previously in our group, chromatin immunoprecipitation followed by ChIP-sequencing was performed to evaluate H3K4me3 histone modifications associated with gene transcription in HeLa cells at normoxia or after 1 hour of hypoxia exposure. More recently, another study investigated H3K4me3 levels following 6 hours of hypoxia also in HeLa cells (86). Using our differential DNA binding analysis, Batie *et al.* (117) and Ortmann *et al.* (86), hallmark pathway association analysis was performed focusing on NF-κB transcriptional signature. These two different datasets containing H3K4me3 enriched regions from studies conducted by Batie *et al.* (117) and Ortmann *et al.* (86) are available in NCBI GEO database with accession numbers GSE120339

(https://www.ncbi.nlm.nih.gov/geo/query/acc.cgi?acc=GSE120339) and GSE159128 (https://www.ncbi.nlm.nih.gov/geo/query/acc.cgi?acc=GSE159128), respectively (**Figure 3.1, A** and **B**). When overlapped, both datasets share 53 genes where H3K4me3 levels are upregulated (**Figure 3.1, C**). As expected, 6 hours of hypoxia exposure induces a higher number of upregulated gene peaks compared to shorter hypoxia time point (**Figure 3.1, C**).

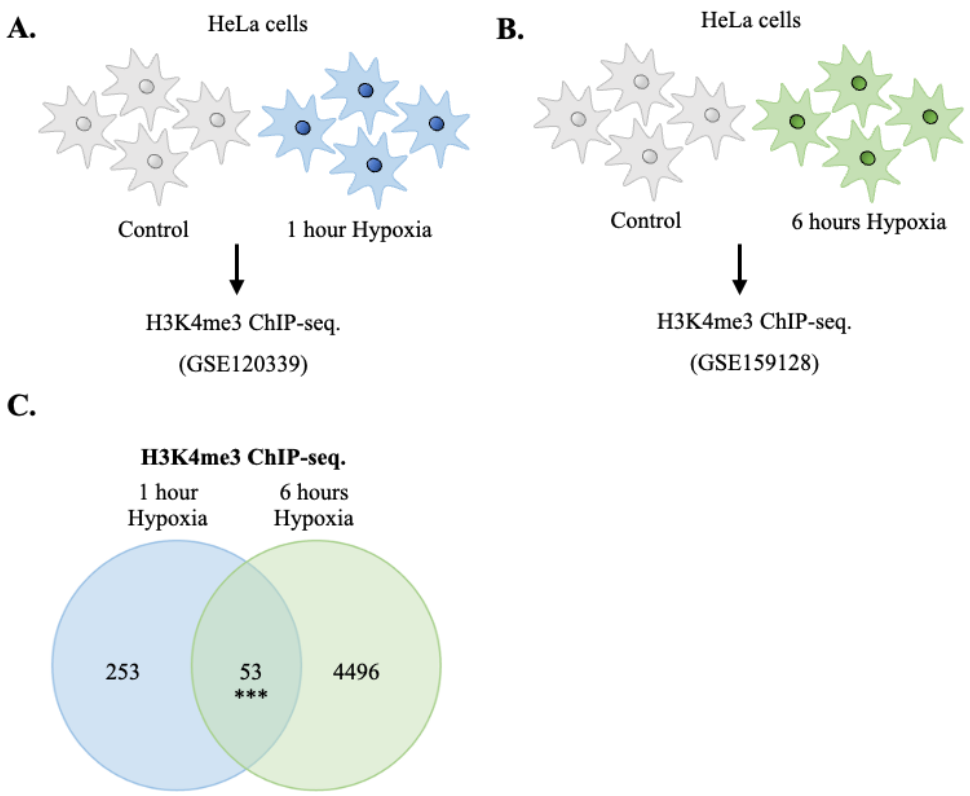

Figure 3.1. H3K4me3 ChIP-seq differential expression peak calling. Experimental design for H3K4me3 ChIP-seq. experiments with **A.** 1 hour or **B.** 6 hours of hypoxia. **C.** Overlap of 1 hour and 6 hours hypoxia H3K4me3 upregulated ChIP-seq gene peaks using low stringency analysis datasets. P value for the overlap was calculated by hypergeometric test. *** $p \leq 0.001$.

Next, pathways enriched with H3K4me3 after 1 hour or 6 hours of hypoxia stimulation were investigated separately as shown in **Tables 3.1** and **3.2**. The pathway enrichment analysis was performed on WEB-based Gene SeT AnaLysis Toolkit (WebGestalt), using hallmark gene sets obtained from Molecular Signature Database (187, 204) Hallmark gene sets were compared with low stringency H3K4me3 hypoxia upregulated gene peaks, which were shown

to be increased at least 2 out of 3 biological replicates of the ChIP-seq experiments. As a result, a list of different pathways was shown to be significantly enriched with H3K4me3 methylation mark. As expected, hypoxia signalling pathway was found as the primary pathway in both 1 hour and 6 hours of hypoxia treated cells' datasets. TNF-α induced NF-κB signalling pathway was identified as the second most enriched pathway when overlapped with 6 hours hypoxia treated dataset (**Table 3.2**). There was no significant overlap with TNF-α induced NF-κB pathway and low stringency H3K4me3 1 hour hypoxia upregulated gene peaks (**Table 3.1**). However, the NF-κB signalling pathway was significantly enriched when overlapped with high stringency H3K4me3 1 hour hypoxia upregulated gene peaks, which were shown to be increased in all biological replicates of the ChIP-seq experiments. This analysis was performed using Molecular Signature Database (MSigDB), and also published in Batie *et al.* (117, 186).

Table 3.1. Pathway association analysis of H3K4me3 ChIP-seq peaks with 1 hour hypoxia treatment. H3K4me3 low stringency ChIP-seq peaks with 1 hour hypoxia treatment overlap with gene groups identified using WEB-based Gene SeT AnaLysis Toolkit. The top 15 signalling pathways are listed with FDR cut off >0.05. Numbers in brackets represent the number of genes in the gene group used as a reference.

Gene Set	Overlapping genes	P Value	FDR
Hypoxia (199)	7	0.0137	0.16783
Epithelial Mesenchymal Transition (199)	7	0.0137	0.16783
KRas Signalling (198)	8	0.0036716	0.16783
IL2 Stat5 Signalling (198)	7	0.013351	0.16783
Spermatogenesis (132)	5	0.027441	0.26892
Mitotic Spindle (197)	6	0.041139	0.28797
G2M Checkpoint (195)	6	0.039437	0.28797
Estrogen Response (198)	5	0.11291	0.55806
E2F Targets (197)	5	0.11112	0.55806
UV Response (143)	4	0.11389	0.55806
Androgen Response (98)	3	0.13395	0.59668
TGF Beta Signalling (53)	2	0.15061	0.615
Glycolysis (197)	4	0.25263	0.88422
MTorck1 Signalling (196)	4	0.24976	0.88422
TNF-α signalling via NF-κB (199)	3	0.48282	1

Table 3.2. Pathway association analysis of H3K4me3 ChIP-seq peaks with 6 hours hypoxia treatment. H3K4me3 low stringency ChIP-seq peaks with 6 hours hypoxia treatment overlap with gene groups identified using WEB-based Gene SeT AnaLysis Toolkit. The top 5 signalling pathways are listed with FDR cut off ≤0.05. Numbers in brackets represent the number of genes in the gene group used as a reference.

Gene Set	Overlapping genes	P Value	FDR
Hypoxia (199)	97	0.00027974	0.002432
TNF-α signalling via NF-κB (199)	78	0.0002978	0.002432
Estrogen Response Early (198)	74	1.5865E-06	2.59E-05
Glycolysis (197)	66	8.10E-08	1.98E-06
Heme Metabolism (193)	65	2.22E-16	1.09E-14

To strengthen the information generated by ChIP-seq in hypoxia induced regulatory mechanisms, a merged list of genes enriched with H3K4me3 methylation mark was overlapped with hypoxia RNA-seq dataset, which was previously produced in the Rocha lab by inducing HeLa cells with 16- or 24-hours of hypoxia. As a result, 473 of these genes were detected in both ChIP-seq and RNA-seq datasets. 80 of them were overlapped with publicly available NF-κB hallmark gene set, where 22 of them was also identified in all 3 datasets (**Figure 3.2**). These statistically significant results indicate that H3K4me3 ChIP-seq and RNA-seq analysis share a group of genes that possibly has similar transcriptional regulatory network, and a list of them is identified to correlate with the NF-κB system.

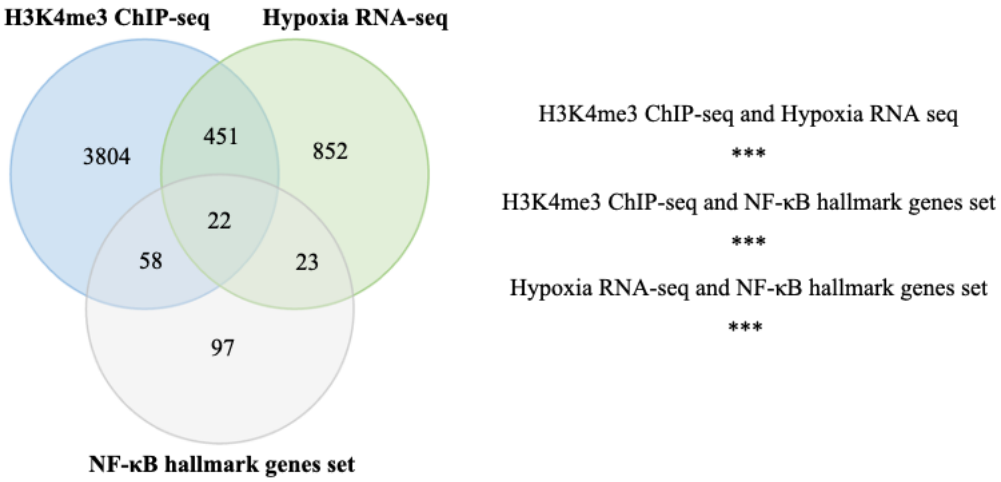

Figure 3.2. Overlap of H3K4me3 ChIP-seq peaks with other datasets. Individual genes included in H3K4me3 ChIP-seq datasets with 1 hour and 6 hours of hypoxia stimulation were compared with upregulated genes in RNA-seq analysis following 16- and 24-hours hypoxia stimulation previously performed in Rocha lab, and publicly available NF-κB hallmark genes set. P value for overlaps were calculated by hypergeometric test. *** $p \leq 0.001$.

From the overlapped lists, genes that are mutual in both H3K4me3 ChIP-seq and NF-κB hallmark gene sets were listed in **Table 3.3**; and genes that are also common in hypoxia RNA-seq were listed in **Table 3.4**. Listed genes were described for their molecular function using the information obtained from GeneCards database (https://www.genecards.org) (**Table 3.3** and **Table 3.4**). Also, Gene Ontology (GO) enrichment analysis was performed using WebGestalt Toolkit looking to further define the gene functions (**Figure 3.3**). Based on this analysis, the top significantly enriched GO terms included "RNA polymerase II proximal promoter sequence-specific DNA binding" and "DNA-binding transcriptional factor activity". These results indicate that high number of H3K4me3 enriched genes that are correlated with the NF-κB system possibly have active roles on the transcriptional machinery.

Next, high stringency H3K4me3 hypoxia upregulated promoter peak changes were selected for further validation by ChIP-qPCR (**Table 3.3** and **Table 3.4**). The selected gene peaks were shown to be increased in all biological replicates of the ChIP-seq experiment. Among the H3K4me3 1 hour hypoxia upregulated high stringency gene peaks, only two of them were identified to overlap with the NF-κB hallmark genes set; EDN1(Endothelin 1), which is mainly known to encode a preproprotein that functions as a vasoconstrictor (205) (**Figure 3.3, A**); and BMP2 (Bone Morphogenetic Protein 2), which belongs to the Tumour Growth Factor (TGF-β) superfamily of proteins and plays a critical role in various developmental processes (206) (**Figure 3.4, B**). The additional genes that belong to the H3K4me3 6-hours hypoxia upregulated gene peaks, included MARCKS (Myristoylated alanine-rich C-kinase substrate), which is an actin filament cross-linking protein and plays important roles in cell motility, phagocytosis, transmembrane transport, and regulation of the cell cycle (207) (**Figure 3.4, C**); KDM6B (Lysine Demethylase 6B, also known as Jumonji Domain-Containing Protein 3 - JMJD3), which controls chromatin organization and gene silencing through demethylation of H3K27me3, also previously shown to involve in the modulation of immune and inflammatory responses (208) (**Figure 3.4, D**); JUN (Jun Proto-Oncogene, AP-1 Transcription Factor Subunit), a transcription factor that involves in cell

cycle progression and antiapoptotic activity cooperating with NF-κB (209) (**Figure 3.4, E**); and DUSP1 (Dual Specificity Phosphatase 1), which has a central role in cellular responses to environmental stress, also several studies have demonstrated that DUSP1 negatively regulates the inflammatory responses (210, 211) (**Figure 3.4, F**).

Table 3.3. HeLa H3K4me3 1 hour or 6 hours hypoxia upregulated ChIP-seq gene peaks that are potential NF-κB target genes with their molecular functions.
Genes identified common in both H3K4me3 ChIP-seq and NF-κB hallmark gene sets. High stringency H3K4me3 hypoxia upregulated promoter peak changes selected for further validation (**bold**). Genes enriched in "DNA-binding transcription factor activity" Gene Ontology is highlighted in blue. Gene function summary was obtained from GeneCards database (https://www.genecards.org).

Gene Name	Ensemble Gene ID	Gene Function Summary
EDN1	**ENSG00000078401**	Vasoconstriction
BMP2	**ENSG00000125845**	Bone and cartilage development
KLF10	ENSG00000155090	Regulation of the circadian clock
CD44	ENSG00000026025	Cell-cell interactions, cell adhesion and migration
KLF6	ENSG00000067057	B-cell growth and development
NFKB2	ENSG00000076513	Immune and inflammatory responses
GADD45B	ENSG00000099822	Regulation of growth and apoptosis
NFKBIA	ENSG00000100767	Immune and inflammatory responses
SLC16A6	ENSG00000108840	Monocarboxylic acid transmembrane transporter activity
RNF19B	ENSG00000116260	Cytotoxic effects of natural killer cells
TRIP10	ENSG00000125462	Actin cytoskeleton organization and signal transduction
STAT5A	ENSG00000126217	Cell growth and division, cell proliferation and differentiation
GCH1	ENSG00000131746	Nitric oxide synthesis
IL15RA	ENSG00000134245	Cell proliferation and expression of apoptosis inhibitors
DRAM1	ENSG00000135736	Autophagy induction
ATF3	ENSG00000162496	Cellular stress response
SERPINB8	ENSG00000166016	Platelet functions and cell-cell adhesion in the skin
SMAD3	ENSG00000166478	Transforming growth factor-beta signalling and cell proliferation
RELA	ENSG00000172530	Immune and inflammatory responses, cell growth and apoptosis
SPHK1	ENSG00000175691	Cell proliferation and survival
PER1	ENSG00000177951	Locomotor activity, metabolism, and behaviour in circadian rhythms
FJX1	ENSG00000178104	Growth and differentiation in *D. melanogaster*
DENND5A	ENSG00000183337	Conversion of GDP to GTP
SOCS3	ENSG00000183691	Negative regulation of cytokine signalling
SNN	ENSG00000183723	Metal ion binding activity
TNFAIP2	ENSG00000184678	Inflammation and angiogenesis
YRDC	ENSG00000188613	Nucleotidyltransferase and tRNA binding
MAP2K3	ENSG00000264364	Expression of glucose transporter
MXD1	ENSG00000267073	Cellular proliferation, differentiation and apoptosis
BCL3	ENSG00000272473	Transcriptional co-activator of NF-κB
PPP1R15A	ENSG00000279708	Apoptosis following ionizing radiation
AREG	ENSG00000079308	Epithelial cell growth
HBEGF	ENSG00000085662	Enables growth factor activity and wound healing

Table 3.3 continued.

Gene Name	Ensemble Gene ID	Gene Function Summary
HES1	ENSG00000088836	Cell proliferation and differentiation
ID2	ENSG00000099331	Negatively regulating cell differentiation
SGK1	ENSG00000099942	Cell survival, neuronal excitability, and renal sodium excretion
NR4A3	ENSG00000100226	Cell proliferation, differentiation, and apoptosis
DUSP1	**ENSG00000120129**	Environmental stress response and negative regulation of cell proliferation
EGR1	ENSG00000100300	Cellular differentiation and mitogenesis
PMEPA1	ENSG00000101335	Negative regulation of transforming growth factor-beta signalling
FOSB	ENSG00000104219	Cell proliferation, differentiation, and transformation
KLF2	ENSG00000104936	Cellular development
ZFP36	ENSG00000105058	Cellular response to cytokine and growth factor stimulus
GFPT2	ENSG00000106477	Controls the flux of glucose into the hexosamine pathway
NINJ1	ENSG00000106538	Cell-cell interactions, inflammation, cell death, and angiogenesis
KLF4	ENSG00000112759	Cell proliferation and differentiation
TUBB2A	ENSG00000114251	Mitosis and intracellular transport
SIK1	ENSG00000115350	Cell cycle regulation, gluconeogenesis and lipogenesis regulation, muscle growth and differentiation
NFKBIE	ENSG00000120708	NF-κB inhibition
RCAN1	ENSG00000130382	Central nervous system development
ICOSLG	ENSG00000130724	Immune and inflammatory responses
SQSTM1	ENSG00000131668	Autophagy. Activation of upstream NF-κB pathway
ZC3H12A	ENSG00000135317	Immune and inflammatory responses, apoptosis and angiogenesis
TNIP2	ENSG00000145569	NF-κB inhibition
JUNB	ENSG00000147533	Immune and inflammatory response
PHLDA2	ENSG00000160570	Placenta growth regulation
CEBPD	ENSG00000160570	Immune and inflammatory responses
MARCKS	**ENSG00000277443**	Cell motility, phagocytosis, membrane trafficking and mitogenesis

Table 3.4. HeLa H3K4me3 1 hour or 6 hours hypoxia upregulated ChIP-seq gene peaks that are potential NF-κB target genes with their molecular functions.

Genes identified common in all three datasets; H3K4me3 ChIP-seq high stringency, NF-κB hallmark genes set, as well as genes Hypoxia RNA-seq data set. High stringency H3K4me3 hypoxia upregulated promoter peak changes selected for further validation (**bold**). Genes enriched in "DNA-binding transcription factor activity" Gene Ontology is highlighted in blue. The gene function summary was obtained from GeneCards database (https://www.genecards.org).

Gene Name	Ensemble Gene ID	Gene Function Summary
SLC2A3	ENSG00000059588	Glucose transport across the cell membrane
F3	ENSG00000117408	Initiates the blood coagulation cascades
TNFSF9	ENSG00000125447	Antigen presentation and cytotoxic T cells generation
KDM6B	**ENSG00000132510**	Chromatin organization and gene activation
DUSP5	ENSG00000137872	Cellular proliferation and differentiation
EFNA1	ENSG00000168348	Cellular migration and adhesion during neuronal, vascular and epithelial development
FOS	ENSG00000169750	Cell proliferation, differentiation, and transformation
PFKFB3	ENSG00000169884	Glycolysis, cell cycle progression and prevention of apoptosis
FOSL1	ENSG00000174915	Cell proliferation, differentiation, and transformation
JUN	**ENSG00000177606**	Immune and inflammatory responses
PLAUR	ENSG00000262454	Localizing and promoting plasmin formation
FOSL2	ENSG00000274833	Cell proliferation, differentiation, and transformation
SERPINE1	ENSG00000072135	Inhibitor of tissue plasminogen activator and and hence fibrinolysis.
VEGFA	ENSG00000084731	Proliferation and migration of vascular endothelial cells
TNFAIP3	ENSG00000099917	Immune and inflammatory responses. NF-κB inhibition
SDC4	ENSG00000101199	Receptor in intracellular signalling
CDKN1A	ENSG00000102007	Cell cycle progression
BHLHE40	ENSG00000108175	Control of circadian rhythm and cell differentiation
RHOB	ENSG00000115694	Apoptosis and cell migration
TNIP1	ENSG00000119771	Autoimmunity and tissue homeostasis. NF-κB inhibition
NFIL3	ENSG00000138821	Regulation of circadian rhythm
MAFF	ENSG00000163754	Cellular stress response

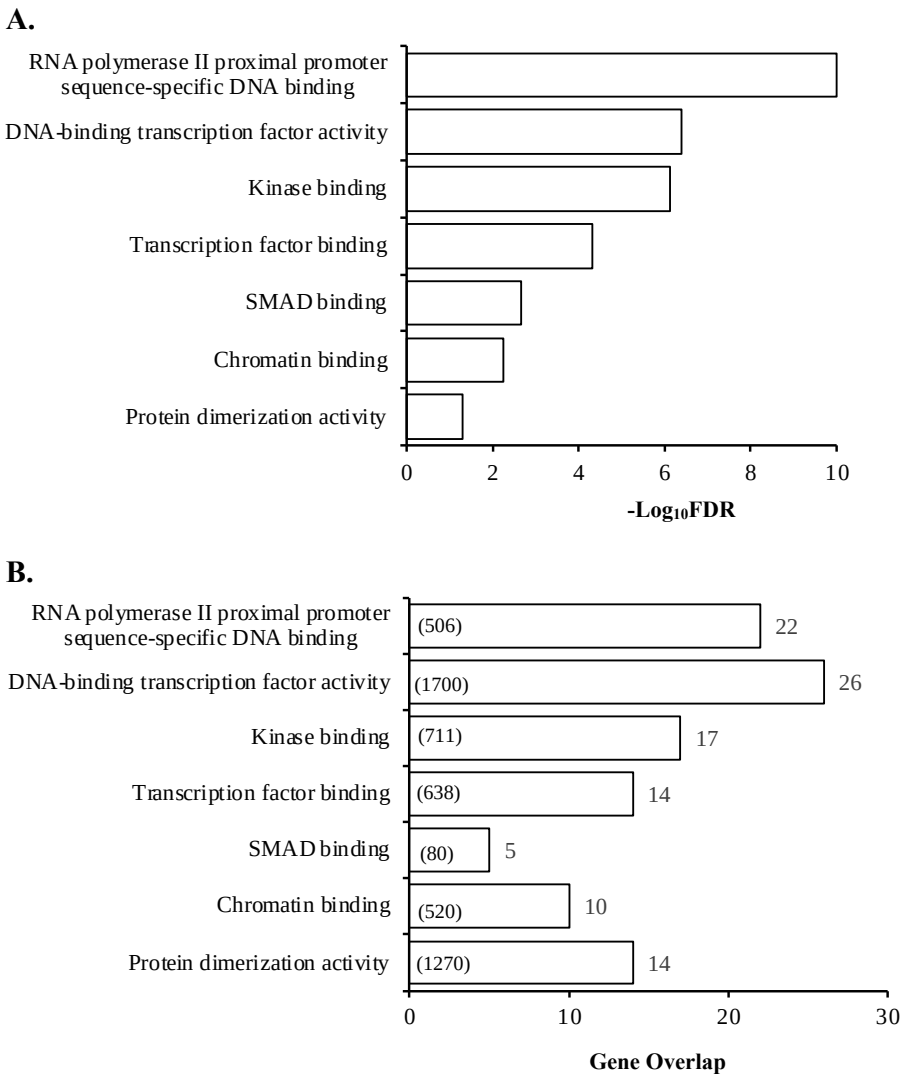

Figure 3.3. Gene Ontology (GO) enrichment analysis of the common genes found in both H3K4me3 ChIP-seq and NF-κB hallmark genes set. A. Top 7 significantly enriched GO terms of the molecular functions were identified using WEB-based Gene SeT AnaLysis Toolkit with FDR cut off ≤0.05. The adjusted statistically significant values were negative 10-base log transformed. **B.** Number of genes overlap in each molecular function category. Numbers in brackets represent the number of genes in each gene group used as a reference.

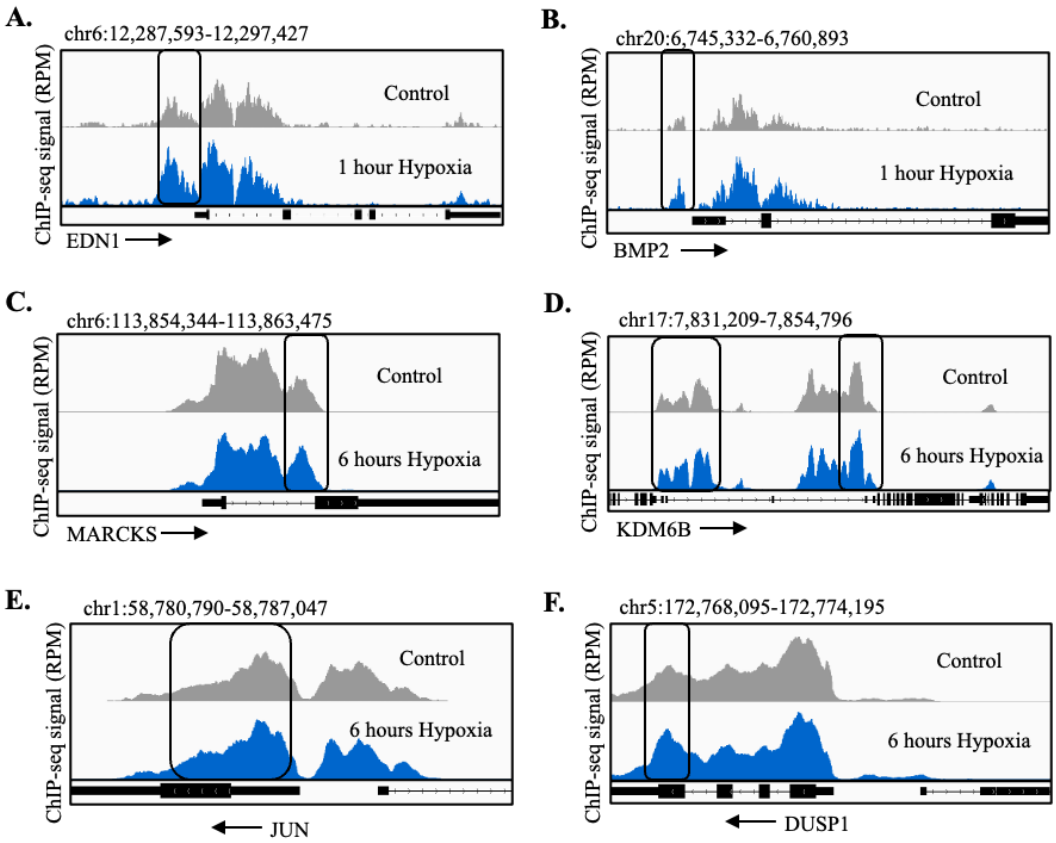

Figure 3.4. Hypoxia ChIP-seq coverage tracks of H3K4me3 peaks at different putative NF-κB target genes. Coverage tracks and peaks from H3K4me3 ChIP-seq 1 hour of hypoxia high stringency dataset at EDN1 (**A**), and BMP2 (**B**); 6 hours of hypoxia high stringency dataset at MARCKS (**C**), KDM6B (**D**), JUN (**E**), and DUSP1 (**F**). Peak start and end area is shown in a black framed rectangle. Forward stranded genes are shown with arrows directing to right side, reverse stranded genes are shown with arrows directing to the left side. Chromosomal information is shown at the top of each image with 3000 bp upstream of transcription start side (TSS) to 3000 bp downstream of transcription end side (TES). Integrative Genomics Viewer (IGV) software was used for the figure illustration.

To validate the effect of hypoxia on the expression of the selected genes, HeLa cells were exposed to 1% oxygen at different time points prior to qPCR analysis (**Figure 3.5**). In this analysis, efficiency of the hypoxia stimulation was measured using a known hypoxia-inducible gene, Carbonic Anhydrase (CA9) (**Figure 3.5, A**). As a result, mRNA expression of all genes was increased at 24 hours of hypoxia (**Figure 3.5**). EDN1 was significantly increased at 1- and 2-hours of hypoxia stimulation, whereas KDM6B, DUSP1, JUN and MARCKS were also increased at 4 hours of hypoxia. These results suggest that H3K4me3 upregulated promoter regions identified at hypoxia lists indicated the hypoxia inducible genes. As BMP2 showed the least increase with hypoxia stimulation in all of the time points, this gene was not included in subsequent analysis (**Figure 3.5, G**).

H3K4me3 levels on the selected genes following 1- and 24-hours of hypoxia stimulation were investigated by using the ChIP-qPCR method. H3K4me3 methylation was quantified using specific set of primers, designed for the predicted binding sites of the genes that were selected based on coordinates obtained in the ChIP-seq experiments (**Figure 3.6, A**). H3K4me3 levels were increased on the selected genes with both hypoxia time points but with statistically significance being mostly observed following 24-hours of hypoxia exposure (**Figure 3.6**). Although t-test was used to statistically analyse the data in Figures 3.5 and 3.6, one-way ANOVA should have been used, as population means of more than two groups were being compared.

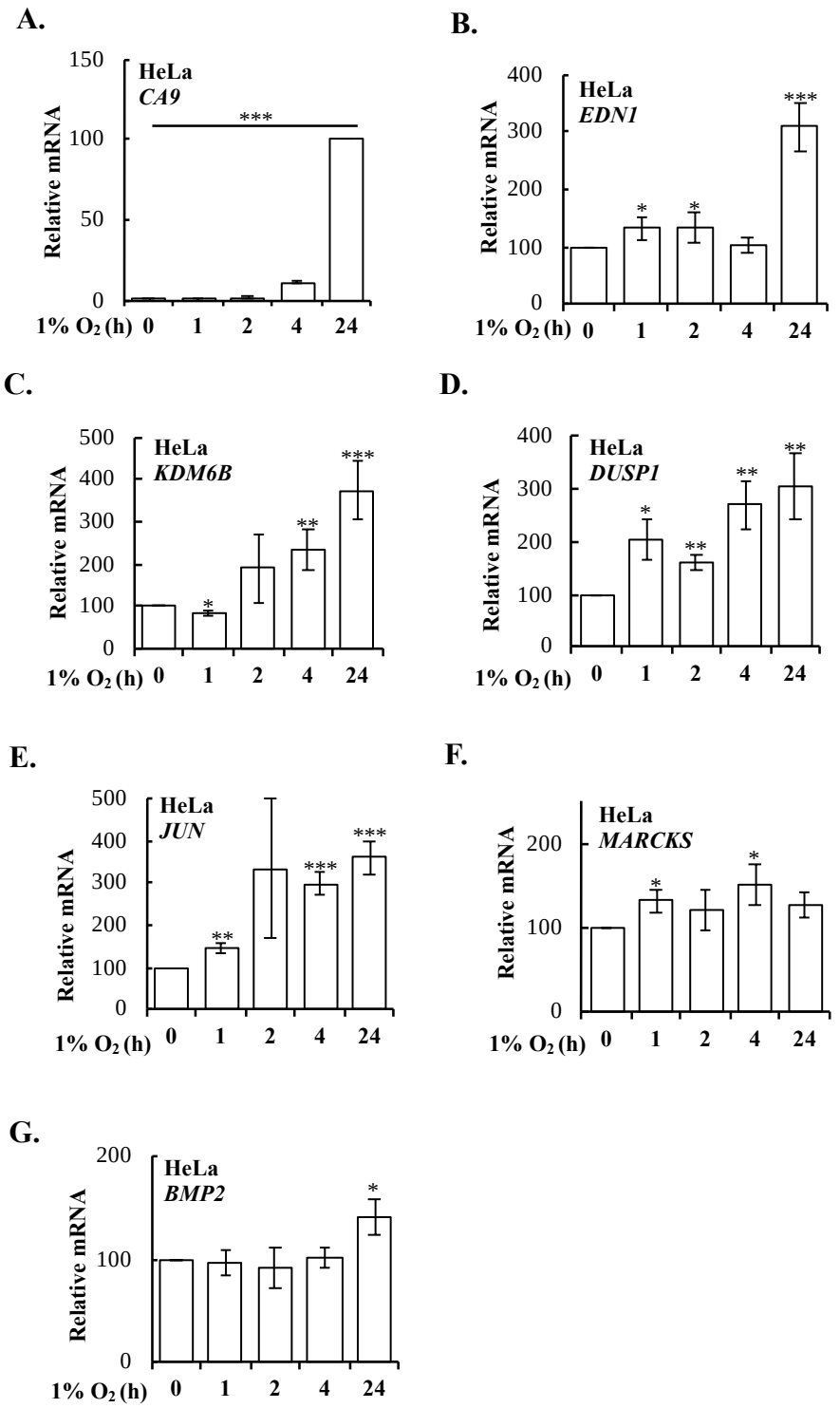

Figure 3.5. Hypoxia induction of genes with H3K4me3 hypoxia upregulated peaks. HeLa cells were exposed to 0, 1, 2, 4, and 24 hours 1% O_2 before proceeding to total RNA extraction and cDNA conversion. Relative mRNA expression levels of the indicated genes were analysed by qPCR using ACTB as a normalising gene. Graphs represent mean and standard error of a minimum of three independent experiments. Student t-test was applied, and significance determined as follows: * $p \leq 0.05$, ** $p \leq 0.01$, *** $p \leq 0.001$.

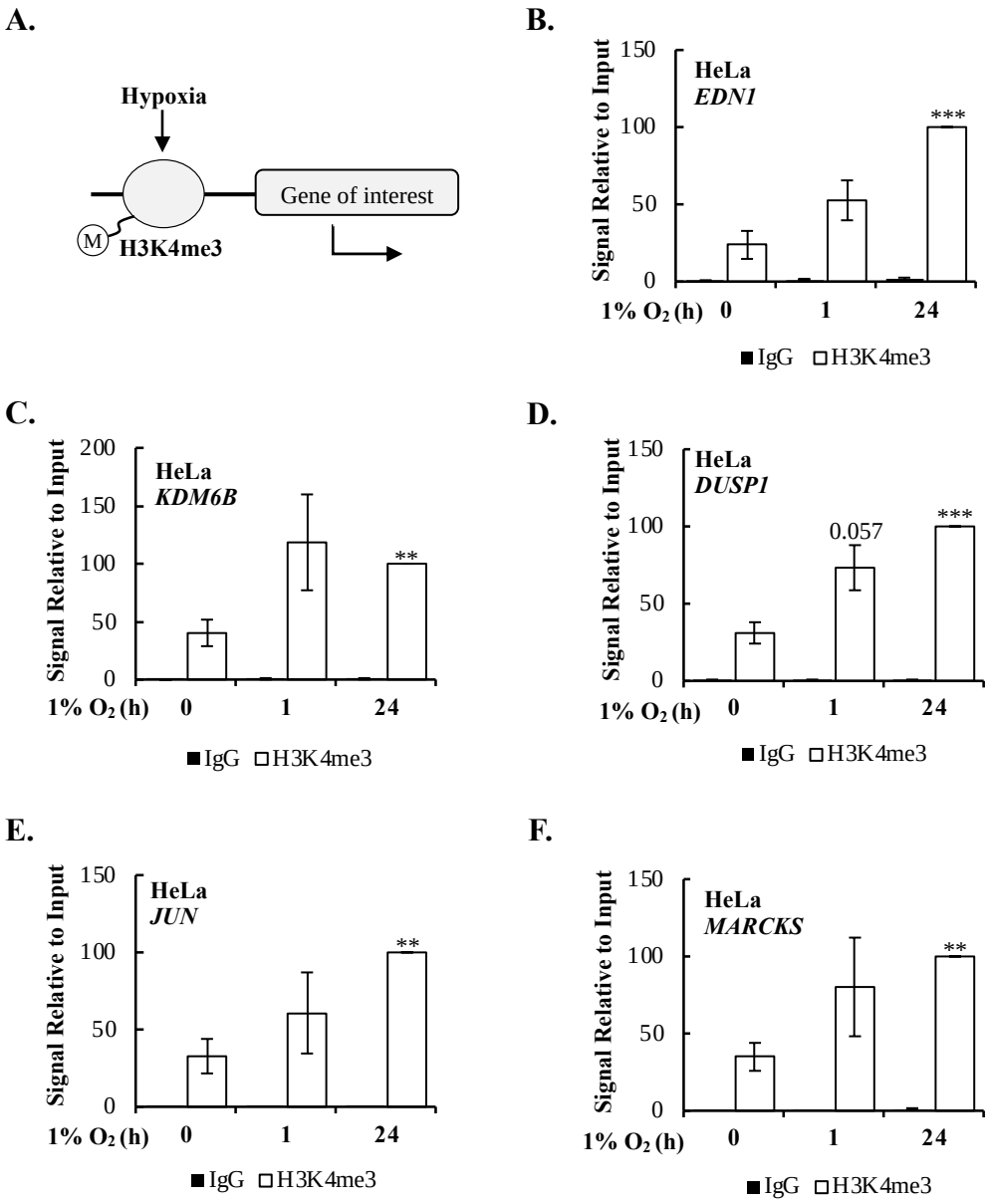

Figure 3.6. H3K4me3 1 hour hypoxia peak change validation by ChIP-qPCR. HeLa cells were exposed to 0, 1 or 24 hours 1% O_2 prior to cross-linking and lysis. ChIP was performed for an IgG control and H3K4me3 enriched genes' promoter regions occupied by the H3K4me3 promoter peaks. DNA was analysed by qPCR with results normalised to 2% input DNA. Graphs represent mean and standard error of a minimum of three independent experiments. Student t-test was applied, and significance determined as follows: * $p \leq 0.05$, ** $p \leq 0.01$, *** $p \leq 0.001$.

Although, the genes selected are reported to be NF-κB dependent, this was further validated by using an overexpression experiment. Cells were transfected with a RelA plasmid prior to qPCR analysis for the genes selected above (**Figure 3.7**, **A**). As predicted, mRNA expression of all genes was increased with RelA overexpression, although JUN, MARCKS and KDM6B failed to reach statistical significance (**Figure 3.7**). These results indicate that upregulated gene peaks identified at H3K4me3 hypoxia lists are associated with NF-κB activation. To further support the connection of these genes with the NF-κB transcriptional response, NF-κB RelA ChIP-seq Atlas dataset was used (https://chip-atlas.org/ (212)) and RelA binding sites were compared with the H3K4me3 gene peaks (**Figure 3.8**, **A**). As a result, there was a statistically significant overlap between H3K4me3 hypoxia enriched genes and the RelA ChIP-seq Atlas dataset. Also, based on the pathway enrichment analysis performed using the hallmark gene sets, hypoxia, and TNF-α stimulated NF-κB were confirmed to be the top two signalling pathways significantly enriched with these genes (**Figure 3.8**, **B**). Importantly, the genes overlapped in the NF-κB hallmark and H3K4me3 gene sets were also identified in the RelA ChIP-seq Atlas data set. This indicates that H3K4me3 enriched genes possibly have RelA binding sites and potentially regulate their transcriptional expression. However, this information will need to be validated with further experiments.

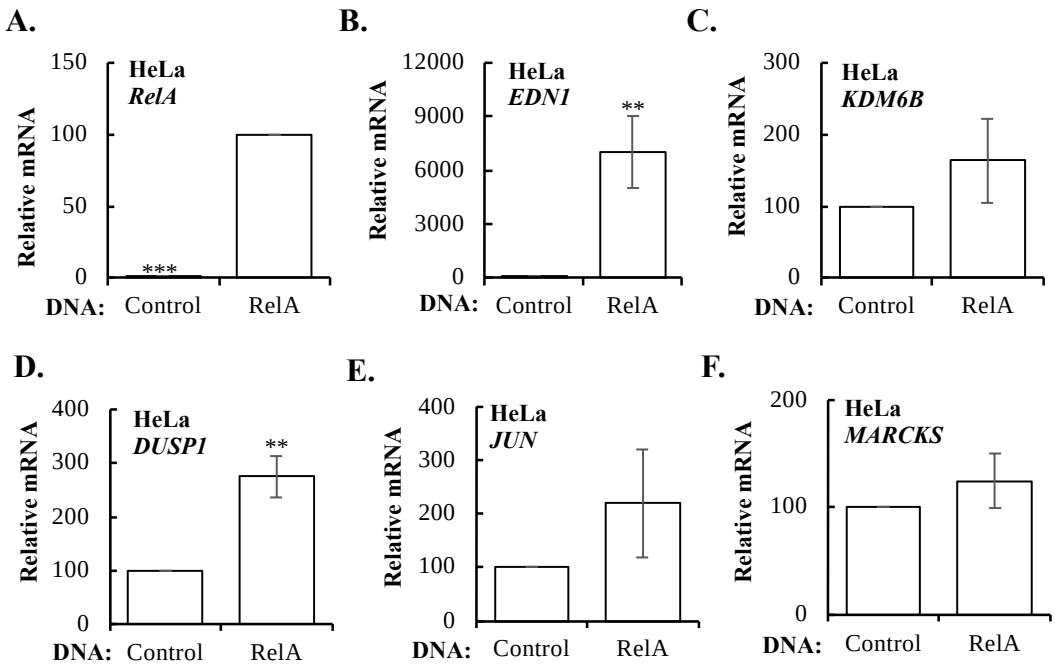

Figure 3.7. RelA overexpression increases the mRNA expression of H3K4me3 hypoxia upregulated peaks. HeLa cells were transfected with control (empty vector) and RelA plasmid DNA 48 hours prior to total RNA extraction and cDNA conversion. Relative mRNA expression levels of the indicated genes were analysed by qPCR using ACTB as a normalising gene. Graphs represent mean and standard error of a minimum of three independent experiments. Student t-test was applied, and significance determined as follows: * $p \leq 0.05$, ** $p \leq 0.01$, *** $p \leq 0.001$.

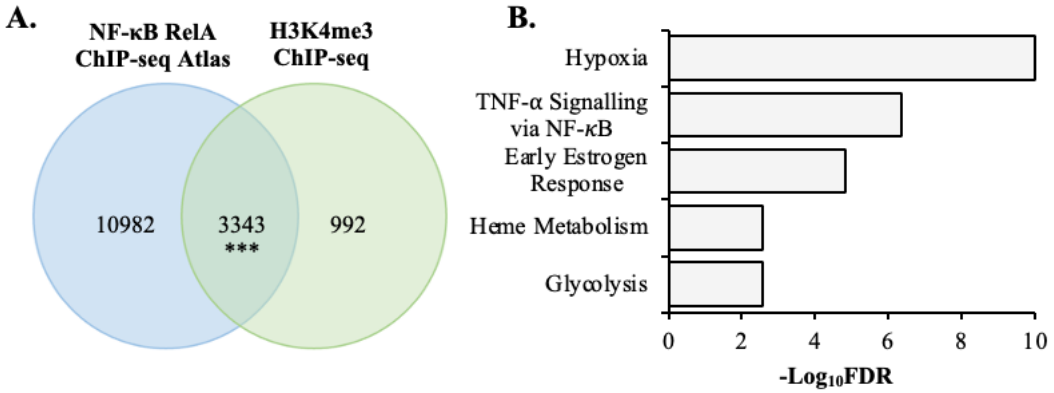

Figure 3.8. Overlap of RelA ChIP-seq Atlas and H3K4me3 ChIP-seq peaks. A. Individual genes included in H3K4me3 ChIP-seq datasets with 1 hour and 6 hours of hypoxia stimulation were compared with publicly available NF-κB RelA ChIP-seq Atlas, containing list of genes with RelA DNA binding sites. **B.** Pathway association analysis of the overlapped genes identified in the H3K4me3 ChIP-seq and NF-κB RelA ChIP-seq Atlas peaks was performed using WEB-based Gene SeT AnaLysis Toolkit with FDR cut off ≤0.05. The adjusted statistically significant values were negative 10-base log transformed. P value for the overlap was calculated by hypergeometric test. *** $p \leq 0.001$.

3.3. Regulation of NF-κB target gene expression and H3K4me3 levels by KDM5A

The results shown above demonstrate that H3K4me3 methylation mark increases with hypoxia stimulation at selected NF-κB target genes (**Figure 3.6**). Previous work has shown that KDM5A depletion can mimic hypoxia-induced cellular responses in this cell system (117). As such, we asked if the KDM5A depletion contributes to the hypoxia induced H3K4me3 levels at the hypoxia upregulated H3K4me3 gene sites. To test this question, KDM5A was depleted using two different oligonucleotides, H3K4me3 was immunoprecipitated with a specific antibody and its levels present at the gene promoters selected were measured using specific primer sets designed for the predicted sites in the genes as obtained by the sequencing experiments (**Figure 3.9, A**). As shown in **Figure 3.9**, **B**, KDM5A mRNA levels were efficiently decreased by using two different siRNA oligonucleotides, specifically designed for targeting distinct sites of the KDM5A RNA sequence. H3K4me3 levels present at all genes were increased with the KDM5A oligo 1 but this was not observed with KDM5A oligo 2 (**Figure 3.9**).

Then, it was investigated if loss of KDM5A activity would contribute to the increase in mRNA expression of the selected genes. Analysis of mRNA levels for the NF-κB dependent genes revealed that all genes were increased by varying degrees upon KDM5A depletion, with KDM6B, JUN and MARKCS increases reaching to statistical significance with both of the KDM5A oligonucleotides (**Figure 3.10**). Overall, like hypoxia stimulation, KDM5A depletion increased the histone methylation mark in all the NF-κB target genes and both conditions increased the mRNA level gene expressions in the similar amounts. These results indicate that KDM5A knock-down mimics hypoxia stimulation and potentially induces the NF-κB transcriptional response.

Based on the analysis obtained with both KDM5A oligos, the data indicates that KDM5A negatively regulates gene transcription of DUSP1, MARKCKS, JUN and KDM6B, whereas only oligo 1 has this effect on the EDN1. In addition, KDM5A oligo 1 leads into the negative regulation of H3K4me3 promoter levels at these genes. However, these experiments

will need to be repeated with another siRNA KDM5A to further support this observation. In addition, experiments that are shown in both Figure 3.9 and Figure 3.10 will need to be re-analysed with one-way ANOVA statistical test, as population means of more than two groups were being compared.

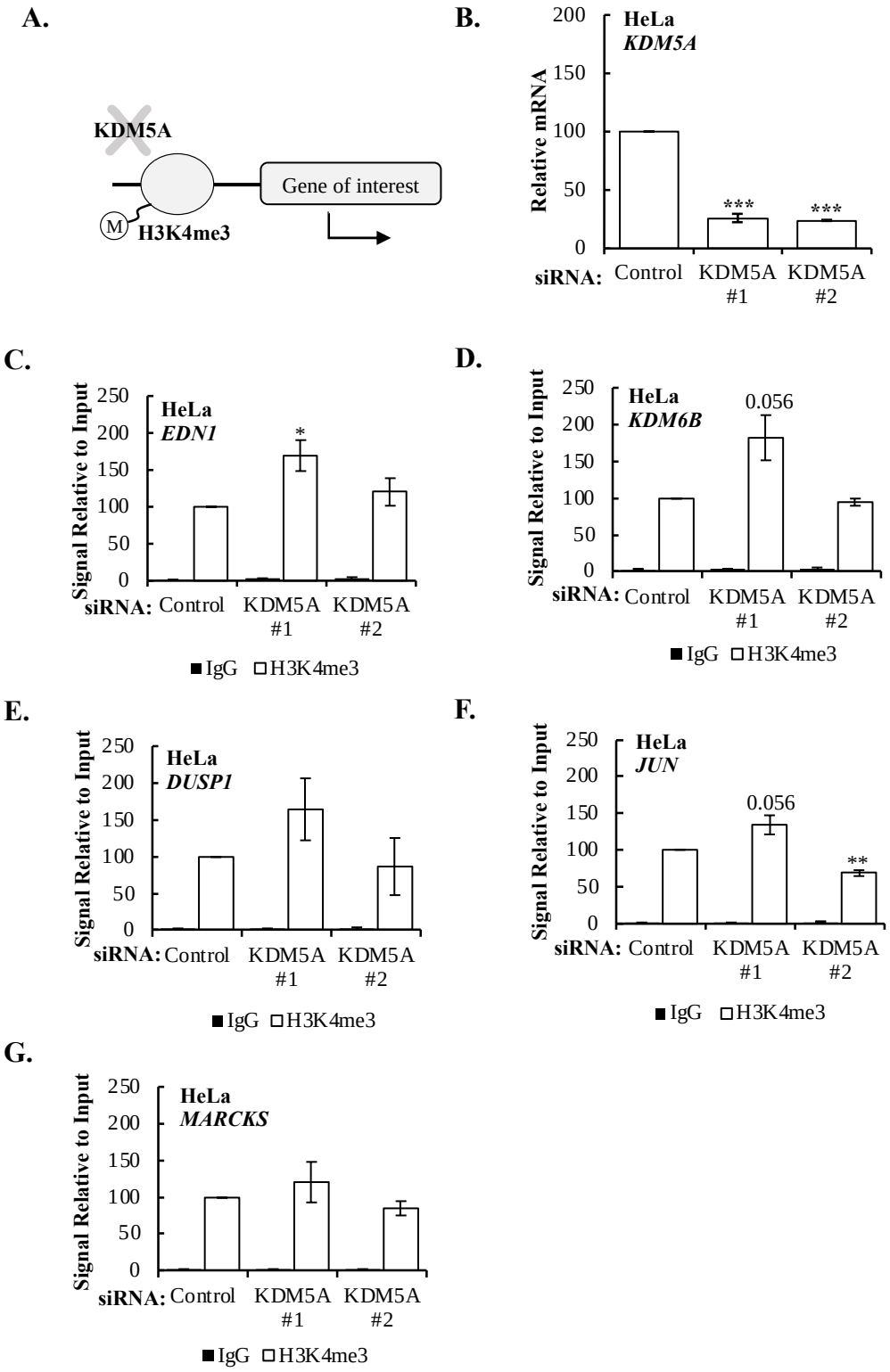

Figure 3.9. Effect of KDM5A depletion on H3K4me3 levels at hypoxia upregulated H3K4me3 peaks. HeLa cells were transfected with control (non-targeting), KDM5A oligo 1 and KDM5A oligo 2 siRNAs 48 hours prior to cross-linking and lysis. ChIPs were performed for an IgG control and H3K4me3 to the indicated gene promoter regions occupied by H3K4me3 promoter peaks. DNA was analysed by qPCR with results normalised to 2% input DNA. Graphs represent mean and standard error of a minimum of three independent experiments. Student t-test was applied, and significance determined as follows: * $p \leq 0.05$, ** $p \leq 0.01$, *** $p \leq 0.001$.

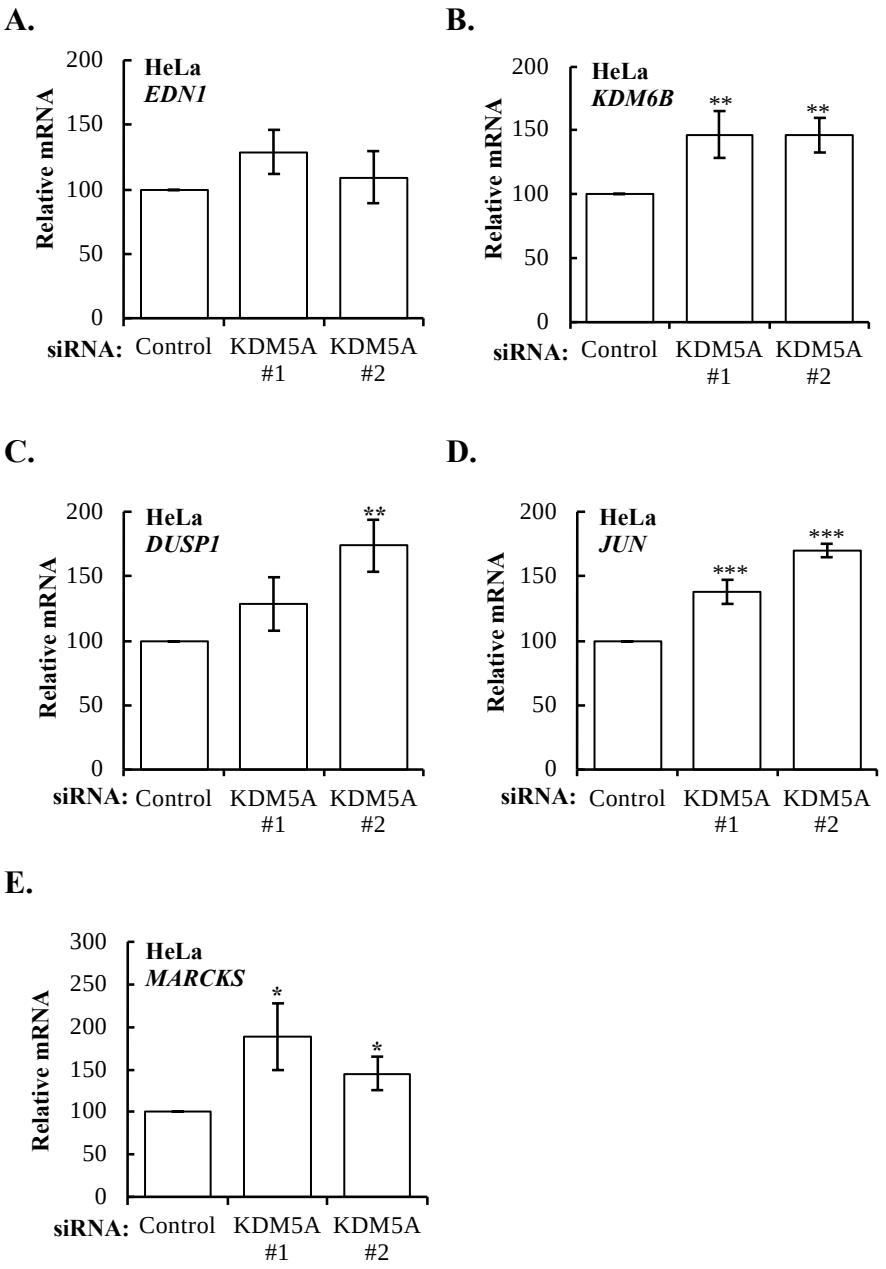

Figure 3.10. Effect of KDM5A depletion on hypoxia upregulated H3K4me3 peaks. HeLa cells were transfected with control (non-targeting), KDM5A oligo 1 and KDM5A oligo 2 siRNAs 48 hours prior to total RNA extraction and cDNA conversion. Relative mRNA expression levels of the indicated genes were analysed by qPCR using 18S as a normalising gene. Graphs represent mean and standard error of a minimum of three independent experiments. Student t-test was applied, and significance determined as follows: * $p \leq 0.05$, ** $p \leq 0.01$, *** $p \leq 0.001$.

3.4. Role of KDM5A on NF-κB transcriptional activity and protein expression

The analysis of the hypoxia ChIP-sequencing experiments for H3K4me3, and subsequent experiments suggest that KDM5A is a potential novel regulator of NF-κB. As a preliminary experiment to determine the role of KDM5A regulation on the NF-κB activity, luciferase experiments in 3 different cell lines were performed (**Figure 3.9**). These cell lines stably express an artificial promoter containing 3x-κB sites in tandem. U2OS and A549 cells express the Promega NF-κB reporter luc2P, while HeLa express 3x-κB ConA luciferase reporter as described in (178).

NF-κB luciferase reporter cells, were transfected with KDM5A siRNA without any additional stimulation. KDM5A knock-down decreased the κB activity in HeLa (**Figure 3.11, B**) and A549 cells (**Figure 3.11, C**) but increased in U2OS cells (**Figure 3.11, D**). This shows that KDM5A has a positive regulatory effect on HeLa and A549 cell lines, but a negative regulatory role on U2OS cells. However, variation in these results could be due to diversity in KDM5A knock-down efficiency in different cell types. Although efficiency of the KDM5A knock-down in HeLa cells was tested (**Figure 3.11**, **A**), A549 and U2OS cells will also need to be tested for such variations.

Given that NF-κB is known to respond to cytokine stimulation, cells were exposed to the canonical NF-κB pathway inducer, Tumour necrosis factor α (TNF-α). Optimum response time points were previously defined for each cell line in the Rocha lab. Following KDM5A depletion and TNF-α stimulation, NF-κB activity in HeLa cells remained lower (**Figure 3.12**, **A**). However, KDM5A depletion and TNF-α stimulation increased in A549 cells but decreased in U2OS cells (**Figure 3.12**, **B** and **C**). This indicated that upon TNF-α stimulation, KDM5A is required to reduce a negative regulatory mechanism in the NF-κB pathway in HeLa and U2OS cell lines but not in A549 cells. Given, the artificial nature of the reporter and lack of chromatin environment of these promoters, additional work is required to fully determine the molecular regulatory mechanism of the NF-κB via KDM5A. Nevertheless, these results suggest that KDM5A might be involved in a variety of mechanisms controlling NF-κB

activity. Although t-test was used to statistically analyse the data in Figure 3.12, one-way ANOVA should have been used, as population means of more than two groups were being compared.

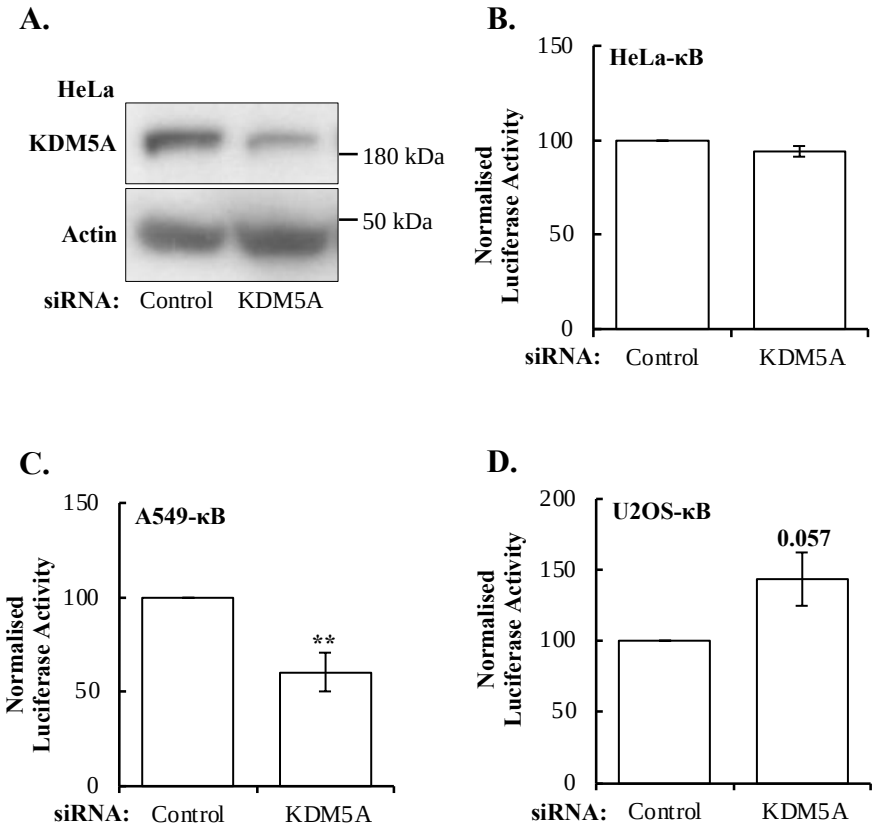

Figure 3.11. KDM5A depletion affects the κB activity differently in different cell lines. Efficiency of the KDM5A knock-down was checked on HeLa cells (**A**). Cells were transfected with siRNA oligonucleotide of control (non-targeting) or KDM5A before whole cell lysis and probing with western blot method. β-Actin was used as a loading control. Blots represent minimum of three independent experiments. HeLa, A549 and U2OS cells, stably transfected with κB luciferase reporter, were transfected with siRNA control (non-targeting) and KDM5A oligonucleotides (**B**), (**C**), and (**D**). Values were normalised to the control sample. All graphs represent mean and standard error of four independent biological experiments. Student t-test was applied, and significance determined as follows: * $p \leq 0.05$, ** $p \leq 0.01$, *** $p \leq 0.001$.

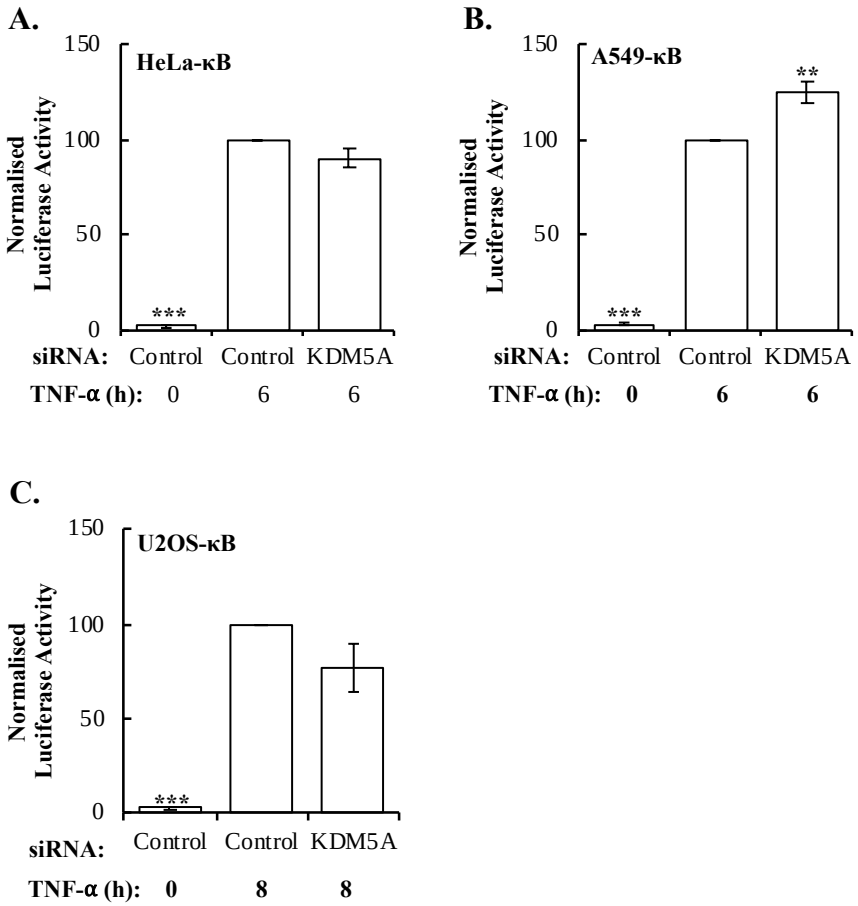

Figure 3.12. KDM5A depletion alters the κB activity in some cell lines following TNF-α stimulation. HeLa, A549, and U2OS, cells, stably transfected with κB luciferase reporter, were transfected with siRNA control (non-targeting) or KDM5A oligonucleotides (**A**), (**B**), and (**C**). 10 ng/mL TNF-α treatment was also added for 6 hours in HeLa (**A**), and A549 (**B**) cells; and for 8 hours in U2OS cells (**C**) prior to luciferase measurements. All the values were normalised to TNF-α treated control samples. All graphs represent mean and standard error of at least three independent biological experiments. Student t-test was applied, and significance determined as follows: * $p \leq 0.05$, ** $p \leq 0.01$, *** $p \leq 0.001$.

The role of KDM5A on NF-κB subunits and their target genes' protein expression was investigated after depleting the KDM5A using an siRNA oligonucleotide and immunoblotting the HeLa cell lysates with specific antibodies (**Figure 3.13**). Based on the two replicates of this experiment, NF-κB RelB protein expression was decreased with KDM5A depletion, and the RelB target gene, cyclinD1 (182, 213) was also reduced. On the other hand, NF-κB cRel protein expression levels increased with KDM5A depletion, however cRel target gene, claspin (214) expression was decreased in both replicates, also suggesting an additional mechanism being involved for the regulation of claspin expression. Furthermore, following KDM5A knockdown, RelA protein expression was increased most noticeably in replicate 1. For RelA, p100, c-IAP1 (215, 216) and BHLHE40 were used as target genes. As a result, BHLHE40 protein expression levels were increased in both replicates, however, p100 was very slightly elevated, and c-IAP1 expression was inconsistent. Overall, these results indicate that KDM5A has a variable impact on the NF-κB subunits and their target genes' protein expression levels. However, this experiment will need to be repeated in order to reach to a clear conclusion. The effect of KDM5A on NF-κB subunits at the protein level and its impact on their transcriptional response could involve their regulatory role on the histones, as well as their non-histone function, which is studied more in detail in **chapter 5**.

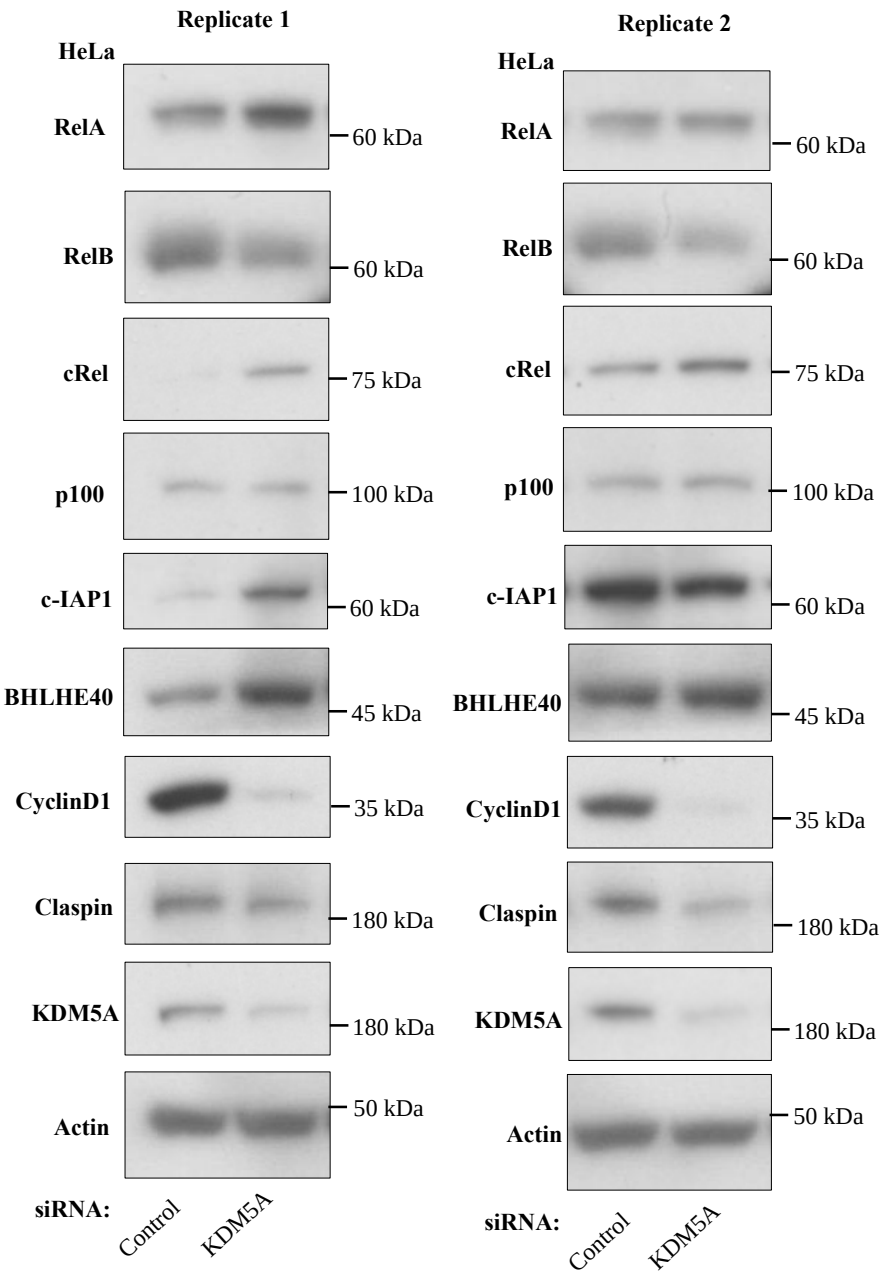

Figure 3.13. KDM5A depletion alters NF-κB subunits and their target genes in protein level. HeLa cells were transfected with siRNA oligonucleotide of control (non-targeting) and KDM5A before whole cell lysis and probing with western blot method. β-Actin was used as a loading control. Blots show two independent replicates of the experiment.

3.5. Discussion

Recent studies have demonstrated that hypoxia induces changes to histone methylation and controls chromatin which plays an important role in the regulation of variety of cellular responses (110, 117). Although it is known that hypoxia intersects with the NF-κB pathway (148), this data revealed yet an unknown link between the role of hypoxia-controlled histone methylation and JmjC histone demethylases and the NF-κB transcriptional response. This study focused on the role of hypoxia controlling H3K4me3 levels via inhibition of the demethylase KDM5A and how this regulates the NF-κB transcriptional response. This data demonstrates that oxygen sensing by chromatin occurring via KDM5A inhibition impacts on other signalling pathways such as NF-κB.

Genome-wide analysis was performed by Michael Batie, to map H3K4me3 enriched genomic regions in HeLa cells, at basal level and following 1 hour (117) and 6 hours hypoxia induction (86); two separate lists of gene peaks were obtained for each dataset (**Figure 3.1**). Pathway enrichment analysis was performed using H3K4me3 upregulated gene peaks, which included genes identified in at least 2 out of 3 biological experiments. This identified genes with statistically significant overlaps with hallmark gene sets (**Tables 3.1** and **3.2**). However, this analysis is limited to overlapping only a defined number of reference genes for each pathway. Thus, some of the TNF-α-induced NF-κB genes might not be included in the hallmark gene sets, therefore, including other publicly available ChIP-seq and RNA-seq datasets with hypoxia or TNF-α stimulation to the comparison, could be more informative.

Combined list of H3K4me3 1 hour and 6 hours hypoxia upregulated gene peaks, were also overlapped with RNA-seq hypoxia and NF-κB hallmark gene sets (**Figure 3.2**). This comparison highlighted potential NF-κB target genes that are associated with H3K4me3 upregulated gene peaks (**Table 3.3**), as well as induced by hypoxia stimulation (**Table 3.4**). From the H3K4me3 1 hour hypoxia upregulated gene peaks, EDN1 was successfully validated to increase with hypoxia stimulation (**Figure 3.5, B**). Also, H3K4me3 6 hours hypoxia upregulated gene peaks, DUSP1, MARCKS, JUN and KDM6B was validated to be hypoxia

inducible (**Figure 3.5, C**, **D**, and **F**). Additionally, their responsiveness to the NF-κB subunit RelA was shown by measuring their mRNA levels following RelA overexpression of the HeLa cells (**Figure 3.7**). All these genes have been shown to have RelA binding sites by ChIP-seq in a variety of different cellular backgrounds, when ChIP-Atlas was used (https://chip-atlas.org/, (212)) (**Figure 3.8**). However, further analysis is necessary to support their connection with the NF-κB transcriptional response. As such a genome-wide analysis of NF-κB RelA binding sites with hypoxia stimulation will enable to identify direct targets of the NF-κB with hypoxia stimulation and differentiate the TNF-α induced gene signatures. At present, even TNF-α ChIP-seq datasets for NF-κB are limited, and such analysis in hypoxia has not been done in any cellular system. In order to do this, a CUT and RUN experiment was planned and optimisation of the assay was initiated (**Chapter 9**).

With the experiments investigating the role of KDM5A on the H3K4me3 hypoxia upregulated gene peaks, KDM5A acts as a negative regulator for H3K4me3 at the EDN1, DUSP1, MARCKS, JUN and KDM6B gene promoters (**Figure 3.9**). Also, based on 1 siRNA oligonucleotide, KDM5A was identified as a negative regulator of these genes (**Figure 3.10**). Additional experiments using an independent siRNA sequence are therefore needed to support these observations. Given these results, KDM5A is anticipated to demethylase H3K4me3 and thus negatively regulate the potential NF-κB target genes. However, this requires additional experimentation. In this case, siRNA or inducible degron systems (217, 218) could be used to deplete the endogenous KDM5A, then rescue experiments with KDM5A wild type or JmjC demethylase dead mutant plasmids, investigating the gene promoter methylation levels and expression of the H3K4me3 upregulated gene peaks could be conducted. Recently Zhou *et al.* has shown that KDM5A significantly downregulates NF-κB RelA mRNA and protein levels in chronic myeloid leukaemia cell lines in a histone demethylation-dependent manner by directly binding to the RelA promoter locus (219). This study supports the direct regulatory role of the KDM5A on RelA through its enzymatic activity (219). However, further work is

needed to clarify this in hypoxia context and by looking at the KDM5A binding to NF-κB target gene promoters and its effect on their expression.

Using a reporter gene assay, a positive regulatory effect of KDM5A on NF-κB activity was observed in HeLa and A549 cells by depleting the KDM5A prior to quantifying the κB activity (**Figure 3.11**, **B** and **C**). Although TNF-α stimulation following KDM5A depletion did not change the NF-κB activity in HeLa cells (**Figure 3.12**, **A**), it increased in A549 cells (**Figure 3.12**, **B**). This indicated that KDM5A is not necessary for NF-κB activity in TNF-α stimulated A549 cells but it is needed in HeLa cells. The results obtained from HeLa cells could be the consequence of the human papilloma virus proteins, E6 and E7 disturbing the normal functioning of protein systems (220). Also, in the case of A549 cells, majority of lung cancer cell lines have been shown to contain mutations in the SWI/SNF subunits, which is a chromatin remodelling complex and a necessary element in transcriptional mechanisms (221).

Moreover, the negative regulatory effect of KDM5A on NF-κB activity was observed in U2OS cells (**Figure 3.11**, **D**). Similar to HeLa cells, TNF-α stimulation following KDM5A depletion decreased the NF-κB activity in U2OS cell lines, showing that KDM5A is necessary for suppressing possible negative regulatory mechanisms present in the NF-κB system (**Figure 3.12**, **C**). Using this artificial luciferase reporter system, it is implied that these promoters do not possess a chromatin environment. This suggests that KDM5A can control NF-κB activity following TNF-α via an intermediary mechanism or by acting on NF-κB subunits directly. Supporting our findings in U2OS cells, another group indicated that KDM5A is necessary for the activation of TNF-α induced NF-κB pathway (222). This study was based on gene set enrichment analysis performed with RNA-seq results obtained from KDM5A knock-out osteosarcoma cells. Additional work investigating how KDM5A depletion alters basal and TNF-α induced genes such as IκB-α, IL-8, TNFAIP3 and others would be interesting to determine KDM5A role in this response.

To this date, several studies have already shown an association between KDM5A and NF-κB with different inducers and in various cellular backgrounds. As such, KDM5A has

been shown to associate with NF-κB p50 and decrease H3K4me3 modification at the promoter region of the cytokine signalling suppressor, SOCS1, leading to the activation of the innate immune response (203). Another study conducted on the model organism, *Drosophila melanogaster* has shown that demethylase activity of KDM5 ortholog transcriptionally regulates the immune deficiency signalling pathway that shares high similarities with the canonical NF-κB pathway in vertebrates, activated by TNF receptor (202). Moreover, KDM5A was shown to be critical for H3K4 demethylation and transcriptional gene silencing by cooperating with E2F, which is a known co-regulator of NF-κB that interacts and represses the activation of the NF-κB during cell cycle progression (223, 224).

Given the importance of NF-κB in regulating wide ranges of different cellular processes including immune and inflammatory responses and regulation of cell growth, survival, and development; understanding its transcriptional machinery has been crucial. Enzymatic deactivation of the KDM5A in hypoxia and the role of H3K4me3 levels has shown a promising mechanism that with further research could clarify the gene expression networks in different physiological and pathological conditions.

To summarise, this chapter has indicated the role of oxygen sensing mechanism of the chromatin and H3K4me3 demethylase, KDM5A on the transcriptional regulation of potential NF-κB target genes. KDM5A is identified as a negative regulator of the H3K4me3 promoter regions and gene expressions that are responsive to both hypoxia and NF-κB RelA, speculating the role of KDM5A on NF-κB transcriptional regulatory mechanisms.

Chapter 4 - NF-κB target genes are enriched in H3K36me3 sites following hypoxia in HeLa cells

4.1. Introduction

This chapter focuses on another hypoxia induced post-translational modification (PTM) on histone 3 (H3). Methylation of the histone 3 lysine 36 (H3K36) is associated with active gene transcription (225), and specifically, trimethylation of the H3K36 (H3K36me3) is enriched on the gene bodies of the actively transcribed genes (197). This methylation mark is deposited by a histone methyltransferase called, SETD2 (226). SETD2 binds to the C-terminal domain of elongation-competent form of RNA polymerase II and catalyses H3K36me3 at the gene bodies of the actively transcribed genes (227). SETD2-dependent trimethylation of the H3K36 supresses false transcriptional initiation within the gene bodies, ensuring fidelity of the gene transcription (228). H3K36me3 plays a role in chromatin modification with its antagonistic effect on other PTMs. As such the presence of H3K36me3 impairs trimethylation of H3K27 by repressing the histone methyltransferase enzyme, polycomb repressive complex 2 (PRC2) (229). Furthermore, H3K36me3 involves in the regulation of mRNA splicing (reviewed in (230)). Also, it is an important methylation mark during DNA damage response, where it serves as the docking site for recruiting a key mismatch repair sensor, hMutSα (hMSH2-hMSH6), which inspects DNA for damage repair during both DNA replication and gene transcription (231).

Trimethylation of the H3K36 can be reversed by KDM4 and KDM2 family members, belonging to the Jumonji C (JmjC)-containing lysine-specific histone demethylases (KDMs). Similar to the key regulators of the hypoxia response, prolyl hydroxylase domain (PHD) and factor inhibiting hypoxia inducible factor (FIH), KDMs are 2-oxoglutarate dependent dioxygenases that require oxygen for their enzymatic activity (39, 99).

As mentioned before, changes in histone methylation have been described in hypoxia in different cellular systems (39, 199). Also, recently it has been shown in multiple studies that chromatin can sense oxygen changes and regulate gene expression through the inactivation of KDMs in hypoxia, independent of the main hypoxia stimulated transcription factor family, hypoxia inducible factor (HIF) (110, 117). In addition, KDM2 and KDM4 members have been

shown to be induced in low oxygen conditions (reviewed in (199); (120)). However, at present it is not known which KDM is responsible for the increase of H3K36me3 in hypoxia.

Activation of the NF-κB is a critical component in the transcriptional response to hypoxia. It has been shown previously that hypoxia stimulation can modulate NF-κB dependent gene expressions (148, 151, 152, 232). Independent to hypoxia stimulation, H3K36me3 histone methylation (233-235), histone demethylases, KDM2 (170, 236, 237) and KDM4 (238, 239) have been linked to NF-κB by regulating a multitude of immune and inflammatory responses. However, further research is needed to elucidate the link between hypoxia and NF-κB transcriptional response in the context of histone methylation.

In this chapter, H3K36me3 levels in response to hypoxia were investigated for their association with the NF-κB transcriptional response. Using Chromatin immunoprecipitation-sequencing (ChIP-seq) datasets, hallmark pathway enrichment analysis was performed focusing on NF-κB transcriptional signature. Identified potential NF-κB target genes were validated for hypoxia stimulation and H3K36me3 methylation. Also, the role of KDM2A, KDM4A, KDM4B and KDM4C in modulating NF-κB activity was determined. This work demonstrates that both hypoxia stimulation and depletion of the H3K36me3 associated KDMs potentially regulate the hypoxia-induced NF-κB target gene signature.

4.2. Identification and validation of potential NF-κB target genes enriched with H3K36me3 with hypoxia stimulation

Previously in our group, chromatin immunoprecipitation (ChIP) followed by sequencing was performed to evaluate H3K36me3 histone modifications associated with gene transcription in HeLa cells at normoxia or after 1 hour of hypoxia exposure (**Figure 4.1**). Using these differential DNA binding analysis from Batie *et al.* (117), dataset available in NCBI GEO database with accession numbers GSE120339 (https://www.ncbi.nlm.nih.gov/geo/query/acc.cgi?acc=GSE120339), hallmark pathway association analysis was performed focusing on NF-κB transcriptional signature (**Table 4.1**).

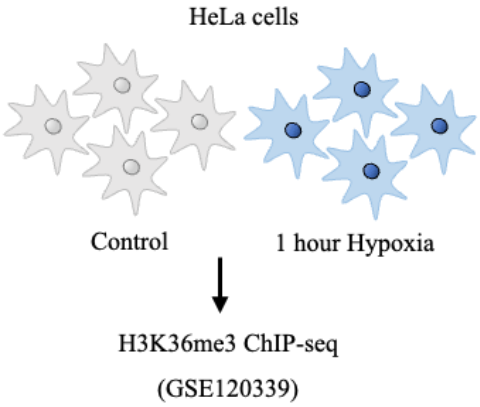

Figure 4.1. H3K36me3 ChIP-seq differential expression peak calling. H3K36me3 ChIP-seq experiment with 1 hour of hypoxia stimulation of HeLa cells.

The pathway enrichment analysis was performed on WEB-based Gene SeT AnaLysis Toolkit (WebGestalt), using hallmark gene sets obtained from Molecular Signature Database (187, 204). Hallmark gene sets were compared with low stringency H3K36me3 hypoxia upregulated gene peaks, which were shown to be increased at least 2 out of 3 biological replicates of the ChIP-seq experiments. As a result, a list of different pathways was shown to be significantly enriched with H3K36me3 methylation mark (**Table 4.1**). Both hypoxia signalling pathway and TNF-α induced NF-κB signalling pathways were identified to be significantly enriched with genes listed in H3K36me3 data set.

Table 4.1. Pathway association analysis of H3K36me3 ChIP-seq peaks after 1 hour hypoxia treatment. H3K36me3 low stringency ChIP-seq peaks with 1 hour hypoxia treatment overlap with gene groups identified using WEB-based Gene SeT AnaLysis Toolkit with FDR cut off ≤0.05. Numbers in brackets represent the number of genes in the gene group used as a reference.

Gene Set	Overlapping genes	P Value	FDR
UV Response (143)	49	1.55E-14	7.62E-13
Mitotic Spindle (197)	45	4.37E-07	1.0702E-05
G2M Checkpoint (195)	43	2.204E-06	3.5998E-05
Epithelial Mesenchymal Transition (197)	43	3.8855E-06	4.7597E-05
Androgen Response (98)	25	2.4738E-05	0.00024243
TNF-α signalling via NF-κB (199)	40	0.00005159	0.00042132
Hypoxia (199)	35	0.0020179	0.014125

To further support the information generated by ChIP-seq in hypoxia induced regulatory mechanisms, a merged list of genes enriched with H3K36me3 methylation mark was overlapped with hypoxia RNA-seq dataset, which was previously produced in the Rocha lab by exposing HeLa cells to 16- and 24-hours of hypoxia. As a result, 94 of these genes were detected in both H3K36me3 ChIP-seq and hypoxia RNA-seq datasets. 40 of them were overlapped with publicly available NF-κB hallmark gene set, where 5 of them were also identified in all 3 datasets (**Figure 4.2**, **A**). These results indicate that H3K36me3 ChIP-seq and hypoxia RNA-seq analysis share a group of genes that possibly has similar transcriptional regulatory network, and a list of them is identified to correlate with the NF-κB system. Furthermore, NF-κB target genes listed by the Gilmore laboratory was used to identify additional genes that overlap with the H3K36me3 ChIP-seq peaks (https://www.bu.edu/nf-kb/gene-resources/target-genes/). Supplementary to the genes identified by overlapping H3K36me3 ChIP-seq with the NF-κB hallmark genes set, 28 more NF-κB target genes were identified from the Gilmore laboratory's genes list (**Figure 4.2**, **B**).

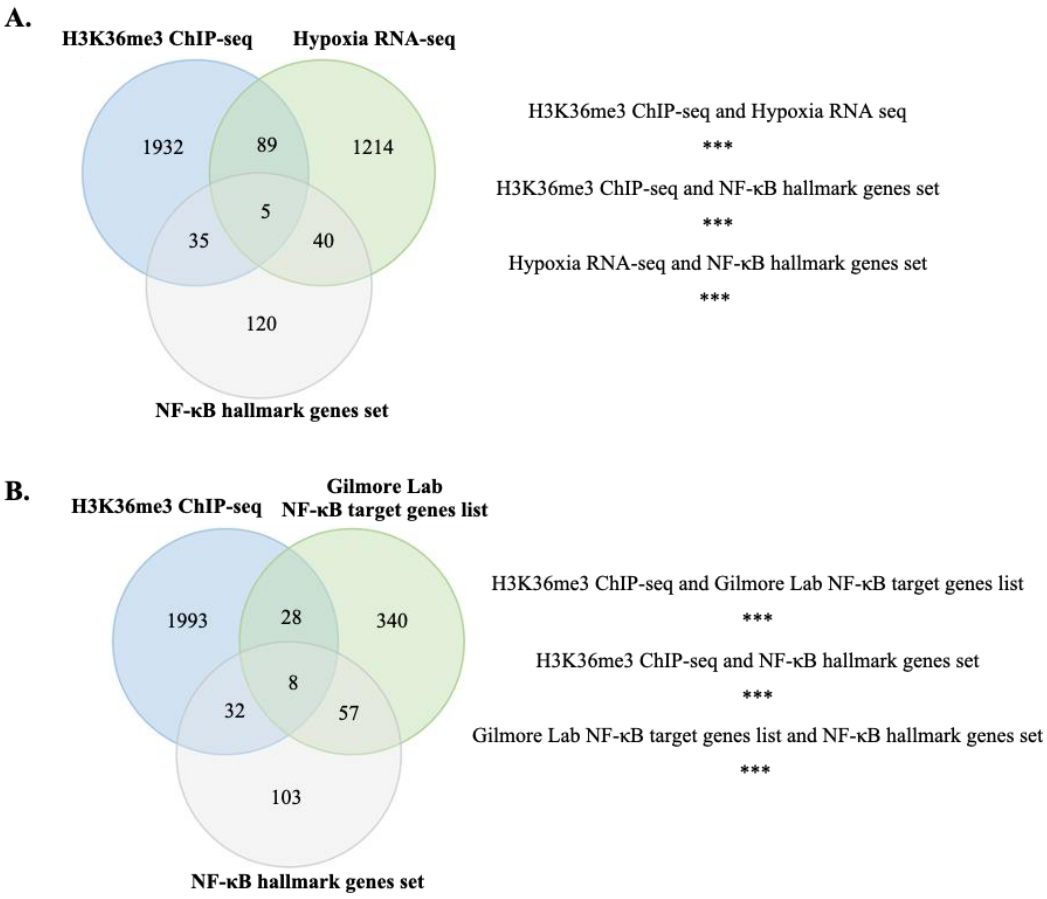

Figure 4.2. Overlap of H3K36me3 ChIP-seq peaks with other datasets. A. Individual genes included in H3K36me3 ChIP-seq dataset with 1 hour of hypoxia stimulation were compared with upregulated genes in RNA-seq analysis following 16- and 24-hours hypoxia stimulation previously performed in Rocha laboratory, and publicly available NF-κB hallmark gene set. **B.** H3K36me3 ChIP-seq dataset was overlapped with NF-κB hallmark gene set and NF-κB target genes list identified by the Gilmore lab. P value for overlaps were calculated by hypergeometric test. *** $p \leq 0.001$.

From the overlapped lists, genes that are present in both H3K36me3 ChIP-seq and NF-κB hallmark genes sets, as well as the genes that are also common in hypoxia RNA-seq gene set are listed in **Table 4.2**. Also, the additional genes identified by overlapping H3K36me3 ChIP-seq and Gilmore laboratory's NF-κB target genes are listed in **Table 4.3**. Listed genes were described for their molecular function using the information obtained from GeneCards database (https://www.genecards.org) (**Table 4.2** and **Table 4.3**). Also, Gene Ontology (GO) enrichment analysis was performed using WebGestalt Toolkit looking to further define the molecular function of the genes found in both NF-κB hallmark genes set and Gilmore laboratory's NF-κB target genes list (**Figure 4.3**). Based on this analysis, the top

significantly enriched GO terms included “cytokine activity” and “Transcription regulatory DNA binding”. These results indicate that high number of H3K36me3 enriched genes that are correlated with the NF-κB system possibly have active roles on the transcriptional machinery.

Next, high stringency H3K36me3 hypoxia upregulated promoter peak changes were selected for further validation by ChIP-qPCR (**Table 4.2** and **Table 4.3**). The selected gene peaks were shown to be increased in all biological replicates of the ChIP-seq experiment (**Figure 4.4**). Among the H3K36me3 hypoxia upregulated high stringency gene peaks, the following were identified in either NF-κB hallmark genes set or Gilmore laboratory’s NF-κB target genes list; BHLHE40 (Basic Helix-Loop-Helix Family Member E40), which encodes a transcriptional regulator, mainly known to control the cell cycle and regulation of the genes associated with the circadian rhythm (240) (**Figure 4.4, A**); FTH1 (Ferritin Heavy Chain 1), which controls intracellular iron distribution, is essential for many biological processes such as DNA and RNA synthesis, cell proliferation and differentiation (241) (**Figure 4.4, B**); DUSP1 (Dual Specificity Phosphatase 1), which has a central role in cellular responses to environmental stress, also negatively regulates the inflammatory responses (210, 211) (**Figure 4.4, C**); MARCKS (Myristoylated alanine-rich C-kinase substrate), which is an actin filament cross-linking protein, plays important roles in cell motility, phagocytosis, transmembrane transport, and regulation of the cell cycle (207) (**Figure 4.4, D**); MYC (MYC Proto-Oncogene, BHLH Transcription Factor), which is known to potentially regulate the transcription of at least 15% of the entire genome with major downstream effectors including those involved in protein translation, cell cycle progression and metabolism (242) (**Figure 4.4, E**); SGK1 (Serum/Glucocorticoid Regulated Kinase 1), which involves in the regulation of ion channels, membrane transporters, cellular enzymes, transcription factors including NF-κB, and cell growth and proliferation (243) (**Figure 4.4, F**); TSC22D1 (Transforming Growth Factor Beta-1-Induced Transcript 4 Protein), which is a transcriptional repressor, involves in cellular differentiation, growth inhibition and apoptosis (244) (**Figure 4.4, G**); CXCL2 (C-X-C Motif Chemokine Ligand 2), which involves in immune and inflammatory responses, specifically

neutrophil trafficking (245) (**Figure 4.4, H**); PTPN13 (Protein Tyrosine Phosphatase Non-Receptor Type 13), which is associated with pro-apoptotic signalling, cytokinesis and cell cycle progression(246) (**Figure 4.4, I**).

Table 4.2. HeLa H3K36me3 hypoxia upregulated ChIP-seq gene peaks that are potential NF-κB target genes with their known molecular functions.

Genes identified common in H3K36me3 ChIP-seq low stringency, and NF-κB hallmark genes. Genes also identified common in Hypoxia RNA-seq data set are listed within the "green box". High stringency H3K36me3 hypoxia upregulated promoter peak changes selected for further validation (**bold**). Genes that are also identified in H3K4me3 ChIP-seq list are marked with "the asterisk". Genes with transcriptional regulatory role are highlighted in blue. Gene function summary was obtained from GeneCards database (https://www.genecards.org).

Gene Name	Ensemble Gene ID	Gene Function Summary
KLF6*	ENSG00000067082	B-cell growth and development
ATP2B1	ENSG00000070961	Intracellular calcium homeostasis
EDN1*	ENSG00000078401	Vasoconstriction
CXCL2	**ENSG00000081041**	Immunoregulatory and inflammatory processes
NFKBIA*	ENSG00000100906	Immune and inflammatory responses
TSC22D1	**ENSG00000102804**	Cellular development and differentiation
NFAT5	ENSG00000102908	Osmotic stress and inflammatory responses
KYNU	ENSG00000115919	Catalyses the cleavage of kynurenine into anthranilic acid
NFE2L2	ENSG00000116044	Oxidative stress response and inflammation
GADD45A	ENSG00000116717	Environmental stress response. DNA excision repair
SGK1*	**ENSG00000118515**	Cell survival, neuronal excitability, and renal sodium excretion
KLF9	ENSG00000119138	Oxidative stress response
DUSP1*	**ENSG00000120129**	Environmental stress response and regulation of cell proliferation
IL6ST	ENSG00000134352	Immune responses, haematopoiesis, pain control and bone metabolism
IL6	ENSG00000136244	Immune and inflammatory responses
TANK	ENSG00000136560	Inflammatory and DNA damage responses
KLF4*	ENSG00000136826	Cell proliferation and differentiation
MYC	**ENSG00000136997**	Cell cycle progression, apoptosis, and cellular transformation
SIK1*	ENSG00000142178	Cell cycle regulation, gluconeogenesis and lipogenesis regulation, muscle growth and differentiation
MCL1	ENSG00000143384	Regulation of apoptosis and cell survival
PLK2	ENSG00000145632	Centriole duplication and G1/S phase transition in cell cycle
TNFAIP8	ENSG00000145779	Regulation of apoptosis
IL18	ENSG00000150782	Immune and inflammatory responses
BTG3	ENSG00000154640	Cell proliferation
MARCKS*	**ENSG00000155130**	Cell motility, phagocytosis, membrane trafficking and mitogenesis
ETS2	ENSG00000157557	Cell development and apoptosis
B4GALT5	ENSG00000158470	Synthesis of lactosylceramide via the transfer of galactose
PDLIM5	ENSG00000163110	Scaffold for the formation of multiprotein complexes
TIPARP	ENSG00000163659	Mono-ADP-ribosylation of glutamate, aspartate, and cysteine residues
CCNL1	ENSG00000163660	Regulation of RNA polymerase II
PTGER4	ENSG00000171522	Cellular responses to Prostaglandin E_2
EIF1	ENSG00000173812	RNA binding activity. Regulation of translational initiation
TGIF1	ENSG00000177426	Transcriptional repression of SMAD2. Inhibition of retinoic acid responsive element
MSC	ENSG00000178860	E2A protein inhibitor. B-cell differentiation
PDE4B	ENSG00000184588	Cellular concentrations of cyclic nucleotides. Signal transduction
PTGS2	ENSG00000073756	Prostaglandin biosynthesis
CCL2	ENSG00000108691	Immunoregulatory and inflammatory processes
F3*	ENSG00000117525	Initiates the blood coagulation cascades
BHLHE40*	**ENSG00000134107**	Control of circadian rhythm and cell differentiation
PNRC1	ENSG00000146278	Signal transduction

Table 4.3. HeLa H3K36me3 hypoxia upregulated ChIP-seq gene peaks that are NF-κB target genes with their molecular functions.

Genes identified common in H3K36me3 ChIP-seq low stringency, and Gilmore lab NF-κB target genes list that is identified additional to NF-κB hallmark genes list. High stringency H3K36me3 hypoxia upregulated promoter peak changes selected for further validation (**bold**). Genes with transcriptional regulatory role are highlighted in blue. Gene function summary was obtained from GeneCards database (https://www.genecards.org).

Gene Name	Ensemble Gene ID	Gene Function Summary
GCLC	ENSG00000001084	Glutathione synthesis
REV3L	ENSG00000009413	Translesion DNA synthesis
GCLM	ENSG00000023909	Glutathione synthesis
VIM	ENSG00000026025	Maintaining cell shape and integrity. Cell attachment, migration, and signalling
KITLG	ENSG00000049130	Cell survival and proliferation, development and migration. Haematopoiesis, stem cell maintenance, and Gametogenesis.
MYLK	ENSG00000065534	Myosin interaction with actin filaments
HIF1A	ENSG00000100644	Metabolic adaptation to hypoxia. Energy metabolism, angiogenesis, and apoptosis
PGK1	ENSG00000102144	Glycolysis
CDK6	ENSG00000105810	Cell cycle progression
TFPI2	ENSG00000105825	Regulation of plasmin-mediated matrix remodelling
NR3C1	ENSG00000113580	Glucocorticoid response. Inflammatory responses, cellular proliferation, and differentiation
SH3BGRL	ENSG00000131171	Protein-to-protein interactions
THBS1	ENSG00000137801	Cell-to-cell and cell-to-matrix interactions
IFI44L	ENSG00000137959	Antiviral and antibacterial responses
NFKBIZ	ENSG00000144802	Regulation of NF-κB transcription factor complexes
CCL28	ENSG00000151882	Immunoregulatory and inflammatory processes
PTPN13	**ENSG00000163629**	Cell growth, differentiation, and mitotic cycle
IL15	ENSG00000164136	T and natural killer cell activation and proliferation
FTH1	**ENSG00000167996**	Intracellular iron storage
BMI1	ENSG00000168283	Embryonic development and self-renewal in somatic stem cells DNA damage repair
PTEN	ENSG00000171862	Cell cycle progression and survival
BDNF	ENSG00000176697	Growth and differentiation of neurons
DPYD	ENSG00000188641	Catalyses the reduction of uracil and thymine
S100A10	ENSG00000197747	Cell cycle progression and differentiation
S100A6	ENSG00000197956	Cell cycle progression and differentiation
MBP	ENSG00000197971	Formation and stabilisation of myelin membrane on nerves
ASPH	ENSG00000198363	Calcium homeostasis
HMGN1	ENSG00000205581	Altering interaction between the DNA and the histone octamer

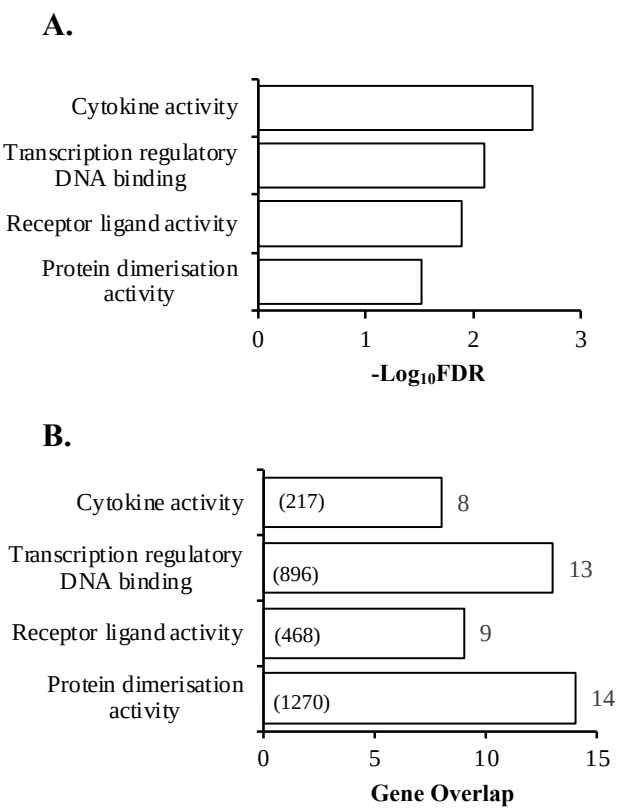

Figure 4.3. Gene Ontology (GO) enrichment analysis of the common genes found in H3K36me3 ChIP-seq and NF-κB hallmark genes set combined with Gilmore lab NF-κB target genes list. A. Top 4 significantly enriched GO terms of the molecular functions were identified using WEB-based Gene SeT AnaLysis Toolkit with FDR cut off ≤0.05. The adjusted statistically significant values were negative 10-base log transformed. **B.** Number of genes overlap in each molecular function category. Numbers in brackets represent the number of genes in each gene group used as a reference.

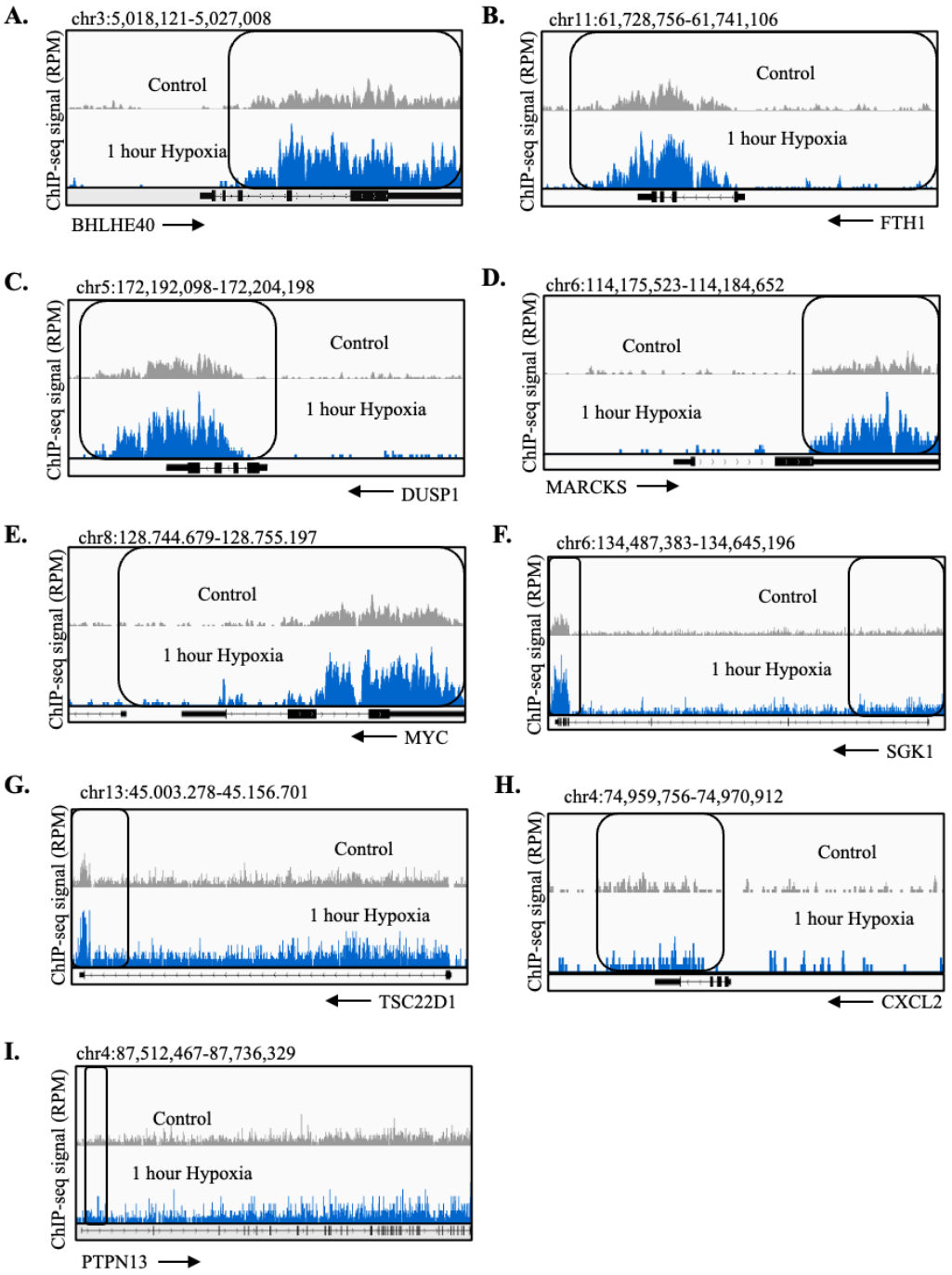

Figure 4.4. Hypoxia ChIP-seq coverage tracks of H3K36me3 peaks at different putative NF-κB target genes. Coverage tracks and peaks from H3K36me3 ChIP-seq 1 hour of hypoxia high stringency dataset at BHLHE40 (**A**), FTH1 (**B**), DUSP1 (**C**), MARCKS (**D**), MYC (**E**), SGK1 (**F**), TSC22D1 (**G**), CXCL2 (H), and PTPN13 (I). Peak start and end area is shown in a black framed rectangle. Forward stranded genes are shown with arrows directing to right side, reverse stranded genes are shown with arrows directing to the left side. Chromosomal information is shown at the top of each image with 3000 bp upstream of transcription start side (TSS) to 3000 bp downstream of transcription end side (TES). Integrative Genomics Viewer (IGV) software was used for the figure illustration.

To validate the effect of hypoxia on the expression of the selected genes, HeLa cells were exposed to 1% oxygen at different time points prior to qPCR analysis (**Figure 4.5**). In this analysis, efficiency of the hypoxia stimulation was measured using a known hypoxia-inducible gene, Carbonic Anhydrase (CA9) (**Figure 3.5, A**). As a result, mRNA expression of DUSP1 and MARCKS was increased at all hypoxia time points as it was shown in the previous chapter (**Figure 3.5**, **D** and **F**). BHLHE40 mRNA expression was increased significantly at all hypoxia time points (**Figure 4.5**, **A**). Also, FTH1 expression was significantly increase at 1 and 24 hours of hypoxia, whereas MYC expression was significantly increased only at 24 hours of hypoxia stimulation (**Figure 4.5**, **B** and **C**). The rest of the selected genes did not show a significant increase by being exposed to 1% oxygen (**Figure 4.5**, **D**, **E**, **F**, and **G**). These results suggest that H3K36me3 hypoxia upregulated promoter regions could identify some of the hypoxia inducible genes. As MYC, SGK1, TSC22D1, CXCL2, and PTPN13 showed the least or no increase with hypoxia stimulation in most of the time points, these genes were not included in subsequent analysis (**Figure 4.5**, **C**, **D**, **E**, **F**, and **G**).

H3K36me3 levels on the selected genes following 1- and 24-hours of hypoxia stimulation were investigated by using the ChIP-qPCR method. H3K36me3 methylation was quantified using specific set of primers designed for the predicted binding sites of the genes selected based on coordinates obtained in the ChIP-sequencing experiments. This experiment was repeated four times by using the Cell Signalling antibody (cat. #4909) while immunoprecipitating the H3K36me3 protein on the cross-linked chromatin (**Figure 4.6, A**). As a result, there was no significant change at the methylation levels with the hypoxia stimulation at BHLHE40 and FTH1 genes (**Figure 4.6, B** and **C**). Hypoxia stimulation increased the H3K36me3 levels at both DUSP1 and MARCKS gene peaks (**Figure 4.6, D** and **F**). However, each replicate of this experiment showed highly variable results and could not reach to a conclusion. In addition, although t-test was used to statistically analyse the data in Figures 4.5 and 4.6, one-way ANOVA should have been used, as population means of more than two groups were being compared.

Previously, a H3K36me3 Active Motif antibody (cat. #61101) was optimised and used in the H3K36me3 ChIP-seq experiments, since it was ChIP-validated by the vendor. To further test the results found in **Figure 4.6**, H3K36me3 hypoxia peak change was investigated using the same antibody that was used in the ChIP-seq experiments (**Figure 4.7**). As a result of the one biological replicate, hypoxia stimulation increased the H3K36me3 levels more than 2-folds in all the investigated gene peaks. This experiment will need to be repeated with the same conditions and antibody.

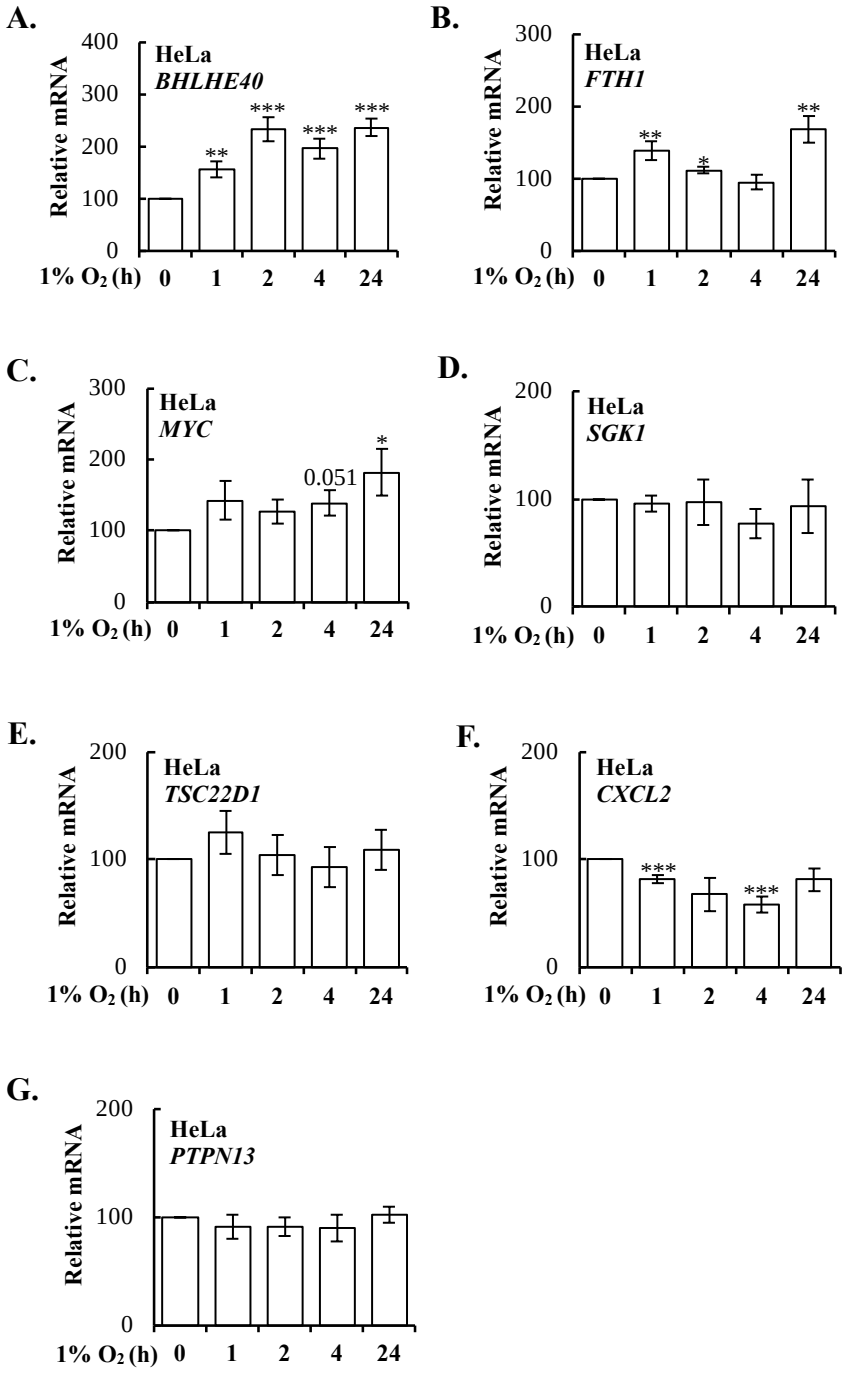

Figure 4.5. Hypoxia induction of genes with H3K36me3 hypoxia upregulated peaks. HeLa cells were exposed to 0, 1, 2, 4, and 24 hours 1% O_2 before proceeding to total RNA extraction and cDNA conversion. Relative mRNA expression levels of the indicated genes were analysed by qPCR using ACTB as a normalising gene. Graphs represent mean and standard error of a minimum of three independent experiments. Student t-test was applied, and significance determined as follows: * $p \leq 0.05$, ** $p \leq 0.01$, *** $p \leq 0.001$.

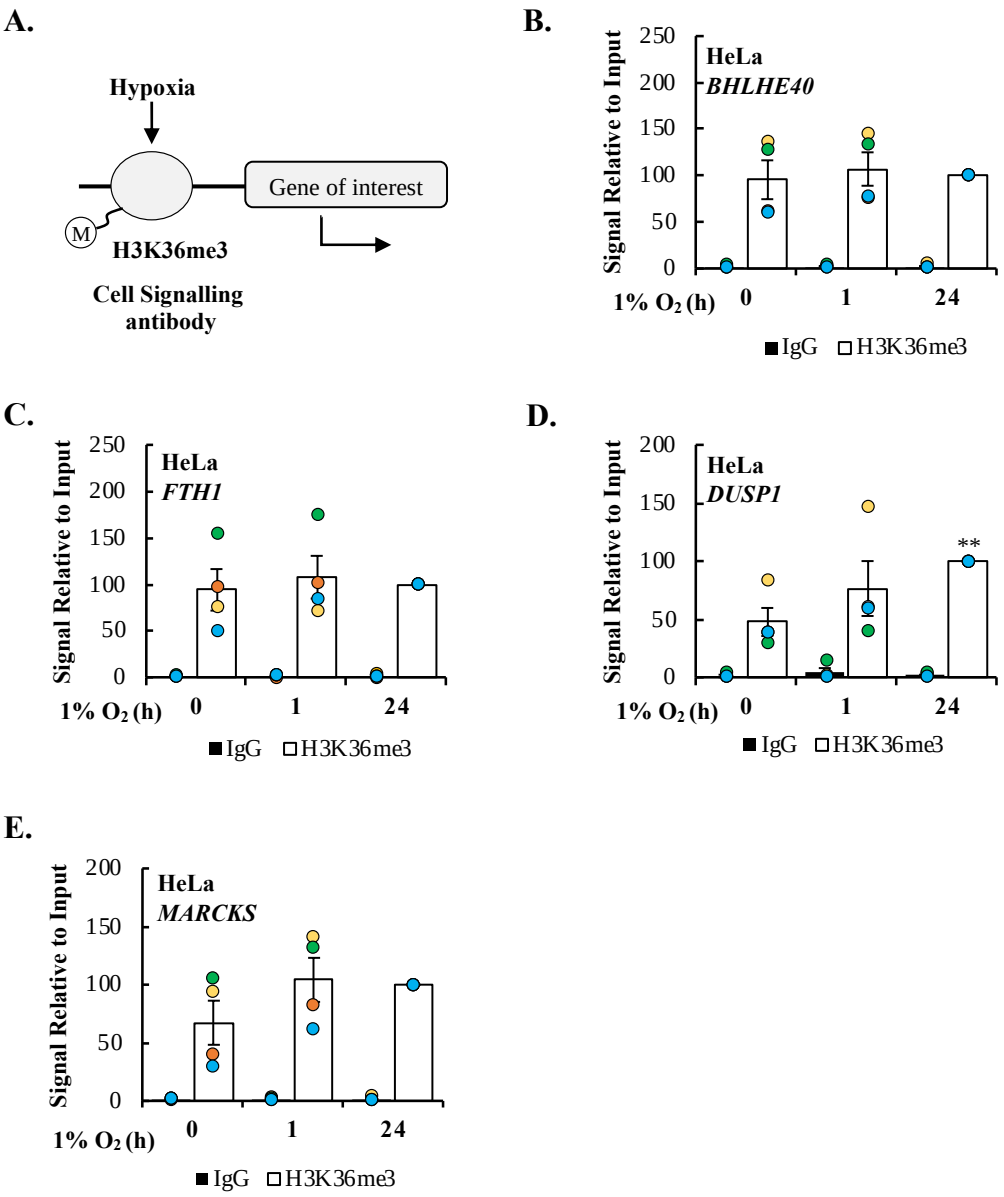

Figure 4.6. H3K36me3 hypoxia peak change validation by ChIP-qPCR. HeLa cells were exposed to 0, 1 or 24 hours 1% O_2 prior to cross-linking and lysis. ChIP was performed for an IgG control and H3K36me3 enriched genes' promoter region occupied by H3K36me3 promoter peak. Cell Signalling antibody (cat. #4909) was used for the immunoprecipitation of the H3K36me3. DNA was analysed by qPCR with results normalised to 2% input DNA. Graphs represent mean and standard error of four independent experiments. Individual replicates are shown scattered on top of each condition, represented with different colours; replicate 1 (orange), replicate 2 (yellow), replicate 3 (green), and replicate 4 (blue). Student t-test was applied, and significance determined as follows: * $p \leq 0.05$, ** $p \leq 0.01$, *** $p \leq 0.001$.

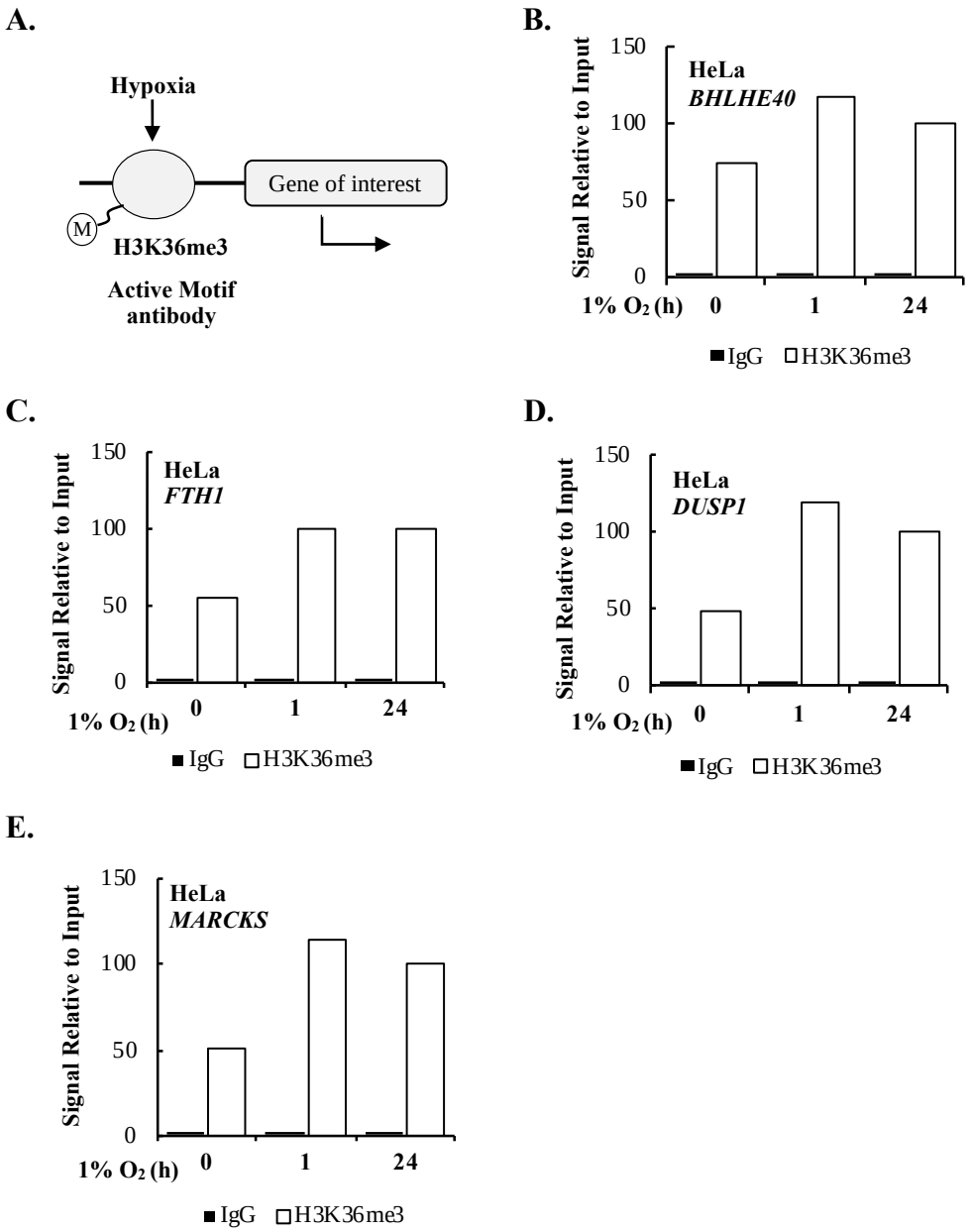

Figure 4.7. H3K36me3 hypoxia peak change validation by ChIP-qPCR. HeLa cells were exposed to 0, 1 or 24 hours 1% O_2 prior to cross-linking and lysis. ChIP was performed for an IgG control and H3K36me3 enriched genes' promoter regions occupied by the H3K36me3 promoter peaks. Active Motif antibody (cat. #61101) was used for the immunoprecipitation of the H3K36me3. DNA was analysed by qPCR with results normalised to 2% input DNA. Graphs represent 1 replicate of the experiment.

Although, the genes selected are reported to be NF-κB dependent, this was further validated by using an overexpression experiment. Cells were transfected with a RelA plasmid prior to qPCR analysis for the genes selected above (**Figure 3.7, A**). As already shown in the previous chapter DUSP1 and MARCKS mRNA level expressions were increased with the RelA overexpression (**Figure 3.7**, **D** and **F**). Additionally, BHLHE40 and FTH1 mRNA expression was significantly increased with RelA overexpression (**Figure 4.8**, **A** and **B**). These results indicate that upregulated gene peaks identified at H3K36me3 hypoxia lists are associated with NF-κB activation.

To further support the connection of these genes with the NF-κB transcriptional response, NF-κB RelA ChIP-seq Atlas dataset was used (https://chip-atlas.org/, (212)) and RelA binding sites were compared with the H3K36me3 gene peaks (**Figure 4.9, A**). As a result, there was a statistically significant overlap between H3K36me3 hypoxia enriched genes and RelA ChIP-seq Atlas dataset. Also, based on the pathway enrichment analysis performed using the hallmark gene sets, both hypoxia, and TNF-α stimulated NF-κB were at the top 8 signalling pathways significantly enriched with these genes (**Figure 4.9, B**). Importantly, the genes overlapped in the NF-κB hallmark and H3K36me3 gene sets were also identified in the RelA ChIP-seq Atlas data set. This indicates that H3K36me3 enriched genes have RelA binding sites and thus RelA potentially regulates their transcriptional expression. However, this needs to be validated with further experiments.

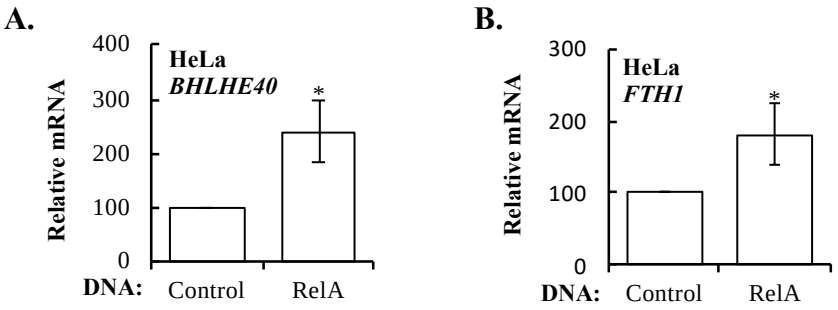

Figure 4.8. RelA overexpression increases the mRNA expression of H3K36me3 hypoxia upregulated peaks. HeLa cells were transfected with control (empty vector) and RelA plasmid DNA 48 hours prior to total RNA extraction and cDNA conversion. Relative mRNA expression levels of the indicated genes were analysed by qPCR using ACTB as a normalising gene. Graphs represent mean and standard error of a minimum of three independent experiments. Student t-test was applied, and significance determined as follows: * $p \leq 0.05$, ** $p \leq 0.01$, *** $p \leq 0.001$.

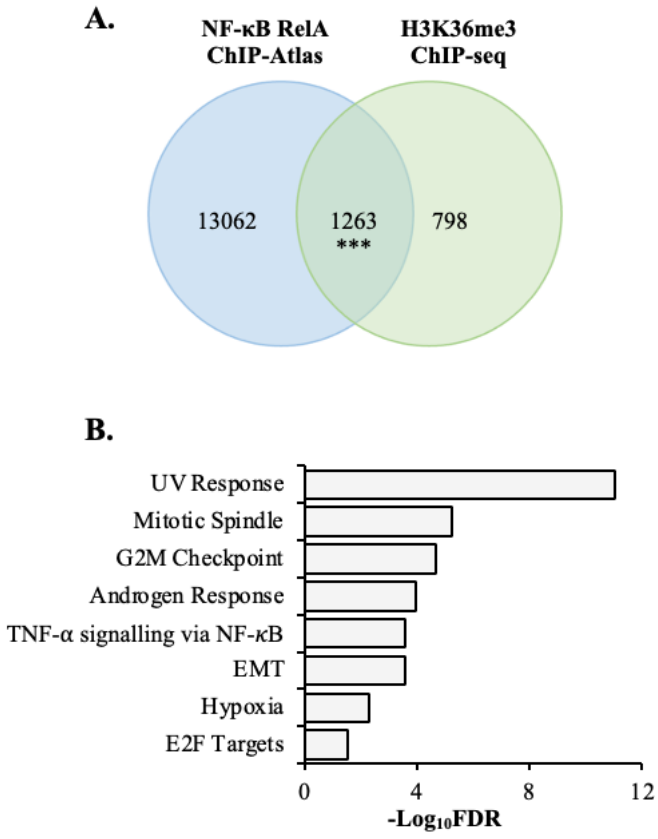

Figure 4.9. Overlap of RelA ChIP-seq Atlas and H3K36me3 ChIP-seq peaks. A. Individual genes included in H3K36me3 ChIP-seq datasets with 1 hour hypoxia stimulation were compared with publicly available NF-κB RelA ChIP-seq Atlas, containing list of genes with RelA DNA binding sites. **B.** Pathway association analysis of the overlapped genes identified in the H3K36me3 ChIP-seq and NF-κB RelA ChIP-seq Atlas peaks was performed using WEB-based Gene SeT AnaLysis Toolkit with FDR cut off ≤0.05. The adjusted statistically significant values were negative 10-base log transformed. P value for the overlap was calculated by hypergeometric test. *** $p \leq 0.001$.

4.3. Regulation of NF-κB target gene expression and H3K36me3 levels by KDMs

The results shown above demonstrate that H3K36me3 methylation mark increases with hypoxia stimulation at selected NF-κB target genes (**Figure 4.7**). Unlike H3K4me3, previous studies had not identified which KDM was responsible for the increases in H3K36me3 observed in hypoxia. As such, we asked which known H3K36me3 associated KDMs contribute to the hypoxia induced histone methylation levels of H3K36me3. First, we investigated if KDM4A, KDM4B, KDM4C and KDM2A depletion could affect the global H3K36me3 levels. To test this, an immunofluorescence (IF) method was used following the siRNA knockdown of the KDMs individually (**Figure 4.14**, **A**). This analysis revealed that H3K36me3 levels significantly increase 1.37- and 1.45-fold with KDM4A or KDM4B depletion, respectively (**Figure 4.10, A** and **B**). KDM2A depletion significantly increased the methylation mark 1.22-fold (**Figure 4.10, A** and **B**). KDM4C depletion increased the H3K36me3 levels by the least amount, which was identified as 1.06-fold. These results suggest that, in HeLa cells, KDM4A and KDM4B are dominant in removing H3K36me3.

Next, the effect of KDM4A knock down on the H3K36me3 levels was tested on the selected H3K36me3 hypoxia upregulated gene peaks. KDM4A was depleted using two different oligonucleotides, then H3K36me3 was immunoprecipitated by using the same Active Motif antibody used in **Figure 4.7**, and its levels present at the gene promoters selected were measured using specific primer sets designed for the predicted sites in the genes as obtained by the sequencing experiments (**Figure 4.11**, **A**). H3K36me3 levels were slightly increased at the BHLHE40 gene with the depletion of KDM4A oligo 1 but not with oligo 2 (**Figure 4.11**, **C**). The methylation levels were also slightly increased at FTH1 and MARCKS gene peaks but not at DUSP1 gene (**Figure 4.11**, **D**, **F** and **E**).

Similarly, the effect of KDM4B knock down on the H3K36me3 levels was tested on the selected H3K36me3 hypoxia upregulated gene peaks by using the same Active Motif antibody used before (**Figure 4.12**, **A**). In this experiment, there was no significant change on the H3K36me3 levels at any of the gene peaks with the KDM4B depletion, except at the

MARCKS gene, there was a significant increase with KDM4B oligo 2 knock down (**Figure 4.12**, **F**). These experiments indicate that KDM4A or KDM4B individual depletion does not impact H3K36me3 levels at the H3K36me3 hypoxia upregulated gene peaks investigated. This suggest that affecting the H3K36me3 levels on these predicted gene peaks might need a combined effort from two or more H3K36me3 associated KDMs. However, this possibility will need to be tested with further experiments. Furthermore, although t-test was used to statistically analyse the data in Figures 4.11 and 4.12, one-way ANOVA should have been used, as population means of more than two groups were being compared.

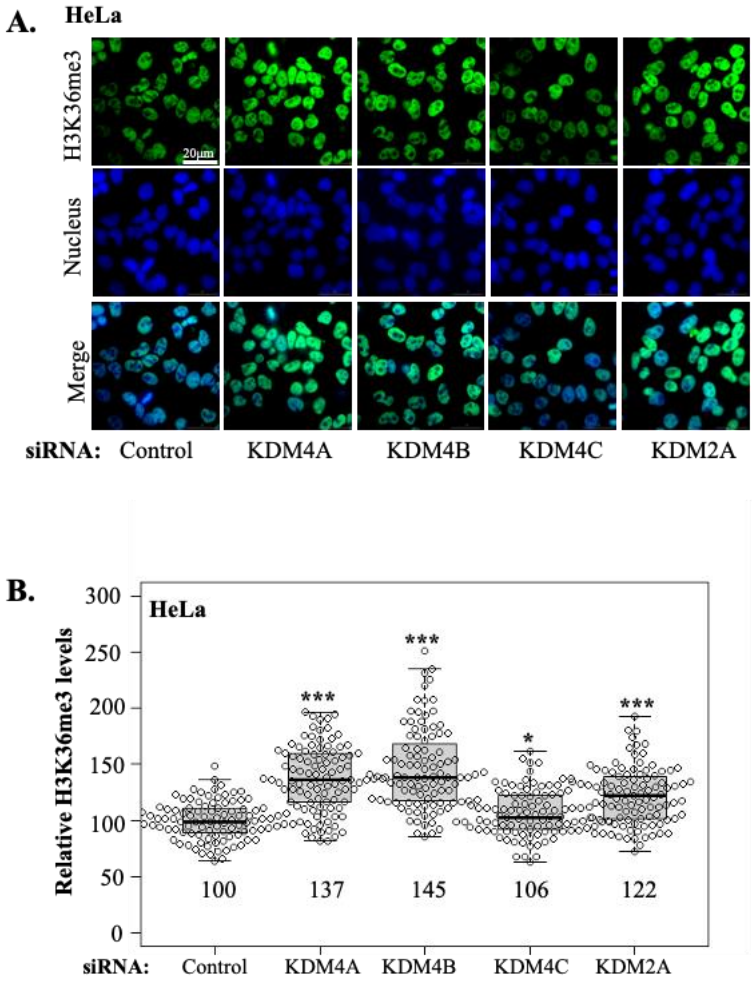

Figure 4.10. Effect of KDM depletion on H3K36me3 levels. HeLa cells were grown on a cover slip and transfected with control (non-targeting), KDM4A, KDM4B, KDM4C or KDM2A siRNAs 48 hours prior to methanol fixation. H3K36me3 levels were analysed by immunofluorescence (IF) microscopy with H3K36me3 immunostaining. **A.** Representative IF microscopy images displaying H3K36me3 (green), cell nuclei (Hoechst staining) (blue) and merging of H3K36me3 and cell nuclei. **B.** Box plot of relative H3K36me3 levels from IF microscopy quantification of 100 cells per condition from two independent experiments. Mean and individual cell data points are shown on the graph. Student t-test was applied, and significance determined as follows: * $p \leq 0.05$, ** $p \leq 0.01$, *** $p \leq 0.001$.

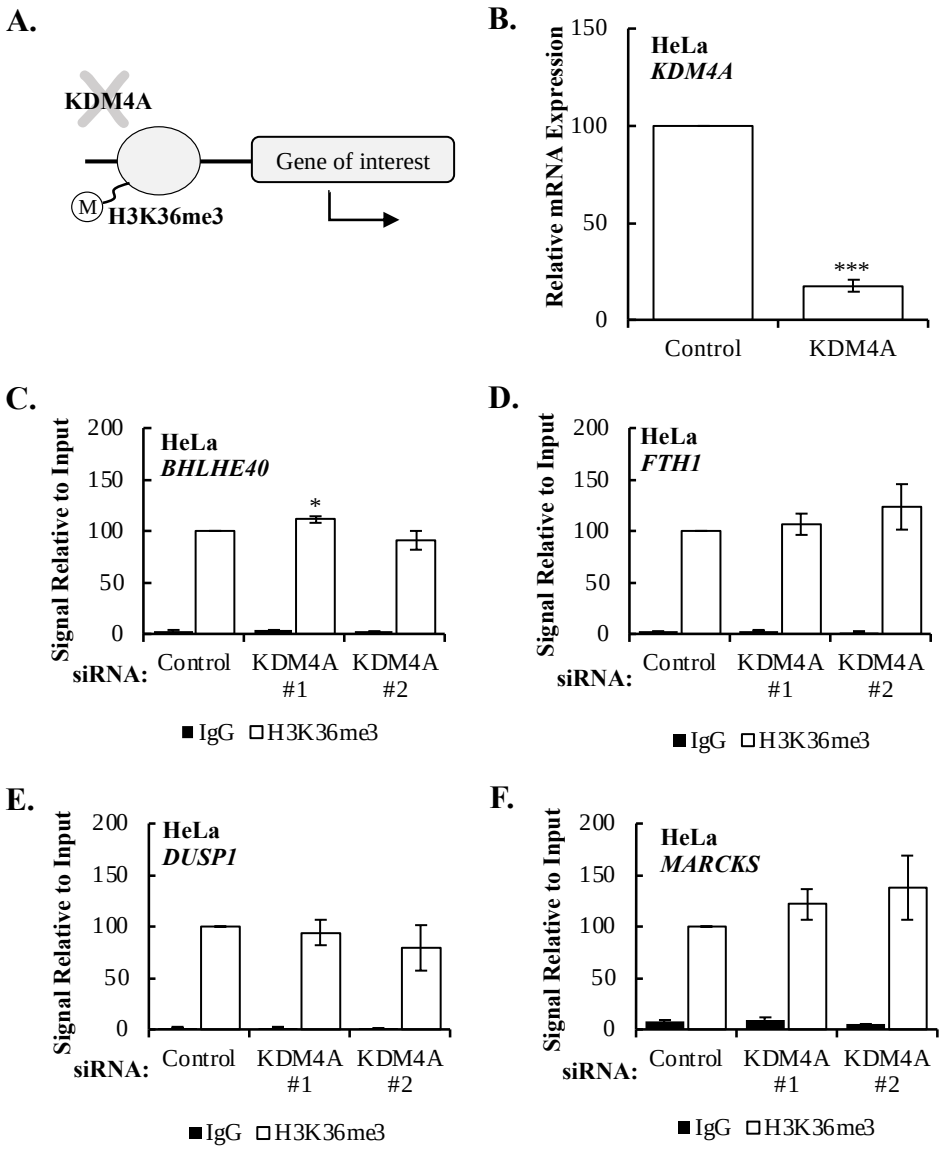

Figure 4.11. Effect of KDM4A depletion on H3K36me3 levels at hypoxia upregulated H3K36me3 peaks. HeLa cells were transfected with control (non-targeting), KDM4A oligo 1 and KDM4A oligo 2 siRNAs 48 hours prior to cross-linking and lysis. ChIPs were performed for an IgG control and H3K36me3 to the indicated gene promoter regions occupied by H3K36me3 promoter peaks. DNA was analysed by qPCR with results normalised to 2% input DNA. Graphs represent mean and standard error of a minimum of three independent experiments. Student t-test was applied, and significance determined as follows: * $p \leq 0.05$, ** $p \leq 0.01$, *** $p \leq 0.001$.

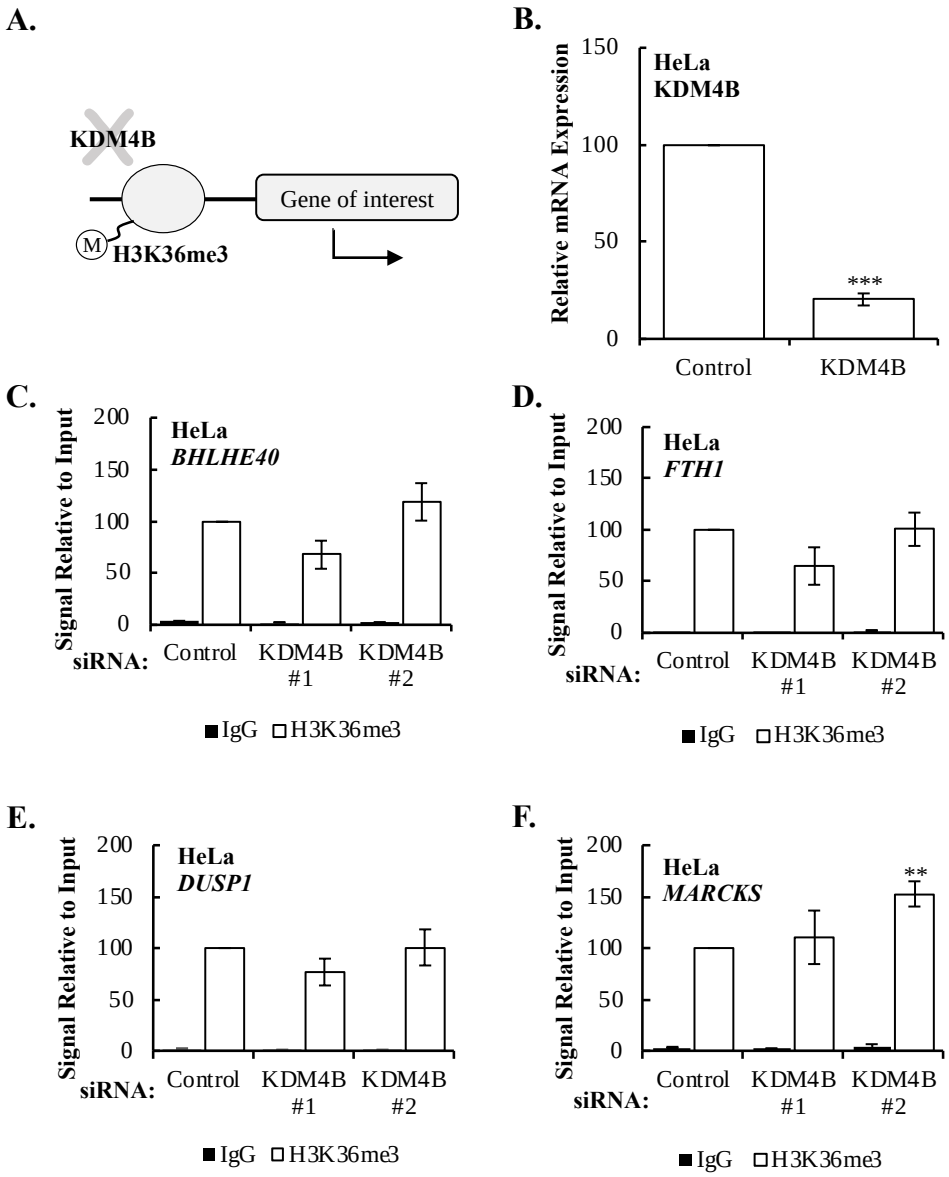

Figure 4.12. Effect of KDM4B depletion on H3K36me3 levels at hypoxia upregulated H3K36me3 peaks. HeLa cells were transfected with control (non-targeting), KDM4B oligo 1 and KDM4B oligo 2 siRNAs 48 hours prior to cross-linking and lysis. ChIPs were performed for an IgG control and H3K36me3 to the indicated gene promoter regions occupied by H3K36me3 promoter peaks. DNA was analysed by qPCR with results normalised to 2% input DNA. Graphs represent mean and standard error of a minimum of three independent experiments. Student t-test was applied, and significance determined as follows: * $p \leq 0.05$, ** $p \leq 0.01$, *** $p \leq 0.001$.

Then, it was investigated if loss of either of the H3K36me3 associated KDMs would contribute to the increase in mRNA expression of the selected genes. First, KDM4A, KDM4B, KDM4C or KDM2A mRNA levels were efficiently decreased by siRNA oligonucleotides (**Figure 4.13**, **A**). KDM4A depletion increased the mRNA expression of all genes, which was significant for FTH1, MARCKS and DUSP1 (**Figure 4.13**, **B**, **C**, **D and E**). Also, KDM4B depletion significantly increased the mRNA expression of all genes. Effect of KDM4C or KDM2A depletions were more variable on the gene expression levels. KDM4C depletion significantly increased the MARCKS mRNA levels (**Figure 4.13**, **D**), whereas KDM2A depletion significantly increased the FTH1 mRNA levels (**Figure 4.13**, **C**). Neither KDM4C, nor KDM2A had a significant effect on rest of the genes tested. This analysis indicated that both KDM4A and KDM4B have an impact on the mRNA expression of the hypoxia upregulated genes. However, KDM4C and KDM2A only effects a few selective genes.

Overall, individual depletion of the KDM4A or KDM4B did not consistently increase H3K36me3 at the analysed genes (**Figure 4.11** and **Figure 4.12**). However, both KDMs' knock down elevated the global methylation marks (**Figure 4.10**) and increased the mRNA of the H3K36me3 hypoxia upregulated genes (**Figure 4.13**). Hypoxia stimulation increased the methylation levels in all H3K36me3 hypoxia upregulated gene peaks but obtained data will need to be supported with more replicates using the ChIP-seq validated antibody. These results indicated that KDM4A and KDM4B have a negative regulatory role on the transcription of BHLHE40, FTH1, DUSP1 and MARCKS. This effect could be through the demethylation of the H3K36me3. Although, individual depletion of KDM4A or KDM4B did not show an effect on the methylation mark on these genes, this could be due to more than one KDM is necessary to impact methylation levels on the genes. Further experiments will be needed to elucidate the role of KDMs on the H3K36me3 hypoxia upregulated gene peaks, thus their potential role on the NF-κB transcriptional response. Also, one-way ANOVA statistical test should have been used in this experiment, as the population means of more than two groups were being compared.

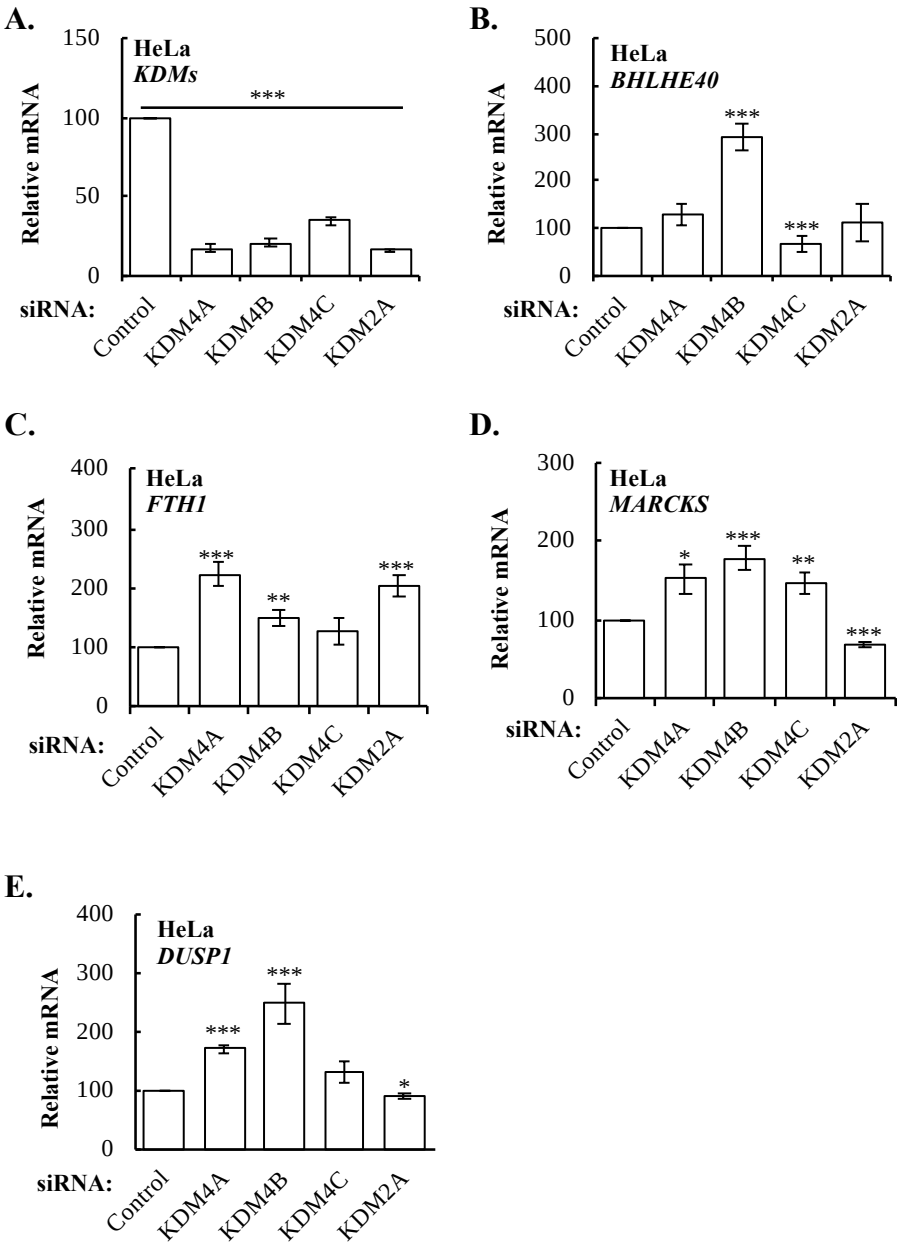

Figure 4.13. Effect of KDM depletion on H3K36me3 levels at hypoxia upregulated H3K36me3 peaks. HeLa cells were transfected with control (non-targeting), KDM4A, KDM4B, KDM4C or KDM2A siRNAs 48 hours prior to total RNA extraction and cDNA conversion. Relative mRNA expression levels of the indicated genes were analysed by qPCR using 18S as a normalising gene. Graphs represent mean and standard error of a minimum of three independent experiments. Student t-test was applied, and significance determined as follows: * $p \leq 0.05$, ** $p \leq 0.01$, *** $p \leq 0.001$.

4.4. Role of KDM4 members and KDM2A on NF-κB transcriptional activity and protein expression

The analysis of the hypoxia ChIP-sequencing experiments for H3K36me3, and subsequent experiments suggest that H3K36me3 associated KDMs might be a novel regulator of NF-κB. As a preliminary experiment to determine the role of KDM4A, KDM4B, KDM4C and KDM2A regulation on the NF-κB activity, independent of chromatin context, luciferase reporter assays in 3 different cell lines were performed (**Figure 4.14**). These cell lines stably express an artificial promoter containing 3x-κB sites in tandem. U2OS and A549 cells express the Promega NF-κB reporter luc2P, while HeLa cells express 3x-κB ConA luciferase reporter as described in (178).

NF-κB luciferase reporter cells, were transfected individually with KDM4A, KDM4B, KDM4C or KDM2A siRNAs without any additional stimulation (**Figure 4.14**, **A**). KDM4A knock down increased the κB activity in all cell lines with statistically significant results in A549 and U2OS cells. KDM4B, KDM4C or KDM2A depletions significantly increased the κB activity in all cell lines, with KDM4B knock down showing the highest impact on A549 and U2OS cell lines and KDM2A knock down showing the highest impact in HeLa cells. These results show that all H3K36me3 associated KDMs have a negative regulatory effect on the NF-κB reporter activity in all cell lines analysed under basal conditions.

Given that NF-κB is best known in response to cytokine stimulation, cells were exposed to the canonical NF-κB pathway inducer, Tumour necrosis factor α (TNF-α) (**Figure 4.15**). Optimum response time points were previously defined for each cell line in the Rocha lab. Following KDM4A, KDM4B, KDM4C or KDM2A depletion with TNF-α stimulation NF-κB activity was significantly decreased in A549 cells (**Figure 4.15**, **B**). KDM4B depletion upon TNF-α stimulation decreased the κB activity in HeLa cells (**Figure 4.15**, **A**). In U2OS cells, all the KDMs' depletion upon TNF-α stimulation increased the κB activity, except KDM2A depletion (**Figure 4.15**, **C**). These results indicated that upon TNF-α, KDM4A,

KDM4B, KDM4C or KDM2A are required for the induction of the NF-κB activity in A549 cells. The same case is observed with KDM4B in HeLa cells but not with KDM2A. KDM4A or KDM4C depletion with TNF-α stimulation increased κB activity in U2OS cells. However, variation in the results that was shown in both Figures 4.14 and 4.15, could be due to diversity in KDMs' knock-down efficiencies in different cell types. Although efficiency of the knock-downs in HeLa cells were tested (**Figure 4.14, A**), A549 and U2OS cells will also need to be tested for such variations. In addition, although t-test was used to statistically analyse these data, one-way ANOVA should have been used, as population means of more than two groups were being compared.

Given, the artificial nature of the reporter and lack of chromatin environment of these promoters, additional work is required to fully determine the molecular regulatory mechanism of the NF-κB via H3K36me3 associated KDMs. Nevertheless, these results suggest that H3K36me3 associated KDMs might be involved in a variety of mechanisms controlling NF-κB activity, which will be dependent on the cellular background analysed.

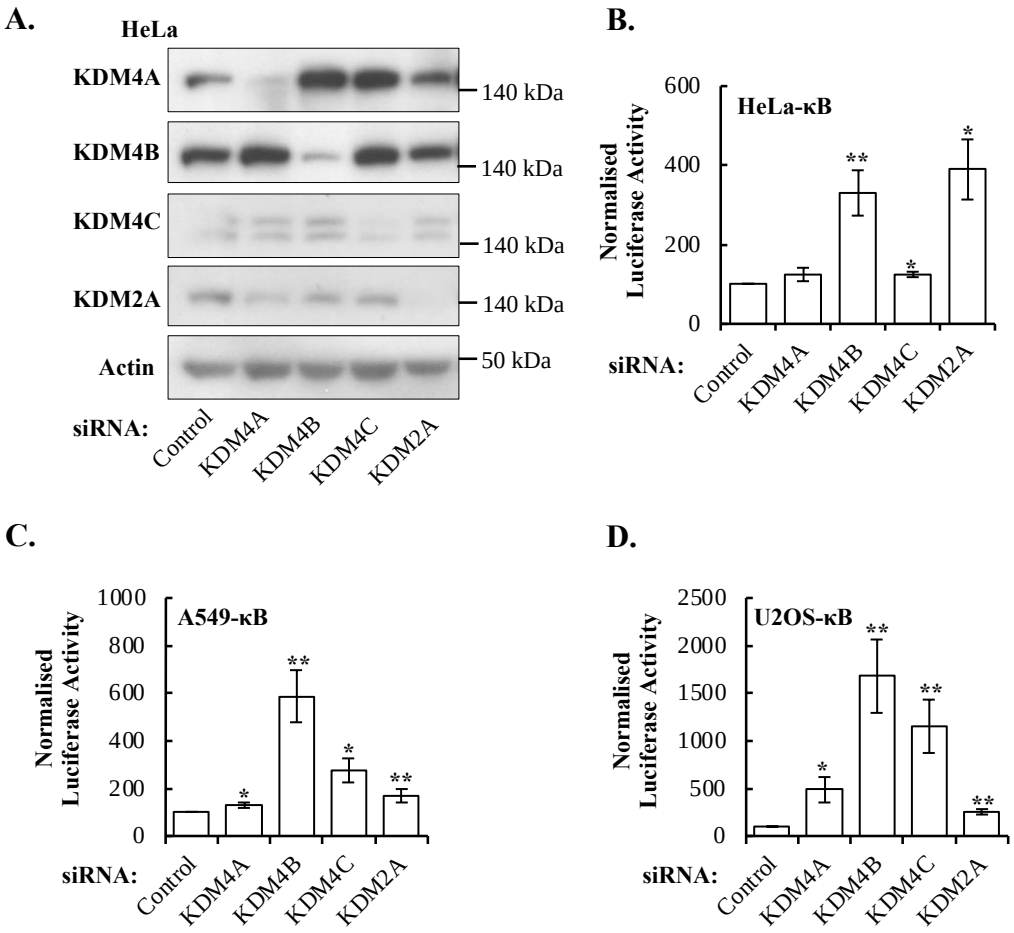

Figure 4.14. KDMs depletion affects the κB activity differently in different cell lines. Efficiency of the KDM knock-downs were checked on HeLa cells (**A**). Cells were transfected with siRNA oligonucleotide of control (non-targeting), KDM4A, KDM4B, KDM4C or KDM2A before whole cell lysis and probing with western blot method. β-Actin was used as a loading control. Blots represent minimum of three independent experiments. HeLa, A549 and U2OS cells, stably transfected with κB luciferase reporter, were transfected with siRNA control (non-targeting), KDM4A, KDM4B, KDM4C or KDM2A (**B**), (**C**), and (**D**). Values were normalised to the control samples. All graphs represent mean and standard error of four independent biological experiments. Student t-test was applied, and significance determined as follows: * $p \leq 0.05$, ** $p \leq 0.01$, *** $p \leq 0.001$.

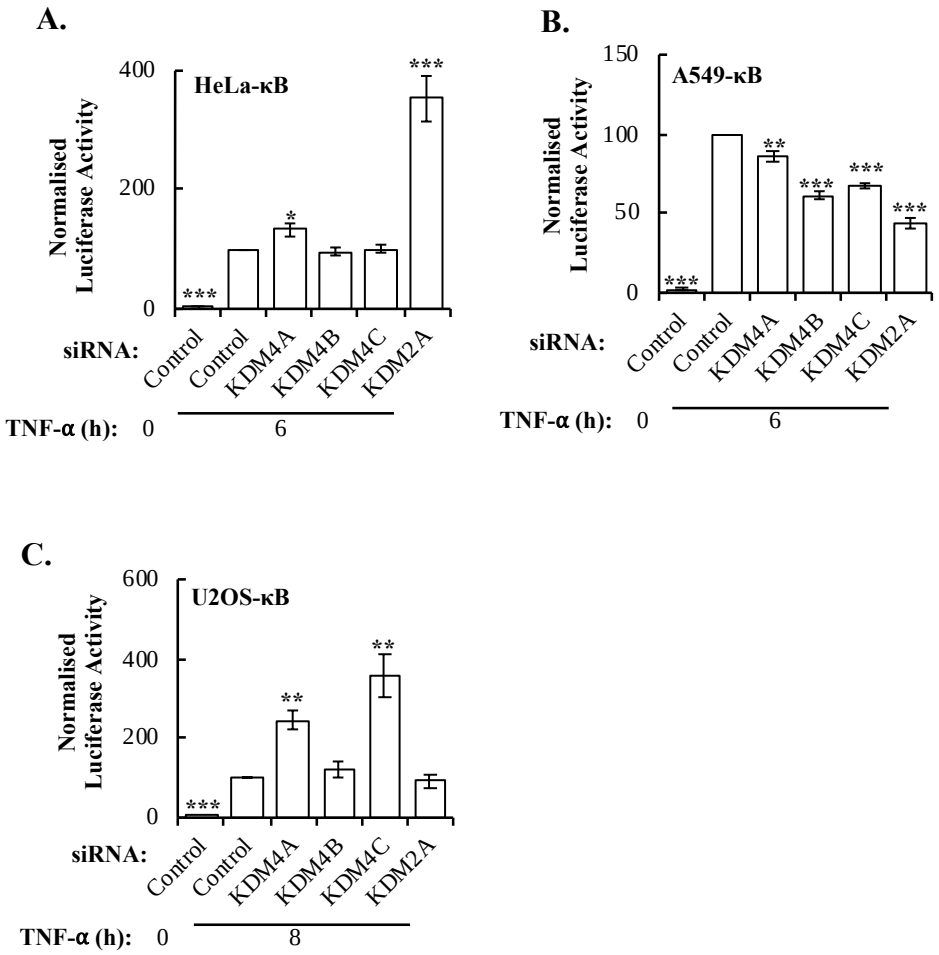

Figure 4.15. KDMs depletion alters the κB activity in some cell lines following TNF-α stimulation. HeLa, A549, and U2OS, cells, stably transfected with κB luciferase reporter, were transfected with siRNA control (non-targeting), KDM4A, KDM4B, KDM4C or KDM2A oligonucleotides (**A**), (**B**), and (**C**). 10 ng/mL TNF-α treatment was also added for 6 hours in HeLa (**A**), and A549 (**B**) cells; and for 8 hours in U2OS cells (**C**) prior to luciferase measurements. All the values were normalised to TNF-α treated control samples. All the graphs represent mean and standard error of at least three independent biological experiments. Student t-test was applied, and significance determined as follows: * $p \leq 0.05$, ** $p \leq 0.01$, *** $p \leq 0.001$.

Role of KDM4 family and KDM2A on NF-κB subunits and their target genes' protein expression levels were investigated after depleting the KDMs using specific siRNA oligonucleotides and immunoblotting the HeLa cell lysate (**Figure 4.16**). Based on the two replicates of this experiment, NF-κB RelB protein expression levels increased with KDM4B, KDM4C and KDM2A knockdowns, while KDM4A depletion was not as effective on the RelB expression. NF-κB cRel protein expression levels were increased with KDM4A and KDM4C depletions, while other KDMs' knockdown did not have a consistent effect on cRel protein

levels. Both RelB target gene, cyclinD1 (182, 213), and cRel target gene, claspin (214) protein expression levels were inconsistent across the two replicates.

NF-κB RelA protein expression levels were not affected with either of the KDM's depletion. P100, c-IAP1 (215, 216), and BHLHE40 was used as RelA target genes. Each KDM had a negative regulatory impact on different RelA target genes. As such, p100 protein expression levels were increased with KDM4B depletion, c-IAP1 levels were increased with KDM4A, KDM4B and KDM4C depletions, and BHLHE40 expression was elevated with KDM4B and KDM4C knockdowns. Overall, these results indicate that each KDM can negatively regulate different NF-κB subunits and their target genes at the protein level. However, this experiment will need to be repeated in order to reach to a clear conclusion. The effect of KDMs on NF-κB subunits at the protein level and its impact on their transcriptional response could involve their regulatory role on histones, as well as their non-histone function, which is studied more in detail in the next chapter.

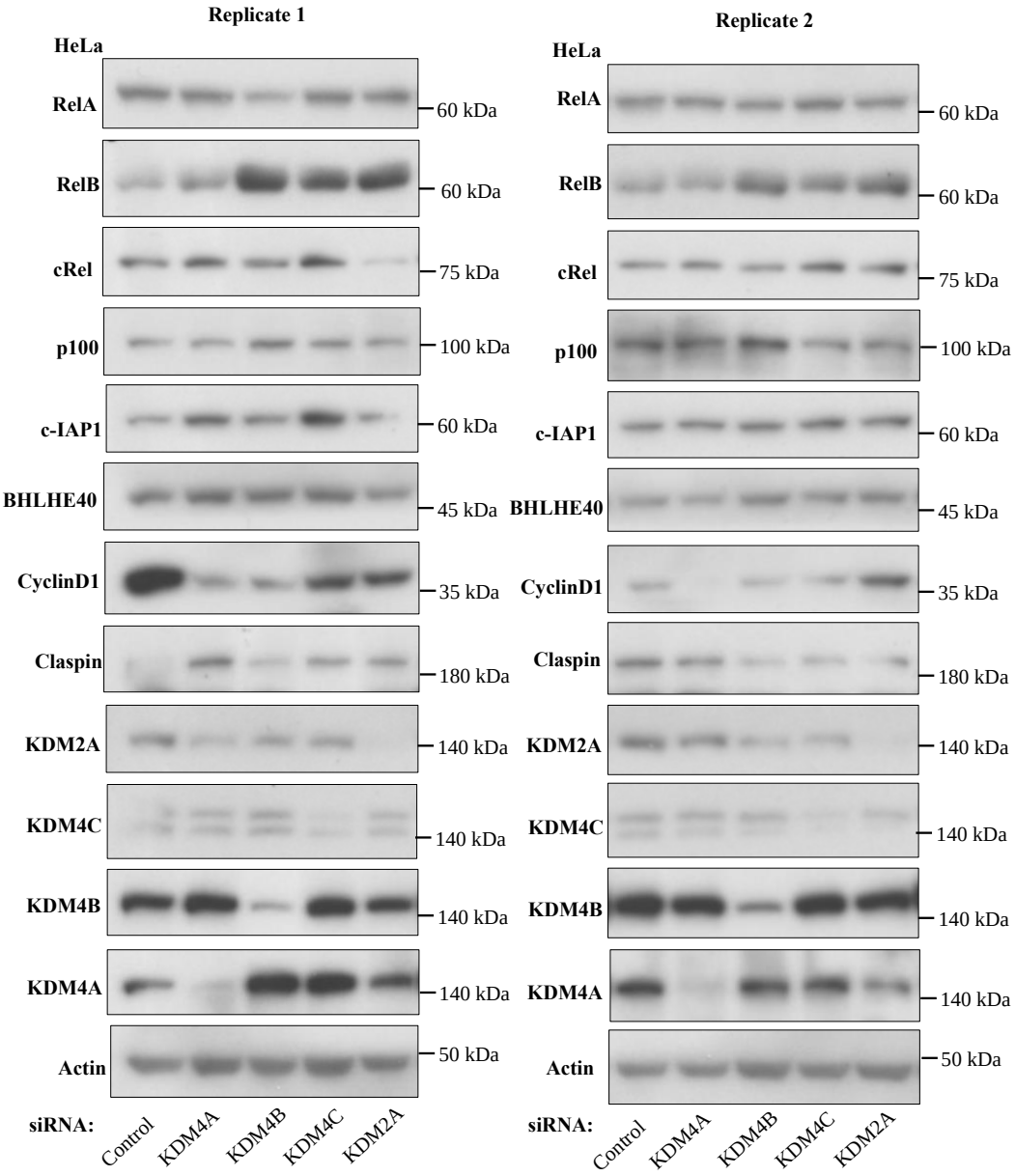

Figure 4.16. KDM4 family and KDM2A depletion alters NF-κB subunits and their target genes in protein level. HeLa cells were transfected with siRNA oligonucleotide of control (non-targeting) and KDM4A, KDM4B, KDM4C, or KDM2A before whole cell lysis and probing with western blot method. β-Actin was used as a loading control. Blots show two independent replicates of the experiment.

4.5. Discussion

Histone lysine methylation represents a key epigenetic function for gene expressions, which has recently been associated with its elevation through decreased oxygen levels and deactivation of the JmjC containing KDMs (100, 110). Although these studies focused on the other demethylases, H3K36me3 hypoxia stimulated ChIP-seq data obtained from Batie *et al.* revealed the potential of this methylation mark in hypoxia stimulated NF-κB transcriptional response. This study focused on the role of hypoxia controlling H3K36me3 levels and investigating the possible KDMs that could be involved in the regulation of the NF-κB transcriptional response.

Genome-wide analysis performed by Michael Batie, to map H3K36me3 enriched genomic regions in HeLa cells, at basal level and following 1 hour hypoxia (117) a list of gene peaks was obtained (**Figure 4.1**). Pathway enrichment analysis was performed using H3K36me3 upregulated low stringency gene peaks, which included genes identified in at least 2 out of 3 biological experiments. This enabled to obtain genes with statistically significant overlaps with hallmark gene sets (**Tables 4.1**). However, as mentioned in the previous chapter, this analysis is limited to overlapping only a defined number of reference genes for each pathway. Thus, some of the TNF-α-induced NF-κB genes might not be included in the hallmark gene sets, therefore, including other publicly available ChIP-seq and RNA-seq datasets with hypoxia or TNF-α stimulation to the comparison, could be more informative.

The list of H3K36me3 hypoxia upregulated gene peaks, were also overlapped with RNA-seq hypoxia and NF-κB hallmark gene sets, as well as with the Gilmore laboratory's NF-κB target genes list (**Figure 4.2**, **A** and **B**). This comparison highlighted potential NF-κB target genes that are associated with H3K36me3 upregulated gene peaks, and the ones that are also induced by hypoxia stimulation (**Table 4.2** and **Table 4.3**). From the H3K36me3 hypoxia upregulated gene peaks, high stringency genes that were identified in all replicates of the H3K36me3 hypoxia ChIP-seq experiment, were selected for further validation. BHLHE40 and FTH1 was validated to significantly increase with hypoxia stimulation (**Figure 4.5**, **A** and **B**).

Also, DUSP1 and MARCKS was confirmed to be hypoxia inducible in the previous chapter (**Figure 3.5**, **D** and **F**). Furthermore, all the hypoxia responsive genes were also shown to respond to the NF-κB subunit RelA by measuring their mRNA levels following RelA overexpression of the HeLa cells (**Figure 4.8** and **Figure 3.7**, **D** and **F**). Additionally, all these genes have been shown to have RelA binding sites by ChIP-seq in a variety of different cellular backgrounds, when ChIP-Atlas was used (https://chip-atlas.org/, (212)) (**Figure 4.9**). However, as it is described in the previous chapter further analysis is necessary to support their connection with the NF-κB transcriptional response by doing genome-wide analysis of NF-κB RelA binding sites with hypoxia stimulation. In order to do this, a CUT and RUN experiment was planned and optimisation of the assay was initiated (**Chapter 9**). This approach will enable to identify direct targets of the NF-κB with hypoxia stimulation and differentiate the TNF-α induced gene signatures.

In the next experiments, we focused on validating the effect of hypoxia stimulation on the H3K36me3 methylation levels. Initially, a Cell Signalling antibody was used at the immunoprecipitation process of the H3K36me3 proteins that were crosslinked to the chromatin (**Figure 4.6**). This experiment could not reach to a conclusion due to high variability between biological replicates, which was thought to be caused by using an antibody that was not validated for this experiment (247). In the next experiment, another H3K36me3 specific antibody produced by Active Motif that was validated and used in the H3K36me3 hypoxia stimulated ChIP-seq experiments was used (100). As a result, hypoxia stimulation increased the methylation levels in all H3K36me3 hypoxia upregulated gene peaks (**Figure 4.7**). However, this experiment will need to be repeated to support the results from the first replicate.

Next, we focused on identifying the KDMs that could be involved in regulating the H3K36me3 hypoxia upregulated gene peaks. Unlike H3K4me3, where KDM5A was identified previously as the main KDM responsible for hypoxia response (117), no information was available for which KDM was responsible for H3K36me3 induction in hypoxia. Initially, H3K36me3 associated KDMs, KDM4A, KDM4B, KDM4C and KDM2A was validated for

their effect on the global H3K36me3 levels in HeLa cells (**Figure 4.10**). KDM4A or KDM4B depletion showed the highest significant increase at the methylation levels, indicating that these are dominant in HeLa cells. Next, KDMs were investigated if they would influence the H3K36me3 levels, similar to hypoxia stimulation, at the H3K36me3 hypoxia upregulated gene peaks by using ChIP-qPCR method (**Figure 4.11** and **Figure 4.12**). Apart from the increased methylation levels at MARCKS gene, there was no significant change on the H3K36me3 levels at rest of the gene peaks with either of the KDMs knock down. This could be due to multiple KDMs being involved on the demethylation of the H3K36me3 levels, thus depletion of only KDM4A or KDM4B might not be sufficient. Supporting this hypothesis, previously, it has been shown that single gene knockouts of KDM4A, KDM4B and KDM4C, as well as double knockouts of KDM4A with KDM4B or KDM4B with KDM4C would maintain viable mouse embryonic stem cells, but combined deficiency of all three KDM4s would be embryonic lethal (248, 249). This indicates that individual KDM4 family members have redundant roles in preventing the accumulation of H3K36me3. In this case, additional experiments, depleting the combination of KDMs is necessary to further investigate their regulatory role at the H3K36me3 hypoxia upregulated gene peaks in HeLa cells.

Using a reporter gene assay, negative regulatory effect of KDM4A, KDM4B, KDM4C and KDM2A on NF-κB activity was observed in HeLa, A549 and U2OS cells by depleting each of the KDMs independently prior to quantifying the κB activity (**Figure 4.14**). Following TNF-α stimulation, depleting either of the KDMs decreased the κB activity in A549 cell lines (**Figure 4.15**, **C**). The same effect happened on HeLa cells with depletion of the KDM4B (**Figure 4.15**, **A**). In U2OS cells, all the KDM4 depletion with TNF-α stimulation increased the κB activity, but this was not the case for KDM2A depletion (**Figure 4.15**, **C**). These results indicated that upon TNF-α, different KDMs could be required for the induction of the NF-κB activity in different cell lines.

The reporters used are artificial in nature and lack of chromatin environment of endogenous promoters, as such the results obtained, point to an effect either on the

transcription factor themselves and/or indirectly alterations of chromatin of NF-κB regulators. Additional work is required to fully determine the molecular regulatory mechanism of the NF-κB via KDM4 family members and KDM2A. In terms of KDM2A, independent to its histone demethylation activity, following interleukin-1β signalling, knockdown of KDM2A increased the mRNA level expression of NF-κB target genes, such as IL-6 and IL-8 in mesenchymal stem cells (236). Also, a recent study has confirmed the negative regulatory role of KDM2A on the NF-κB in MCF-7 breast cancer cell lines (237). Furthermore, *Lu et al.* showed that JmjC domain, and especially the H3K36 demethylase activity that is encoded within this domain is needed for the negative regulatory effect of KDM2A on NF-κB in human 293 cells (170). The same group has also shown a non-canonical function of KDM2A, where it negatively regulates the NF-κB RelA through reversing methylation of the lysine residues by directly binding to the NF-κB subunit (35), which could explain the role of KDM2A on the NF-κB activity in the luciferase system. It is thus possible that KDM4 family members also directly demethylate NF-κB subunits, a hypothesis that will require investigation in the future. Nevertheless, these results suggest that these KDMs might be involved in a variety of mechanisms controlling NF-κB activity. Additional work investigating how KDM4 family and KDM2A depletion alter basal and TNF-α induced genes such as IκB-α, IL-8, TNFAIP3 and others would be interesting to determine KDM4 and KDM2A's role in the canonical NF-κB pathway.

Several studies have also shown an association between KDM4 family and NF-κB with different inducers and in various cellular backgrounds. Studies that linked KDM4 family and NF-κB majorly focused on their demethylation activity on H3K9me2/3, which is a mark for transcriptional repression. Based on the kinetic analysis of the KDM4 family, this might be because, although KDM4A, KDM4B and KDM4C accept both H3K9 and H3K36 as substrates, demethylation at H3K9 compared to H3K36, occurs with a higher affinity and efficiency (250). KDM4B accumulation at the RelA promoter, has been shown to increase the NF-κB expression and its corresponding inflammatory response by depleting H3K9me3(238).

Moreover, KDM4A and KDM4C has been shown to form a complex with NF-κB in response to T follicular helper cell-derived signals and mediates the cell cycle progression of the activated B cells through demethylation of H3K9 (239).

Furthermore, several studies have focused on the association between H3K36me3 and NF-κB transcriptional response. It has been shown that Lipopolysaccharides (LPS) stimulation enhances H3K36me3 chromatin occupancy in inflammatory genes such as IL-1β (234). This study has shown that increased H3K36me3 levels is correlated with elevated pro-IL-1β at the protein level, however its' link with NF-κB was not established. Another group has shown decreased H3K36me3 levels on the pro-inflammatory mediator, TNF-α promoter in rat spleen samples, following a corticosteroid drug treatment, which is known to reduce inflammation and suppress immune system (235). In this study, while decrease in H3K36me3 levels were compatible with decreased TNF-α mRNA expression, their correlation was not clarified.

To summarise, this chapter has indicated the role of oxygen sensing mechanism of chromatin on the transcriptional regulation of potential NF-κB target genes. Enzymatic activity of KDM4A and KDM4B is suggested as a potential regulator of the H3K36me3 regions and gene expression that are responsive to both hypoxia and NF-κB RelA. The results presented here also lead to a speculating the role of KDM4 in controlling NF-κB transcriptional activity.

Chapter 5 - Non-Histone role of KDMs regulating NF-κB in HeLa cells

5.1. Introduction

Given the role of NF-κB in a wide range of crucial cellular and physiological processes, activity of the NF-κB is regulated by many mechanisms including various post-translational modifications (PTMs), such as ubiquitination, phosphorylation, acetylation, sumoylation, and nitrosylation (147). Methylation has also been reported but has not been studied widely. It has been suggested that histone-modifying enzymes not only modify histone proteins, but are also involved in the modification of non-histone proteins including NF-κB. To date, NF-κB RelA protein has been discovered to have six methylated lysine (K) sites, which are modified by different histone modifying enzymes (35, 166, 170-173). Specifically, K37, K218 and K221 sites are located within the Rel homology domain (RHD) of the RelA protein, which is known with its function for protein dimerization, inhibition of NF-κB and its inhibitor, IκB interaction, as well as nuclear targeting, and DNA binding (176).

Lysine methylation can occur in different forms and can lead into distinctive functional outcomes depending on the molecular role of the methylated binding protein. Lu *et al.* have identified that NF-κB RelA protein can be monomethylated on K218 and dimethylated on K221 sites, catalysed by the H3K36 methyltransferase, the nuclear receptor-binding SET domain-containing protein 1 (NSD1) in response to cytokine stimulation, and the methyl groups can be removed by the H3K36 demethylase, KDM2A (35, 170). Based on gene expression profiling of Lu *et al.*, using RelA plasmid DNA in mouse embryonic fibroblast cells (MEFs), about 80% of genes were not activated by the RelA overexpression, when both K218 and K221 sites were mutated (35). Also, about 87% of the RelA-dependent genes were shown to be downregulated by overexpression of the KDM2A in MEFs. The data obtained by Lu and colleagues suggested that K218 and K221 methylation sites are important for NF-κB transcriptional response and KDM2A has a direct negative regulatory role on most of the RelA-dependent genes (35).

In the previous chapter, it was shown that KDM4 and KDM2A, which belongs to the Jumonji C (JmjC)-containing lysine-specific histone demethylases (KDMs), have a negative

regulatory role in NF-κB transcriptional activity. As the luciferase method that was used to measure the κB activity does not involve a chromatin system, it raises the possibility of a non-canonical function of the KDMs. This has directed us to investigate the role of KDMs in the regulation of possible methylations on NF-κB proteins.

This chapter investigates the functional significance of lysine residues identified to be conserved in all NF-κB subunits for their potential of being methylated. Mutation of the identified lysine residues has shown to alter the NF-κB transcriptional activity in different cellular backgrounds. The conducted preliminary work has shown potential methylation sites on the NF-κB proteins in HeLa cells and the possible interaction of KDM5A with the NF-κB subunits, RelA and p50.

5.2. Identification of the NF-κB lysine residues as potential methylation targets

As mentioned above, several methylation sites had been previously identified in the NF-κB RelA (p65) subunit (35, 166, 170-173). To determine if these sites are conserved in different species, sequence similarity search was applied focusing on the K218 and K221 residues of the NF-κB RelA using Jalview software (251) (**Figure 5.1**). Orthologous sequences of the Rel Homology Domain (RHD) were obtained for different organisms from the UniProt proteome database with the following UniProt entry identifiers; *H.* sapiens, Q04206-1; *M. musculus*, Q04207; *G. gallus*, P98152; *X. laevis*, Q04865; and *D. melanogaster* Dorsal, P15330 and *D. melanogaster* Dif, P98149. As a result, it was demonstrated that the K218 and K221 methylation sites in human are evolutionarily conserved in other organisms, such as mice, chicken, frog, and the fruit fly. Based on this information, it could be hypothesised that these sites are functionally important for RelA.

As the methylation sites investigated above are located in the RHD, which is the most conserved domain between NF-κB subunits, the conservation of these sites was investigated across all NF-κB proteins. Sequence alignment analysis of all NF-κB subunits was also performed using Jalview software (**Figure 5.2**, **A**). Canonical protein sequences for each NF-

κB subunit' RHD were obtained with the following UniProt entry identifiers; RelA (p65), Q04206-1; RelB, Q01201; NF-κB1 (p50), P19838; NF-κB2 (p52), Q00653; and cRel, Q04864. As a result, the amino acid motif containing the K218 and K221 sites were discovered to be conserved in all five NF-κB subunits. Location of this amino acid motif and thus the lysine residues was different for each NF-κB subunit due to different number of amino acids existing in their protein sequences. RelA K218 and K221 was aligned with K210 and K213 in cRel; K327 and K330 in RelB; K275 and K278 in NF-κB1; and K252 and K255 in NF-κB2. In the protein data bank (PDB) repository, the structure of RelA-p50 heterodimer bound to the tandem κB sites of the Human Immunodeficiency Virus (HIV)-1 Long Terminal Repeat (LTR) is available with the PDB code, 3GUT. Using such structure, a representative diagram of RelA-p50 heterodimer with aligned lysine residues was shown while bound to the HIV-1 LTR, was produced using PyMOL software (Delano Scientific, LLC) (**Figure 5.2**, **B**). DNA helix is shown to be coated by RelA-p50 heterodimer, forming a nearly complete circle around the DNA. Unlike most DNA-binding proteins, which use α-helices, NF-κB dimers use loops in order to mediate DNA contacts (252, 253). Structural modelling has identified that RelA contacts DNA through few residues, and among them the recently identified methylation sites, K218 and K221 are found to be located on the loop L4 with the ability to bind to DNA on κB sites (252, 254). Lu *et al.* have shown that both K218 and K221 residues, which are located in the DNA binding domain of RelA, increases gene expression by facilitating RelA promoter binding ability (171). NF-κB heterodimer RelA-p50 structure has been studied on a number of different DNA sites, where it has been determined that RelA-p50 dimer bind to the same or closely related DNA sequences (252, 254-257). Given the structural similarities of RelA and p50, it is possible that p50 lysine residues that are aligned with K218 and K221 are also involved in increasing the DNA binding affinity of the p50. This could also be applied to other NF-κB subunits as they are identified to share the same amino acid motif within aligned lysine residues (**Figure 5.2**, **A**). The results obtained in the similarity analysis suggest that apart from RelA, other NF-κB subunits could also potentially be methylated and demethylated by specific

enzymes, contributing to the regulation of the NF-κB transcriptional response. Given the function of the RHD, it is also possible that these putative methylated lysine sites contribute to NF-κB protein homo- or hetero-dimerization, as well as detachment of the NF-κB proteins from their inhibitor followed by their nuclear localisation. Also, potential methylation of the identified NF-κB lysine sites could contribute to recruiting additional factors such as NF-κB co-activators that are necessary for a complete NF-κB transcriptional response. Thus, further study investigating the functional role of these putative methylated lysine sites on NF-κB is necessary. To start such investigation, effect of the potentially methylated lysine sites on NF-κB transcriptional activity is tested and described in the next section.

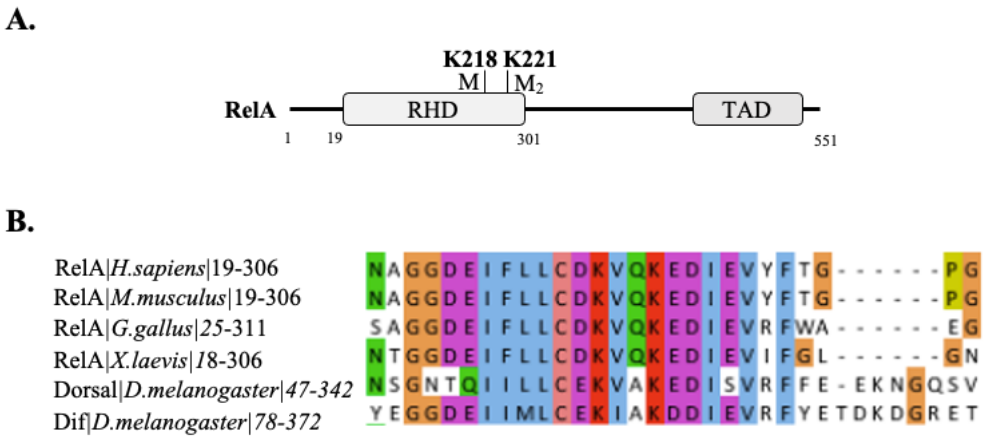

Figure 5.1. NF-κB RelA protein methylation sites via KDM2A. A. Visual illustration of NF-κB RelA protein structure showing mono-methylation (M) on Lysine 218 residue (K218) and di-methylation (M_2) of the Lysine 221 residue (K221) on the amino acid sequence of the Rel Homology Domain (RHD). **B.** Sequence alignment diagram for the NF-κB RelA RHD K218 and K221 sites in different species. Red highlighted section indicates conserved Lysine (K) residues.

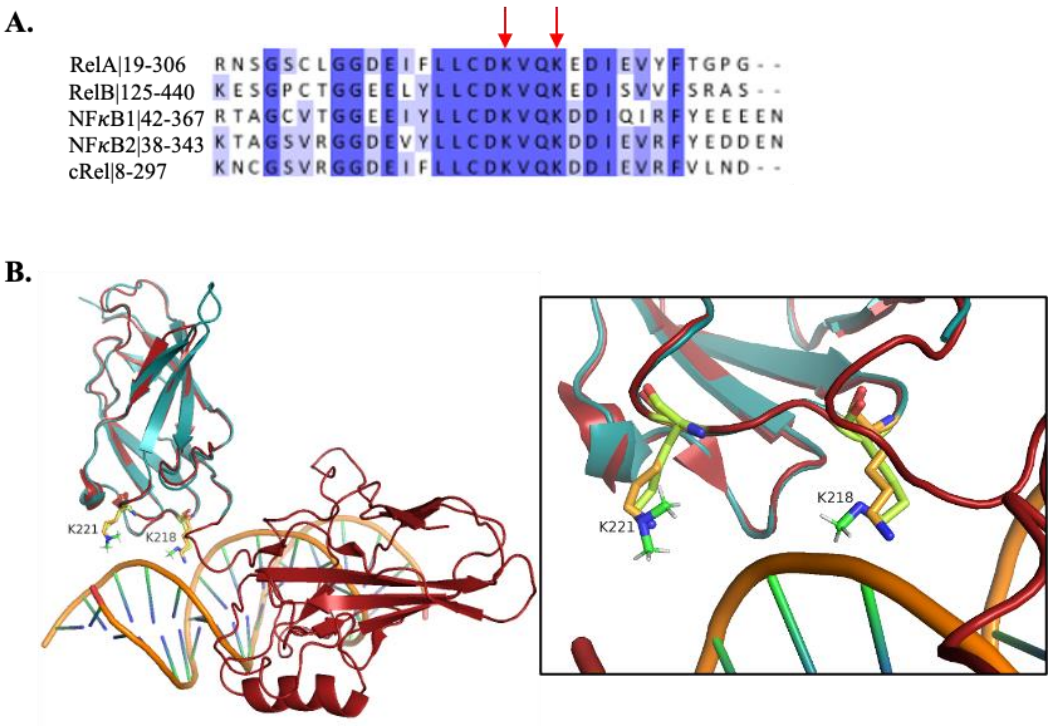

Figure 5.2. NF-κB subunits potential methylation sites. A. Sequence alignment diagram for the NF-κB subunits aligning with the RelA K218 and K221 sites on the Rel Homology Domain (RHD). Red arrows indicate conserved Lysine (K) residues. **B.** A stereo cartoon diagram of a representative alignment of RelA (red, PDB code, 3GUT) and NF-κB1 p50 (cyan, PDB code, 1NFI) bound to Human Immunodeficiency Virus (HIV)-1 Long Terminal Repeat (LTR) DNA (orange). Magnified diagram at the right-side shows overlapping K218 and K221 residues with methyl groups, C (green) and H3 (white) added to each of the N-terminus (blue). Structure figure was generated with PyMOL (Delano Scientific, LLC).

5.3. Functional analysis of putative methylated lysine sites on NF-κB transcriptional activity

To gain an insight into the functional contribution of the identified conserved lysine residues towards the NF-κB transcriptional activity in different cell lines, lysine (K) residues were mutated into alanine (A). NF-κB mutants were generated with altered lysine sites from their corresponding wild-type plasmid DNA using site directed mutagenesis (**Figure 5.3**).

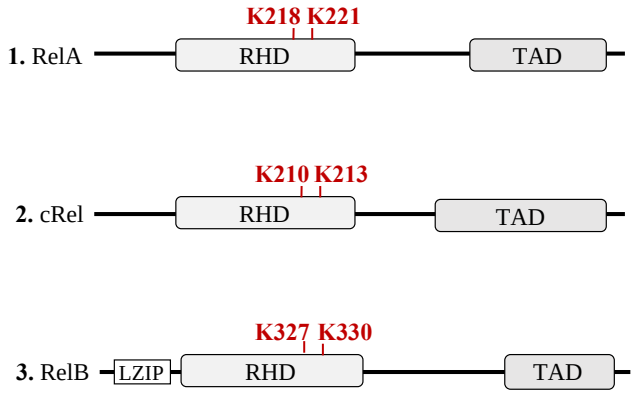

#.	Mutant	Abbreviation	Description
1.	-	RelA WT	RelA wild type
	RelA; K218A	RelA K218A	RelA lysine 218 residue loss of function
	RelA; K221A	RelA K221A	RelA lysine 221 residue loss of function
	RelA (K218A); K221A	RelA DM	RelA both lysine residues loss of function
2.	-	cRel WT	cRel wild type
	cRel; K210A	cRel K210A	cRel lysine 210 residue loss of function
	cRel; K213A	cRel K213A	cRel lysine 213 residue loss of function
	cRel (K210A); K213A	cRel DM	cRel both lysine residues loss of function
3.	-	RelB WT	RelB wild type
	RelB; K327A	RelB K327A	RelB lysine 327 residue loss of function
	RelB; K330A	RelB K330A	RelB lysine 330 residue loss of function
	RelB (K327A); K330A	RelB DM	RelB both lysine residues loss of function

Figure 5.3. NF-*κ*B subunits potential methylation sites mutants. Schematic diagram of NF-*κ*B subunits RelA, cRel and RelB with the list of mutant plasmid DNA generated. Lysine residues that are shown in "red" are converted to alanine using site directed mutagenesis method. Two single mutations and a double mutation was produced for each NF-*κ*B subunit using their wild type of plasmid DNA.

NF-κB mutants were then transiently expressed in HeLa-κB, A549-κB, and U2OS-κB luciferase cells and exposed or not to canonical NF-κB pathway inducer, Tumour necrosis factor α (TNF-α) for the optimum amount of time that was previously defined for each cell line in the Rocha lab.

In HeLa cells, NF-κB activity was significantly increased with the overexpression of RelA wild type (WT), and increased with the RelA single mutants, K218 and K221 (**Figure 5.4**, **A**). However, compared to the RelA WT, κB activity was decreased with both single

mutants and this reduced activity was really evident when cells expressed the double mutant (DM) (**Figure 5.4**, **A**).

In A549 cells, surprisingly RelA WT plasmid was not able to induce κB activity. This was also seen when the DM was expressed in these cells (**Figure 5.4**, **B**). However, both of the single mutants increased κB activity in A549 cells (**Figure 5.4**, **B**).

In U2OS cells, RelA WT and both of the single mutants significantly increased the NF-κB activity. On the other hand, a significant decrease in the κB activity was observed with RelA DM expression, suggesting a dominant negative effect of these mutations (**Figure 5.4**, **C**). These results indicate that, mutation in one of the RelA lysine residues is not sufficient to remove NF-κB activity in either of the cell lines, however altering both of the RelA lysine sites substantially decrease κB activity in all cell lines.

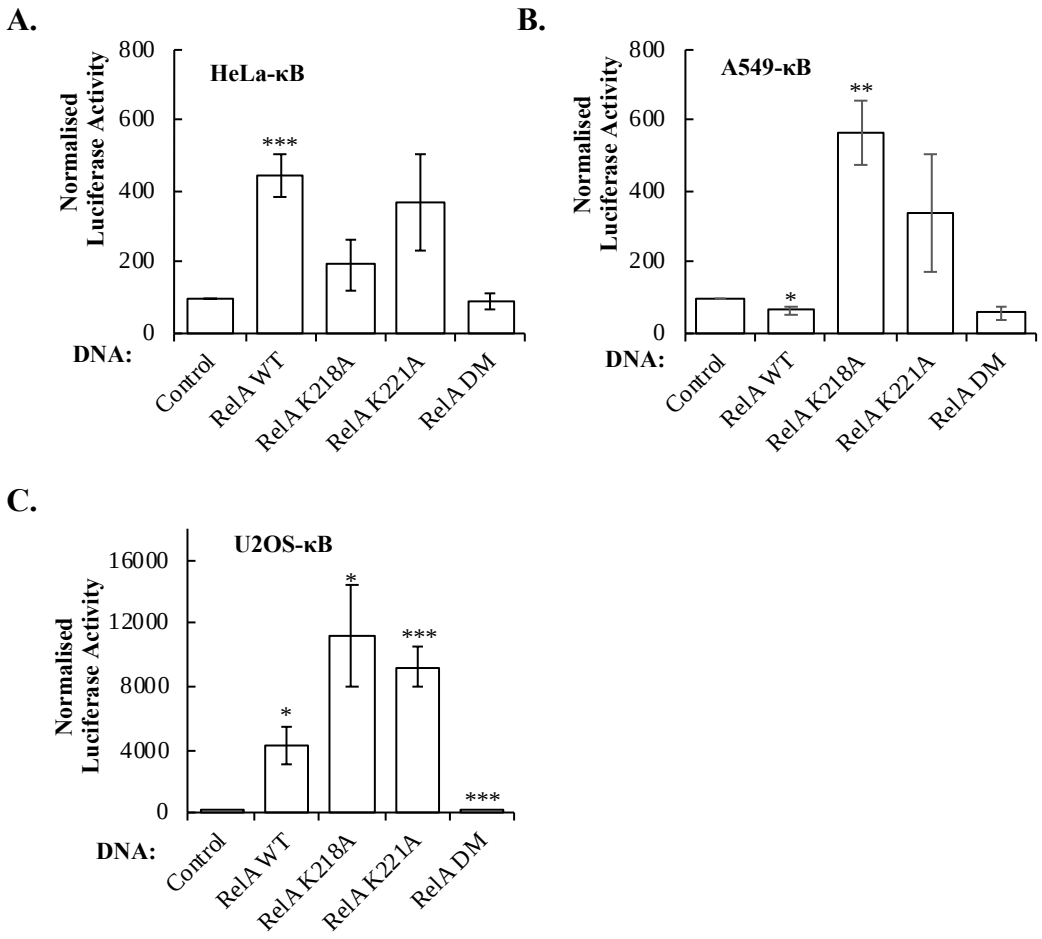

Figure 5.4. NF-κB RelA mutants expression alter the κB activity in different cell lines. HeLa, A549, and U2OS, cells, stably transfected with κB luciferase reporter, were transiently transfected with the following plasmid DNAs; control (empty vector), RelA WT (wild type), RelA K218A, RelA K221A or RelA DM (double mutant) prior to luciferase measurements. All the values were normalised to control samples. All the graphs represent mean and standard error of at least three independent biological experiments. Student t-test was applied, and significance determined as follows: * $p \leq 0.05$, ** $p \leq 0.01$, *** $p \leq 0.001$.

To investigate the relevance of these lysine residues in TNF-α induced NF-κB activity, these experiments were repeated in the presence of this cytokine. In HeLa and U2OS cell lines, following overexpression of the RelA plasmids and TNF-α stimulation, RelA WT and all of its single mutants increased the κB activity (**Figure 5.5**, **A** and **C**). However, in A549 cells, no significant difference is observed between WT and mutants (**Figure 5.5**, **B**). Interestingly in U2OS cells, expression of RelA DM and stimulation with TNF-α, still resulted in reduced κB activity when compared to the WT. These results suggest that upon TNF-α,

most cells can rely on endogenous RelA for activation of the reporter and that cell type specific responses are seen for each of the mutants analysed.

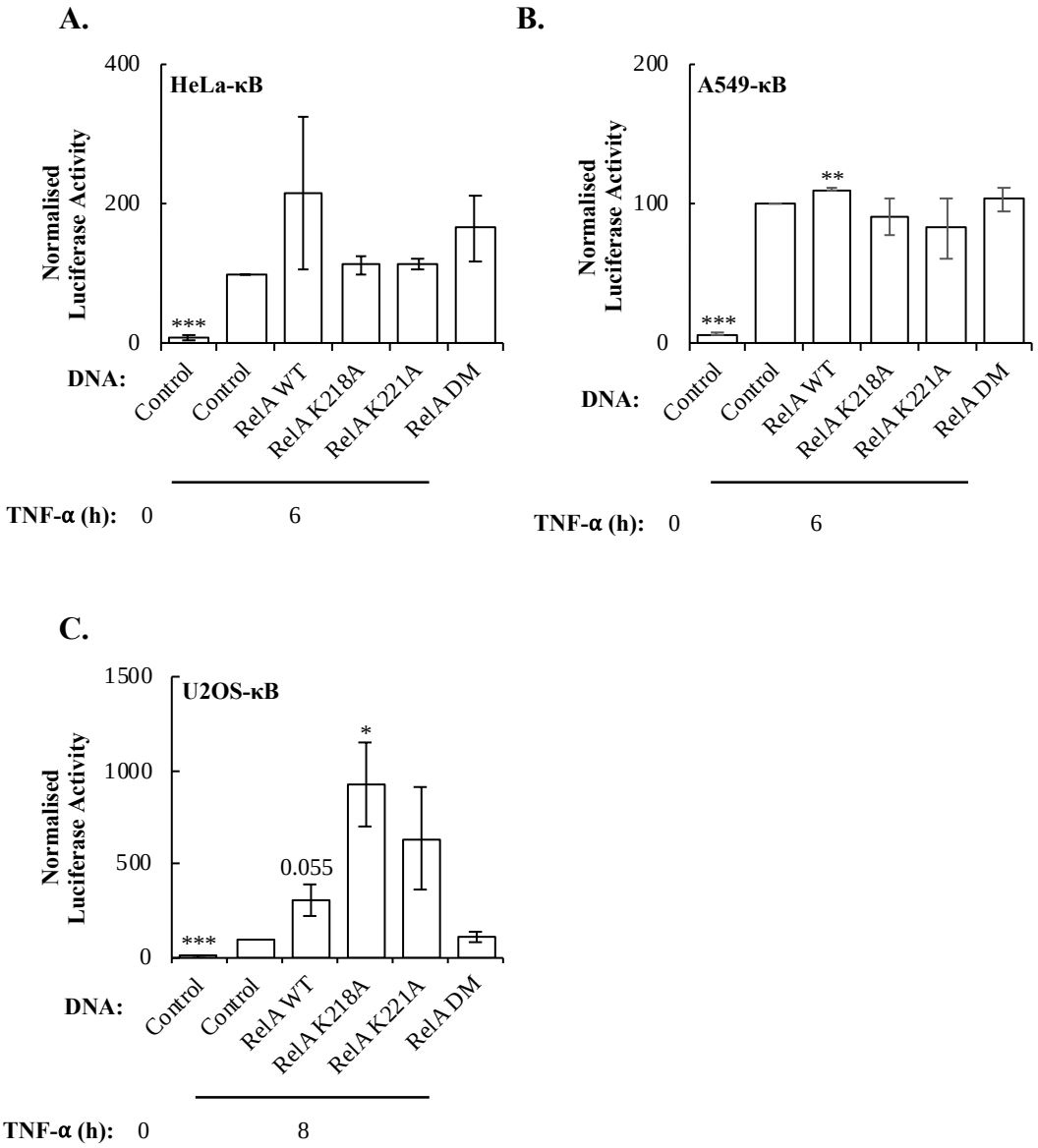

Figure 5.5. NF-κB RelA mutants expression alter the κB activity in different cell lines following TNF-α stimulation. HeLa, A549, and U2OS, cells, stably transfected with κB luciferase reporter, were transiently transfected with the following plasmid DNAs; control (empty vector), RelA WT (wild type), RelA K218A, RelA K221A or RelA DM (double mutant). 10 ng/mL TNF-α treatment was also added for 6 hours in HeLa (**A**), and A549 (**B**) cells; and for 8 hours in U2OS cells (**C**) prior to luciferase measurements. All the values were normalised to TNF-α treated control samples. All the graphs represent mean and standard error of at least three independent biological experiments. Student t-test was applied, and significance determined as follows: * $p \leq 0.05$, ** $p \leq 0.01$, *** $p \leq 0.001$.

Given the degree of conservation of the putative lysine methylation sites, the analysis was repeated using RelB and a similar experimental setting as RelA, across three different reporter cell lines. NF-κB activity was increased with the overexpression of RelB WT and its mutants both in A549 and U2OS cells, however this was not statistically significant (**Figure 5.6**, **B** and **C**). Also, compared to the WT, κB activity was decreased with both single mutants and DM in A549 cells (**Figure 5.6**, **B**). In HeLa cells none of the RelB plasmids were able to induce κB activity (**Figure 5.6**, **A**). Following overexpression of the RelB mutants and TNF-α stimulation, once again no increase in NF-κB activity was observed in HeLa cells (**Figure 5.7**, **A**). In A549 and U2OS cells, no differences were observed between WT and mutants (**Figure 5.7**, **B** and **C**). These results indicate that RelB lysine sites are only necessary for the NF-κB activity in A549, but TNF-α stimulation removes this requirement, possibly by regulating endogenous protein PTMs.

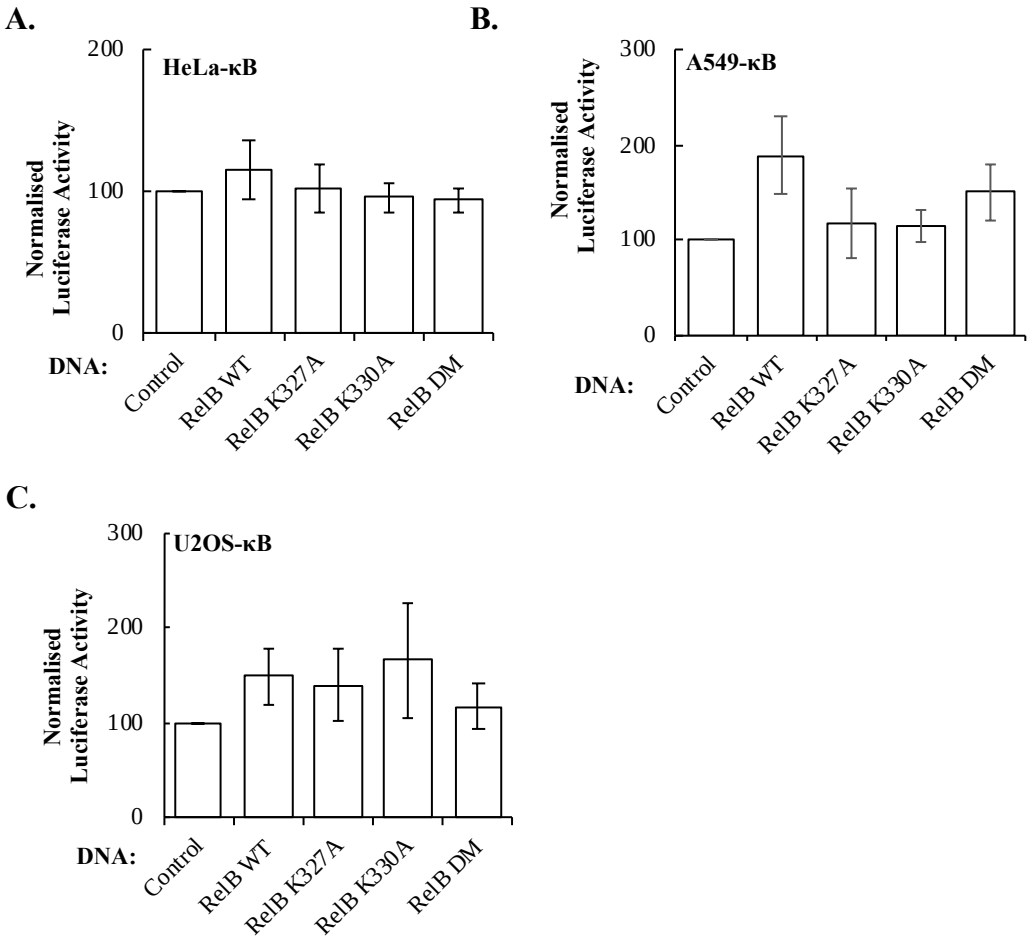

Figure 5.6. NF-κB RelB mutants expression alter the κB activity in different cell lines. HeLa, A549, and U2OS, cells, stably transfected with κB luciferase reporter, were transiently transfected with the following plasmid DNAs; control (empty vector), RelB WT (wild type), RelB K327A, RelB K330A or RelB DM (double mutant) prior to luciferase measurements. All the values were normalised to control samples. All the graphs represent mean and standard error of at least three independent biological experiments. Student t-test was applied, and significance determined as follows: * $p \leq 0.05$, ** $p \leq 0.01$, *** $p \leq 0.001$.

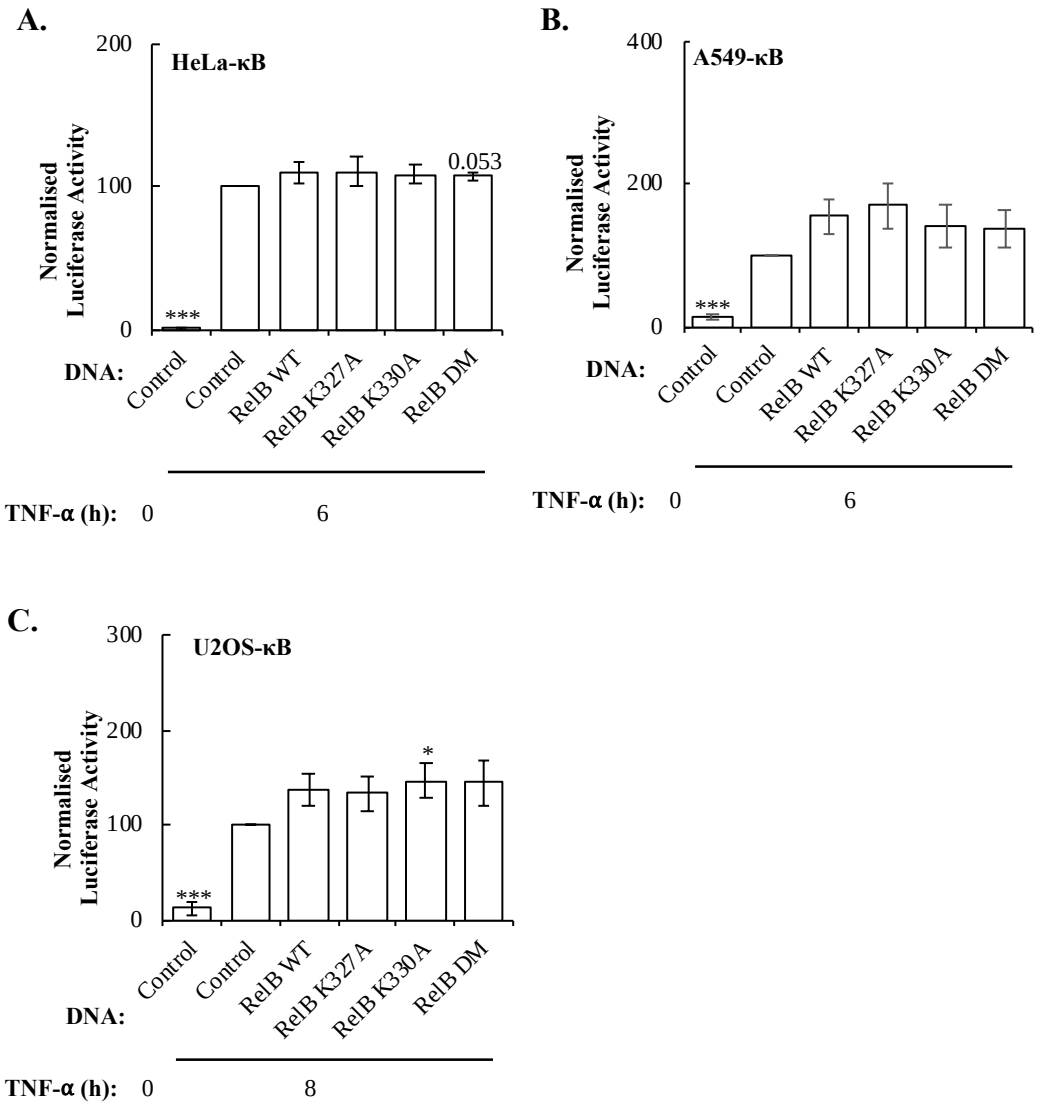

Figure 5.7. NF-κB RelB mutants expression alter the κB activity in different cell lines following TNF-α stimulation. HeLa, A549, and U2OS, cells, stably transfected with κB luciferase reporter, were transiently transfected with the following plasmid DNAs; control (empty vector), RelB WT (wild type), RelB K327A, RelB K330A or RelB DM (double mutant). 10 ng/mL TNF-α treatment was also added for 6 hours in HeLa (**A**), and A549 (**B**) cells; and for 8 hours in U2OS cells (**C**) prior to luciferase measurements. All the values were normalised to TNF-α treated control samples. All the graphs represent mean and standard error of at least three independent biological experiments. Student t-test was applied, and significance determined as follows: * $p \leq 0.05$, ** $p \leq 0.01$, *** $p \leq 0.001$.

Finally, the role of the identified conserved lysine sites was investigated in cRel. Overexpression of the cRel WT and its mutants increased the NF-κB activity in all cell lines (**Figure 5.8**). However, in HeLa cells no differences were observed between WT and mutants (**Figure 5.8**, **A**). On the other hand, in A549 and U2OS cells, that express the same reporter, single lysine mutants' overexpression resulted in higher κB activity (**Figure 5.8**, **B** and **C**).

Following TNF-α stimulation, overexpression of the cRel WT and its mutants significantly increased the NF-κB activity in U2OS cells, with slightly less activity for the DM (**Figure 5.9**, **C**). In HeLa and A549 cells no significant difference was observed between WT and mutants following TNF-α treatment (**Figure 5.9**, **A** and **B)**. These data suggest that upon TNF-α stimulation, cRel lysine methylation sites do not have a significant change to NF-κB activity in the cells analysed.

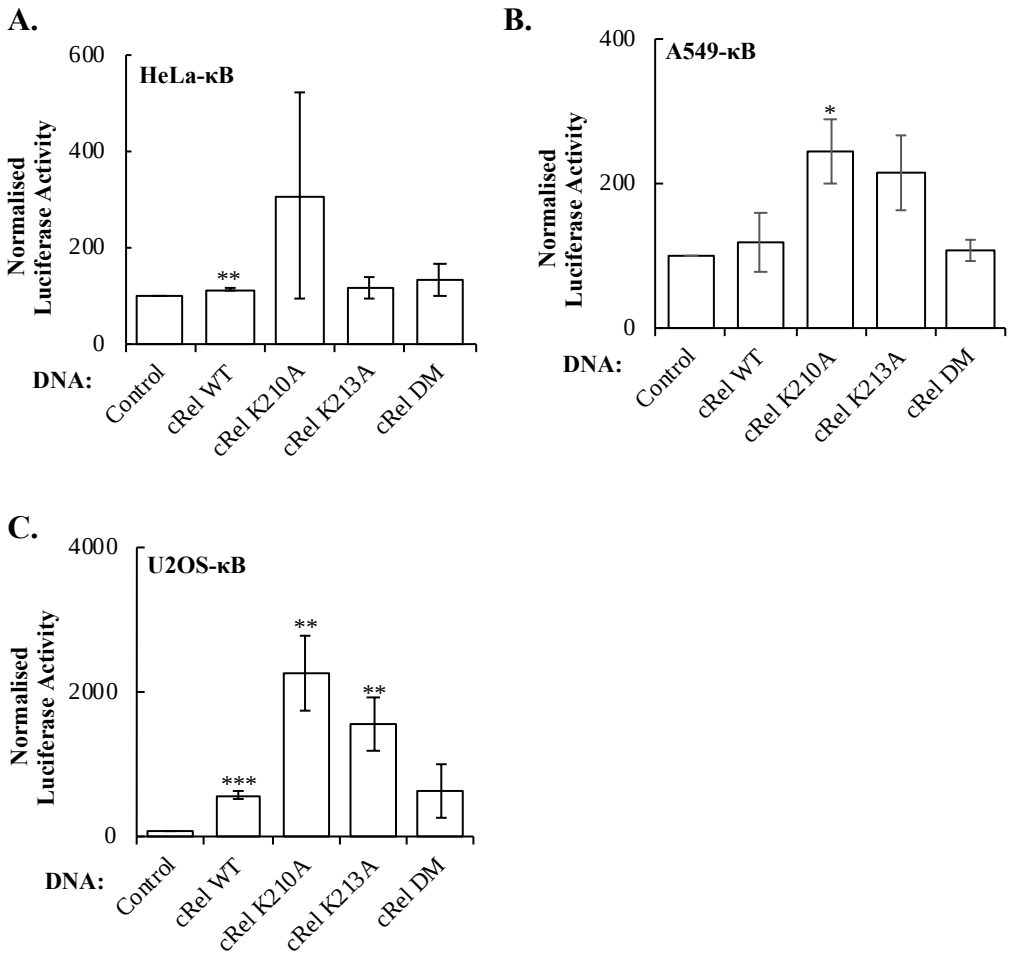

Figure 5.8. NF-κB cRel mutants expression alter the κB activity in different cell lines. HeLa, A549, and U2OS, cells, stably transfected with κB luciferase reporter, were transiently transfected with the following plasmid DNAs; control (empty vector), cRel WT (wild type), cRel K210A, cRel K213A or cRel DM (double mutant) prior to luciferase measurements. All the values were normalised to control samples. All the graphs represent mean and standard error of at least three independent biological experiments. Student t-test was applied, and significance determined as follows: * $p \leq 0.05$, ** $p \leq 0.01$, *** $p \leq 0.001$.

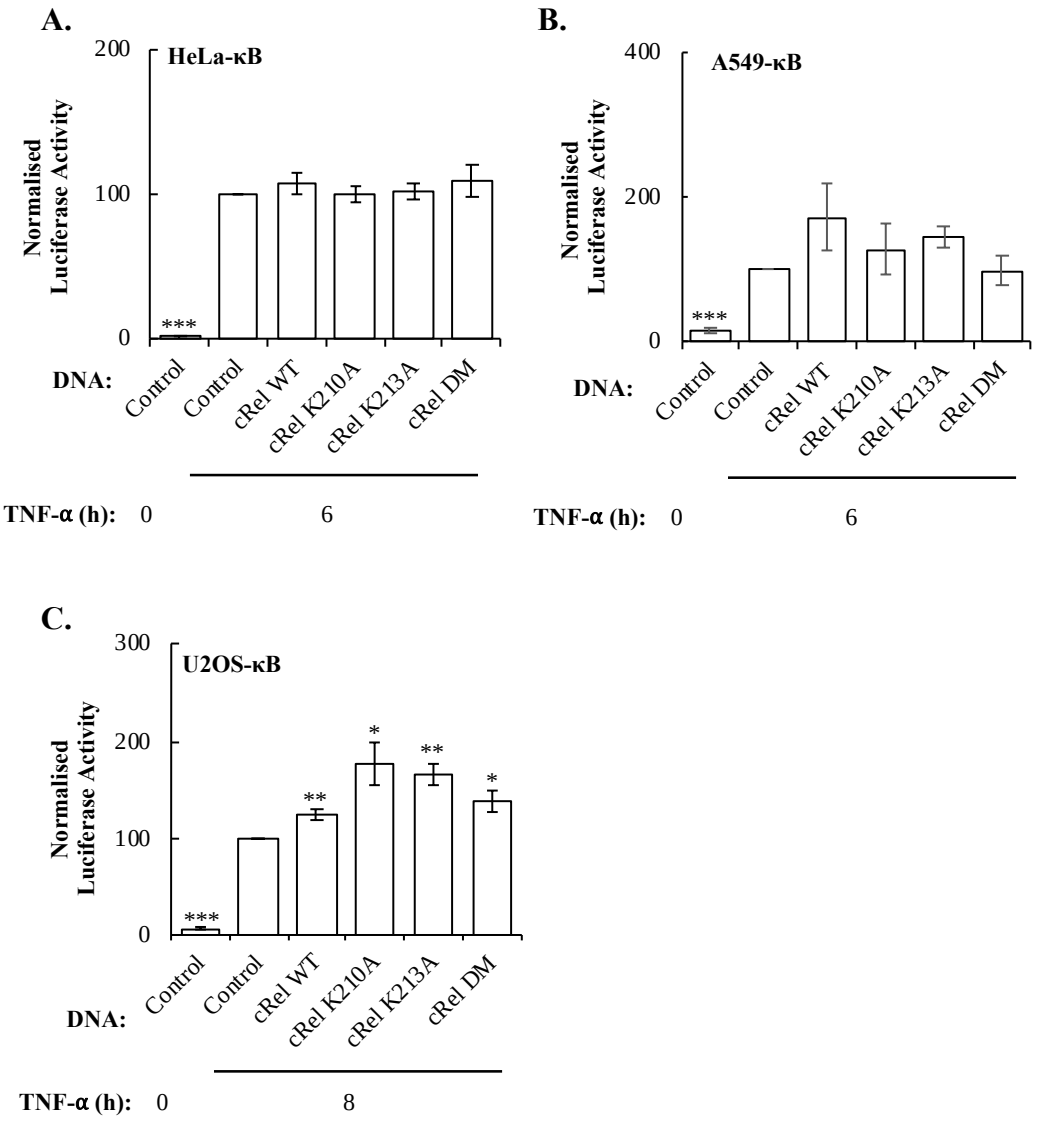

Figure 5.9. NF-κB cRel mutants expression alter the κB activity in different cell lines following TNF-α stimulation. HeLa, A549, and U2OS, cells, stably transfected with κB luciferase reporter, were transiently transfected with the following plasmid DNAs; control (empty vector), cRel WT (wild type), cRel K210A, cRel K213A or cRel DM (double mutant). 10 ng/mL TNF-α treatment was also added for 6 hours in HeLa (**A**), and A549 (**B**) cells; and for 8 hours in U2OS cells (**C**) prior to luciferase measurements. All the values were normalised to TNF-α treated control samples. All the graphs represent mean and standard error of at least three independent biological experiments. Student t-test was applied, and significance determined as follows: * $p \leq 0.05$, ** $p \leq 0.01$, *** $p \leq 0.001$.

Given that reporter gene assays are quite artificial, and NF-κB has many possible intricate mechanisms controlling its genes, it was important to analyse the role of the lysine mutants of RelA on its target genes' mRNA expression levels. To do so, cells were transfected with WT and lysine mutants prior to lysis, RNA extraction, cDNA conversion and qPCR analysis (**Figure 5.10**). This analysis revealed that, both single mutants, K218 and K221, and the double mutant RelA had significantly lower RelA expression compared to the WT (**Figure 5.10**, **A**). Similarly, IL8 expression was decreased with both of the single mutants and the double mutant, when compared to the RelA WT plasmid (**Figure 5.10**, **C**). Interestingly, and despite reduced expression levels, IκBα mRNA was lower with K218A and DM plasmids, but higher with the K221A plasmid, when compared to the RelA WT (**Figure 5.10**, **B**). On the other hand, single mutant plasmids but not the DM elevated the p100 mRNA level (**Figure 5.10**, **D**). These results revealed that K218 and K221 methylation sites are necessary for the complete NF-κB RelA transcriptional response. Each of the methylation site has an impact on different RelA target genes. Although DM reduced the IκBα and IL8 expression evidently, its impact on the p100 expression was not recognisable. Additional experiments investigating the role of cRel and RelB mutants on the NF-κB transcriptional response will need to be completed with future experiments.

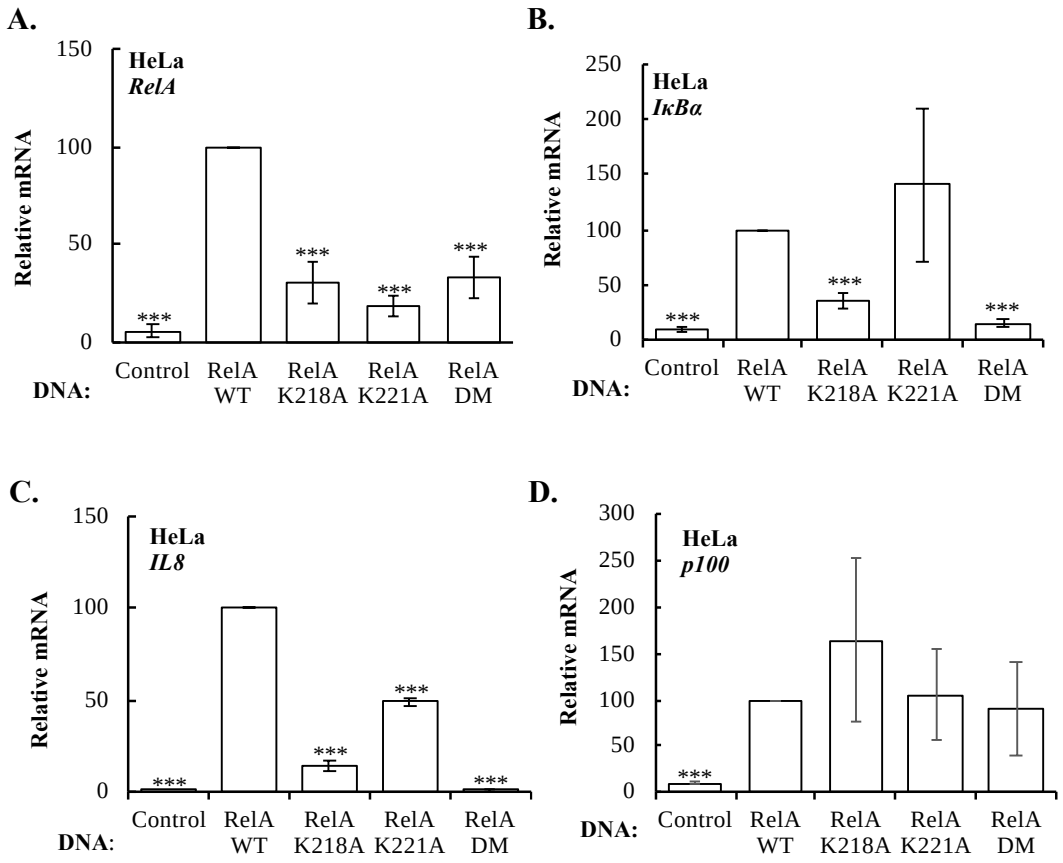

Figure 5.10. RelA mutants' overexpression alters the mRNA expression of RelA and its target genes. HeLa cells were transfected with the following plasmid DNAs; control (empty vector) and RelA WT (wild type), RelA K218A, RelA K221A, and RelA DM (double mutant), 48 hours prior to total RNA extraction and cDNA conversion. Relative mRNA expression levels of the indicated genes were analysed by qPCR using ACTB as a normalising gene. Graphs represent mean and standard error of a minimum of three independent experiments. Student t-test was applied, and significance determined as follows: * $p \leq 0.05$, ** $p \leq 0.01$, *** $p \leq 0.001$.

As the mRNA levels for WT and the lysine mutants were very different, NF-κB mutants were studied for their effect on the protein expression levels of RelA, cRel or RelB as well as some of their target genes (**Figure 5.11**). Western blot analysis revealed that all of NF-κB WT and mutants displayed variable protein expression across three biological replicates, suggesting a combination of variability in transfection efficiency and expression ability. Based on the results of two replicates, the RelA target gene, p100 showed an increase with K218 and K221 single mutants' overexpression, compared to the RelA WT, very likely due to increased expression levels of these mutants (**Figure 5.11**, **A**). Also, consistent to the level of RelA expression, RelA DM induced lower levels of p100 expression in both of the replicates. Similar to RelA results, cRel and RelB expression levels were variable between replicates (**Figure 5.11**, **B** and **C**). The cRel target gene, Claspin (214) was induced in replicates where good expression of cRel WT could be observed (**Figure 5.11**, **B**). Replicate 3 revealed detectable expression of WT and cRel mutants, and under these conditions, only WT and cRel K213A single mutant induced Claspin levels (**Figure 5.11**, **B**). Interestingly, while cRel DM could be detected in all replicates, this failed to induce Claspin when compared to WT (**Figure 5.11**, **B**).

For RelB, CyclinD1 was used as a target gene (182, 213). Expression of RelB WT and mutants revealed to be the most variable between replicates (**Figure 5.11**, **C**). CyclinD1 protein expression levels increased in a similar level to the level of RelB expression (**Figure 5.11**, **C**), suggesting that this target is unaffected by mutation of lysine sites in the RHD. Overall, these results indicate that transiently transfected plasmids express inconsistent protein expressions, and this also affects their target genes' protein expressions. However, it also suggests that at least for RelA and cRel, the lysine sites investigated could be involved in target specificity.

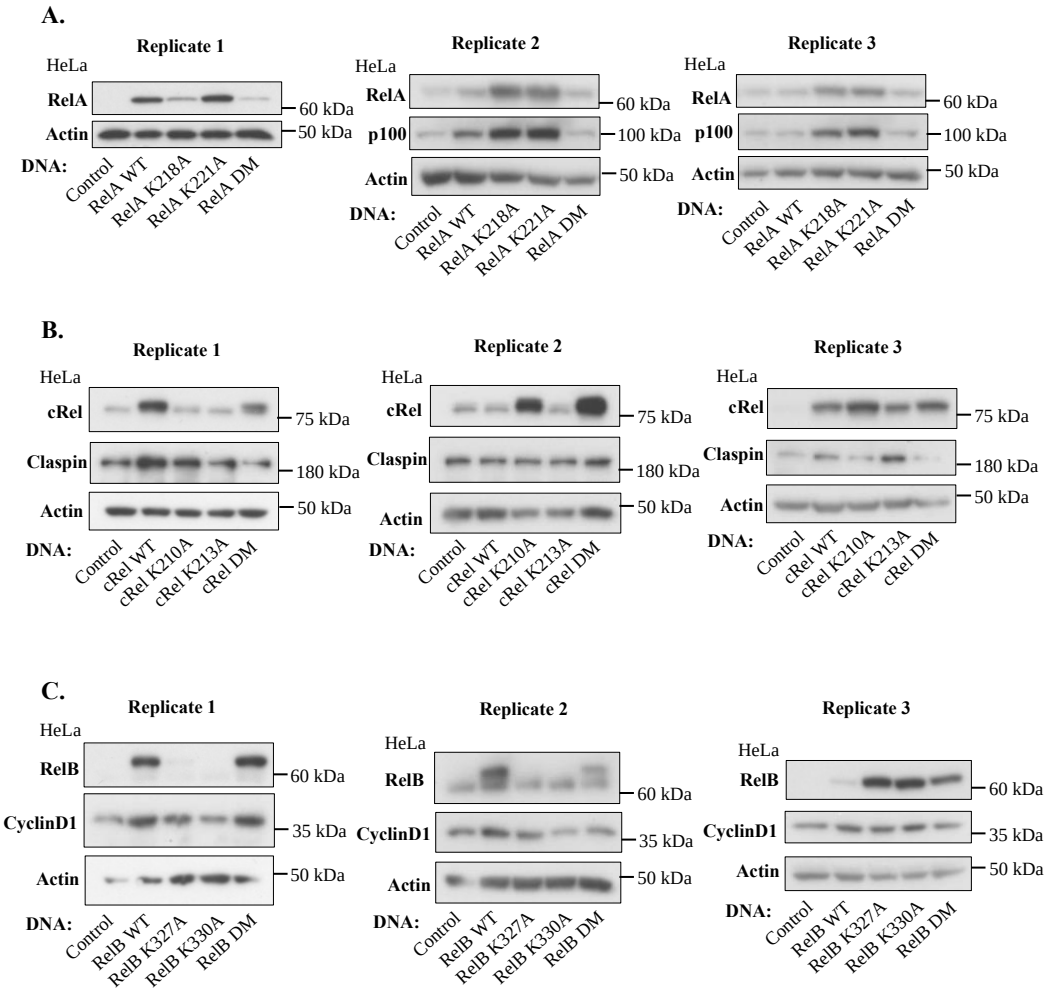

Figure 5.11. NF-*κ*B mutants' protein expression on NF-*κ*B subunits and their target genes. Protein expression levels of the mutated NF-*κ*B subunits RelA (**A**), cRel (**B**), and RelB (**C**) were analysed on HeLa cells. Cells were transfected with the following plasmid DNA before whole cell lysis and probing with western blot method; empty vector (control), RelA WT (wild type), RelA K218A, RelA K221A, and RelA DM (double mutant) (**A**); cRel WT, cRel K210A, cRel K213A, and cRel DM (**B**); RelB WT, RelB K327A, RelB K330A, and RelB DM (**C**). β-Actin was used as a loading control. Blots show three independent replicates of the experiment.

5.4. Putative methylation of the NF-κB proteins and their interaction with KDMs

Given that there have been reports of methylation on RelA in the literature (35, 166, 170-173), it was next investigated if specific NF-κB subunits could be methylated. To this end, overexpression with RelA or p50 plasmid DNAs in HeLa cells, followed by immunoprecipitation (IP) and western blot method was used. In addition, Desferrioxamine (DFX) treatment for 1 hour was also included as a control. DFX is an iron chelator which specifically inhibits molecules that needs iron for their activity, including the KDMs (117). In

DFX exposed cells, demethylating activity of the KDMs should be suppressed. After immunoprecipitation of RelA or p50 using specific antibodies, a pan-methyl lysine antibody was used that specifically identifies trimethylation (**Figure 5.12**). This analysis revealed that in both replicate 1 and 2, RelA has associated trimethylation, but this was insensitive to 1-hour DFX treatment (**Figure 5.12**, **A**). When analysing p50, replicate 1 has shown an associated trimethylation with and without DFX (**Figure 5.12**, **B**). Interestingly, replicate 2 of the p50 protein analysis has shown association with trimethylation only after the addition of DFX. These results suggest that methylation is a modification that also occur in HeLa cells, however, these experiments will need to be repeated in order to have three independent biological replicates with consistent results, and using denaturating conditions, preserving only covalent modifications such as methylation.

These experiments were repeated but instead additional pan-methyl lysine antibodies that specifically detect mono- or dimethylation were used (**Figure 5.13**). Following overexpression of HeLa cells with RelA plasmid DNA and 1-hour DFX treatment, RelA protein was immunoprecipitated followed by western blot analysis. Successful overexpression of RelA was identified at around 65 kDa molecular weight (MW) on the IP lane (**Figure 5.13**, **A**). Interestingly, in the RelA IP lanes, even at endogenous levels, a higher mobility band of around 75 kDa was observed (**Figure 5.13**, **A**), which was lost in the RelA overexpressing, DFX treated cells. This suggests additional modifications such as ubiquitination, which have been previously reported for RelA (258-260). Based only on 1 biological replicate, mono- and dimethylation was identified to associate with the RelA protein in the band around 75 kDa MW, and decreased methylation levels were observed with the DFX treatment, where reduced 75 kDa band was observed for RelA (**Figure 5.13**, **B** and **C**). Also, methylation was observed in DFX treated cells at endogenous level of RelA (**Figure 5.13**, **B** and **C**). These results could suggest that mono- and dimethylation of the RelA in HeLa cells might be leading or associated with other PTMs. This experiment also will need to be repeated in order to reach a conclusion, also including denaturating lysis conditions.

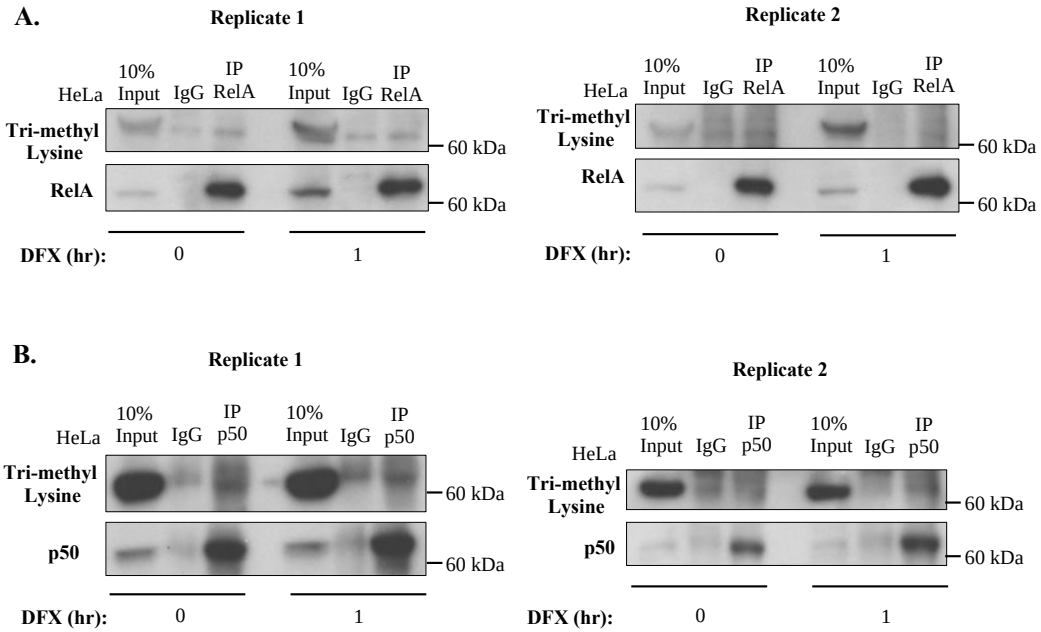

Figure 5.12. Tri-methylation of the NF-κB subunits RelA and p50. HeLa cells were transfected with control (empty vector) and RelA or p50 plasmid DNA, prior to treatment with 200 µM DFX (Desferrioxamine) for 1 hour. Cells were lysed in RIPA buffer, and 250 µg from original lysates were used to immunoprecipitate RelA (**A**) or p50 (**B**). Rabbit IgG was used as antibody control. Immunoprecipitated complexes were analysed by Western blot using the indicated antibodies. Blots show two independent replicates of the experiments. Inputs correspond to 10% of the starting material.

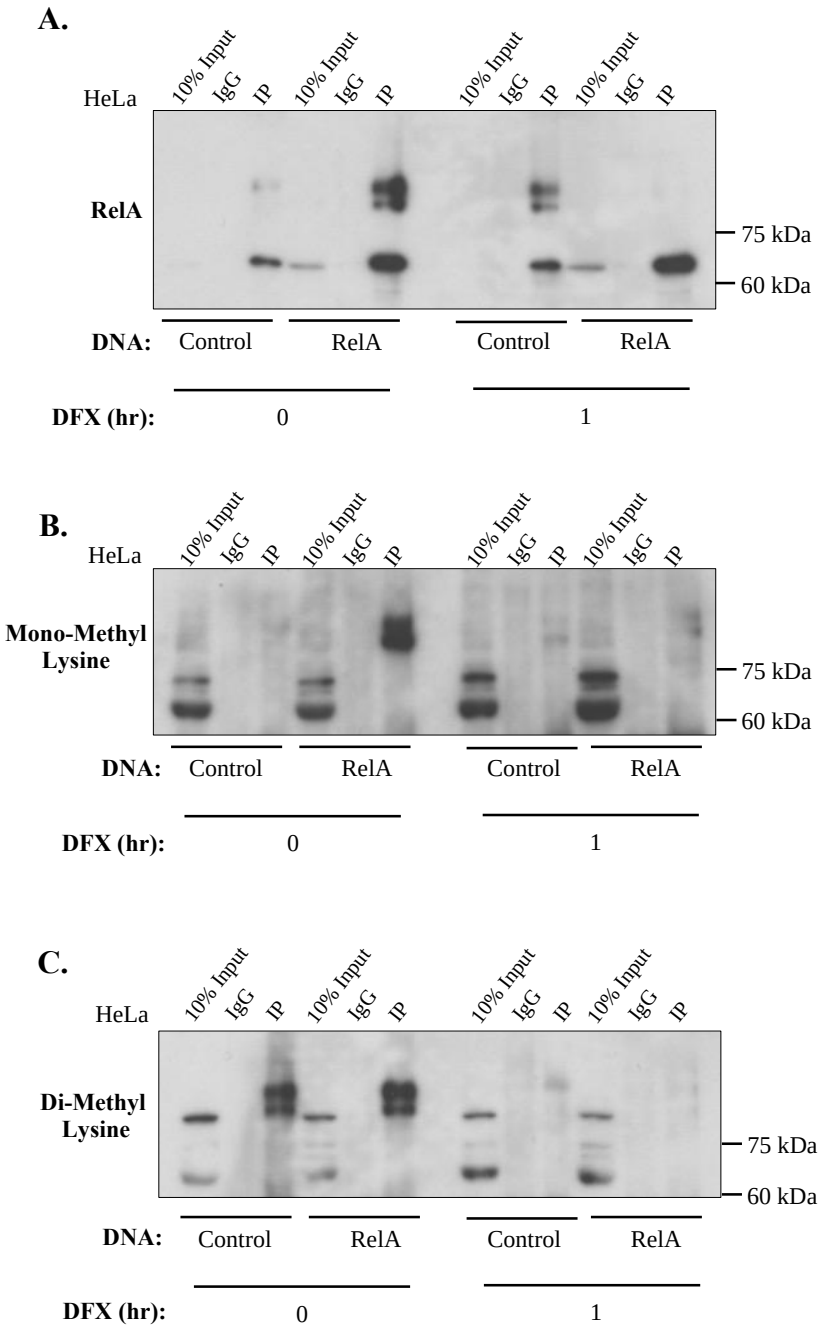

Figure 5.13. Mono- and Di-methylation of the NF-κB subunits RelA and p50. HeLa cells were transfected with control (empty vector) or RelA plasmid DNA, prior to treatment with 200 µM DFX (Desferrioxamine) for 1 hour. Cells were lysed in RIPA buffer, and 166.7 µg from original lysates were used to immunoprecipitate RelA. Rabbit IgG was used as antibody control. Immunoprecipitated complexes were analysed by Western blot using the indicated antibodies; RelA (**A**), Mono-methyl Lysine (**B**), Di-methyl Lysine (**C**). Blots show one independent replicate of the experiment. Inputs correspond to 10% of the starting material.

Given the results obtained with H3K4me3 levels at NF-κB targets and KDM5A involvement in controlling NF-κB, plus the potential methylation of NF-κB subunits, it was hypothesised that a physical complex between NF-κB and KDM5A could occur. As such, following the overexpression of RelA and KDM5A in HeLa cells, the IP western blot method was used (**Figure 5.14**). RelA was immunoprecipitated and its interaction with KDM5A was investigated by western blot using a KDM5A specific antibody. Despite not ideal, as a very strong lysis buffer was used (RIPA), this approach detected KDM5A in the IP lanes at slightly higher levels than those obtained with the IgG control. This suggests an interaction between these two proteins is possible, however the experiment will need to be repeated for reaching to a clear conclusion. Furthermore, a milder lysis buffer, preserving protein-protein interactions should be used.

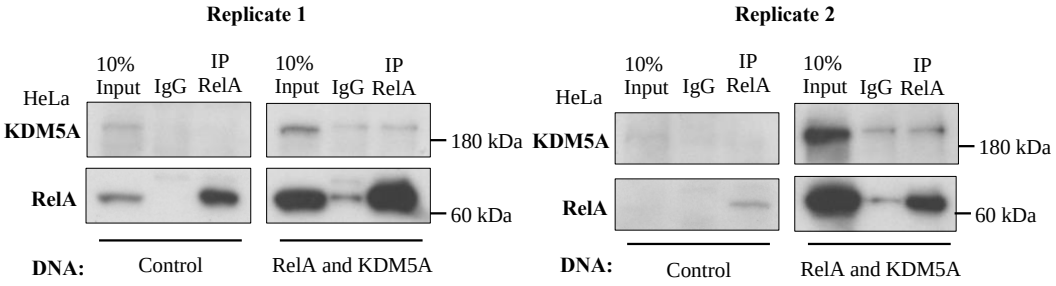

Figure 5.14. NF-κB RelA and KDM5A binding. HeLa cells were transfected with control (empty vector) or RelA and KDM5A plasmid DNAs. Cells were lysed in RIPA buffer, and 250 µg from original lysates were used to immunoprecipitate RelA. Rabbit IgG was used as antibody control. Immunoprecipitated complexes were analysed by Western blot using the indicated antibodies. Blots show two independent replicates of the experiment. Inputs correspond to 10% of the starting material.

5.5. Discussion

Following on investigating the role of KDMs on NF-κB transcriptional response through their histone demethylation activity in the previous chapters; in this chapter, we have investigated the potential methylation of the NF-κB proteins and their effect on the NF-κB transcriptional activity. NF-κB RelA protein was previously shown to have several methylated lysine (K) sites, which are modified by different histone modifying enzymes (35, 166, 170-173). Specifically, Lu and colleagues has found that the RelA K218 and K221 sites are important for the RelA-dependent gene activation and majority of the activated genes can be downregulated by the histone demethylating enzyme, KDM2A (35).

K218 and K221 sites are located at the Rel Homology Domain (RHD) of the RelA structure, and this domain is known with its function for protein dimerization, IκB inhibition and DNA binding (176). Crystal structure of the NF-κB shows that Rel dimers use loops instead of α-helices for contacting with DNA (252, 253). K218 and K221 are found to be located at the loop L4 and are one of the few residues that directly contact the κB site on the DNA (252, 254). The sequence similarity analysis focusing on the K218 and K221 residues of the NF-κB RelA shows that these two sites are evolutionarily conserved in mouse, chicken, frog, and the fly (**Figure 5.1**, **B**). Also, this similarity was shown by Lu and colleagues on several other organisms (35). We have shown that these RelA lysine sites are also conserved in other NF-κB subunits (**Figure 5.2**, **A**). This has suggested that apart from RelA, other NF-κB proteins could also potentially be methylated, contributing to the regulation of the NF-κB transcriptional response. To further investigate the functional contribution of the identified conserved lysine residues on NF-κB transcriptional activity, selected lysine sites were mutated into alanine and NF-κB mutant plasmids were generated with site directed mutagenesis in order to disable the possible methylation at these residues (**Figure 5.3**).

NF-κB mutants were transiently expressed in HeLa-κB, A549-κB, and U2OS-κB luciferase cells and exposed or not to canonical NF-κB pathway inducer, Tumour necrosis factor α (TNF-α). Consistent with the results found in 293C6 cell lines by Lu *et al.* (35), all

RelA mutants increased the NF-κB activity in HeLa cells, however RelA K218 and K221 single mutants decreased the κB activity compared to the wild type, with the reduced activity being more evident with the expression of double mutant plasmid (**Figure 5.4**, **A**). Overall, each of the putative methylation site showed a diverse impact on different cell lines (**Figure 5.4**, **Figure 5.6**, and **Figure 5.8**). However, upon TNF-α stimulation none of the lysine sites were necessary for elevating the NF-κB activity (**Figure 5.5**, **Figure 5.7**, and **Figure 5.9**). As it is mentioned previously, RelA has identified to be methylated at multiple lysine residues upon cytokine stimulation. Thus, inducing the cells with TNF-α could be elevating the methylation of lysine residues on endogenous NF-κB subunits. As such, Ea and colleagues have shown that RelA is monomethylated by lysine methyltransferase Set9 at K37 in response to TNF-α stimulation (172). It was identified that K37 methylation of RelA regulates DNA binding, its promoter recruitment and subsequently the induction of a group of NF-κB target genes. It would therefore be interesting to analyse the effects of this residue in our cellular systems as well.

Gene expression analysis has also shown a variable impact on different RelA target genes when RelA lysine mutants were overexpressed (**Figure 5.10**). Similar to luciferase results, RelA mRNA levels were lower in the mutants' expression, compared to the wild type (**Figure 5.10**, **A**). Analysis of RelA target genes demonstrated variable ability of lysine mutants to induce their expression, when compared to wild type. Supporting our findings, Lu and colleagues has shown that although half of the IL1β-induced NF-κB target genes were downregulated with K218-K221 mutant expression; some of the NF-κB target genes were classified as upregulated or insensitive to the lysine mutations (171). In that study, ChIP-sequencing analysis of binding by K218-K221 double mutant revealed that methylation of K218-K221 sites, which are located on the DNA binding domain of RelA, enhances gene expression mainly by mediating binding to promoters (171). Decreased promoter binding in response to the K218-K221 double mutation correlated with either decreased gene expression

or no significant effect on the gene expression. This indicates that additional factors are involved for the expression of some genes, when K218-K221 sites are unable to be methylated.

NF-κB mutants protein expression levels of RelA, cRel or RelB as well as their target genes also revealed variable levels (**Figure 5.11**). The variable protein expression across replicates could be a combination of variability in transfection efficiency and also expression ability of the mutants. Repeating these experiments with stably transfected cell lines containing NF-κB WT and the lysine mutants' plasmid sequences would clarify the effect of potentially methylated lysine sites on NF-κB protein expressions and their role in NF-κB target gene specificity. Ideally, knock-in mutations using CRISPR would ultimately reveal the functional significance of these sites in the control of expression levels of NF-κB proteins as well as their transcriptional activity.

Several reports of methylation on RelA exist in the literature (35, 166, 170-173). Here, it was also investigated if specific NF-κB subunits could be methylated. Both RelA and p50 were shown to be associated with trimethylation in HeLa cells (**Figure 5.12**). Also, RelA was associated with both mono- and di-methylation without DFX treatment. However, these experiment apart from preliminary, also have technical problems. Ideally, these experiments should be repeated using denaturing lysis conditions, where all interacting proteins are lost but covalent modifications are preserved. In addition, analysis using mass spectrometry would identify all potential methylation sites on NF-κB.

Given the variable nature of the expression of the lysine mutants, it would be possible to speculate that methylation is needed for protein stability. This could be analysed in stable cells lines using cycloheximide chase experiments. Also, to further investigate the role of methylation in the NF-κB activation, two necessary steps for the NF-κB activation could be analysed: IκBα degradation or production, and RelA nuclear translocation. Cellular fractionation into cytoplasmic and nuclear compartments would need to be prepared after TNF-α stimulation and broad methylation inhibitor, methylthioadenosine (MTA) treatment and immunoblot for IκBα and RelA in both of the cellular locations.

In the future experiments, characterising the NF-κB mutants for their impact in cellular processes is fundamental. As such, investigating the role of mutated lysine sites in cell proliferation, cell death and colony formation would clarify the role of the lysine sites on regulating cellular development and survival. Furthermore, lysine sites could also impact the NF-κB transcriptional response via regulating the NF-κB oligomerisation, nuclear localization, and DNA binding. Lu *et al.* has shown that overexpression of K218-K221 mutants decrease the ability of both the RelA-RelA homodimer and RelA-p50 heterodimer to bind to DNA, compared to the RelA wild type in electrophoretic mobility shift assay (EMSA) (35). However, the ratio of the dimerization with the K218-K221 mutant was similar to the RelA wild type, suggesting that the lysine mutation in RelA did not impact its binding to p50. Further experiments investigating other NF-κB subunits for their oligomerisation and DNA binding will clarify the role of the lysine sites on NF-κB transcriptional response.

It has been shown that post-translational methylation associates with other types of PTMs. For instance, damage-specific DNA binding protein 1 (DDB1)/cullin4 (CUL4) E3 ubiquitin ligase complex and a DDB1-CUL4-associated factor 1 (DCAF1) adaptor recognises monomethylated lysine residues on its substrate and promotes ubiquitylation (261). RelA lysine sites that are subject to methylation are also shown to be modified by acetylation and ubiquitylation, suggesting that the crosstalk between several PTMs is involved in regulating RelA and controlling transcription in gene-specific manner (173, 262, 263). TNF-α stimulated acetylation of K310 is shown to inhibit the K314 and K315 methylation of RelA, which is important for the ubiquitylation and degradation of chromatin-associated RelA (173, 262). Furthermore, RelA K218 and K221 methylation sites also shown to be targeted for acetylation (263), however, their association with ubiquitylation is not clear. It will be of great interest to explore whether a crosstalk between post-translational methylation and other PTMs, similar to those identified with RelA, would apply to other NF-κB subunits.

We then investigated if RelA and KDM5A interacts with each other (**Figure 5.14**). Despite of using a strong lysis buffer (RIPA), a slight interaction was detected with two

biological replicates. This experiment will need to be repeated with milder lysis buffer in order to conserve even possible weaker interactions between NF-κB and KDMs. Also, doing a nuclear extraction would be more efficient as it has been stated in multiple studies that methylation of NF-κB takes place after they bind to DNA. Lu and group have shown that RelA is not associated with histone modifying enzymes KDM2A and NSD1 until it is activated, suggesting that the lysine modification of NF-κB happens only after it is dissociated IκB and enters the nucleus (35, 170). Also, Ea and group has shown that K37 methylation of RelA was only identified in nuclear fraction of the cell lysates, suggesting that RelA methylation is restricted to the nucleus (172).

Furthermore, based on co-immunoprecipitation data, KDM4A and KDM4C forms a complex with NF-κB in response to T follicular helper cell-derived signals and mediates the cell cycle progression of the activated B cells (239). In that study interaction between the KDMs and NF-κB RelA was detected after 24 hours of stimulation but not 48 hours, which shows that their association is time dependent upon stimulation. Another study suggested that RelA physically interact with KDM4A at the interferon type I promoter region (168), however clear function of this interaction has not been clarified. Also, it has been reported that KDM4B induces changes in chromatin structure near osteoclast-related gene promoters through H3K9 demethylation, leading to NF-κB RelA recruitment via a direct interaction with KDM4B (264). Overall, these studies support our hypothesis on the close regulation of NF-κB by KDMs.

It has also shown that RelA and histone methylations might involve in a cooperative mechanism for regulating NF-κB transcriptional response. Levy and colleagues have reported that mono-methylation of RelA K310 site under unstimulated conditions downregulates the NF-κB target gene expressions by G9A-like protein (GLP)-mediated H3K9 di-methylation, which leads to chromatin silencing (166). On the other hand, upon TNF-α and LPS stimulation, phosphorylation of RelA at serine 311 blocked this mechanism and led to transcriptional activation (166). In the future studies, it would be interesting to further

investigate the link between methylation of NF-κB subunits and histone proteins for the regulation of NF-κB activation and target gene expressions.

To summarise, this chapter has suggested that methylation of NF-κB subunits as an additional mechanism that could regulate the NF-κB activation and transcriptional response. Previously identified RelA K218 and K221 methylation sites were discovered to be conserved in all NF-κB subunits. These potential methylation sites have shown to alter the NF-κB transcriptional activity in different cell types. Also, the preliminary work looking at the direct interactions between NF-κB subunits and KDMs showed a potential association between these proteins.

Chapter 6 - Identification of hypoxia inducible NF-κB target genes signature using publicly available RNA-sequencing datasets

6.1. Introduction

Maintaining the oxygen homeostasis is essential to support different cellular metabolism and physiological functions. Hypoxia induces multiple adaptive mechanisms, aiming to balance the oxygen supply and demand in multicellular organisms (265). This response can be variable depending on tissue type, and duration and the degree of the oxygen concentration both in physiological and pathological states.

Most of the responses to hypoxia are coordinated at the transcriptional level, with the hypoxia inducible factor (HIF) being the main transcription factor family controlling the changes in gene expression levels (266). Transcriptional response required for maintaining oxygen homeostasis and its alteration in different disease states has been studied extensively to identify the complete set of genes regulated by hypoxia using different gene profiling techniques (reviewed in (75)). When collectively analysed, these data revealed a cell or tissue specific transcriptome responses, with an underlying cell type independent, also known as "core" hypoxia responsive gene signature (88, 91, 267-269). Most recently, the Del Peso group produced a robust hypoxic signature applying meta-analysis techniques on an extensive number of RNA sequencing samples collected from various studies that included 33 different cell types (91). This approach enabled the identification of a comprehensive core gene signature that is regulated by hypoxia.

NF-κB is a key transcription factor which has recognised as an important player in the cellular response to hypoxia (148). The hypoxia induced NF-κB transcriptional response has been studied by several groups (148, 151, 152, 232). However, the complete mechanisms explaining the oxygen regulation of the NF-κB pathway and hypoxia stimulated NF-κB target gene expression profile still remain an area for investigation.

In this chapter, to characterise the hypoxia inducible NF-κB target gene signature in different cell lines, a bioinformatics approach was used. Publicly available hypoxia transcriptomics were analysed, specifically, the RNA-sequencing data, and integrated with a list of validated NF-κB target genes listed by the Gilmore laboratory. This approach has

identified cell type specific hypoxia inducible NF-κB target gene signatures. Also, cell type independent NF-κB target genes were identified using hypoxia inducible core gene signature meta-analysis from the Del Paso group (91). These signatures will be useful resource for future work uncovering the mechanistic link between hypoxia and NF-κB.

6.2. Hypoxia inducible NF-κB target gene signatures in different cell types

To identify hypoxia inducible NF-κB target genes, a bioinformatics approach was used as summarised in **Figure 6.1**. First of all, hypoxia transcriptomics datasets containing gene transcriptional responses to hypoxia, were selected from the NCBI Gene Expression Omnibus (GEO) (183), and raw data files were downloaded from the NCBI sequencing read archive (SRA). The downloaded hypoxia RNA-sequencing datasets contained 3 biological replicates with 24 hours of 1% oxygen treatment performed in human cell lines in different tissues (**Table 6.1** and **Table 6.2**).

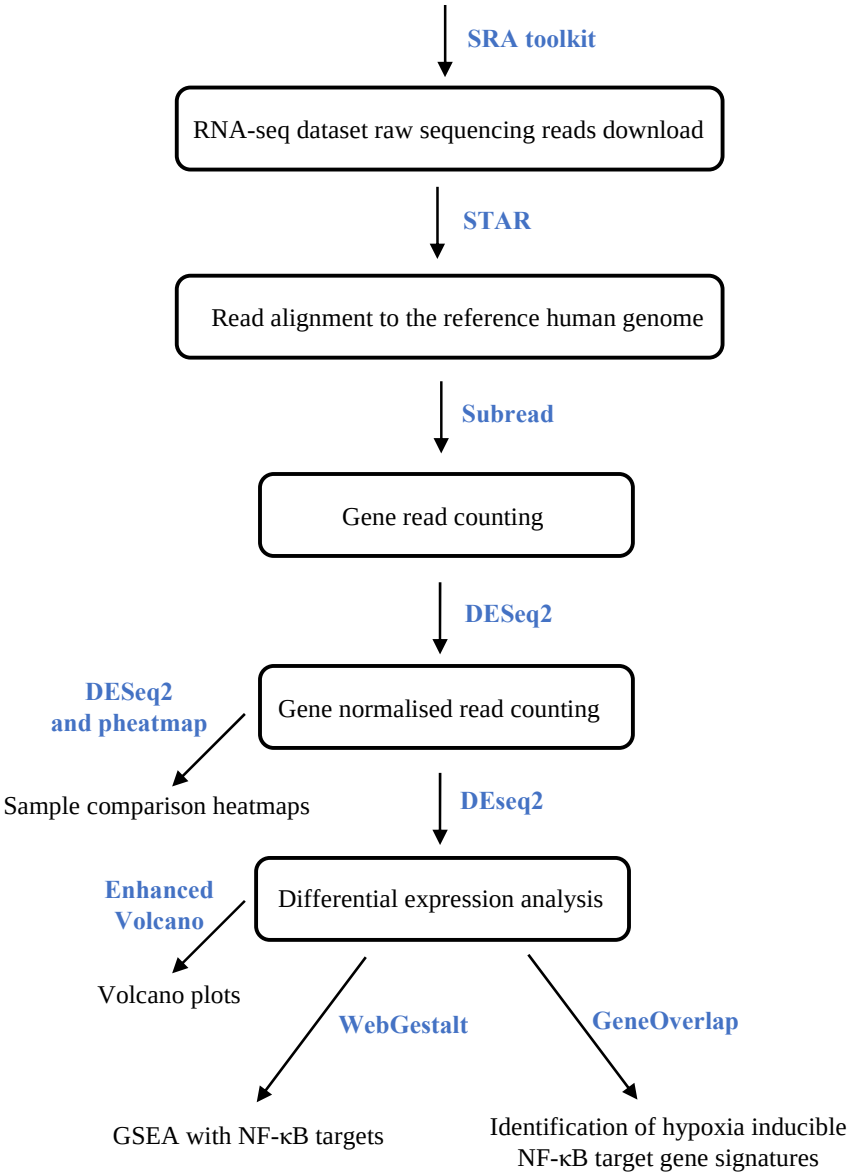

Figure 6.1. Bioinformatics analysis workflow. Flow chart summarising bioinformatics analysis pipeline. Software tools used at each stage are shown in blue.

Table 6.1. Summary of hypoxia RNA-sequencing dataset information. CML; Chronic myelogenous leukaemia

Cell line	Tissue	Type	Control	Hypoxia	NCBI GEO ID
HeLa	Cervical adenocarcinoma	Epithelial	21% oxygen	24 hours, 1% oxygen	GSE186370
MCF-7	Breast adenocarcinoma	Epithelial			GSE153291
A549	Lung carcinoma	Epithelial			GSE186370
HCT116	Colorectal carcinoma	Epithelial			GSE81513
K562	Bone CML	Lymphoblast			GSE144527
U87	Brain glioblastoma	Epithelial			GSE78025
501-mel	Skin melanoma	Epithelial			GSE132624

Table 6.2. Sequence Read Archive (SRA) accession numbers for hypoxia RNA-sequencing datasets.

Cell line	Control #1	Control #2	Control #3	Hypoxia #1	Hypoxia #2	Hypoxia #3
HeLa	SRR16531798	SRR16531799	SRR16531800	SRR16531804	SRR16531805	SRR16531806
MCF-7	SRR12094720	SRR12094721	SRR12094722	SRR12094723	SRR12094724	SRR12094725
A549	SRR16531807	SRR16531808	SRR16531809	SRR16531810	SRR16531811	SRR16531812
HCT116	SRR3535647	SRR3535651	SRR3535655	SRR3535683	SRR3535687	SRR3535691
K562	SRR10989435	SRR10989436	SRR10989437	SRR10989459	SRR10989460	SRR10989461
U87	SRR3175550	SRR3175551	SRR3175552	SRR3175553	SRR3175554	SRR3175555
501-mel	SRR9283239	SRR9283240	SRR9283241	SRR9283245	SRR9283246	SRR9283247

The RNA sequencing datasets were then aligned to the human reference genome, and gene read counting was applied. For the initial investigation of the data, sample-to-sample correlation heatmaps were generated using normalised read count data for each cell line (**Figure 6.2**). As hypoxia is known to alter the transcription of a high number of genes (75, 91), it is expected that samples will cluster by treatment (i.e., control or hypoxia). As predicted, HeLa, HCT116, MCF-7, 501-mel, K562, A549 and U87 cell line samples clustered by treatment (**Figure 6.2**, **B**, **C**, **D**, **E**, **F**, **G**, and **H**). On the other hand, human umbilical vein endothelial cells (HUVEC) did not show any clustering in the same treatment types (**Figure 6.2**, **A**).

Next, differential expression analysis was performed, where normalised read count data was used to discover quantitative changes in gene expression levels of hypoxia treated samples compared to control. Differential expression analysis was used to generate volcano

plots, visualising the effect of hypoxia on gene expression levels in each cell line (**Figure 6.3**). The effect size cut off of log2 fold change greater than 0.58 was applied to identify the differentially expressed genes (DEGs) in hypoxia compared to control conditions in each cell line. This log2 fold change cut off was chosen to set a minimum value for the effect size whilst avoiding discarding the potential biologically relevant data points that could occur when using higher effect size cut-offs. Additionally, statistical significance cut-off of FDR less than 0.05 was applied. As a result, the number of changes in all cell lines were similar to other RNA-sequencing dataset analysis (75, 91), where the numbers of DEGs are comparable to what was previously reported (**Figure 6.3**). U87 and HCT116 cell lines showed the highest number of repressed and induced list of genes (**Figure 6.3**, **H** and **C**), indicating that brain glioblastoma and colorectal carcinoma tissue types are the most responsive to the 24 hours of 1% oxygen. Hela cells had almost 5 times more upregulated list of genes than the downregulated (**Figure 6.3**, **B**). 501-mel, K652, and A549 had about 2 times more of upregulated genes than the downregulated, whereas MCF-7 cells had almost equal amount of the increased and decreased list of genes (**Figure 6.3**, **E**, **F**, **G**, and **D**). These results indicated that, each cell line respond to hypoxia differently. The tissue type-specific hypoxia response was previously reported by Puente-Santamaria and colleagues, where endothelial cells had significantly distinct gene expression pattern compared to other analysed cell types (91). However, reason behind the variable gene expression patterns in different cell lines and the possible differences in their response mechanisms has not been studied and will need to be clarified in the future analysis. On the other hand, HUVEC cells showed the lowest transcriptional response (**Figure 6.3**, **A**). Due to high sample variability and low number of gene changes, HUVEC cells were excluded from the downstream analysis (**Figure 6.2**, **A** and **Figure 6.3**, **A**).

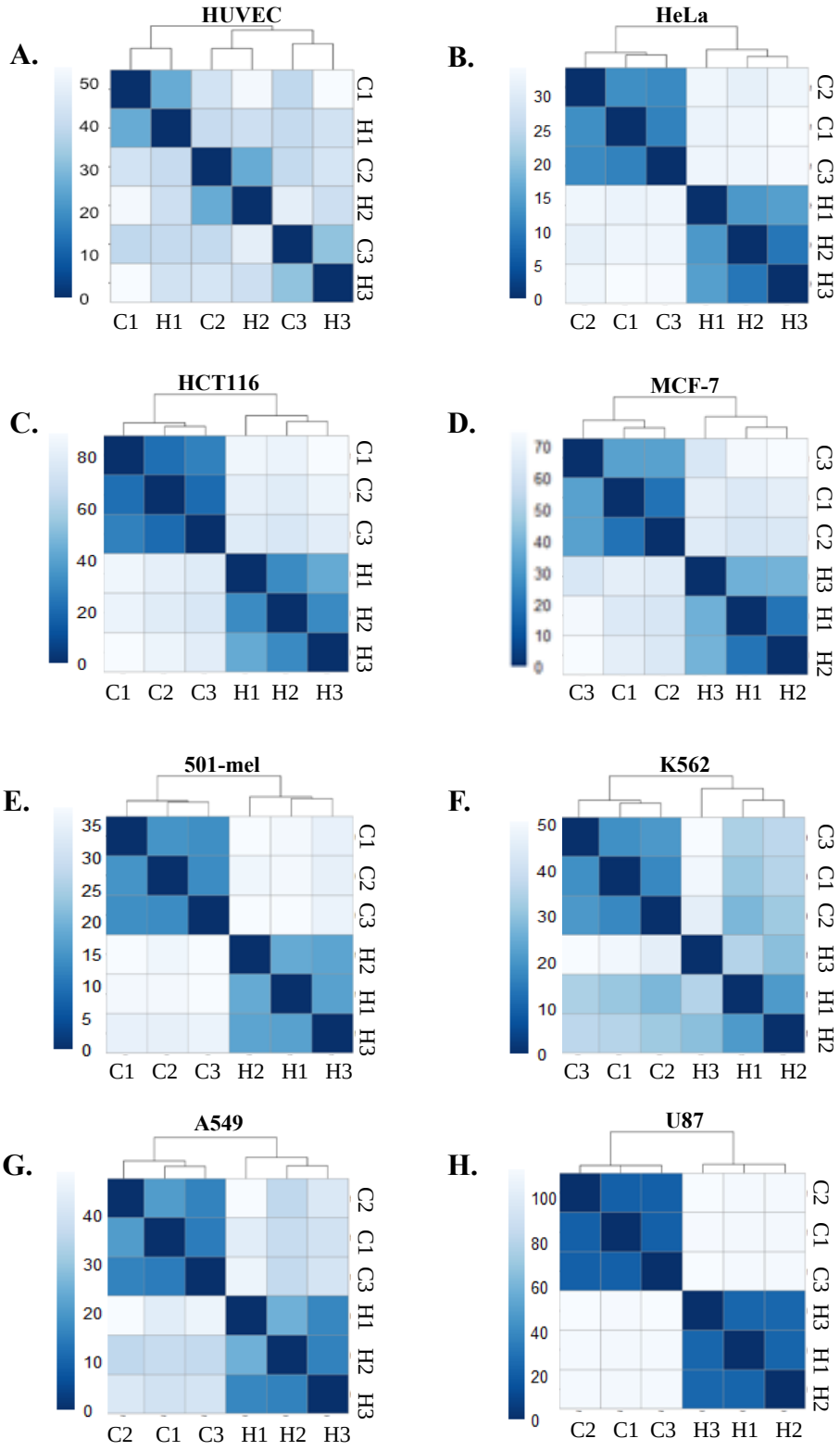

Figure 6.2. Sample comparison heatmaps. Sample to sample distance heatmaps of normalised read counts from RNA-sequencing in the indicated cell lines. Hierarchal clustering is also shown. C; Control (21% oxygen), H; Hypoxia (24 hours, 1% oxygen).

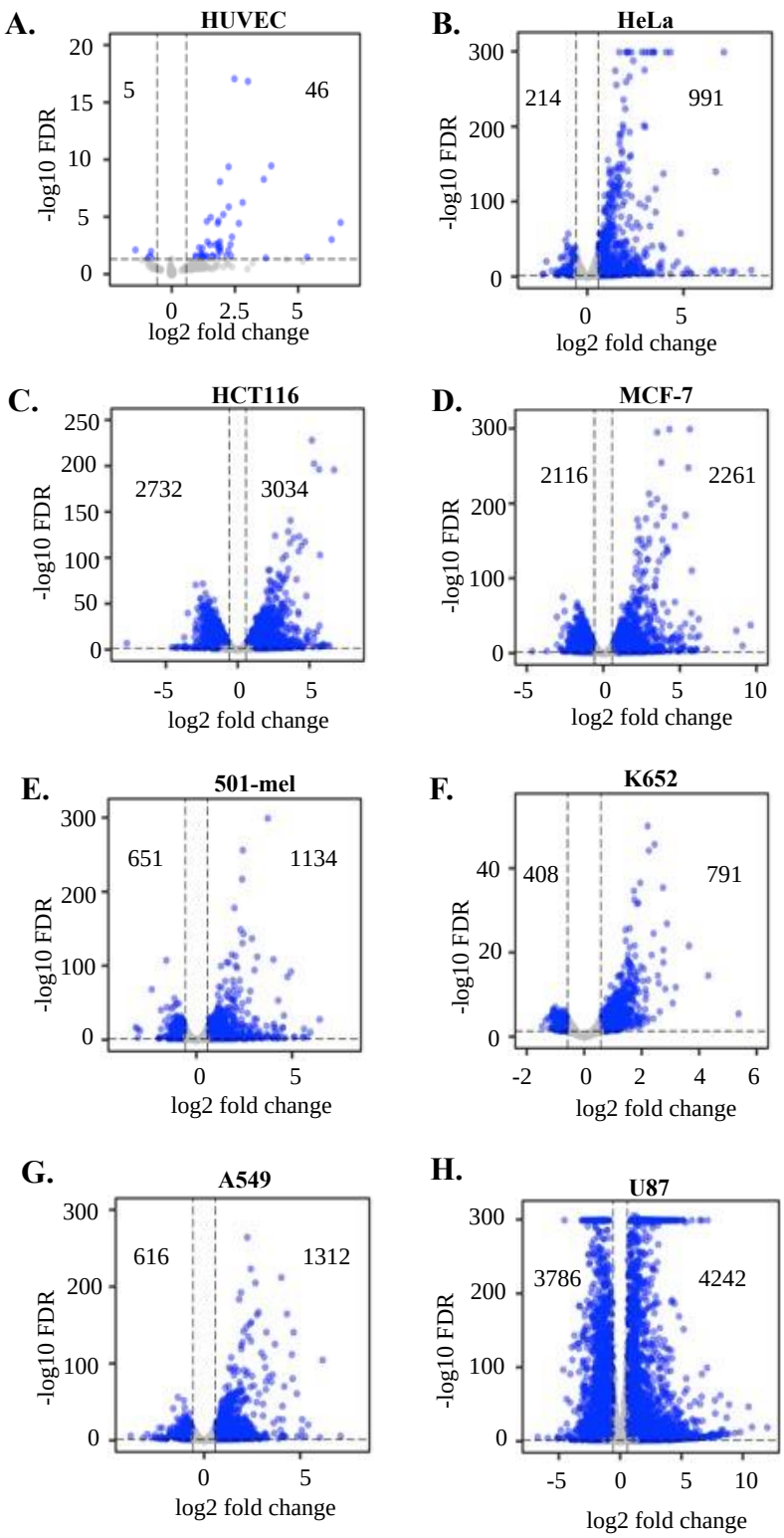

Figure 6.3. Differential expression analysis volcano plots. Volcano plots displaying differential expression analysis comparing hypoxia (24 hours, 1% oxygen) to control (21% oxygen) from RNA-sequencing in the indicated cell lines. Blue points; differentially expressed genes (DEGs) with the following cut-off values; FDR < 0.05 (-log10 FDR < 1.3) and log2 fold change in RNA levels > 0.58. Number of upregulated (right side) and downregulated (left side) DEGs are labelled.

In order to investigate the link between NF-κB target genes and hypoxia responsive genes, Gene Set Enrichment Analysis (GSEA) was applied (186), using the NF-κB target genes list that was obtained from the Gilmore laboratory (https://www.bu.edu/nf-kb/gene-resources/target-genes/). This analysis compared the list of NF-κB target genes with the list of genes obtained from the differential expression analysis of the hypoxia transcriptomic experiments across different cell types (**Figure 6.4**). A positive normalised enrichment score (NES) was obtained in all cell lines, indicating that NF-κB target genes are enriched at hypoxia upregulated genes. The enrichment was statistically significant in all cell lines with an FDR value below 0.05, except for K562 cells.

The link between NF-κB target genes and hypoxia upregulated genes was further investigated by overlapping the Gilmore laboratory NF-κB target genes list with the lists of hypoxia upregulated genes obtained from the differential expression analysis in different cell lines (**Figure 6.5**, **A**). Overall, 132 different genes were identified as hypoxia inducible NF-κB target genes. For each cell line, overlap of hypoxia upregulated genes with NF-κB target genes was statistically significant, with a *P* value of below 0.05 (**Figure 6.5**, **B**). These results further demonstrate that hypoxia inducible genes are associated with the NF-κB target genes across all different cell types investigated.

To elucidate the NF-κB target genes that are upregulated in hypoxia, independent of cell type, NF-κB target genes were overlapped with the list of core hypoxia upregulated genes, obtained from the hypoxia RNA-sequencing meta-analysis study of the Del Peso group, which is based on 33 different cell types (91). As a result, 11 core hypoxia upregulated NF-κB target genes were identified, which were also statistically significant (**Figure 6.5**, **A** and **B**). Taken together, this analysis uncovered the hypoxia inducible NF-κB target genes signature in individual cell types, as well as the NF-κB target genes that are hypoxia-inducible independent of the cell type (**Table 6.3**). Although all of the cell types had a shared NF-κB target genes signature, majority of the hypoxia upregulated genes identified was unique to individual cell line types.

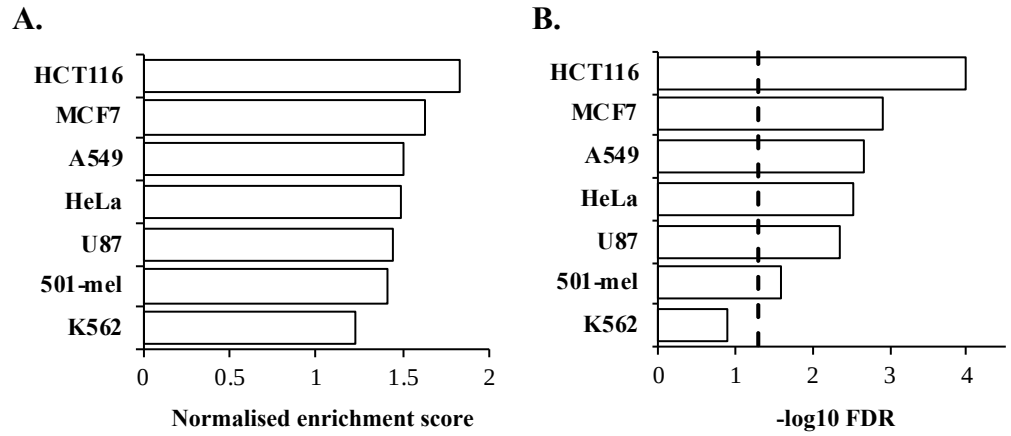

Figure 6.4. NF-κB target gene enrichment analysis with hypoxia RNA-sequencing. Gene Set Enrichment Analysis (GSEA) comparing NF-κB target genes from the Gilmore lab to a list of genes ranked by log2 fold change in RNA levels in hypoxia (24 hours, 1% oxygen) compared to control (21% oxygen) from RNA-sequencing in the indicated cell lines. Graph depicts normalised enrichment scores from GSEA in the indicated cell lines (**A**). Graph depicts statistical significance (-log10 FDR) from GSEA in the indicated cell lines (**B**). Dashed line shows statistical significance threshold of FDR 0.05 (-log10 FDR 1.3).

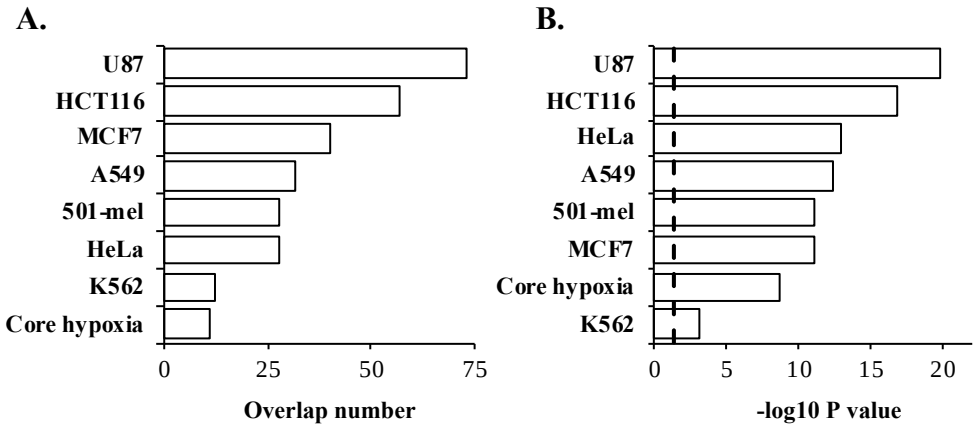

Figure 6.5. Overlap analysis of hypoxia upregulated genes and NF-κB target genes. Overlap of NF-κB target genes from the Gilmore laboratory with hypoxia upregulated genes determined by RNA-sequencing comparing hypoxia (24 hours 1% oxygen) with control (21% oxygen) or core hypoxia upregulated genes determined by RNA-sequencing meta-analysis (91). Gene overlap analysis (**A**). Statistical significance (-log10 P) from overlap analysis (**B**). Dashed line shows statistical significance threshold of P 0.05 (-log10 P 1.3).

Next, we asked if hypoxia upregulated NF-κB target genes identified in different cell lines and the core hypoxia induced NF-κB target genes overlap with the genes identified in the previous chapters that investigated the role of H3K4me3 and H3K36me3 histone marks on the NF-κB transcriptional response with hypoxia stimulation (**Chapter 3** and **Chapter 4**). When H3K36me3 ChIP-sequencing peaks with 1 hour hypoxia treatment overlapped with the hypoxia upregulated NF-κB target genes listed in Table 6.3; only FTH1 gene in the HCT116 cell line was found to be common in both gene sets (**Table 6.3**). H3K4me3 ChIP-sequencing peaks with 1 hour and 6 hours hypoxia treatments were overlapped with the hypoxia upregulated NF-κB target genes listed in Table 6.3, and 8 genes were found to be common in both data sets, which 3 of them were the core hypoxia induced NF-κB target genes (**Table 6.3**). These findings indicate that some of the cell-specific and the core hypoxia induced NF-κB target genes could potentially be regulated through H3K4me3 or H3K36me3 histone marks. Repeating the experiments performed in Chapters 3 and 4 using different cell types would further validate this hypothesis.

Table 6.3. Hypoxia upregulated NF-κB target genes in different cell lines. The list of genes was obtained by overlapping NF-κB target genes from the Gilmore laboratory with hypoxia upregulated genes determined by 24 hours hypoxia RNA-sequencing or core hypoxia upregulated genes determined by RNA-sequencing meta-analysis. Cell type-independent, "Core" hypoxia upregulated NF-κB target genes determined by RNA-sequencing meta-analysis are listed in blue. Hypoxia upregulated NF-κB target genes overlapped with the H3K36me3 1 hour hypoxia ChIP-sequencing high stringency dataset is shown with the green asterisk "*". Hypoxia upregulated NF-κB target genes overlapped with the H3K4me3 1 hour and 6 hours hypoxia ChIP-sequencing high stringency datasets is shown with the red asterisk "*"

Cell Lines	Hypoxia upregulated NF-κB target genes
HeLa	TNFRSF9, PTGS2, IL11, PDGFB, LIPG, AMH, EBI3, SERPINE1, SOD2, IL1A, FN1, F3, TNFAIP3, SDC4, BMP4, SLC6A6, IL1RN, IER3, TLR2, TNIP1, LCN2, VEGFC, CCL28, TERT, OLR1, BNIP3, TNFSF15, F8
HCT116	SERPINB1, TRAF1, MYLK, BCL3*, NFKB2*, NOS1, TGM1, IL11, PDGFB, NFKBIA*, RELB, SERPINE1, SCNN1A, FN1, IGFBP2, TNFAIP3, PLAU, SDC4, SOX9, ADORA2A, SAT1, APOE, ASS1, SH3BGRL, SLC6A6, PIM1, IER3, TRPC1, TNIP1, EGFR, NR4A2, REL, ELF3, CTSB, ABCA1, RAG1, NOD2, FTH1*, IRF2, TAP1, JUNB*, KRT15, LAMB2, BNIP3, MTHFR, IRF7, BACE1, PLCD1, S100A4, SERPINA1, S100A6, MBP, ASPH, TGM2, AGER, TAPBP, HLA-B
MCF-7	VIM, FSTL3, NFKB2*, BLNK, GADD45B*, HMOX1, PDGFB, SERPINE1, TNFAIP3, SNAI1, BMP4, SOX9, C3, SAT1, IL1RN, PIM1, IER3, TNIP1, EGFR, VEGFC, CCL28, TFF3, ELF3, RAG1, NOD2, FTH1*, IL12A, PTAFR, FABP6, JUNB*, KRT15, BNIP3, OXTR, PLCD1, S100A4, SERPINA1, S100A6, ASPH, HLA-G, HLA-B
501-mel	VIM, ST6GAL1, GADD45B*, FCGRT, CCND1, FN1, SDC4, SAT1, APOE, SLC6A6, LGALS3, SERPINE2, PIM1, IER3, CYP19A1, TP53, NFKBIZ, TNIP1, PTEN, BNIP3, MTHFR, UPP1, APOD, S100A4, MBP, ASPH, HLA-G, HLA-B
K562	ST6GAL1, CCND1, APOE, SLC6A6, PIM1, ERBB2, TNIP1, CD3G, REL, JUNB*, BNIP3, F8
A549	VIM, TNFRSF9, TRAF1, PTGS2, IL11, PDGFB, LIPG, AMH, SERPINE1, SOD2, F3, INHBA, SDC4, SOX9, BMP2*, SLC6A6, LGALS3, IL6, IRF4, BCL2A1, TRPC1, TNIP1, EGFR, VEGFC, CCL28, NR4A2, ABCA1, JUNB*, BNIP3, S100A4, CEBPD*, HLA-B
U87	GCLC, ATP1A2, NLRP2, VIM, TNIP3, FSTL3, PTGS2, NFKB2*, EDN1*, TGM1, GADD45B*, MADCAM1, HMOX1, PDGFB, BDKRB1, NFKBIA*, TNFSF13B, RELB, FCGRT, SERPINE1, APOC3, CYP27B1, UPK1B, IL1A, CCL20, FN1, F3, TNFAIP3, CCND2, INHBA, TWIST1, SDC4, TREM1, C3, CCR7, TICAM1, LBP, SAT1, APOE, SLC6A6, IL6, IL1RN, IER3, TLR2, NFKBIZ, TRPC1, TNIP1, EGFR, SLC16A1, TFF3, ELF3, TERT, CSF2, ABCA1, NOD2, DNASE1L2, FTH1*, FABP6, JUNB*, PTEN, LAMB2, PLK3, BNIP3, UPP1, IRF7, KRT3, ASPH, AGER, HLA-G, CEBPD*, HLA-B, CCL4, CCL3
Core	GADD45B*, IER3, JUNB*, BNIP3, CEBPD*, TNIP1, FN1, PIM1, HLA-B, TNFAIP3, SLC6A6

To further support the connection of the identified genes with the NF-κB transcriptional response, NF-κB RelA ChIP-sequencing Atlas dataset was used (https://chip-atlas.org/, (212)) and RelA binding sites were compared with the hypoxia-inducible NF-κB target genes signature. Overall, 116 of the 132 genes were found to be common in RelA ChIP-sequencing Atlas dataset, and all of the 11-core hypoxia upregulated NF-κB target genes were involved in this group of genes (**Figure 6.6**, **A**). This indicates that most of the hypoxia-inducible NF-κB target genes signature potentially have RelA binding sites and thus RelA potentially regulates their transcriptional expression. As mentioned above, apart from having a shared NF-κB target genes signature, there was a group of genes specific to individual cell lines. It could be hypothesised that differential RelA binding could be the cause of variable hypoxia inducible gene selection across different cell types. However, this needs to be validated with further experiments.

To investigate, if there is a differential NF-κB subunit usage across different cell types, hypoxia-inducible NF-κB target genes were compared with the ChIP-sequencing Atlas datasets of the other NF-κB subunits, including cRel, RelB, NF-κB1, and NF-κB2 (**Figure 6.6**, **B**, **C**, **D**, **E**). Each of the NF-κB subunit's ChIP-sequencing Atlas dataset overlapped with different number of hypoxia-inducible NF-κB target genes. Although each subunit had shared hypoxia-inducible NF-κB target gene binding sites within the same cell type, they also had gene binding sites specific to individual NF-κB subunits (**Tables 6.4**, **6.5**, **6.6**, **6.7**, and **6.8**). RelA ChIP-sequencing Atlas dataset contained all of the gene binding sites identified in rest of the NF-κB subunits, however a group of genes were exclusive to the RelA subunit (**Table 6.4**). These results indicate that most of the hypoxia-inducible NF-κB target genes signature predominantly have RelA binding sites, however different combinations of homo- or heterodimerisation of the NF-κB subunits could be the reason for cell type-dependent hypoxia-inducible NF-κB target genes signature. This needs to be investigated with further experiments.

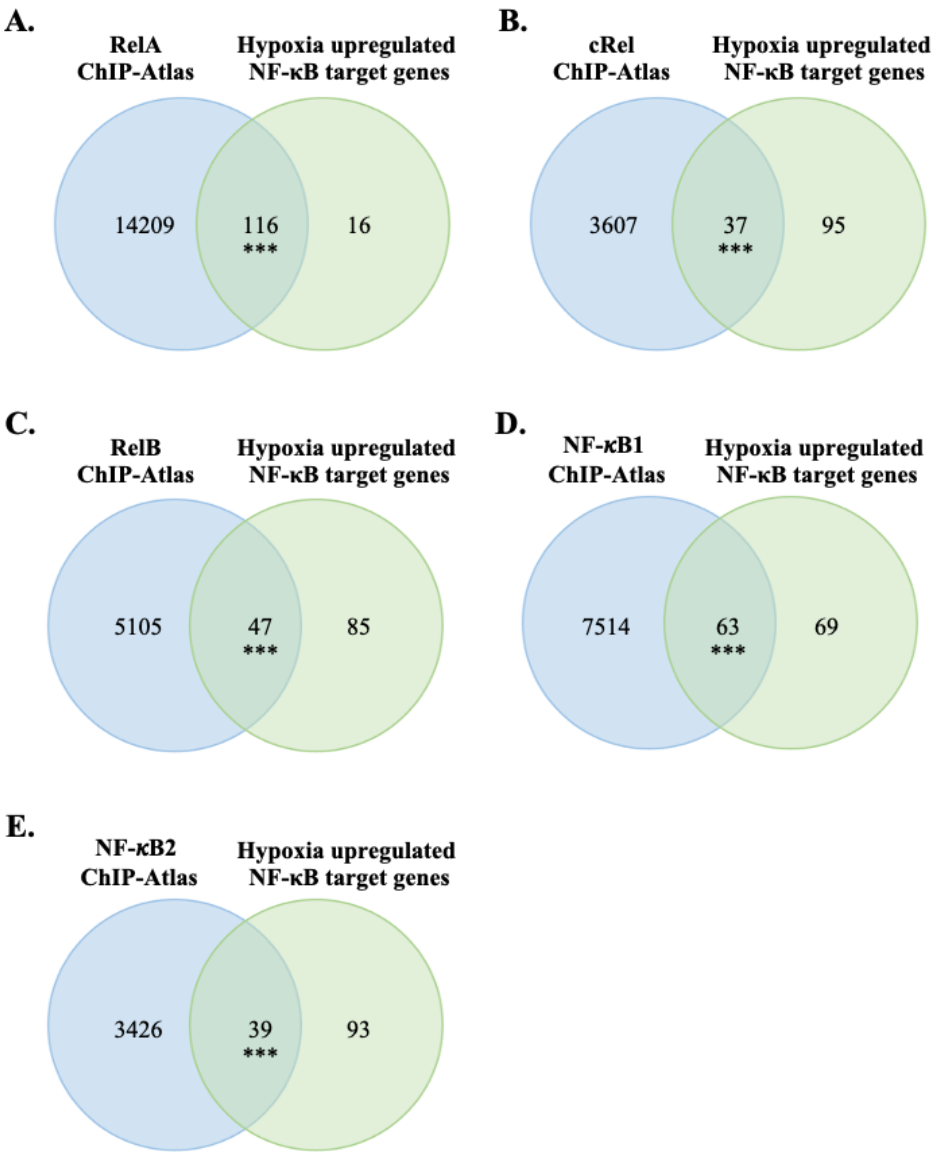

Figure 6.6. Overlap of NF-κB subunits ChIP-sequencing Atlas and Hypoxia upregulated NF-κB target genes. Hypoxia upregulated NF-κB target genes determined by 24 hours hypoxia RNA-sequencing and core hypoxia upregulated genes determined by RNA-sequencing meta-analysis, were compared with publicly available ChIP-seq Atlas for RelA (**A**), cRel (**B**), RelB (**C**), NF-κB1 (**D**), and NF-κB2 (**E**), containing list of genes with each NF-κB subunit's DNA binding sites. P value for overlaps were calculated by hypergeometric test. *** $p \leq 0.001$.

Table 6.4. Hypoxia upregulated NF-κB target genes overlapped with RelA ChIP-sequencing Atlas in different cell lines. The list of genes was obtained by overlapping hypoxia upregulated NF-κB target genes listed in Table 6.3 with RelA ChIP-sequencing Atlas. Genes only identified in RelA but no other NF-κB subunits' ChIP-sequencing Atlas are underlined. Cell type-independent, "Core" hypoxia upregulated NF-κB target genes determined by RNA-sequencing meta-analysis are listed in blue.

Cell Lines	Hypoxia upregulated RelA target genes
HeLa	TNFRSF9, PTGS2, IL11, PDGFB, LIPG, EBI3, SERPINE1, SOD2, IL1A, FN1, F3, TNFAIP3, SDC4, BMP4, SLC6A6, IL1RN, IER3, TLR2, TNIP1, LCN2, VEGFC, CCL28, OLR1, BNIP3, TNFSF15, F8
HCT116	SERPINB1, TRAF1, MYLK, BCL3, NFKB2, IL11, PDGFB, NFKBIA, RELB, SERPINE1, SCNN1A, FN1, IGFBP2, TNFAIP3, PLAU, SDC4, SOX9, ADORA2A, APOE, ASS1, SH3BGRL, SLC6A6, PIM1, IER3, TRPC1, TNIP1, EGFR, NR4A2, REL, ELF3, CTSB, ABCA1, RAG1, NOD2, FTH1, IRF2, TAP1, JUNB, LAMB2, BNIP3, MTHFR, IRF7, BACE1, S100A4, SERPINA1, S100A6, MBP, ASPH, TGM2, TAPBP, HLA-B
MCF-7	VIM, FSTL3, NFKB2, BLNK, GADD45B, HMOX1, PDGFB, SERPINE1, TNFAIP3, SNAI1, BMP4, SOX9, C3, IL1RN, PIM1, IER3, TNIP1, EGFR, VEGFC, CCL28, ELF3, RAG1, NOD2, FTH1, IL12A, PTAFR, FABP6, JUNB, BNIP3, OXTR, S100A4, SERPINA1, S100A6, ASPH, HLA-B
501-mel	VIM, ST6GAL1, GADD45B, FCGRT, CCND1, FN1, SDC4, APOE, SLC6A6, LGALS3, SERPINE2, PIM1, IER3, CYP19A1, TP53, NFKBIZ, TNIP1, PTEN, BNIP3, MTHFR, UPP1, APOD, S100A4, MBP, ASPH, HLA-B
K562	ST6GAL1, CCND1, APOE, SLC6A6, PIM1, ERBB2, TNIP1, REL, JUNB, BNIP3, F8
A549	VIM, TNFRSF9, TRAF1, PTGS2, IL11, PDGFB, LIPG, SERPINE1, SOD2, F3, INHBA, SDC4, SOX9, BMP2, SLC6A6, LGALS3, IL6, IRF4, BCL2A1, TRPC1, TNIP1, EGFR, VEGFC, CCL28, NR4A2, ABCA1, JUNB, BNIP3, S100A4, CEBPD, HLA-B
U87	GCLC, VIM, TNIP3, FSTL3, PTGS2, NFKB2, EDN1, GADD45B, MADCAM1, HMOX1, PDGFB, BDKRB1, NFKBIA, TNFSF13B, RELB, FCGRT, SERPINE1, APOC3, CYP27B1, IL1A, CCL20, FN1, F3, TNFAIP3, CCND2, INHBA, TWIST1, SDC4, TREM1, C3, CCR7, TICAM1, LBP, APOE, SLC6A6, IL6, IL1RN, IER3, TLR2, NFKBIZ, TRPC1, TNIP1, EGFR, SLC16A1, ELF3, CSF2, ABCA1, NOD2, FTH1, FABP6, JUNB, PTEN, LAMB2, PLK3, BNIP3, UPP1, IRF7, ASPH, CEBPD, HLA-B, CCL4, CCL3
Core	GADD45B, IER3, JUNB, BNIP3, CEBPD, TNIP1, FN1, PIM1, HLA-B, TNFAIP3, SLC6A6

Table 6.5. Hypoxia upregulated NF-κB target genes overlapped with cRel ChIP-sequencing Atlas in different cell lines. The list of genes was obtained by overlapping hypoxia upregulated NF-κB target genes listed in Table 6.3 with cRel ChIP-sequencing Atlas. Cell type-independent, "Core" hypoxia upregulated NF-κB target genes determined by RNA-sequencing meta-analysis are listed in blue.

Cell Lines	Hypoxia upregulated cRel target genes
HeLa	EBI3, SOD2, FN1, TNFAIP3, IER3, TLR2, TNIP1, BNIP3
HCT116	TRAF1, BCL3, NFKB2, NFKBIA, RELB, TNFAIP3, TNIP1, NR4A2, REL, CTSB, FTH1, IRF2, TAP1, JUNB, BNIP3, MTHFR, IRF7, TAPBP, HLA-B
MCF-7	NFKB2, GADD45B, HMOX1, TNFAIP3, IER3, TNIP1, FTH1, JUNB, BNIP3, HLA-B
501-mel	ST6GAL1, GADD45B, FN1, IER3, TP53, NFKBIZ, TNIP1, BNIP3, MTHFR, HLA-B
K562	ST6GAL1, TNIP1, REL, JUNB, BNIP3
A549	TRAF1, SOD2, BMP2, BCL2A1, TNIP1, NR4A2, IRF4, JUNB, BNIP3, HLA-B
U87	NFKB2, GADD45B, HMOX1, NFKBIA, RELB, FN1, TNFAIP3, CCR7, TICAM1, IER3, TLR2, NFKBIZ, TNIP1, SLC16A1, JUNB, PLK3, BNIP3, IRF7, HLA-B, CCL3, FTH1
Core	GADD45B, IER3, JUNB, BNIP3, TNIP1, FN1, HLA-B, TNFAIP3

Table 6.6. Hypoxia upregulated NF-κB target genes overlapped with RelB ChIP-sequencing Atlas in different cell lines. The list of genes was obtained by overlapping hypoxia upregulated NF-κB target genes listed in Table 6.3 with RelB ChIP-sequencing Atlas. Cell type-independent, "Core" hypoxia upregulated NF-κB target genes determined by RNA-sequencing meta-analysis are listed in blue.

Cell Lines	Hypoxia upregulated RelB target genes
HeLa	TNFRSF9, EBI3, SOD2, TNFAIP3, SDC4, IER3, TLR2, TNIP1, BNIP3, TNFSF15, F8
HCT116	TRAF1, BCL3, NFKB2, NFKBIA, RELB, TNFAIP3, SDC4, NOS1, IER3, TNIP1, NR4A2, REL, ELF3, CTSB, RAG1, NOD2, IRF2, TAP1, BNIP3, MTHFR, IRF7, S100A6, TAPBP, HLA-B
MCF-7	VIM, NFKB2, GADD45B, HMOX1, TNFAIP3, IER3, ELF3, RAG1, TNIP1, NOD2, BNIP3, OXTR, S100A6, HLA-B
501-mel	VIM, ST6GAL1, GADD45B, SDC4, LGALS3, SERPINE2, IER3, TP53, NFKBIZ, TNIP1, BNIP3, MTHFR, UPP1, HLA-B
K562	ST6GAL1, TNIP1, REL, BNIP3, F8
A549	VIM, TNFRSF9, TRAF1, SOD2, SDC4, LGALS3, TNIP1, NR4A2, BNIP3, HLA-B
U87	VIM, NFKB2, GADD45B, HMOX1, NFKBIA, TNFSF13B, RELB, TNFAIP3, CCND2, SDC4, CCR7, TICAM1, IER3, TLR2, NFKBIZ, TNIP1, SLC16A1, ELF3, NOD2, BNIP3, UPP1, IRF7, HLA-B, CCL4, CCL3
Core	GADD45B, IER3, BNIP3, TNIP1, HLA-B, TNFAIP3

Table 6.7. Hypoxia upregulated NF-κB target genes overlapped with NF-κB1 ChIP-sequencing Atlas in different cell lines. The list of genes was obtained by overlapping hypoxia upregulated NF-κB target genes listed in Table 6.3 with NF-κB1 ChIP-sequencing Atlas. Cell type-independent, "Core" hypoxia upregulated NF-κB target genes determined by RNA-sequencing meta-analysis are listed in blue.

Cell Lines	Hypoxia upregulated NF-κB1 target genes
HeLa	TNFRSF9, EBI3, SOD2, IL1A, FN1, TNFAIP3, SDC4, IER3, TLR2, TNIP1, LCN2, OLR1, BNIP3, F8
HCT116	TRAF1, BCL3, NFKB2, NFKBIA, RELB, FN1, TNFAIP3, SDC4, ADORA2A, ASS1, PIM1, IER3, TRPC1, TNIP1, NR4A2, REL, ELF3, CTSB, RAG1, NOD2, FTH1, IRF2, TAP1, BNIP3, MTHFR, IRF7, ASPH, TAPBP, HLA-B
MCF-7	VIM, NFKB2, GADD45B, TNFAIP3, C3, PIM1, IER3, TNIP1, ELF3, RAG1, NOD2, FTH1, IL12A, PTAFR, FABP6, BNIP3, OXTR, ASPH, HLA-B
501-mel	VIM, GADD45B, FN1, SDC4, PIM1, IER3, TP53, NFKBIZ, TNIP1, PTEN, BNIP3, MTHFR, UPP1, ASPH, HLA-B
K562	PIM1, TNIP1, REL, BNIP3, F8
A549	VIM, TNFRSF9, TRAF1, SOD2, SDC4, IL6, IRF4, BCL2A1, TRPC1, TNIP1, NR4A2, BNIP3, HLA-B
U87	GCLC, VIM, TNIP3, NFKB2, GADD45B, BDKRB1, NFKBIA, RELB, IL1A, CCL20, FN1, TNFAIP3, CCND2, SDC4, TREM1, C3, CCR7, TICAM1, IL6, IER3, TLR2, NFKBIZ, TRPC1, TNIP1, SLC16A1, ELF3, CSF2, NOD2, FABP6, PTEN, PLK3, BNIP3, UPP1, IRF7, ASPH, HLA-B, CCL3, FTH1
Core	GADD45B, IER3, BNIP3, TNIP1, FN1, PIM1, HLA-B, TNFAIP3

Table 6.8. Hypoxia upregulated NF-κB target genes overlapped with NF-κB2 ChIP-sequencing Atlas in different cell lines. The list of genes was obtained by overlapping hypoxia upregulated NF-κB target genes listed in Table 6.3 with NF-κB2 ChIP-sequencing Atlas. Cell type-independent, "Core" hypoxia upregulated NF-κB target genes determined by RNA-sequencing meta-analysis are listed in blue.

Cell Lines	Hypoxia upregulated NF-κB2 target genes
HeLa	TNFRSF9, EBI3, SOD2, FN1, TNFAIP3, SDC4, TNIP1, BNIP3, F8
HCT116	TRAF1, BCL3, NFKB2, NFKBIA, RELB, FN1, TNFAIP3, SDC4, TNIP1, NR4A2, REL, NOD2, IRF2, TAP1, BNIP3, IRF7, TAPBP, HLA-B
MCF-7	VIM, NFKB2, GADD45B, TNFAIP3, TNIP1, NOD2, IL12A, BNIP3, OXTR, HLA-B
501-mel	VIM, GADD45B, CCND1, FN1, SDC4, TP53, NFKBIZ, TNIP1, PTEN, BNIP3, HLA-B
K562	CCND1, TNIP1, REL, BNIP3, F8
A549	VIM, TNFRSF9, TRAF1, SOD2, SDC4, IL6, TNIP1, NR4A2, BNIP3, HLA-B
U87	VIM, TNIP3, NFKB2, GADD45B, NFKBIA, RELB, FN1, TNFAIP3, CCND2, SDC4, CCR7, TICAM1, IL6, NFKBIZ, TNIP1, SLC16A1, CSF2, NOD2, PTEN, BNIP3, IRF7, HLA-B, CCL3, GCLC
Core	GADD45B, BNIP3, TNIP1, FN1, HLA-B, TNFAIP3

6.3. Discussion

Cells respond to hypoxia by altering their gene expression pattern in order to maintain optimum oxygen levels in physiological states and pathological conditions. While transcriptional responses to hypoxia are well characterised (reviewed in (75)), transcriptome wide characterisation of hypoxia inducible NF-κB target genes are lacking. To address this, a bioinformatics approach was used (**Figure 6.1**), analysing publicly available hypoxia transcriptomics, specifically RNA-sequencing data with 24 hours of 1% oxygen treatment performed in human cell lines in different tissues (**Table 6.1** and **Table 6.2**). By integrating this analysis with a list of validated NF-κB target genes obtained from the Gilmore laboratory, this approach has identified cell type specific and cell type independent hypoxia inducible NF-κB target gene signatures.

Based on the volcano plots generated using differential expression analysis of the RNA-sequencing data with 24 hours of 1% oxygen treatment, hypoxia stimulation had variable effects on each cell line (**Figure 6.3**). It is known that in different human tissue types, oxygen partial pressure can vary significantly, and some tissue types are referred as oxy-regulators, which the energy consumption rate remains constant irrespective of oxygen availability (53). For instance, brain tissue is known to be extremely sensitive to oxygen deprivation due representing the largest source of energy consumption in the human body (270). Thus, this might also be relevant in a cellular level, as U87, brain glioblastoma cell type showed the highest number of altered genes in the differential expression analysis (**Figure 6.3**, **H**). It is previously shown that the transcriptional response to hypoxia varies among different cell-lines, such as renal tubule cells were shown to have the greatest gene expression signature, when compared to breast epithelial cells, smooth muscle cells and endothelial cells using the data obtained from DNA microarrays (92). These variations could be linked to the variation in expression of the HIF subunits across different cell types. In the future experiments, each cell type will need to be investigated for their endogenous HIF levels, as well as the change in expression levels of HIF subunits following hypoxia stimulation.

The Gene Set Enrichment Analysis (GSEA) comparing the NF-κB target genes list with hypoxia stimulated RNA-sequencing data, has shown that NF-κB target genes are enriched at hypoxia upregulated genes (**Figure 6.4**). The number of hypoxia upregulated NF-κB target genes were variable across different cell lines (**Figure 6.5**). A group of genes were identified to be common in all cell types but mainly each cell line had their own independent hypoxia inducible NF-κB target genes signature (**Table 6.3**). Given the complex nature of the NF-κB family of transcription factors, this is not too surprising. In the future studies, it will be important to validate these genes signatures by hypoxia time-course qPCR analysis.

As many stimuli, hypoxia also induces NF-κB transiently, leading to time-dependent transcriptional outputs, which is a fundamental feature of NF-κB activation (148, 271, 272). It is expected that NF-κB target genes express a distinct kinetic pattern in different cell types and with different hypoxia time-points. Also, expression levels and activities of the different subunits may be variable in different cell types, which could help determine cell type-specific differences in which NF-κB target genes are activated in hypoxia. By studying different time-points of hypoxia induction with the DNA binding and activation of diverse NF-κB subunits would give a more in-depth understanding to variable NF-κB transcriptional responses in different cell types.

Upon hypoxia stimulation, apart from HIFs, there are wide-range of factors that can affect the NF-κB transcriptional response, including other transcription factors and enzymes (reviewed in (106)). As mentioned in the previous chapters, histone methylation and JmjC-containing histone lysine demethylases (KDMs) potentially play an important role in regulating hypoxia stimulated NF-κB transcriptional response. In the future experiments, it will be interesting to determine the role of KDMs and histone methylation in the NF-κB target gene signature of various cell lines, which will also elucidate their possible role in variable hypoxia inducible gene selection across different cell types.

In order to identify other transcriptional regulators and co-regulators that are potentially involved in the regulation of the hypoxia-induced NF-κB target genes, motif

enrichment analysis, looking at overrepresented DNA binding sites at the gene promoters, will be performed using publicly available ChIP-sequencing datasets (273).

Recent work on genome wide mapping of chromatin accessibility using ATAC-sequencing has shown that hypoxia alters chromatin accessibility at subsets of hypoxia responsive genes (96-98). Comparative analysis between hypoxia induced NF-κB target genes with ATAC-sequencing data will determine if these genes are located at accessible chromatin sites under normal oxygen condition and if they have increased chromatin accessibility in response to hypoxia.

Furthermore, hypoxia inducible NF-κB target genes were analysed for their different biological processes and the associated molecular pathways across different cell types (data not shown), by using the gene ontology database on WEB-based Gene SeT AnaLysis Toolkit (WebGestalt) (204). As low number of genes were uploaded, most of the ontology terms were not statistically significant, and also, they were categorised too broad and not described clearly. Thus, enrichment analysis showing ontology terms for molecular function and biological processes over-represented in cell type-specific and core hypoxia upregulated NF-κB target genes were not presented in this chapter.

Hypoxia and NF-κB are both associated with different pathological conditions, most notably cancer (reviewed in (150)). Hypoxia in many different human cancers is associated with metastasis, tumour recurrence, resistance to chemotherapy, and radiation, invasion, and decreased patient survival. Thus, hypoxia gene signatures are often considered crucial for being prognostic markers and biomarkers of certain tumour types (274, 275). In the future studies, integrative analysis with The Cancer Genome Atlas (TCGA) dataset (276), could be performed to explore if the hypoxia inducible NF-κB gene signatures are elevated in certain tumours compared to their normal tissue counterparts, and if their expression is correlated with poor patient survival.

To summarise, this chapter has identified the cell type specific and the core hypoxia inducible NF-κB target genes signature. These signatures will be a useful resource for future

work uncovering the mechanisms involved in hypoxia stimulated NF-κB transcriptional response.

Chapter 7 - Discussion

7.1. Introduction

The crosstalk between hypoxia and inflammation, and also between the two major transcription factors involved in these stress responses, HIF and NF-κB, has been widely demonstrated (reviewed in (149, 150, 156, 277)). Although an extensive list of NF-κB target genes is known in response to various stimuli (https://www.bu.edu/nf-kb/gene-resources/target-genes/), a comprehensive analysis of hypoxia-induced NF-κB transcriptional response is still lacking. A detailed understanding of the mechanisms controlling the NF-κB target gene signature following exposure to low oxygen tension will be an important resource for finding novel therapeutic strategies against pathological conditions that are linked to the deregulation of oxygen homeostasis and NF-κB response, such as immune diseases and several types of cancer (150, 277).

The aim of this thesis was to study the role of JmjC histone lysine demethylases (KDMs) in the regulation of hypoxia-induced NF-κB transcriptional response. Overall, this study proposed that KDMs are novel regulators of NF-κB target gene signature either by modulating histone methylation marks and/ or by directly binding to NF-κB subunits. In addition, cell type-specific and core hypoxia-stimulated NF-κB target genes are identified using 7 different cancer types and cell type-independent meta-analysis of a group of hypoxia-induced RNA-sequencing experiments, respectively (91). All these findings will be an essential reference in guiding future research uncovering the link between hypoxia and NF-κB.

7.2. Hypoxia-induced NF-κB transcriptional response and histone methylation dynamics

The link between NF-κB transcriptional response and histone modifications has been described in multiple studies in different cellular backgrounds (reviewed in (158, 278, 279)). For instance, H3K4 trimethylation upregulated NF-κB target genes, following lipopolysaccharide (LPS) stimulation in periodontal ligament cells and human endothelial cells, respectively (29, 280). Several studies have suggested that histone methylation is necessary for NF-κB recruitment to promoter regions and target gene expressions (29, 164). Although an association between histone methylations and NF-κB transcriptional response has been described, the regulatory link between methyltransferases and NF-κB in different stimuli has not been clarified. NF-κB-dependent histone modifications have also been described in multiple studies (165, 166). This includes SETD6-mediated methylation of RelA protein interacting with histone lysine methyltransferase, G9A-like protein (GLP) and downregulating NF-κB target genes by dimethylation of H3K9 (166). However, further work is needed to understand the association between NF-κB protein methylation and histone methylation, in terms of NF-κB transcriptional response. Additionally, increased methylation levels of histones that are linked to repressed gene expressions, such as H3K9me3 are shown to suppress the pro-inflammatory cytokines (281). Depending on the context, KDMs play a critical role in contributing to the histone methylation dynamics by reversing the methylation marks.

In this thesis we initially focused on studying the role of hypoxia induced H3K4me3 levels via inhibition of KDM5A and how this regulates the NF-κB transcriptional response. KDM5A was identified as the most abundant KDM5 family member in our experimental cell model, HeLa (100). Also, sequence and structural analysis comparing other KDM5 members identified that KDM5B and KDM5C are highly similar to the KDM5A with conserved domains that control demethylase activity (100). It is hypothesised that apart from oxygen affinity in a given cell type, variable levels of the respective enzymes could lead into cell type-

specific transcriptional responses with hypoxia stimulation (100). Based on the findings in this thesis, hypoxia-induced gene signatures controlled by KDM5A, also include NF-κB target genes. Previously, KDM5B inhibition has shown to increase the innate immune response to respiratory syncytial virus infection in bone marrow-derived dendritic cells by increasing the H3K4me3 levels on promoters of specific inflammatory genes (282). In addition, KDM5C alterations has been correlated with increased tumour immunogenicity and inflamed anti-tumour immunity (283). Given the importance of both KDM5B and KDM5C in different cancer types (283-287), investigating the role of these enzymes in the control of NF-κB target gene signature in response to hypoxia across different tissue types will enable the design of future targeted therapies. As KDM5 inhibition seems to provide a robust and reversible control of innate immune response, a significant effort has been invested to develop KDM5 inhibitors for clinical applications. Among all, a pan-KDM5 inhibitor, GS-5801 has recently entered phase 1 clinical trials for treatment of chronic hepatitis B infection (288, 289). However, further work is necessary to identify the level of cooperation between these enzymes and other possible coregulators to prevent off-target effects that could cause in different physiological and disease processes.

Histone demethylation is an organised transcriptional mechanism regulating the gene activation and repression. While H3K4me3 and H3K36me3 methylation have been related with active gene transcription, certain methylation marks, such as H3K9me3 and H3K27me3, are linked to gene repression (39). In a recent study, it has been shown that depletion of H3K36me2 and gain of H3K27me3 work simultaneously in transcriptional silencing of innate immunity genes (290). This study also supports our work on NF-κB target gene activation through increased H3K36me3 levels. Histone methylation marks associated with both active and repressed transcriptions have been shown to control changes in chromatin and gene expressions with hypoxia stimulation (110, 117). It is thus likely that a chromatin crosstalk between transcription activating, and repressing mechanisms is triggered with hypoxia stimulation. Comparing ChIP-sequencing data containing both H3K4/K36me3 hypoxia

upregulated and H3K27me3 hypoxia downregulated gene peaks that are NF-κB target genes, will identify the genes potentially affected by both of these mechanisms.

Despite the extensive knowledge about hypoxia upregulated genes, molecular mechanisms behind transcriptional repression and downregulated gene signatures upon hypoxia stimulation are less well understood (76). While a number of upregulated genes are identified to be conserved with hypoxia stimulation in all cell types, less conservation was identified within hypoxia-repressed genes (88, 91, 267-269). However, functional enrichment analysis on the core hypoxic signatures has shown that like hypoxia-induced genes, hypoxia-repressed genes are also involved in critical molecular functions, such as cell cycle progression and DNA replication and repair (91). Hypoxia-altered NF-κB gene signature also includes a cascade of down-regulated genes. Unlike, HIF, NF-κB is known to induce transcriptional repression of certain targets (reviewed in (76, 133)). As such, hypoxia induced repression of NF-κB genes could be both by directly interacting with the subset of genes and by modulating expression of other transcription factors. Down-regulation of these genes could be due to decreased amount of NF-κB in the nucleus at that particular time-point of the hypoxia stimulation. Another possibility is that DNA-bound NF-κB might interfere with the progression of RNA polymerases, thereby reducing the transcriptional output. NF-κB-dependent transcriptional repression could be part of a negative regulatory feedback mechanism. Future studies focusing on the molecular function of the repressed NF-κB target genes, combined with their link in different biological processes upon both hypoxia and cytokine stimulation will further clarify the complexity of the NF-κB transcriptional gene regulations. In the future studies, comparing both hypoxia-induced and -repressed NF-κB target gene profiles will improve the understanding on the feedback mechanisms of the NF-κB transcriptional response and the mechanistic link between hypoxia and NF-κB.

7.3. Hypoxia-induced NF-κB transcriptional response and potential direct methylation of NF-κB subunits.

Further to the role of KDMs on NF-κB transcriptional response through their histone demethylation activity, the non-histone role of KDM2A on NF-κB RelA led to an interrelated hypothesis (35); KDMs might influence the NF-κB transcriptional response simultaneously with both its enzymatic activity on histones but also acting directly on NF-κB proteins. Apart from KDM2A and RelA interaction, there are other KDMs that are also shown to directly bind to the RelA upon various stimulations, such as KDM4B, following stimulation by receptor activator of NF-κB ligand (RANKL) (264), KDM4A and KDM4C following stimulation of B cells by T follicular helper cell-derived signals (239). However, studies focused on hypoxia stimulation are still lacking. Future studies analysing non-chromatin methylomes following hypoxia stimulation in different tissue types will reveal possible novel KDM targets, including other NF-κB subunits and their co-regulator proteins, as well as other transcription factors that could eventually influence the NF-κB transcriptional response. Previously, a mass spectrometry-based comprehensive methylome study was conducted to characterize global protein lysine methylation patterns in human cells and identified that more than 500 different intracellular sites can be methylated (291). Over the years, a number of studies has shown the functional importance of these protein lysine methylation sites, and also suggested that reversible methyl modifications could occur in various non-histone proteins (reviewed in (33)). The future developments on potent and specific KDM inhibitors will contribute to the understanding of non-histone demethylation role of the KDMs.

Besides their demethylation effect on proteins, KDMs are also known with their non-demethylation functions (42, 46, 47). The use of wild type and demethylation dead versions of KDMs and the use of drugs inhibiting KDM demethylase activity can be used to differentiate between demethylase and non-demethylase functions of KDMs in regulating NF-κB target genes in response to hypoxia.

7.4. Hypoxia-induced NF-κB transcriptional response across distinct cellular systems

There have been large-scale transcriptome profiling experiments that focused on characterising transcriptional activity in different cancer types. For instance, Zodro *et al.* has performed a meta-analysis on different stages of clear cell renal cell carcinoma microarray datasets derived from normal and cancerous histopathology tissue samples (292). This study could classify the upregulated genes into pathways known to be deregulated in cancer, including immune and inflammatory responses, DNA damage response, angiogenesis, and apoptosis, which are also transcriptional responses of hypoxia and NF-κB pathways (reviewed in (150)). Although the study of Zodro *et al.* was conducted without additional stimulation, tumour microenvironment is known to be hypoxic with altered inflammatory system (reviewed in (150)). In another study, RNA-sequencing analysis of 31 different breast cancer cell lines produced a hypoxic breast cancer gene signature (293). However, correlation of NF-κB target genes signature with conserved hypoxia-altered gene signatures within a particular disease model is still lacking. Such a work would be crucial on identifying more specific gene candidates that could be used as diagnostic and/ or prognostic biomarkers. Beside investigating the effect of hypoxia by using transcriptome analysis derived from bulk cell analysis, single cell response of transcriptome changes with hypoxia stimulation would be critical to discover unique characteristics of individual cells. So far single cell RNA-sequencing has been performed in hypoxic retina (294) and lung following intermittent hypoxia exposure (295). Using such analysis will determine the cell type-specific NF-κB activation following hypoxia stimulation, and the cell specific NF-κB genes signature. This will support the knowledge on the complex molecular systems and propose new targeted therapeutic approaches.

Response to low oxygen tensions is a well-orchestrated event at the molecular level, which apart from including changes in chromatin, and the transcriptome, also involve adaptations in the epi-transcriptome, the proteome, and the metabolome (75). Future work combining the knowledge in other fields will also improve the understanding in different physiological and pathological states. Characterising the dependence of NF-κB on histone

modification changes in hypoxia and identifying co-regulators of NF-κB is still required for defining the full mechanism behind the regulation of NF-κB transcriptional response in hypoxia.

7.5. Final Remarks

The findings described in this thesis provide evidence for the role of hypoxia-induced NF-κB transcriptional response, through histone methylation dynamics, mediated by KDMs. Also, complexity of the NF-κB transactivation mechanism was highlighted by describing a potential non-histone role of KDMs on the NF-κB subunits. In addition, the results from this thesis identified the hypoxia-induced NF-κB target gene signature across different cell lines, where majority of the gene signature is cell type-specific. A better understanding of the contributors to this specificity by identifying other chromatin co-regulators will improve the knowledge of the cellular response to hypoxia and potentially reveal new drug targets involved in both hypoxia and NF-κB pathways.

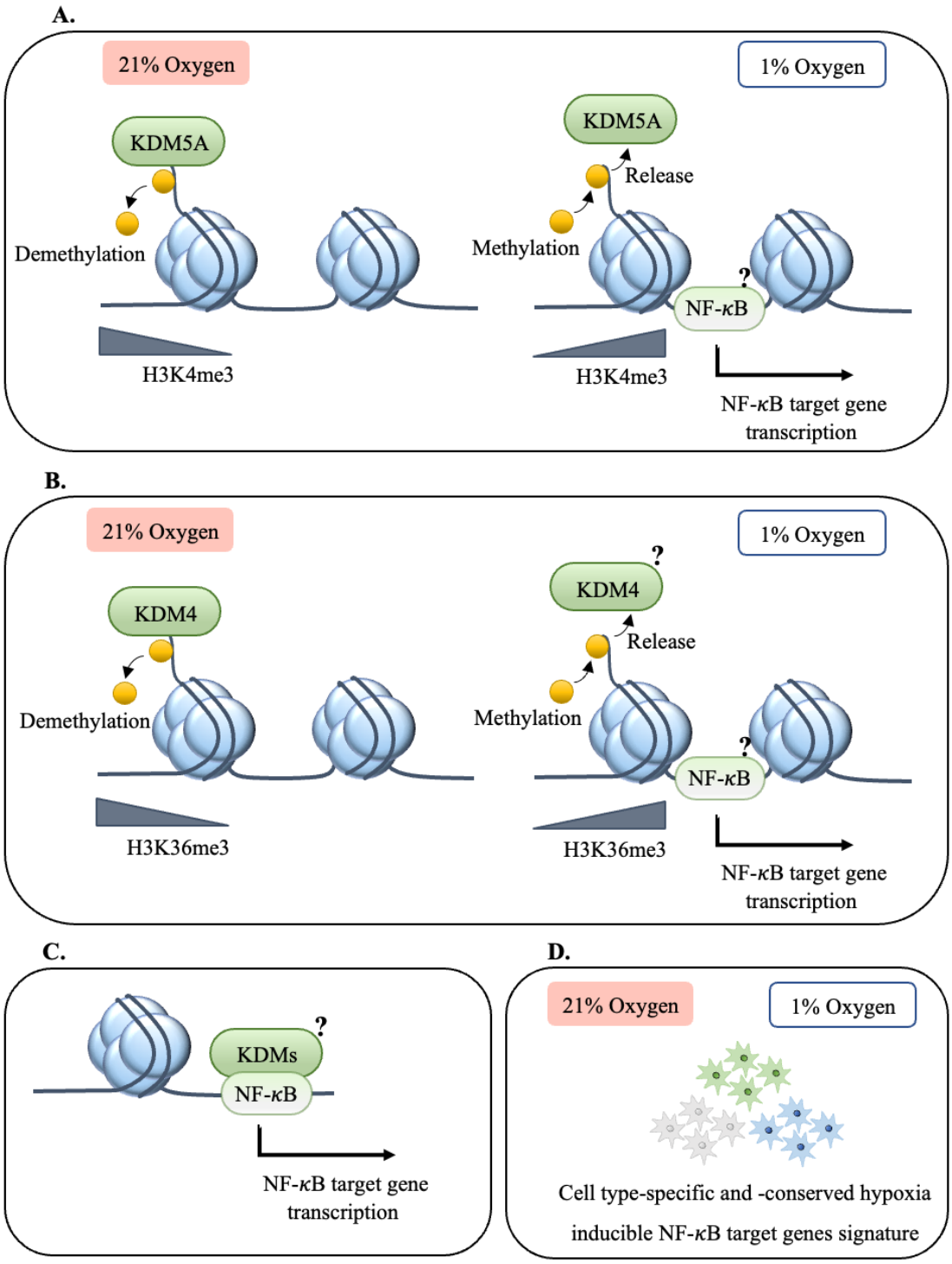

Figure 7.1. Summary illustration of the results chapters. Chapter 3 (**A**), Chapter 4 (**B**), Chapter 5 (**C**), Chapter 6 (**D**). Briefly, KDM5A is identified as a negative regulator of the H3K4me3 promoter regions and gene expressions that are responsive to both hypoxia and NF-κB, speculating the role of KDM5A on NF-κB transcriptional response. Enzymatic activity of KDM4 family is suggested as a potential regulator of the H3K36me3 regions and gene expression that are responsive to both hypoxia and NF-κB, also speculating the role of KDM4s in controlling NF-κB transcriptional activity. Non-histone role of KDMs regulating NF-κB is suggested as a potential mechanism for controlling NF-κB transcriptional response. Finally, cell type-specific and -conserved hypoxia inducible NF-κB target genes signature is identified using publicly available RNA sequencing datasets.

Chapter 8 - Bibliography

1. Malik S, Roeder RG. The metazoan Mediator co-activator complex as an integrative hub for transcriptional regulation. Nat Rev Genet. 2010;11(11):761-72.
2. Saunders A, Core LJ, Lis JT. Breaking barriers to transcription elongation. Nat Rev Mol Cell Biol. 2006;7(8):557-67.
3. Sandelin A, Carninci P, Lenhard B, Ponjavic J, Hayashizaki Y, Hume DA. Mammalian RNA polymerase II core promoters: insights from genome-wide studies. Nat Rev Genet. 2007;8(6):424-36.
4. Koch F, Jourquin F, Ferrier P, Andrau JC. Genome-wide RNA polymerase II: not genes only! Trends in biochemical sciences. 2008;33(6):265-73.
5. Heidemann M, Hintermair C, Voss K, Eick D. Dynamic phosphorylation patterns of RNA polymerase II CTD during transcription. Biochimica et biophysica acta. 2013;1829(1):55-62.
6. Zheng H, Xie W. The role of 3D genome organization in development and cell differentiation. Nat Rev Mol Cell Biol. 2019;20(9):535-50.
7. Li B, Carey M, Workman JL. The role of chromatin during transcription. Cell. 2007;128(4):707-19.
8. Luger K, Mader AW, Richmond RK, Sargent DF, Richmond TJ. Crystal structure of the nucleosome core particle at 2.8 A resolution. Nature. 1997;389(6648):251-60.
9. Henikoff S, Furuyama T, Ahmad K. Histone variants, nucleosome assembly and epigenetic inheritance. Trends Genet. 2004;20(7):320-6.
10. Tremethick DJ. Higher-order structures of chromatin: the elusive 30 nm fiber. Cell. 2007;128(4):651-4.
11. Woodcock CL, Dimitrov S. Higher-order structure of chromatin and chromosomes. Curr Opin Genet Dev. 2001;11(2):130-5.
12. Woodcock CL, Ghosh RP. Chromatin higher-order structure and dynamics. Cold Spring Harbor perspectives in biology. 2010;2(5):a000596.
13. Luger K, Dechassa ML, Tremethick DJ. New insights into nucleosome and chromatin structure: an ordered state or a disordered affair? Nat Rev Mol Cell Biol. 2012;13(7):436-47.
14. Reyes AA, Marcum RD, He Y. Structure and Function of Chromatin Remodelers. J Mol Biol. 2021;433(14):166929.
15. Owen-Hughes T, Gkikopoulos T. Making sense of transcribing chromatin. Current opinion in cell biology. 2012;24(3):296-304.
16. Lleres D, James J, Swift S, Norman DG, Lamond AI. Quantitative analysis of chromatin compaction in living cells using FLIM-FRET. J Cell Biol. 2009;187(4):481-96.
17. Justin N, De Marco V, Aasland R, Gamblin SJ. Reading, writing and editing methylated lysines on histone tails: new insights from recent structural studies. Curr Opin Struct Biol. 2010;20(6):730-8.
18. Murn J, Shi Y. The winding path of protein methylation research: milestones and new frontiers. Nat Rev Mol Cell Biol. 2017;18(8):517-27.
19. Lee BM, Mahadevan LC. Stability of histone modifications across mammalian genomes: implications for 'epigenetic' marking. J Cell Biochem. 2009;108(1):22-34.
20. Kouzarides T. Chromatin modifications and their function. Cell. 2007;128(4):693-705.
21. Husmann D, Gozani O. Histone lysine methyltransferases in biology and disease. Nat Struct Mol Biol. 2019;26(10):880-9.
22. Hyun K, Jeon J, Park K, Kim J. Writing, erasing and reading histone lysine methylations. Exp Mol Med. 2017;49(4):e324.
23. Kuo AJ, Cheung P, Chen K, Zee BM, Kioi M, Lauring J, et al. NSD2 links dimethylation of histone H3 at lysine 36 to oncogenic programming. Mol Cell. 2011;44(4):609-20.

24. Edmunds JW, Mahadevan LC, Clayton AL. Dynamic histone H3 methylation during gene induction: HYPB/Setd2 mediates all H3K36 trimethylation. EMBO J. 2008;27(2):406-20.
25. Schotta G, Sengupta R, Kubicek S, Malin S, Kauer M, Callen E, et al. A chromatin-wide transition to H4K20 monomethylation impairs genome integrity and programmed DNA rearrangements in the mouse. Genes Dev. 2008;22(15):2048-61.
26. Shinsky SA, Monteith KE, Viggiano S, Cosgrove MS. Biochemical reconstitution and phylogenetic comparison of human SET1 family core complexes involved in histone methylation. J Biol Chem. 2015;290(10):6361-75.
27. Nishioka K, Chuikov S, Sarma K, Erdjument-Bromage H, Allis CD, Tempst P, et al. Set9, a novel histone H3 methyltransferase that facilitates transcription by precluding histone tail modifications required for heterochromatin formation. Genes Dev. 2002;16(4):479-89.
28. Tusi BK, Deng C, Salz T, Zeumer L, Li Y, So CW, et al. Setd1a regulates progenitor B-cell-to-precursor B-cell development through histone H3 lysine 4 trimethylation and Ig heavy-chain rearrangement. FASEB J. 2015;29(4):1505-15.
29. Francis M, Gopinathan G, Salapatas A, Nares S, Gonzalez M, Diekwisch TGH, et al. SETD1 and NF-kappaB Regulate Periodontal Inflammation through H3K4 Trimethylation. J Dent Res. 2020;99(13):1486-93.
30. Hayashi K, Yoshida K, Matsui Y. A histone H3 methyltransferase controls epigenetic events required for meiotic prophase. Nature. 2005;438(7066):374-8.
31. Carlson SM, Gozani O. Nonhistone Lysine Methylation in the Regulation of Cancer Pathways. Cold Spring Harb Perspect Med. 2016;6(11).
32. Huang J, Berger SL. The emerging field of dynamic lysine methylation of non-histone proteins. Curr Opin Genet Dev. 2008;18(2):152-8.
33. Levy D. Lysine methylation signaling of non-histone proteins in the nucleus. Cell Mol Life Sci. 2019;76(15):2873-83.
34. Pradhan S, Chin HG, Esteve PO, Jacobsen SE. SET7/9 mediated methylation of non-histone proteins in mammalian cells. Epigenetics. 2009;4(6):383-7.
35. Lu T, Jackson MW, Wang B, Yang M, Chance MR, Miyagi M, et al. Regulation of NF-kappaB by NSD1/FBXL11-dependent reversible lysine methylation of p65. Proceedings of the National Academy of Sciences of the United States of America. 2010;107(1):46-51.
36. Shi Y, Lan F, Matson C, Mulligan P, Whetstine JR, Cole PA, et al. Histone demethylation mediated by the nuclear amine oxidase homolog LSD1. Cell. 2004;119(7):941-53.
37. Shi Y, Whetstine JR. Dynamic regulation of histone lysine methylation by demethylases. Mol Cell. 2007;25(1):1-14.
38. Kooistra SM, Helin K. Molecular mechanisms and potential functions of histone demethylases. Nature reviews Molecular cell biology. 2012;13(5):297-311.
39. Shmakova A, Batie M, Druker J, Rocha S. Chromatin and oxygen sensing in the context of JmjC histone demethylases. Biochem J. 2014;462(3):385-95.
40. Chen Z, Zang J, Whetstine J, Hong X, Davrazou F, Kutateladze TG, et al. Structural insights into histone demethylation by JMJD2 family members. Cell. 2006;125(4):691-702.
41. Markolovic S, Leissing TM, Chowdhury R, Wilkins SE, Lu X, Schofield CJ. Structure-function relationships of human JmjC oxygenases-demethylases versus hydroxylases. Curr Opin Struct Biol. 2016;41:62-72.
42. Turberfield AH, Kondo T, Nakayama M, Koseki Y, King HW, Koseki H, et al. KDM2 proteins constrain transcription from CpG island gene promoters independently of their histone demethylase activity. Nucleic Acids Res. 2019;47(17):9005-23.
43. Upadhyay AK, Judge RA, Li L, Pithawalla R, Simanis J, Bodelle PM, et al. Targeting lysine specific demethylase 4A (KDM4A) tandem TUDOR domain - A fragment based approach. Bioorg Med Chem Lett. 2018;28(10):1708-13.
44. Berry WL, Janknecht R. KDM4/JMJD2 histone demethylases: epigenetic regulators in cancer cells. Cancer Res. 2013;73(10):2936-42.

45. Ponnaluri VK, Vavilala DT, Putty S, Gutheil WG, Mukherji M. Identification of non-histone substrates for JMJD2A-C histone demethylases. Biochem Biophys Res Commun. 2009;390(2):280-4.
46. Hua C, Chen J, Li S, Zhou J, Fu J, Sun W, et al. KDM6 Demethylases and Their Roles in Human Cancers. Front Oncol. 2021;11:779918.
47. Zhou Q, Zhang Y, Wang B, Zhou W, Bi Y, Huai W, et al. KDM2B promotes IL-6 production and inflammatory responses through Brg1-mediated chromatin remodeling. Cell Mol Immunol. 2019.
48. Farcas AM, Blackledge NP, Sudbery I, Long HK, McGouran JF, Rose NR, et al. KDM2B links the Polycomb Repressive Complex 1 (PRC1) to recognition of CpG islands. Elife. 2012;1:e00205.
49. Hammarlund EU, Flashman E, Mohlin S, Licausi F. Oxygen-sensing mechanisms across eukaryotic kingdoms and their roles in complex multicellularity. Science. 2020;370(6515).
50. Kenneth NS, Rocha S. Regulation of gene expression by hypoxia. Biochem J. 2008;414(1):19-29.
51. Xie H, Simon MC. Oxygen availability and metabolic reprogramming in cancer. J Biol Chem. 2017;292(41):16825-32.
52. Kaelin WG, Jr., Ratcliffe PJ. Oxygen sensing by metazoans: the central role of the HIF hydroxylase pathway. Mol Cell. 2008;30(4):393-402.
53. Stamati K, Mudera V, Cheema U. Evolution of oxygen utilization in multicellular organisms and implications for cell signalling in tissue engineering. Journal of tissue engineering. 2011;2(1):2041731411432365.
54. Lin Q, Kim Y, Alarcon RM, Yun Z. Oxygen and Cell Fate Decisions. Gene Regul Syst Bio. 2008;2:43-51.
55. Liao D, Johnson RS. Hypoxia: a key regulator of angiogenesis in cancer. Cancer Metastasis Rev. 2007;26(2):281-90.
56. Sormendi S, Wielockx B. Hypoxia Pathway Proteins As Central Mediators of Metabolism in the Tumor Cells and Their Microenvironment. Front Immunol. 2018;9:40.
57. Hong WX, Hu MS, Esquivel M, Liang GY, Rennert RC, McArdle A, et al. The Role of Hypoxia-Inducible Factor in Wound Healing. Adv Wound Care (New Rochelle). 2014;3(5):390-9.
58. Petousi N, Robbins PA. Human adaptation to the hypoxia of high altitude: the Tibetan paradigm from the pregenomic to the postgenomic era. Journal of applied physiology. 2014;116(7):875-84.
59. Erkan M, Kurtoglu M, Kleeff J. The role of hypoxia in pancreatic cancer: a potential therapeutic target? Expert Rev Gastroenterol Hepatol. 2016;10(3):301-16.
60. Favaro E, Lord S, Harris AL, Buffa FM. Gene expression and hypoxia in breast cancer. Genome Med. 2011;3(8):55.
61. Michiels C. Physiological and pathological responses to hypoxia. Am J Pathol. 2004;164(6):1875-82.
62. Wang GL, Jiang BH, Rue EA, Semenza GL. Hypoxia-inducible factor 1 is a basic-helix-loop-helix-PAS heterodimer regulated by cellular O2 tension. Proc Natl Acad Sci U S A. 1995;92(12):5510-4.
63. Fribourgh JL, Partch CL. Assembly and function of bHLH-PAS complexes. Proc Natl Acad Sci U S A. 2017;114(21):5330-2.
64. Jiang BH, Rue E, Wang GL, Roe R, Semenza GL. Dimerization, DNA binding, and transactivation properties of hypoxia-inducible factor 1. J Biol Chem. 1996;271(30):17771-8.
65. Rocha S. Gene regulation under low oxygen: holding your breath for transcription. Trends Biochem Sci. 2007;32(8):389-97.
66. Lando D, Peet DJ, Whelan DA, Gorman JJ, Whitelaw ML. Asparagine hydroxylation of the HIF transactivation domain a hypoxic switch. Science. 2002;295(5556):858-61.
67. Hu CJ, Sataur A, Wang L, Chen H, Simon MC. The N-terminal transactivation domain confers target gene specificity of hypoxia-inducible factors HIF-1alpha and HIF-2alpha. Mol Biol Cell. 2007;18(11):4528-42.

68. Mandl M, Depping R. Hypoxia-inducible aryl hydrocarbon receptor nuclear translocator (ARNT) (HIF-1beta): is it a rare exception? Mol Med. 2014;20(1):215-20.
69. Bruegge K, Jelkmann W, Metzen E. Hydroxylation of hypoxia-inducible transcription factors and chemical compounds targeting the HIF-alpha hydroxylases. Curr Med Chem. 2007;14(17):1853-62.
70. Fandrey J, Gorr TA, Gassmann M. Regulating cellular oxygen sensing by hydroxylation. Cardiovasc Res. 2006;71(4):642-51.
71. An J, Rettig MB. Mechanism of von Hippel-Lindau protein-mediated suppression of nuclear factor kappa B activity. Mol Cell Biol. 2005;25(17):7546-56.
72. Appelhoff RJ, Tian YM, Raval RR, Turley H, Harris AL, Pugh CW, et al. Differential function of the prolyl hydroxylases PHD1, PHD2, and PHD3 in the regulation of hypoxia-inducible factor. J Biol Chem. 2004;279(37):38458-65.
73. Mahon PC, Hirota K, Semenza GL. FIH-1: a novel protein that interacts with HIF-1alpha and VHL to mediate repression of HIF-1 transcriptional activity. Genes Dev. 2001;15(20):2675-86.
74. Koivunen P, Hirsila M, Gunzler V, Kivirikko KI, Myllyharju J. Catalytic properties of the asparaginyl hydroxylase (FIH) in the oxygen sensing pathway are distinct from those of its prolyl 4-hydroxylases. J Biol Chem. 2004;279(11):9899-904.
75. Batie M, Kenneth NS, Rocha S. Systems approaches to understand oxygen sensing: how multi-omics has driven advances in understanding oxygen-based signalling. Biochem J. 2022;479(3):245-57.
76. Batie M, Del Peso L, Rocha S. Hypoxia and Chromatin: A Focus on Transcriptional Repression Mechanisms. Biomedicines. 2018;6(2).
77. Semenza GL, Jiang BH, Leung SW, Passantino R, Concordet JP, Maire P, et al. Hypoxia response elements in the aldolase A, enolase 1, and lactate dehydrogenase A gene promoters contain essential binding sites for hypoxia-inducible factor 1. J Biol Chem. 1996;271(51):32529-37.
78. Choudhry H, Schodel J, Oikonomopoulos S, Camps C, Grampp S, Harris AL, et al. Extensive regulation of the non-coding transcriptome by hypoxia: role of HIF in releasing paused RNApol2. EMBO Rep. 2014;15(1):70-6.
79. Galbraith MD, Allen MA, Bensard CL, Wang X, Schwinn MK, Qin B, et al. HIF1A employs CDK8-mediator to stimulate RNAPII elongation in response to hypoxia. Cell. 2013;153(6):1327-39.
80. Andrysik Z, Bender H, Galbraith MD, Espinosa JM. Multi-omics analysis reveals contextual tumor suppressive and oncogenic gene modules within the acute hypoxic response. Nat Commun. 2021;12(1):1375.
81. Schodel J, Mole DR, Ratcliffe PJ. Pan-genomic binding of hypoxia-inducible transcription factors. Biol Chem. 2013;394(4):507-17.
82. Schodel J, Oikonomopoulos S, Ragoussis J, Pugh CW, Ratcliffe PJ, Mole DR. High-resolution genome-wide mapping of HIF-binding sites by ChIP-seq. Blood. 2011;117(23):e207-17.
83. Xia X, Kung AL. Preferential binding of HIF-1 to transcriptionally active loci determines cell-type specific response to hypoxia. Genome biology. 2009;10(10):R113.
84. Mole DR, Blancher C, Copley RR, Pollard PJ, Gleadle JM, Ragoussis J, et al. Genome-wide association of hypoxia-inducible factor (HIF)-1alpha and HIF-2alpha DNA binding with expression profiling of hypoxia-inducible transcripts. J Biol Chem. 2009;284(25):16767-75.
85. Perez-Perri JI, Dengler VL, Audetat KA, Pandey A, Bonner EA, Urh M, et al. The TIP60 Complex Is a Conserved Coactivator of HIF1A. Cell Rep. 2016;16(1):37-47.
86. Ortmann BM, Burrows N, Lobb IT, Arnaiz E, Wit N, Bailey PSJ, et al. The HIF complex recruits the histone methyltransferase SET1B to activate specific hypoxia-inducible genes. Nat Genet. 2021;53(7):1022-35.
87. Wenger RH, Stiehl DP, Camenisch G. Integration of oxygen signaling at the consensus HRE. Sci STKE. 2005;2005(306):re12.

88. Benita Y, Kikuchi H, Smith AD, Zhang MQ, Chung DC, Xavier RJ. An integrative genomics approach identifies Hypoxia Inducible Factor-1 (HIF-1)-target genes that form the core response to hypoxia. Nucleic Acids Res. 2009;37(14):4587-602.
89. Hu CJ, Iyer S, Sataur A, Covello KL, Chodosh LA, Simon MC. Differential regulation of the transcriptional activities of hypoxia-inducible factor 1 alpha (HIF-1alpha) and HIF-2alpha in stem cells. Mol Cell Biol. 2006;26(9):3514-26.
90. Bracken CP, Fedele AO, Linke S, Balrak W, Lisy K, Whitelaw ML, et al. Cell-specific regulation of hypoxia-inducible factor (HIF)-1alpha and HIF-2alpha stabilization and transactivation in a graded oxygen environment. J Biol Chem. 2006;281(32):22575-85.
91. Puente-Santamaria L, Sanchez-Gonzalez L, Pescador N, Martinez-Costa O, Ramos-Ruiz R, Del Peso L. Formal Meta-Analysis of Hypoxic Gene Expression Profiles Reveals a Universal Gene Signature. Biomedicines. 2022;10(9).
92. Chi JT, Wang Z, Nuyten DS, Rodriguez EH, Schaner ME, Salim A, et al. Gene expression programs in response to hypoxia: cell type specificity and prognostic significance in human cancers. PLoS Med. 2006;3(3):e47.
93. Dengler VL, Galbraith M, Espinosa JM. Transcriptional regulation by hypoxia inducible factors. Crit Rev Biochem Mol Biol. 2014;49(1):1-15.
94. Schofield CJ, Ratcliffe PJ. Oxygen sensing by HIF hydroxylases. Nat Rev Mol Cell Biol. 2004;5(5):343-54.
95. Lombardi O, Li R, Halim S, Choudhry H, Ratcliffe PJ, Mole DR. Pan-cancer analysis of tissue and single-cell HIF-pathway activation using a conserved gene signature. Cell Rep. 2022;41(7):111652.
96. Xin J, Zhang H, He Y, Duren Z, Bai C, Chen L, et al. Chromatin accessibility landscape and regulatory network of high-altitude hypoxia adaptation. Nat Commun. 2020;11(1):4928.
97. Wang J, Wang Y, Duan Z, Hu W. Hypoxia-induced alterations of transcriptome and chromatin accessibility in HL-1 cells. IUBMB Life. 2020;72(8):1737-46.
98. Batie M, Frost J, Shakir D, Rocha S. Regulation of chromatin accessibility by hypoxia and HIF. Biochem J. 2022;479(6):767-86.
99. Hancock RL, Dunne K, Walport LJ, Flashman E, Kawamura A. Epigenetic regulation by histone demethylases in hypoxia. Epigenomics. 2015;7(5):791-811.
100. Batie M, Rocha S. JmjC histone demethylases act as chromatin oxygen sensors. Mol Cell Oncol. 2019;6(4):1608501.
101. Batie M, Rocha S. Gene transcription and chromatin regulation in hypoxia. Biochem Soc Trans. 2020;48(3):1121-8.
102. Kenneth NS, Mudie S, van Uden P, Rocha S. SWI/SNF regulates the cellular response to hypoxia. J Biol Chem. 2009;284(7):4123-31.
103. Melvin A, Mudie S, Rocha S. The chromatin remodeler ISWI regulates the cellular response to hypoxia: role of FIH. Mol Biol Cell. 2011;22(21):4171-81.
104. Yoo YG, Kong G, Lee MO. Metastasis-associated protein 1 enhances stability of hypoxia-inducible factor-1alpha protein by recruiting histone deacetylase 1. EMBO J. 2006;25(6):1231-41.
105. Frost J, Frost M, Batie M, Jiang H, Rocha S. Roles of HIF and 2-Oxoglutarate-Dependent Dioxygenases in Controlling Gene Expression in Hypoxia. Cancers (Basel). 2021;13(2).
106. Wilson JW, Shakir D, Batie M, Frost M, Rocha S. Oxygen-sensing mechanisms in cells. FEBS J. 2020;287(18):3888-906.
107. Kim I, Park JW. Hypoxia-driven epigenetic regulation in cancer progression: A focus on histone methylation and its modifying enzymes. Cancer Lett. 2020;489:41-9.
108. Sanchez-Fernandez EM, Tarhonskaya H, Al-Qahtani K, Hopkinson RJ, McCullagh JS, Schofield CJ, et al. Investigations on the oxygen dependence of a 2-oxoglutarate histone demethylase. The Biochemical journal. 2013;449(2):491-6.
109. Hancock RL, Masson N, Dunne K, Flashman E, Kawamura A. The Activity of JmjC Histone Lysine Demethylase KDM4A is Highly Sensitive to Oxygen Concentrations. ACS chemical biology. 2017;12(4):1011-9.

110. Chakraborty AA, Laukka T, Myllykoski M, Ringel AE, Booker MA, Tolstorukov MY, et al. Histone demethylase KDM6A directly senses oxygen to control chromatin and cell fate. Science. 2019;363(6432):1217-22.
111. Xia X, Lemieux ME, Li W, Carroll JS, Brown M, Liu XS, et al. Integrative analysis of HIF binding and transactivation reveals its role in maintaining histone methylation homeostasis. Proc Natl Acad Sci U S A. 2009;106(11):4260-5.
112. Johnson AB, Denko N, Barton MC. Hypoxia induces a novel signature of chromatin modifications and global repression of transcription. Mutation research. 2008;640(1-2):174-9.
113. Zhou X, Sun H, Chen H, Zavadil J, Kluz T, Arita A, et al. Hypoxia induces trimethylated H3 lysine 4 by inhibition of JARID1A demethylase. Cancer research. 2010;70(10):4214-21.
114. Tausendschon M, Dehne N, Brune B. Hypoxia causes epigenetic gene regulation in macrophages by attenuating Jumonji histone demethylase activity. Cytokine. 2011;53(2):256-62.
115. Prickaerts P, Adriaens ME, Beucken TV, Koch E, Dubois L, Dahlmans VE, et al. Hypoxia increases genome-wide bivalent epigenetic marking by specific gain of H3K27me3. Epigenetics & chromatin. 2016;9:46.
116. Gallipoli P, Huntly BJP. Histone modifiers are oxygen sensors. Science. 2019;363(6432):1148-9.
117. Batie M, Frost J, Frost M, Wilson JW, Schofield P, Rocha S. Hypoxia induces rapid changes to histone methylation and reprograms chromatin. Science. 2019;363(6432):1222-6.
118. Liu X, Wang J, Boyer JA, Gong W, Zhao S, Xie L, et al. Histone H3 proline 16 hydroxylation regulates mammalian gene expression. Nat Genet. 2022;54(11):1721-35.
119. Nathan JA. Chromatin oxygen sensing by histone H3 prolyl hydroxylation. Nat Genet. 2022;54(11):1585-6.
120. Batie M, Druker J, D'Ignazio L, Rocha S. KDM2 Family Members are Regulated by HIF-1 in Hypoxia. Cells. 2017;6(1).
121. Luo W, Chang R, Zhong J, Pandey A, Semenza GL. Histone demethylase JMJD2C is a coactivator for hypoxia-inducible factor 1 that is required for breast cancer progression. Proc Natl Acad Sci U S A. 2012;109(49):E3367-76.
122. Krieg AJ, Rankin EB, Chan D, Razorenova O, Fernandez S, Giaccia AJ. Regulation of the histone demethylase JMJD1A by hypoxia-inducible factor 1 alpha enhances hypoxic gene expression and tumor growth. Molecular and cellular biology. 2010;30(1):344-53.
123. Nakayama K, Kataoka N. Regulation of Gene Expression under Hypoxic Conditions. Int J Mol Sci. 2019;20(13).
124. Sen R, Baltimore D. Multiple nuclear factors interact with the immunoglobulin enhancer sequences. Cell. 1986;46(5):705-16.
125. Liu T, Zhang L, Joo D, Sun SC. NF-kappaB signaling in inflammation. Signal Transduct Target Ther. 2017;2.
126. Xia ZB, Meng FR, Fang YX, Wu X, Zhang CW, Liu Y, et al. Inhibition of NF-kappaB signaling pathway induces apoptosis and suppresses proliferation and angiogenesis of human fibroblast-like synovial cells in rheumatoid arthritis. Medicine (Baltimore). 2018;97(23):e10920.
127. Qin ZH, Tao LY, Chen X. Dual roles of NF-kappaB in cell survival and implications of NF-kappaB inhibitors in neuroprotective therapy. Acta Pharmacol Sin. 2007;28(12):1859-72.
128. Gerondakis S, Siebenlist U. Roles of the NF-kappaB pathway in lymphocyte development and function. Cold Spring Harb Perspect Biol. 2010;2(5):a000182.
129. Almaden JV, Liu YC, Yang E, Otero DC, Birnbaum H, Davis-Turak J, et al. B-cell survival and development controlled by the coordination of NF-kappaB family members RelB and cRel. Blood. 2016;127(10):1276-86.
130. Volcic M, Karl S, Baumann B, Salles D, Daniel P, Fulda S, et al. NF-kappaB regulates DNA double-strand break repair in conjunction with BRCA1-CtIP complexes. Nucleic Acids Res. 2012;40(1):181-95.

131. Xu RX, Liu RY, Wu CM, Zhao YS, Li Y, Yao YQ, et al. DNA damage-induced NF-kappaB activation in human glioblastoma cells promotes miR-181b expression and cell proliferation. Cell Physiol Biochem. 2015;35(3):913-25.
132. Taniguchi K, Karin M. NF-kappaB, inflammation, immunity and cancer: coming of age. Nat Rev Immunol. 2018;18(5):309-24.
133. Perkins ND, Gilmore TD. Good cop, bad cop: the different faces of NF-kappaB. Cell Death Differ. 2006;13(5):759-72.
134. Caamano J, Hunter CA. NF-kappaB family of transcription factors: central regulators of innate and adaptive immune functions. Clin Microbiol Rev. 2002;15(3):414-29.
135. Mukherjee SP, Behar M, Birnbaum HA, Hoffmann A, Wright PE, Ghosh G. Analysis of the RelA:CBP/p300 interaction reveals its involvement in NF-kappaB-driven transcription. PLoS Biol. 2013;11(9):e1001647.
136. O'Shea JM, Perkins ND. Regulation of the RelA (p65) transactivation domain. Biochem Soc Trans. 2008;36(Pt 4):603-8.
137. Burkhart BA, Hebbar PB, Trotter KW, Archer TK. Chromatin-dependent E1A activity modulates NF-kappaB RelA-mediated repression of glucocorticoid receptor-dependent transcription. J Biol Chem. 2005;280(8):6349-58.
138. Hayden MS, Ghosh S. Signaling to NF-kappaB. Genes Dev. 2004;18(18):2195-224.
139. Marienfeld R, May MJ, Berberich I, Serfling E, Ghosh S, Neumann M. RelB forms transcriptionally inactive complexes with RelA/p65. J Biol Chem. 2003;278(22):19852-60.
140. Mulero MC, Wang VY, Huxford T, Ghosh G. Genome reading by the NF-kappaB transcription factors. Nucleic Acids Res. 2019;47(19):9967-89.
141. Perkins ND. Achieving transcriptional specificity with NF-kappa B. Int J Biochem Cell Biol. 1997;29(12):1433-48.
142. Saccani S, Pantano S, Natoli G. Modulation of NF-kappaB activity by exchange of dimers. Mol Cell. 2003;11(6):1563-74.
143. Oeckinghaus A, Ghosh S. The NF-kappaB family of transcription factors and its regulation. Cold Spring Harb Perspect Biol. 2009;1(4):a000034.
144. Sun SC. Non-canonical NF-kappaB signaling pathway. Cell Res. 2011;21(1):71-85.
145. Xiao G, Harhaj EW, Sun SC. NF-kappaB-inducing kinase regulates the processing of NF-kappaB2 p100. Mol Cell. 2001;7(2):401-9.
146. Perkins ND. Integrating cell-signalling pathways with NF-kappaB and IKK function. Nat Rev Mol Cell Biol. 2007;8(1):49-62.
147. Perkins ND. Post-translational modifications regulating the activity and function of the nuclear factor kappa B pathway. Oncogene. 2006;25(51):6717-30.
148. Culver C, Sundqvist A, Mudie S, Melvin A, Xirodimas D, Rocha S. Mechanism of hypoxia-induced NF-kappaB. Mol Cell Biol. 2010;30(20):4901-21.
149. D'Ignazio L, Rocha S. Hypoxia Induced NF-kappaB. Cells. 2016;5(1).
150. D'Ignazio L, Batie M, Rocha S. Hypoxia and Inflammation in Cancer, Focus on HIF and NF-kappaB. Biomedicines. 2017;5(2).
151. Patel H, Zaghloul N, Lin K, Liu SF, Miller EJ, Ahmed M. Hypoxia-induced activation of specific members of the NF-kB family and its relevance to pulmonary vascular remodeling. Int J Biochem Cell Biol. 2017;92:141-7.
152. Al-Anazi A, Parhar R, Saleh S, Al-Hijailan R, Inglis A, Al-Jufan M, et al. Data on hypoxia-induced VEGF, leptin and NF-kB p65 expression. Data Brief. 2018;21:2395-7.
153. Melvin A, Mudie S, Rocha S. Further insights into the mechanism of hypoxia-induced NFkappaB. [corrected]. Cell Cycle. 2011;10(6):879-82.
154. Bandarra D, Biddlestone J, Mudie S, Muller HA, Rocha S. HIF-1alpha restricts NF-kappaB-dependent gene expression to control innate immunity signals. Dis Model Mech. 2015;8(2):169-81.
155. D'Ignazio L, Shakir D, Batie M, Muller HA, Rocha S. HIF-1beta Positively Regulates NF-kappaB Activity via Direct Control of TRAF6. Int J Mol Sci. 2020;21(8).
156. Bandarra D, Rocha S. Tale of two transcription factors: NF-κB and HIF crosstalk. OA Molecular & Cell Biology. 2013;1(1):1-7.

157. Brignall R, Moody AT, Mathew S, Gaudet S. Considering Abundance, Affinity, and Binding Site Availability in the NF-kappaB Target Selection Puzzle. Front Immunol. 2019;10:609.
158. Natoli G, Saccani S, Bosisio D, Marazzi I. Interactions of NF-kappaB with chromatin: the art of being at the right place at the right time. Nat Immunol. 2005;6(5):439-45.
159. Liu T, Zhang L, Joo D, Sun SC. NF-kappaB signaling in inflammation. Signal Transduct Target Ther. 2017;2:17023-.
160. Saccani S, Pantano S, Natoli G. Two waves of nuclear factor kappaB recruitment to target promoters. J Exp Med. 2001;193(12):1351-9.
161. Bacher S, Meier-Soelch J, Kracht M, Schmitz ML. Regulation of Transcription Factor NF-kappaB in Its Natural Habitat: The Nucleus. Cells. 2021;10(4).
162. Zhang Q, Cao X. Epigenetic regulation of the innate immune response to infection. Nat Rev Immunol. 2019;19(7):417-32.
163. Vandenbon A, Kumagai Y, Lin M, Suzuki Y, Nakai K. Waves of chromatin modifications in mouse dendritic cells in response to LPS stimulation. Genome Biol. 2018;19(1):138.
164. Li Y, Reddy MA, Miao F, Shanmugam N, Yee JK, Hawkins D, et al. Role of the histone H3 lysine 4 methyltransferase, SET7/9, in the regulation of NF-kappaB-dependent inflammatory genes. Relevance to diabetes and inflammation. J Biol Chem. 2008;283(39):26771-81.
165. Wang X, Zhu K, Li S, Liao Y, Du R, Zhang X, et al. MLL1, a H3K4 methyltransferase, regulates the TNFalpha-stimulated activation of genes downstream of NF-kappaB. J Cell Sci. 2012;125(Pt 17):4058-66.
166. Levy D, Kuo AJ, Chang Y, Schaefer U, Kitson C, Cheung P, et al. Lysine methylation of the NF-kappaB subunit RelA by SETD6 couples activity of the histone methyltransferase GLP at chromatin to tonic repression of NF-kappaB signaling. Nat Immunol. 2011;12(1):29-36.
167. Li X, Zhang Q, Shi Q, Liu Y, Zhao K, Shen Q, et al. Demethylase Kdm6a epigenetically promotes IL-6 and IFN-beta production in macrophages. J Autoimmun. 2017;80:85-94.
168. Jin J, Hu H, Li HS, Yu J, Xiao Y, Brittain GC, et al. Noncanonical NF-kappaB pathway controls the production of type I interferons in antiviral innate immunity. Immunity. 2014;40(3):342-54.
169. Zhu Y, van Essen D, Saccani S. Cell-type-specific control of enhancer activity by H3K9 trimethylation. Mol Cell. 2012;46(4):408-23.
170. Lu T, Jackson MW, Singhi AD, Kandel ES, Yang M, Zhang Y, et al. Validation-based insertional mutagenesis identifies lysine demethylase FBXL11 as a negative regulator of NFkappaB. Proc Natl Acad Sci U S A. 2009;106(38):16339-44.
171. Lu T, Yang M, Huang DB, Wei H, Ozer GH, Ghosh G, et al. Role of lysine methylation of NF-kappaB in differential gene regulation. Proc Natl Acad Sci U S A. 2013;110(33):13510-5.
172. Ea CK, Baltimore D. Regulation of NF-kappaB activity through lysine monomethylation of p65. Proc Natl Acad Sci U S A. 2009;106(45):18972-7.
173. Yang XD, Huang B, Li M, Lamb A, Kelleher NL, Chen LF. Negative regulation of NF-kappaB action by Set9-mediated lysine methylation of the RelA subunit. EMBO J. 2009;28(8):1055-66.
174. Wei H, Wang B, Miyagi M, She Y, Gopalan B, Huang DB, et al. PRMT5 dimethylates R30 of the p65 subunit to activate NF-kappaB. Proc Natl Acad Sci U S A. 2013;110(33):13516-21.
175. Lu T, Stark GR. Using sequential immunoprecipitation and mass spectrometry to identify methylation of NF-kappaB. Methods Mol Biol. 2015;1280:383-93.
176. Hayden MS, Ghosh S. Shared principles in NF-kappaB signaling. Cell. 2008;132(3):344-62.
177. Zhang T, Park KA, Li Y, Byun HS, Jeon J, Lee Y, et al. PHF20 regulates NF-kappaB signalling by disrupting recruitment of PP2A to p65. Nat Commun. 2013;4:2062.

178. Rodriguez MS, Thompson J, Hay RT, Dargemont C. Nuclear retention of IkappaBalpha protects it from signal-induced degradation and inhibits nuclear factor kappaB transcriptional activation. J Biol Chem. 1999;274(13):9108-15.
179. Kenneth NS, Mudie S, Naron S, Rocha S. TfR1 interacts with the IKK complex and is involved in IKK-NF-kappaB signalling. Biochem J. 2013;449(1):275-84.
180. Hanahan D, Jessee J, Bloom FR. Plasmid transformation of Escherichia coli and other bacteria. Methods Enzymol. 1991;204:63-113.
181. Allan C, Burel JM, Moore J, Blackburn C, Linkert M, Loynton S, et al. OMERO: flexible, model-driven data management for experimental biology. Nature methods. 2012;9(3):245-53.
182. Schumm K, Rocha S, Caamano J, Perkins ND. Regulation of p53 tumour suppressor target gene expression by the p52 NF-kappaB subunit. The EMBO journal. 2006;25(20):4820-32.
183. Edgar R, Domrachev M, Lash AE. Gene Expression Omnibus: NCBI gene expression and hybridization array data repository. Nucleic Acids Res. 2002;30(1):207-10.
184. Robinson JT, Thorvaldsdottir H, Winckler W, Guttman M, Lander ES, Getz G, et al. Integrative genomics viewer. Nat Biotechnol. 2011;29(1):24-6.
185. Liao Y, Wang J, Jaehnig EJ, Shi Z, Zhang B. WebGestalt 2019: gene set analysis toolkit with revamped UIs and APIs. Nucleic Acids Res. 2019;47(W1):W199-W205.
186. Subramanian A, Tamayo P, Mootha VK, Mukherjee S, Ebert BL, Gillette MA, et al. Gene set enrichment analysis: a knowledge-based approach for interpreting genome-wide expression profiles. Proc Natl Acad Sci U S A. 2005;102(43):15545-50.
187. Liberzon A, Birger C, Thorvaldsdottir H, Ghandi M, Mesirov JP, Tamayo P. The Molecular Signatures Database (MSigDB) hallmark gene set collection. Cell Syst. 2015;1(6):417-25.
188. Heberle H, Meirelles GV, da Silva FR, Telles GP, Minghim R. InteractiVenn: a web-based tool for the analysis of sets through Venn diagrams. BMC Bioinformatics. 2015;16:169.
189. Ashburner M, Ball CA, Blake JA, Botstein D, Butler H, Cherry JM, et al. Gene ontology: tool for the unification of biology. The Gene Ontology Consortium. Nat Genet. 2000;25(1):25-9.
190. Dobin A, Davis CA, Schlesinger F, Drenkow J, Zaleski C, Jha S, et al. STAR: ultrafast universal RNA-seq aligner. Bioinformatics. 2013;29(1):15-21.
191. Liao Y, Smyth GK, Shi W. The Subread aligner: fast, accurate and scalable read mapping by seed-and-vote. Nucleic Acids Res. 2013;41(10):e108.
192. Love MI, Huber W, Anders S. Moderated estimation of fold change and dispersion for RNA-seq data with DESeq2. Genome Biol. 2014;15(12):550.
193. Durinck S, Moreau Y, Kasprzyk A, Davis S, De Moor B, Brazma A, et al. BioMart and Bioconductor: a powerful link between biological databases and microarray data analysis. Bioinformatics. 2005;21(16):3439-40.
194. Greer EL, Shi Y. Histone methylation: a dynamic mark in health, disease and inheritance. Nat Rev Genet. 2012;13(5):343-57.
195. Rivera C, Gurard-Levin ZA, Almouzni G, Loyola A. Histone lysine methylation and chromatin replication. Biochim Biophys Acta. 2014;1839(12):1433-9.
196. Gong F, Clouaire T, Aguirrebengoa M, Legube G, Miller KM. Histone demethylase KDM5A regulates the ZMYND8-NuRD chromatin remodeler to promote DNA repair. J Cell Biol. 2017;216(7):1959-74.
197. Mikkelsen TS, Ku M, Jaffe DB, Issac B, Lieberman E, Giannoukos G, et al. Genome-wide maps of chromatin state in pluripotent and lineage-committed cells. Nature. 2007;448(7153):553-60.
198. Santos-Rosa H, Schneider R, Bannister AJ, Sherriff J, Bernstein BE, Emre NC, et al. Active genes are tri-methylated at K4 of histone H3. Nature. 2002;419(6905):407-11.
199. Melvin A, Rocha S. Chromatin as an oxygen sensor and active player in the hypoxia response. Cellular signalling. 2012;24(1):35-43.
200. Castellano-Castillo D, Denechaud PD, Fajas L, Moreno-Indias I, Oliva-Olivera W, Tinahones F, et al. Human adipose tissue H3K4me3 histone mark in adipogenic, lipid

metabolism and inflammatory genes is positively associated with BMI and HOMA-IR. PLoS One. 2019;14(4):e0215083.
201. Yu L, Fang F, Dai X, Xu H, Qi X, Fang M, et al. MKL1 defines the H3K4Me3 landscape for NF-kappaB dependent inflammatory response. Sci Rep. 2017;7(1):191.
202. Chen K, Luan X, Liu Q, Wang J, Chang X, Snijders AM, et al. Drosophila Histone Demethylase KDM5 Regulates Social Behavior through Immune Control and Gut Microbiota Maintenance. Cell Host Microbe. 2019;25(4):537-52 e8.
203. Zhao D, Zhang Q, Liu Y, Li X, Zhao K, Ding Y, et al. H3K4me3 Demethylase Kdm5a Is Required for NK Cell Activation by Associating with p50 to Suppress SOCS1. Cell Rep. 2016;15(2):288-99.
204. Wang J, Vasaikar S, Shi Z, Greer M, Zhang B. WebGestalt 2017: a more comprehensive, powerful, flexible and interactive gene set enrichment analysis toolkit. Nucleic Acids Res. 2017;45(W1):W130-W7.
205. Kowalczyk A, Kleniewska P, Kolodziejczyk M, Skibska B, Goraca A. The role of endothelin-1 and endothelin receptor antagonists in inflammatory response and sepsis. Arch Immunol Ther Exp (Warsz). 2015;63(1):41-52.
206. Halloran D, Durbano HW, Nohe A. Bone Morphogenetic Protein-2 in Development and Bone Homeostasis. J Dev Biol. 2020;8(3).
207. Prieto D, Zolessi FR. Functional Diversification of the Four MARCKS Family Members in Zebrafish Neural Development. J Exp Zool B Mol Dev Evol. 2017;328(1-2):119-38.
208. Salminen A, Kaarniranta K, Hiltunen M, Kauppinen A. Histone demethylase Jumonji D3 (JMJD3/KDM6B) at the nexus of epigenetic regulation of inflammation and the aging process. J Mol Med (Berl). 2014;92(10):1035-43.
209. Wisdom R, Johnson RS, Moore C. c-Jun regulates cell cycle progression and apoptosis by distinct mechanisms. EMBO J. 1999;18(1):188-97.
210. Smallie T, Ross EA, Ammit AJ, Cunliffe HE, Tang T, Rosner DR, et al. Dual-Specificity Phosphatase 1 and Tristetraprolin Cooperate To Regulate Macrophage Responses to Lipopolysaccharide. J Immunol. 2015;195(1):277-88.
211. Vattakuzhi Y, Abraham SM, Freidin A, Clark AR, Horwood NJ. Dual-specificity phosphatase 1-null mice exhibit spontaneous osteolytic disease and enhanced inflammatory osteolysis in experimental arthritis. Arthritis Rheum. 2012;64(7):2201-10.
212. Oki S, Ohta T, Shioi G, Hatanaka H, Ogasawara O, Okuda Y, et al. ChIP-Atlas: a data-mining suite powered by full integration of public ChIP-seq data. EMBO Rep. 2018;19(12).
213. Rocha S, Campbell KJ, Perkins ND. p53- and Mdm2-independent repression of NF-kappa B transactivation by the ARF tumor suppressor. Mol Cell. 2003;12(1):15-25.
214. Kenneth NS, Mudie S, Rocha S. IKK and NF-kappaB-mediated regulation of Claspin impacts on ATR checkpoint function. EMBO J. 2010;29(17):2966-78.
215. Lombardi L, Ciana P, Cappellini C, Trecca D, Guerrini L, Migliazza A, et al. Structural and functional characterization of the promoter regions of the NFKB2 gene. Nucleic Acids Res. 1995;23(12):2328-36.
216. Kucharczak J, Simmons MJ, Fan Y, Gelinas C. To be, or not to be: NF-kappaB is the answer--role of Rel/NF-kappaB in the regulation of apoptosis. Oncogene. 2003;22(56):8961-82.
217. Natsume T, Kiyomitsu T, Saga Y, Kanemaki MT. Rapid Protein Depletion in Human Cells by Auxin-Inducible Degron Tagging with Short Homology Donors. Cell Rep. 2016;15(1):210-8.
218. Bond AG, Craigon C, Chan KH, Testa A, Karapetsas A, Fasimoye R, et al. Development of BromoTag: A "Bump-and-Hole"-PROTAC System to Induce Potent, Rapid, and Selective Degradation of Tagged Target Proteins. J Med Chem. 2021;64(20):15477-502.
219. Zhou M, Yin X, Zheng L, Fu Y, Wang Y, Cui Z, et al. miR-181d/RBP2/NF-kappaB p65 Feedback Regulation Promotes Chronic Myeloid Leukemia Blast Crisis. Front Oncol. 2021;11:654411.

220. Yeo-Teh NSL, Ito Y, Jha S. High-Risk Human Papillomaviral Oncogenes E6 and E7 Target Key Cellular Pathways to Achieve Oncogenesis. Int J Mol Sci. 2018;19(6).
221. Kadoch C, Crabtree GR. Mammalian SWI/SNF chromatin remodeling complexes and cancer: Mechanistic insights gained from human genomics. Sci Adv. 2015;1(5):e1500447.
222. Peng D, Lin B, Xie M, Zhang P, Guo Q, Li Q, et al. Histone demethylase KDM5A promotes tumorigenesis of osteosarcoma tumor. Cell Death Discov. 2021;7(1):9.
223. Beshiri ML, Holmes KB, Richter WF, Hess S, Islam AB, Yan Q, et al. Coordinated repression of cell cycle genes by KDM5A and E2F4 during differentiation. Proc Natl Acad Sci U S A. 2012;109(45):18499-504.
224. Ankers JM, Awais R, Jones NA, Boyd J, Ryan S, Adamson AD, et al. Dynamic NF-kappaB and E2F interactions control the priority and timing of inflammatory signalling and cell proliferation. Elife. 2016;5.
225. Vakoc CR, Sachdeva MM, Wang H, Blobel GA. Profile of histone lysine methylation across transcribed mammalian chromatin. Mol Cell Biol. 2006;26(24):9185-95.
226. Wagner EJ, Carpenter PB. Understanding the language of Lys36 methylation at histone H3. Nat Rev Mol Cell Biol. 2012;13(2):115-26.
227. Li M, Phatnani HP, Guan Z, Sage H, Greenleaf AL, Zhou P. Solution structure of the Set2-Rpb1 interacting domain of human Set2 and its interaction with the hyperphosphorylated C-terminal domain of Rpb1. Proc Natl Acad Sci U S A. 2005;102(49):17636-41.
228. Carvalho S, Raposo AC, Martins FB, Grosso AR, Sridhara SC, Rino J, et al. Histone methyltransferase SETD2 coordinates FACT recruitment with nucleosome dynamics during transcription. Nucleic Acids Res. 2013;41(5):2881-93.
229. Schmitges FW, Prusty AB, Faty M, Stutzer A, Lingaraju GM, Aiwazian J, et al. Histone methylation by PRC2 is inhibited by active chromatin marks. Mol Cell. 2011;42(3):330-41.
230. Li J, Ahn JH, Wang GG. Understanding histone H3 lysine 36 methylation and its deregulation in disease. Cell Mol Life Sci. 2019;76(15):2899-916.
231. Li F, Mao G, Tong D, Huang J, Gu L, Yang W, et al. The histone mark H3K36me3 regulates human DNA mismatch repair through its interaction with MutSalpha. Cell. 2013;153(3):590-600.
232. Li S, Qian XH, Zhou W, Zhang Y, Feng J, Wan NS, et al. Time-dependent inflammatory factor production and NFkappaB activation in a rodent model of intermittent hypoxia. Swiss Med Wkly. 2011;141:w13309.
233. Fujisawa K, Shimo M, Taguchi YH, Ikematsu S, Miyata R. PCA-based unsupervised feature extraction for gene expression analysis of COVID-19 patients. Sci Rep. 2021;11(1):17351.
234. Yu W, Wang Z, Zhang K, Chi Z, Xu T, Jiang D, et al. One-Carbon Metabolism Supports S-Adenosylmethionine and Histone Methylation to Drive Inflammatory Macrophages. Mol Cell. 2019;75(6):1147-60 e5.
235. Yu HR, Kuo HC, Chen CC, Sheen JM, Tiao MM, Chen YC, et al. Prenatal dexamethasone exposure in rats results in long-term epigenetic histone modifications and tumour necrosis factor-alpha production decrease. Immunology. 2014;143(4):651-60.
236. Du J, Ma Y, Ma P, Wang S, Fan Z. Demethylation of epiregulin gene by histone demethylase FBXL11 and BCL6 corepressor inhibits osteo/dentinogenic differentiation. Stem Cells. 2013;31(1):126-36.
237. Chen Y, Tang W, Zhu X, Zhang L, Zhu Y, Xiao H, et al. Nuclear receptor binding SET domain protein 1 promotes epithelial-mesenchymal transition in paclitaxel-resistant breast cancer cells via regulating nuclear factor kappa B and F-box and leucine-rich repeat protein 11. Bioengineered. 2021;12(2):11506-19.
238. Liu D, Perkins JT, Petriello MC, Hennig B. Exposure to coplanar PCBs induces endothelial cell inflammation through epigenetic regulation of NF-kappaB subunit p65. Toxicol Appl Pharmacol. 2015;289(3):457-65.
239. Hung KH, Woo YH, Lin IY, Liu CH, Wang LC, Chen HY, et al. The KDM4A/KDM4C/NF-kappaB and WDR5 epigenetic cascade regulates the activation of B cells. Nucleic Acids Res. 2018;46(11):5547-60.

240. Kiss Z, Mudryj M, Ghosh PM. Non-circadian aspects of BHLHE40 cellular function in cancer. Genes Cancer. 2020;11(1-2):1-19.
241. Mesquita G, Silva T, Gomes AC, Oliveira PF, Alves MG, Fernandes R, et al. H-Ferritin is essential for macrophages' capacity to store or detoxify exogenously added iron. Sci Rep. 2020;10(1):3061.
242. Dang CV, O'Donnell KA, Zeller KI, Nguyen T, Osthus RC, Li F. The c-Myc target gene network. Semin Cancer Biol. 2006;16(4):253-64.
243. Lang F, Bohmer C, Palmada M, Seebohm G, Strutz-Seebohm N, Vallon V. (Patho)physiological significance of the serum- and glucocorticoid-inducible kinase isoforms. Physiol Rev. 2006;86(4):1151-78.
244. Kamimura R, Uchida D, Kanno SI, Shiraishi R, Hyodo T, Sawatani Y, et al. Identification of Binding Proteins for TSC22D1 Family Proteins Using Mass Spectrometry. Int J Mol Sci. 2021;22(20).
245. Sokol CL, Luster AD. The chemokine system in innate immunity. Cold Spring Harb Perspect Biol. 2015;7(5).
246. Sardina JL, Lopez-Ruano G, Prieto-Bermejo R, Sanchez-Sanchez B, Perez-Fernandez A, Sanchez-Abarca LI, et al. PTPN13 regulates cellular signalling and beta-catenin function during megakaryocytic differentiation. Biochim Biophys Acta. 2014;1843(12):2886-99.
247. Baker M. Reproducibility crisis: Blame it on the antibodies. Nature. 2015;521(7552):274-6.
248. Pedersen MT, Kooistra SM, Radzisheuskaya A, Laugesen A, Johansen JV, Hayward DG, et al. Continual removal of H3K9 promoter methylation by Jmjd2 demethylases is vital for ESC self-renewal and early development. EMBO J. 2016;35(14):1550-64.
249. Pedersen MT, Agger K, Laugesen A, Johansen JV, Cloos PA, Christensen J, et al. The demethylase JMJD2C localizes to H3K4me3-positive transcription start sites and is dispensable for embryonic development. Mol Cell Biol. 2014;34(6):1031-45.
250. Hillringhaus L, Yue WW, Rose NR, Ng SS, Gileadi C, Loenarz C, et al. Structural and evolutionary basis for the dual substrate selectivity of human KDM4 histone demethylase family. J Biol Chem. 2011;286(48):41616-25.
251. Waterhouse AM, Procter JB, Martin DM, Clamp M, Barton GJ. Jalview Version 2--a multiple sequence alignment editor and analysis workbench. Bioinformatics. 2009;25(9):1189-91.
252. Chen FE, Huang DB, Chen YQ, Ghosh G. Crystal structure of p50/p65 heterodimer of transcription factor NF-kappaB bound to DNA. Nature. 1998;391(6665):410-3.
253. Chen FE, Ghosh G. Regulation of DNA binding by Rel/NF-kappaB transcription factors: structural views. Oncogene. 1999;18(49):6845-52.
254. Panne D, Maniatis T, Harrison SC. An atomic model of the interferon-beta enhanceosome. Cell. 2007;129(6):1111-23.
255. Chen-Park FE, Huang DB, Noro B, Thanos D, Ghosh G. The kappa B DNA sequence from the HIV long terminal repeat functions as an allosteric regulator of HIV transcription. J Biol Chem. 2002;277(27):24701-8.
256. Berkowitz B, Huang DB, Chen-Park FE, Sigler PB, Ghosh G. The x-ray crystal structure of the NF-kappa B p50.p65 heterodimer bound to the interferon beta -kappa B site. J Biol Chem. 2002;277(27):24694-700.
257. Stroud JC, Oltman A, Han A, Bates DL, Chen L. Structural basis of HIV-1 activation by NF-kappaB--a higher-order complex of p50:RelA bound to the HIV-1 LTR. J Mol Biol. 2009;393(1):98-112.
258. Collins PE, Mitxitorena I, Carmody RJ. The Ubiquitination of NF-kappaB Subunits in the Control of Transcription. Cells. 2016;5(2).
259. Hochrainer K, Racchumi G, Zhang S, Iadecola C, Anrather J. Monoubiquitination of nuclear RelA negatively regulates NF-kappaB activity independent of proteasomal degradation. Cell Mol Life Sci. 2012;69(12):2057-73.
260. Li H, Wittwer T, Weber A, Schneider H, Moreno R, Maine GN, et al. Regulation of NF-kappaB activity by competition between RelA acetylation and ubiquitination. Oncogene. 2012;31(5):611-23.

261. Lee JM, Lee JS, Kim H, Kim K, Park H, Kim JY, et al. EZH2 generates a methyl degron that is recognized by the DCAF1/DDB1/CUL4 E3 ubiquitin ligase complex. Mol Cell. 2012;48(4):572-86.
262. Yang XD, Tajkhorshid E, Chen LF. Functional interplay between acetylation and methylation of the RelA subunit of NF-kappaB. Mol Cell Biol. 2010;30(9):2170-80.
263. Chen LF, Mu Y, Greene WC. Acetylation of RelA at discrete sites regulates distinct nuclear functions of NF-kappaB. EMBO J. 2002;21(23):6539-48.
264. Yi SJ, Jang YJ, Kim HJ, Lee K, Lee H, Kim Y, et al. The KDM4B-CCAR1-MED1 axis is a critical regulator of osteoclast differentiation and bone homeostasis. Bone Res. 2021;9(1):27.
265. Semenza GL. Hypoxia-inducible factors in physiology and medicine. Cell. 2012;148(3):399-408.
266. Elvidge GP, Glenny L, Appelhoff RJ, Ratcliffe PJ, Ragoussis J, Gleadle JM. Concordant regulation of gene expression by hypoxia and 2-oxoglutarate-dependent dioxygenase inhibition: the role of HIF-1alpha, HIF-2alpha, and other pathways. J Biol Chem. 2006;281(22):15215-26.
267. Ono Y, Bono H. Multi-Omic Meta-Analysis of Transcriptomes and the Bibliome Uncovers Novel Hypoxia-Inducible Genes. Biomedicines. 2021;9(5).
268. Bono H, Hirota K. Meta-Analysis of Hypoxic Transcriptomes from Public Databases. Biomedicines. 2020;8(1).
269. Ortiz-Barahona A, Villar D, Pescador N, Amigo J, del Peso L. Genome-wide identification of hypoxia-inducible factor binding sites and target genes by a probabilistic model integrating transcription-profiling data and in silico binding site prediction. Nucleic Acids Res. 2010;38(7):2332-45.
270. Jain V, Langham MC, Wehrli FW. MRI estimation of global brain oxygen consumption rate. J Cereb Blood Flow Metab. 2010;30(9):1598-607.
271. Zhao M, Joy J, Zhou W, De S, Wood WH, 3rd, Becker KG, et al. Transcriptional outcomes and kinetic patterning of gene expression in response to NF-kappaB activation. PLoS Biol. 2018;16(9):e2006347.
272. Fitzpatrick SF, Tambuwala MM, Bruning U, Schaible B, Scholz CC, Byrne A, et al. An intact canonical NF-kappaB pathway is required for inflammatory gene expression in response to hypoxia. J Immunol. 2011;186(2):1091-6.
273. Boeva V. Analysis of Genomic Sequence Motifs for Deciphering Transcription Factor Binding and Transcriptional Regulation in Eukaryotic Cells. Front Genet. 2016;7:24.
274. Winter SC, Buffa FM, Silva P, Miller C, Valentine HR, Turley H, et al. Relation of a hypoxia metagene derived from head and neck cancer to prognosis of multiple cancers. Cancer Res. 2007;67(7):3441-9.
275. Liu D, Hu Z, Jiang J, Zhang J, Hu C, Huang J, et al. Five hypoxia and immunity related genes as potential biomarkers for the prognosis of osteosarcoma. Sci Rep. 2022;12(1):1617.
276. Cancer Genome Atlas Research N, Weinstein JN, Collisson EA, Mills GB, Shaw KR, Ozenberger BA, et al. The Cancer Genome Atlas Pan-Cancer analysis project. Nat Genet. 2013;45(10):1113-20.
277. D'Ignazio L, Bandarra D, Rocha S. NF-kappaB and HIF crosstalk in immune responses. FEBS J. 2016;283(3):413-24.
278. Medzhitov R, Horng T. Transcriptional control of the inflammatory response. Nat Rev Immunol. 2009;9(10):692-703.
279. Bhatt D, Ghosh S. Regulation of the NF-kappaB-Mediated Transcription of Inflammatory Genes. Front Immunol. 2014;5:71.
280. Shamloul A, Steinemann G, Roos K, Liem CH, Bernd J, Braun T, et al. The Methyltransferase Smyd1 Mediates LPS-Triggered Up-Regulation of IL-6 in Endothelial Cells. Cells. 2021;10(12).
281. Chen TT, Wu SM, Ho SC, Chuang HC, Liu CY, Chan YF, et al. SUV39H1 Reduction Is Implicated in Abnormal Inflammation in COPD. Sci Rep. 2017;7:46667.

282. Ptaschinski C, Mukherjee S, Moore ML, Albert M, Helin K, Kunkel SL, et al. RSV-Induced H3K4 Demethylase KDM5B Leads to Regulation of Dendritic Cell-Derived Innate Cytokines and Exacerbates Pathogenesis In Vivo. PLoS Pathog. 2015;11(6):e1004978.
283. Chen XJ, Ren AQ, Zheng L, Zheng ED. Predictive Value of KDM5C Alterations for Immune Checkpoint Inhibitors Treatment Outcomes in Patients With Cancer. Front Immunol. 2021;12:664847.
284. Roesch A, Mueller AM, Stempfl T, Moehle C, Landthaler M, Vogt T. RBP2-H1/JARID1B is a transcriptional regulator with a tumor suppressive potential in melanoma cells. Int J Cancer. 2008;122(5):1047-57.
285. Catteau A, Rosewell I, Solomon E, Taylor-Papadimitriou J. A short region of the promoter of the breast cancer associated PLU-1 gene can regulate transcription in vitro and in vivo. Int J Oncol. 2004;25(1):5-16.
286. Madsen B, Tarsounas M, Burchell JM, Hall D, Poulsom R, Taylor-Papadimitriou J. PLU-1, a transcriptional repressor and putative testis-cancer antigen, has a specific expression and localisation pattern during meiosis. Chromosoma. 2003;112(3):124-32.
287. Xiao Q, Wang CY, Gao C, Chen JD, Chen JJ, Wang Z, et al. Regulation of KDM5C stability and enhancer reprogramming in breast cancer. Cell Death Dis. 2022;13(10):843.
288. Yang GJ, Zhu MH, Lu XJ, Liu YJ, Lu JF, Leung CH, et al. The emerging role of KDM5A in human cancer. J Hematol Oncol. 2021;14(1):30.
289. Gilmore S, D. T, Dick R, Appleby T, Birkus G, Willkom M, et al. Antiviral activity of GS-5801, a liver-targeted prodrug of a lysine demethylase 5 inhibitor, in a hepatitis B virus primary human hepatocyte infection model. Journal of Hepatology. 2017;66(1):S690-1.
290. Li Y, Goldberg EM, Chen X, Xu X, McGuire JT, Leuzzi G, et al. Histone methylation antagonism drives tumor immune evasion in squamous cell carcinomas. Mol Cell. 2022;82(20):3901-18 e7.
291. Cao XJ, Arnaudo AM, Garcia BA. Large-scale global identification of protein lysine methylation in vivo. Epigenetics. 2013;8(5):477-85.
292. Zodro E, Jaroszewski M, Ida A, Wrzesinski T, Kwias Z, Bluyssen H, et al. FUT11 as a potential biomarker of clear cell renal cell carcinoma progression based on meta-analysis of gene expression data. Tumour Biol. 2014;35(3):2607-17.
293. Ye IC, Fertig EJ, DiGiacomo JW, Considine M, Godet I, Gilkes DM. Molecular Portrait of Hypoxia in Breast Cancer: A Prognostic Signature and Novel HIF-Regulated Genes. Mol Cancer Res. 2018;16(12):1889-901.
294. Heng JS, Rattner A, Stein-O'Brien GL, Winer BL, Jones BW, Vernon HJ, et al. Hypoxia tolerance in the Norrin-deficient retina and the chronically hypoxic brain studied at single-cell resolution. Proc Natl Acad Sci U S A. 2019;116(18):9103-14.
295. Wu G, Lee YY, Gulla EM, Potter A, Kitzmiller J, Ruben MD, et al. Short-term exposure to intermittent hypoxia leads to changes in gene expression seen in chronic pulmonary disease. Elife. 2021;10.

Chapter 9 - Appendix

9.1. Optimisation of CUT and RUN technique for detecting RelA DNA binding sites following hypoxia stimulation

To identify NF-κB RelA binding sites on the DNA in HeLa cells following hypoxia stimulation, it was decided to use a novel technique called CUT and RUN sequencing, which aims to achieve the same objective as the Chromatin Immunoprecipitation (ChIP)-sequencing method. Compared to ChIP, CUT and RUN sequencing is a more rapid and cost-effective method and can be applied for targeting many types of proteins including histone modifications and transcription factors. The CUT and RUN assay start with immobilising the cells using magnetic beads coated with Concanavalin A, a lectin that binds to proteins. Next, cells are permeabilised by using a buffer that contains digitonin, a non-ionic detergent. Permeabilization step allows the target specific antibody and pAG-MNase (i.e., Protein A and Protein G IgG binding domains fused to micrococcal nuclease) to access and bind to the proteins of interest. The pAG-MNase cleaves DNA close to where antibody is bound. Cleaved chromatin fragments diffuse into the supernatant, while remaining chromatin is left inside the immobilised cells bound to the beads. Although above mentioned steps are applied for IgG and target specific antibody, input sample is treated separately as the target specific chromatin fragmentation is not needed, thus the chromatin is sheared by using a sonicator. In the final step, all samples including target DNA and input DNA are purified using a column kit.

Prior to performing the planned experiment, the assay was optimised for our experimental needs. This included optimising the digitonin concentration for the cell lines used by following manufacturer's instructions. As a result, manufacturer's recommended digitonin concentration was identified as the most efficient one, corresponding to 2.5 μL digitonin in 100 μL digitonin buffer. Furthermore, to optimise the sonication conditions for shearing the chromatin in the input sample, different sonication settings were tested, and the following set-up was decided to be the most efficient one; 20 cycles at 50% amplitude, 15 sec on 30 secs off (**Figure 9.1**). Next, optimum concentration of the input sample was determined using the positive control antibody, H3K4me3 and the primer, RPL30, provided by the kit (**Figure 9.2**).

This approach also confirmed the high efficiency of the CUT and RUN protocol as all of the input dilution factors showed around 15-fold increase in H3K4me3 levels at the RPL30 gene promoter.

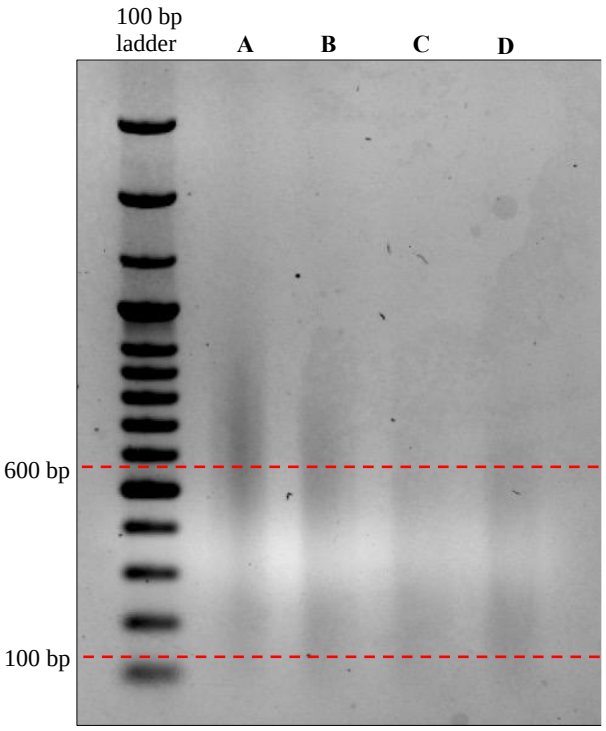

Figure 9.1. Sonication optimisation for the input sample. 100,000 HeLa cells were collected into 1.5 mL Eppendorf tubes for each sonication condition and cell solution was prepared according to manufacturer's instructions. Following sonication conditions were tested; 5 cycles at 50% amplitude, 15 sec on 30 secs off (**A**); 10 cycles at 50% amplitude, 15 sec on 30 secs off (**B**); 15 cycles at 50% amplitude, 15 sec on 30 secs off (**C**), 20 cycles at 50% amplitude, 15 sec on 30 secs off (**D**). 20 µL sample was loaded on a 1% agarose gel with 100 bp DNA marker. The efficient chromatin shearing condition was decided based on the DNA length; area covering the 100-600 bp length is shown between the red dashed lines.

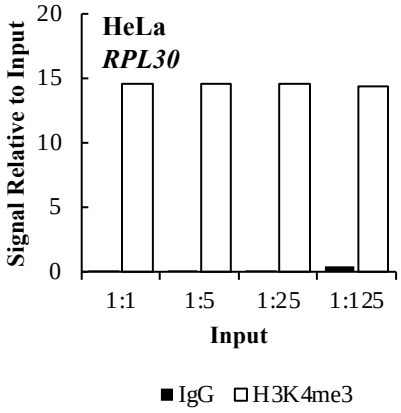

Figure 9.2. Dilution optimisation for the input sample. 100,000 HeLa cells were collected and CUT and RUN procedure was applied according to manufacturer's instructions. Input sample was aliquoted into 1.5 mL Eppendorf tubes with 1:1, 1:5, 1:25 and 1:125 dilution factors. The assay was performed for targeting IgG control and H3K4me3 enriched genes' promoter regions. Positive control qPCR primer supplied in the assay kit, RPL30 was used for the detection of the targeted enriched regions. The graph represents 1 replicate of the experiment.

To detect NF-κB RelA DNA binding sites, initially cells were stimulated with the canonical NF-κB pathway inducer, Tumour necrosis factor α (TNF-α). Following the preparation of the cells according to manufacturer's instructions, efficiency of the Cell Signalling RelA antibody was tested, comparing the difference between overnight or 2 hours antibody incubation (**Figure 9.3**, **A** and **B**). After following the CUT and RUN procedure as per manufacturer's instructions, obtained DNA was analysed using IL8-κB primers, which is a well-known NF-κB target gene. As a result, both of the incubation times had similar efficiency, however, there was also an off-target antibody binding as RelA abundancy was detected on the IL8-κB negative control site.

To prevent any possible re-oxygenation in the cells following hypoxia stimulation, we worked on optimising the CUT and RUN assay to involve formaldehyde fixation step. However, following a mild formaldehyde fixation step, the Cell Signalling RelA antibody lost its efficiency (**Figure 9.3**, **C**). This could be due to formaldehyde disturbing the epitope binding sites for the antibody or affecting the pH levels that could be a problem for the optimum working environment of the kit buffers.

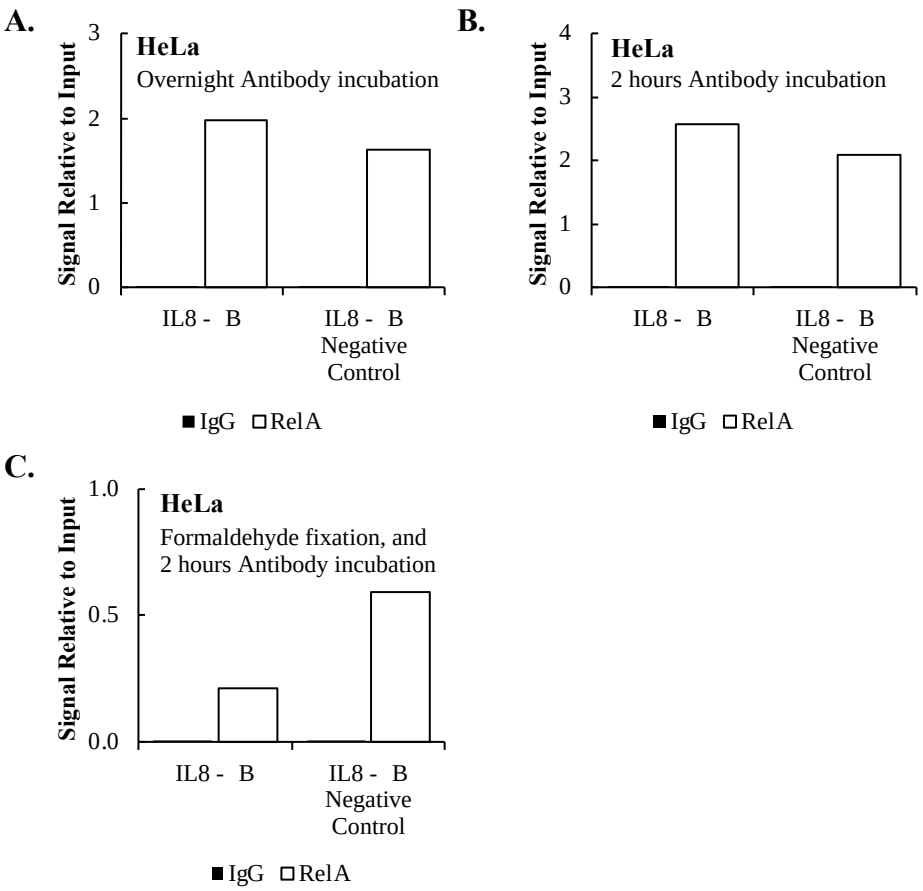

Figure 9.3. Cell Signalling RelA antibody optimisation. HeLa cells were treated with 10 ng/μL TNF-α for 2 hours prior to collection and CUT and RUN procedure application. The assay was performed for an IgG control and IL8-κB enriched genes' promoter regions occupied by the RelA promoter peaks. Cell Signalling antibody (cat. #8242) was used for targeting RelA. The RelA antibody incubation was performed overnight (**A**), for 2 hours (**B**), or for 2 hours following formaldehyde fixation of the cells (**C**). DNA was analysed by qPCR with results normalised to input DNA. IL8-κB negative control represents a DNA region on the IL8 gene that does not include NF-κB binding sites. Graphs represent 1 replicate of the experiment.

Next the CUT and RUN assay was used with the formaldehyde fixation step on the Active motif RelA antibody (**Figure 9.4**). First replicate revealed a positive result, although there was also off-target binding (**Figure 9.4**, **A**). In addition, efficiency of the assay was tested following formaldehyde fixation by investigating H3K4me3 abundancy on the positive control gene, RPL30 (**Figure 9.4**, **B**). This experiment successfully demonstrated around 20-fold increase in the methylation mark levels compared to input. However, when this experiment was repeated the second time, neither the RelA antibody nor the positive control H3K4me3 antibody gave as efficient signal to noise ratio (**Figure 9.4**, **C** and **D**). This might be due to pAG-MNase digestion step could not be performed at the exact recommended temperature, which is 4°C. Also, incubation time of the samples for releasing DNA fragments into the solution might need optimising.

Finally, instead of the formaldehyde fixation, a nuclear extraction method was used based on the manufacturer's instructions (**Figure 9.5**). However, RelA specific DNA binding could not be detected. Also, positive control H3K4me3 levels were low at the RPL30 gene promoter site. These results suggest additional optimisations are needed prior to conduct the line of investigation needed on RelA binding across the genome in hypoxia.

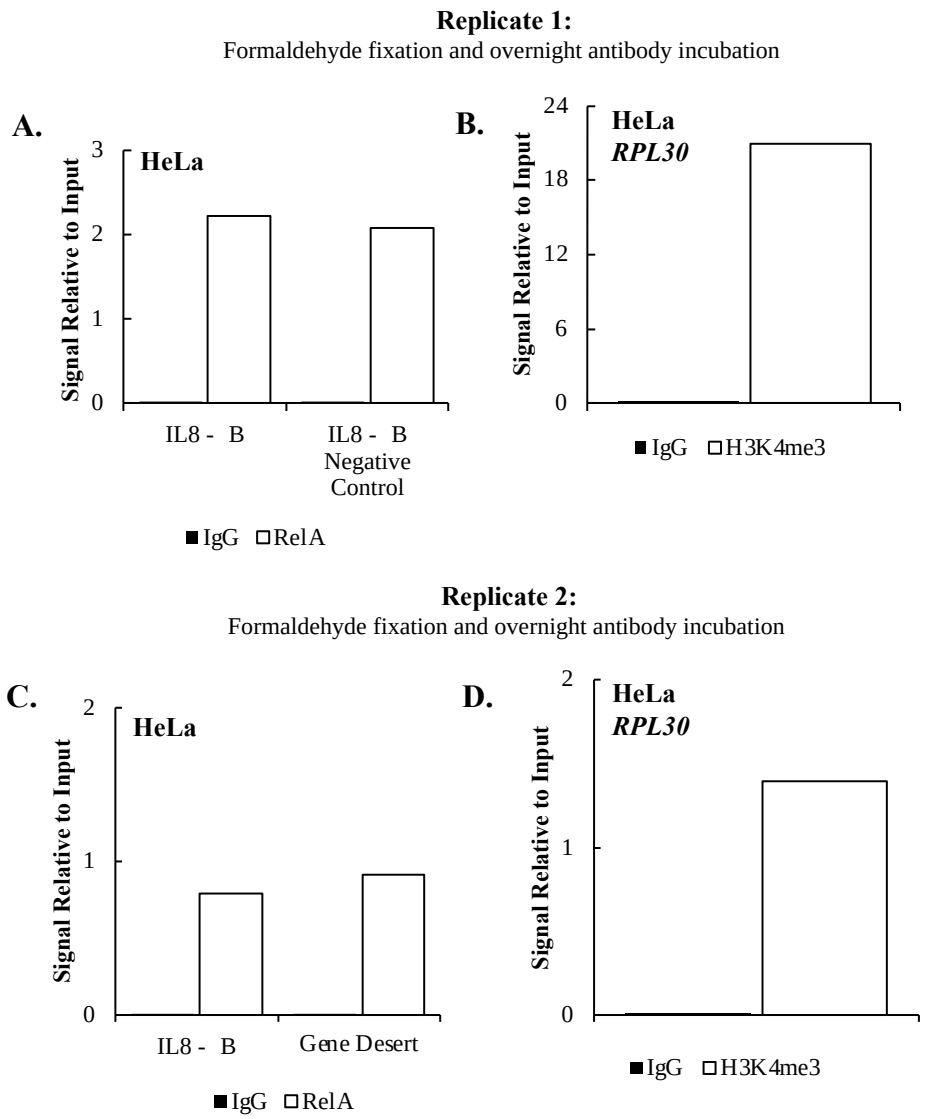

Figure 9.4. Active motif RelA antibody optimisation following formaldehyde fixation of the cells. HeLa cells were treated with 10 ng/μL TNF-α for 2 hours prior to formaldehyde fixation and quenching steps (**A**), (**B**), (**C**), (**D**). Collected cells were then processed according to manufacturer's instructions. The assay was performed for an IgG control and IL8-κB enriched genes' promoter regions occupied by the RelA promoter peaks. Active motif antibody (cat. #39369) was used for targeting RelA by incubating the cells with the antibody overnight (**A**), (**C**). The assay was also performed for targeting H3K4me3 enriched genes' promoter regions (**B**), (**D**). Positive control qPCR primer supplied in the assay kit, RPL30 was used for the detection of the targeted enriched regions. DNA was analysed by qPCR with results normalised to input DNA. IL8-κB negative control represents a DNA region on the IL8 gene that does not include NF-κB binding sites. Gene Desert is used as a negative control as it represents an intergenic DNA region (i.e., non-protein-coding). Graphs represent 2 separate replicates of the experiment.

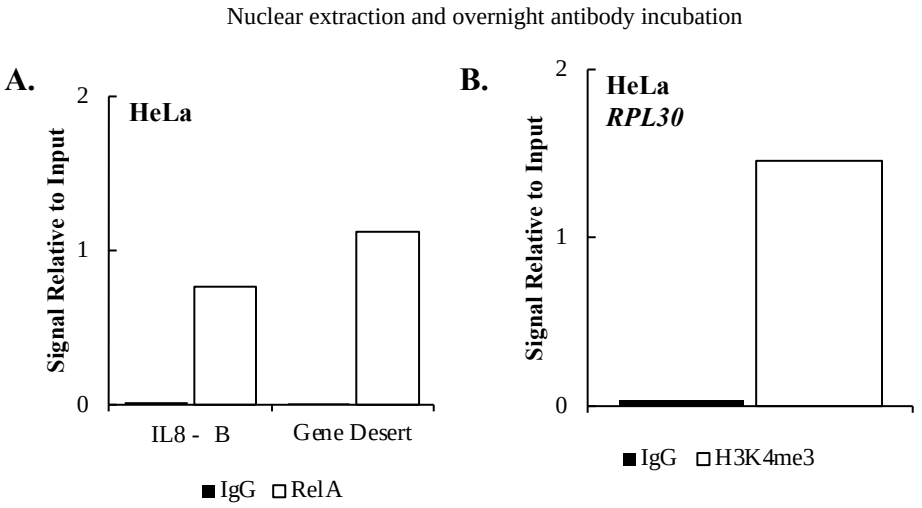

Figure 9.5. Active motif RelA antibody optimisation following nuclear extraction of the cells. HeLa cells were treated with 10 ng/μL TNF-α for 2 hours prior to nuclear extraction procedure according to manufacturer's instructions. The assay was performed for an IgG control and IL8-κB enriched genes' promoter regions occupied by the RelA promoter peaks. Active motif antibody (cat. #39369) was used for targeting RelA by incubating the cells with the antibody overnight (**A**). The assay was also performed for targeting H3K4me3 enriched genes' promoter regions (**B**). Positive control qPCR primer supplied in the assay kit, RPL30 was used for the detection of the targeted enriched regions. DNA was analysed by qPCR with results normalised to input DNA. Gene Desert is used as a negative control as it represents an intergenic DNA region (i.e., non-protein-coding). Graphs represent 1 replicate of the experiment.